SPIG 2026

33rd SUMMER SCHOOL AND
INTERNATIONAL SYMPOSIUM ON
THE PHYSICS OF IONIZED GASES

August 25-28, 2026
Belgrade, Serbia

BOOK OF ABSTRACTS

Editors

Dragana Marić · Saša Dujko · Sanja Tošić
Jelena Marjanović · Bratislav Obradović

33rd Summer School and International Symposium on the Physics of Ionized Gases

SPIG 2026

BOOK OF ABSTRACTS

Editors:

Dragana Marić, Saša Dujko, Sanja Tošić,
Jelena Marjanović and Bratislav Obradović

Serbian Academy
of Sciences and Arts

Institute of Physics Belgrade
University of Belgrade

Belgrade 2026

BOOK OF ABSTRACTS of the 33rd Summer School and International Symposium on the Physics of Ionized Gases

25-28 August 2026, Belgrade, Serbia

Editors:

Dragana Marić, Saša Dujko, Sanja Tošić,
Jelena Marjanović and Bratislav Obradović

Publishers:

Serbian Academy of Sciences and Arts
Kneza Mihaila 35
11000 Belgrade, Serbia

Institute of Physics Belgrade
Pregrevica 118
11080 Belgrade, Serbia

Computer processing: Sanja Tošić, Jelena Marjanović and Dragana Marić

Printed by: Serbian Academy of Sciences and Arts, Belgrade

Number of copies: 200

ISBN: 978-86-6184-132-3

SPIG 2026

Scientific committee

B. Obradović (Chair), Serbia

A. Antoniou, Greece
J. Burgdörfer, Austria
J. Cvetić, Serbia
M. Ćosić, Serbia
J. Kovačević-Dojčinović, Serbia
K. Kutasi, Hungary
M. Kuzmanović, Serbia
V. Lazić, Italy
D. Marić, Serbia
N. J. Mason, UK
N. Milojević, Serbia
A. Milosavljević, France
V. Milosavljević, Serbia
D. Milošević, BH
L. Nahon, France
G. Poparić, Serbia
I. Radović, Serbia
P. Ranitović, Serbia
P. Rousseau, France
I. Savić, Serbia
Y. Serruys, France
T. Silva, Portugal
N. Simonović, Serbia
V. Srećković, Serbia
M. Škorić, Japan
S. Tošić, Serbia
M. Trtica, Serbia
R. White, Australia

Advisory Committee

D. Belić
N. Bibić
M. S. Dimitrijević
S. Đurović
N. Konjević
M.M. Kuraica
J. Labat
G. Malović
I. Mančev
B. P. Marinković
M. Milosavljević
Z. Mišković
Z. Lj. Petrović
L. Č. Popović
B. Stanić

Organizing Committee

S. Dujko (Co-chair)
D. Marić (Co-chair)
J. Marjanović (Secretary)
Z. Lj. Petrović
S. Tošić
N. Cvetanović
D. Bošnjaković
I. Simonović

ACKNOWLEDGEMENTS

The 33rd Summer School and International Symposium on the Physics of Ionized Gases

– SPIG 2026 –

is organized by the

Institute of Physics Belgrade

and

Serbian Academy of Sciences and Arts

under the auspices and with the support of the

Ministry of Science, Technological Development and Innovation of the Republic of Serbia

with technical support from

PANACOMP - Zemlja Čuda d.o.o.

and with support from our sponsors

RoentDek Handels GmbH and **Bel Systems d.o.o. Beograd**

CONTENTS

Section 1. ATOMIC COLLISION PROCESSES

Plenary Lectures

Topical Lectures

Progress Reports

Poster Presentations

Topical Lectures

Progress Reports

Poster Presentations

Topical Lectures

Progress Reports

Poster Presentations

Poster Presentations

3rd Workshop on Swarm Physics and Gaseous Dielectrics (SPGD)

5th Workshop on X-ray and VUV Interaction with Biomolecules in Gas Phase (XiBiGP)

PREFACE

Continuing a tradition established in the early 1960s, the *33rd Summer School and International Symposium on the Physics of Ionized Gases* (SPIG 2026) once again brings together leading researchers from around the world to present and discuss state-of-the-art research and the latest applications in the field. Over more than six decades, SPIG has developed into a distinguished international forum that fosters interdisciplinary dialogue, encourages collaboration across scientific fields, and reflects the continuous progress of modern plasma physics.

The Symposium is organized by the Institute of Physics Belgrade and the Serbian Academy of Sciences and Arts, with support from the Ministry of Science, Technological Development and Innovation of the Republic of Serbia. It will be held at the Serbian Academy of Sciences and Arts in Belgrade, Serbia, from 25 to 28 August 2026.

The scientific programme of SPIG encompasses four major research areas that have long formed the core of the conference:

- Atomic Collision Processes (Electron and Photon Interactions with Atomic Particles, Heavy Particle Collisions, Swarms and Transport Phenomena),
- Particle and Laser Beam Interactions with Solids (Atomic Collisions in Solids, Sputtering and Deposition, Laser and Plasma Interaction with Surfaces),
- Low Temperature Plasmas (Plasma Spectroscopy and Diagnostic Methods, Gas Discharges, Plasma Applications and Devices), and
- General Plasmas (Fusion Plasmas, Astrophysical Plasmas and Collective Phenomena).

In addition to the main conference program, the SPIG 2026 includes two workshops that are thematically aligned with the conference scope and contribute significantly to its scientific breadth:

- 3rd Workshop on Swarm Physics and Gaseous Dielectrics (SPGD),
- 5th Workshop on X-ray and VUV Interaction with Biomolecules in Gas Phase (XiBiGP).

This publication includes abstracts of Plenary Lectures, Topical Invited Talks, Progress Reports, associated Workshop Lectures, and Poster Presentations to be presented at the conference.

The Editors express their sincere gratitude to the members of the Scientific and Advisory Committees of SPIG 2026 for proposing invited lectures and reviewing abstracts, and to the Chairs of the associated workshops for their dedication. We particularly acknowledge the invaluable support of all members of the Local Organizing Committee for their commitment and hard work in preparing and coordinating the conference.

We are deeply grateful to the sponsors of SPIG 2026 and its workshops, RoentDek Handels GmbH and Bel Systems d.o.o. Beograd, whose support has contributed significantly to the realization of this event.

Finally, we thank all invited speakers and participants for contributing to the 33rd SPIG. We wish everyone a pleasant stay in Belgrade, inspiring discussions, valuable scientific exchange, and a successful conference.

Editors:

Dragana Marić, Saša Dujko, Sanja Tošić,
Jelena Marjanović and Bratislav Obradović

Belgrade, 2026

Section 1.

ATOMIC COLLISION PROCESSES

PHOTON-INDUCED DESORPTION FROM MOLECULAR ICES: WHAT IS CURRENTLY KNOWN FROM LABORATORY ASTROPHYSICS EXPERIMENTS

Mathieu Bertin, Antoine Hacquard, Ferdinand Benoit, Daniela Torres-Diaz, Romain Basalgète, Xavier Michaut, Géraldine Féraud, Laurent Philippe and Jean-Hugues Fillion

Sorbonne Université, MONARIS, UMR8233, F-75005 Paris, France

Mathieu.bertin@sorbonne-universite.fr

Desorption induced by photons, usually referred to as photodesorption, is considered one of the main non-thermal desorption processes invoked to explain the abnormally high gas phase abundances of molecules in the cold interstellar medium. It can indeed contribute to maintain a budget of gaseous molecules in the coldest regions (clouds and disks) where they should be depleted onto the icy grains. It is also sometimes thought to be potentially at the origin of the gas phase observation of complex species, such as small organics, that are believed to be formed in or on the ice mantles.

This has motivated numerous experimental studies that aimed at both providing photodesorption yields for a collection of astrophysically-relevent molecules, and identifying the physical-chemical parameters that drive the efficiency of the process. Originally, photodesorption was mostly studied from pure molecular ices, made of "simple" species (H_2O, CO or CO_2) and in the vacuum-UV (7 – 13.6 eV) range using broadband discharge lamps presenting a strong contribution at the H Ly-alpha. However, these last years, the studies progressively aimed more complex systems (organic species, composite ices), harnessed different light sources (monochromatic laser sources and tunable synchrotron sources) and even explored other photon energy domains (soft X-rays), gaining thereby more insights into the microscopic mechanisms of the photodesorption, and in some case benefitting from evolved quantum chemical simulations.

In this presentation, I will show some of the main outcomes of these experimental approach to the UV photodesorption, by developing the cases of some molecular ices. I will go through the photodesorption of some systems, such as the CO ice photodesorption, mechanism of which has been recently more constrained, or the

case of mixed ices with organic molecules, such as HCOOH, $HCOOCH_3$ or CH_3CN. I will also present the limits of what has been done and propose some tracks to follow for future studies.

ELECTRON-PHONON-PHOTON INTERACTION IN POLAR 2D CRYSTALS

Vito Despoja[1], Ivan Radović[2], Zoran L. Mišković[3] and V. M. Silkin[4]

[1]*Centre for Advanced Laser Techniques, Institute of Physics, Bijenička 46, 10000 Zagreb, Croatia*

[2]*Department of Atomic Physics, Vinča Institute of Nuclear Sciences–National Institute of the Republic of Serbia, University of Belgrade, P. O. Box 522, 11001 Belgrade, Serbia*

[3]*Department of Applied Mathematics, and Waterloo Institute for Nanotechnology, University of Waterloo, Waterloo, Ontario, Canada N2L 3G1*

[4]*Departamento de Polímeros y Materiales Avanzados: Física, Química y Tecnología, Facultad de Ciencias Químicas, Universidad del País Vasco (UPV-EHU), Apdo. 1072, 20080 San Sebastián, Spain*

vdespoja@ifs.hr

In the first part of the presentation theoretical formulation of the electron-phonon-photon interaction from the first principles is briefly presented. It is shown that the Electrodynamic Fröhlich Electron-Phonon Vertex in $c \to 0$ limit collapses into its electrostatic or longitudinal counterpart (Verdi *et al.* 2015). The derived formulation is applied to study phonon and photon self-energies in two-dimensional (2D) hexagonal boron nitride (hBN) and hafnium disulfide (HfS_2). Due to electronic screening, the longitudinal optical (LO) phonons (ω_{LO}) in the short wavelength limit show characteristic linear dispersion (Sohier *et al.* 2017), while in the long wavelength limit hybridize with plasmons, free photons (Despoja *et al.* 2026) and cavity photons (Kowalski *et al.* 2025). The cavity photon causes Rabi splitting (Ω) of more than 5% of the ω_{LO}. On the other hand, a few nanometers thick hBN or HfS_2 slabs cause the ultrastrong cavity photon splitting of more than 10% of the cavity photon energy (Barra-Burillo *et al*. 2021). In this way, quantum effects were clearly manifested on a macroscopic scale.

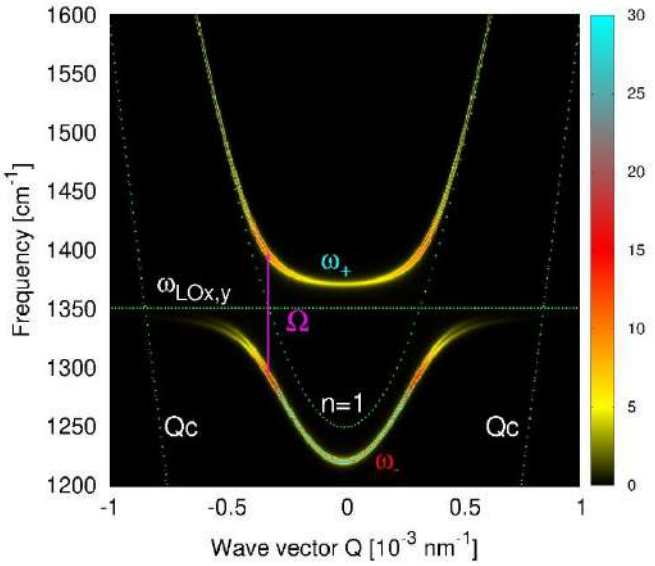

Figure 1: The spectral function of the cavity mode n=1 in 4μm thick cavity in which is inserted 20 atomic layers thick hBN slab (~6nm).

References

Barra-Burillo M, Muniain U, Catalano S, Autore M, Casanova F, Hueso L E, Aizpurua J, Esteban R and Hillenbrand R (2021) *Nat Commun*, **12**, 6206.

Despoja V, Radović I, Mišković Z L, and Silkin V M (2026) *Phys. Rev.* B **113**, 195432.

Kowalski R A, Mueller N S, Álvarez-Pérez G, *et al.* (2025) *Nat. Mater.* **24**, 1735.

Sohier T, Gibertini M, Calandra M, Mauri F and Marzari N (2017) *Nano Lett.* **17**, 6, 3758.

Verdi C and Giustino F (2015) *Phys. Rev. Lett.* **115**, 176401.

NEW PARADIGMS IN AMO DATA COLLECTIONS; THE NEED FOR COMPILATIONS OF HIGHER EXCITED STATES OF POLYATOMIC MOLECULES

Nigel J Mason[1,2]

[1]*Physics and Astronomy, School of Engineering, Mathematics and Physics,University of Kent, Canterbury, CT2 7NH, United Kingdom*

[2]*HUN-REN ATOMKI, Bem square 18, 4026 Debrecen, Hungary*

n.j.mason@kent.ac.uk

The excitation of electronically excited states of molecular systems plays an important role in many disparate areas of science and technology. Radiative decay of such states is the basis of the terrestrial aurorae and is observed in many plasmas, being used to identify component molecular species. Alternative pathways of decay lead to molecular fragmentation yielding neutral or ionic fragments which may dominate chemistry in the local medium.

Photoabsorption spectra provide detailed information upon these electronically excited states and their simultaneous ro-vibrational excitation often providing 'finger-prints' to identify the molecular species. Excited states may be valence or Rydberg, the latter coupled to photoionization. Electron impact excitation can lead to the population of 'forbidden' states with new decay pathways or the formation of 'metastable' states which can transfer energy to other atoms and molecules.

Therefore, the characterization of the electronic states of molecules is an essential part of study of any molecular system and has been the subject of experimental and computational studies for many decades. For decades, Melvin Robin's three-volume series, "Higher Excited States of Polyatomic Molecules[1]", has provided an indispensable reference for understanding the electronic states of molecular systems. However, while these volumes guided generations, recent technological advances and emerging application areas—from laser techniques to spectroscopy in the solid (ice) phase, and the rapid progress in theoretical calculations – demand an updated, comprehensive review.

In this presentation I will discuss the MOLESs project (MOlecular Excited State spectroscopy)[2] an international initiative born from the need to modernize and expand this classic series. The project will assemble authoritative and complete data on the excited states of molecules (valence and Rydberg). It will present their experimental absorption spectra and compare experiment with theoretical derivations of excitation energies and spectra (e.g., using DFT & TDTFT).

MOLESs data will be published in both e-book format and on-line with recommended data sets. Teams will work together on literature reviews, data compilation, and identifying future research needs. The project aims not only to preserve historical data but also standardize future contributions using FAIR procedures. We welcome collaborators who have experimental and/or computational data sets and who wish to join us in the project.

In this presentation I will also review new methodologies being used to collate and prepare such data using next generation AI and machine learning architectures, highlighting advantages and disadvantages of such data generation

Figure 1: The MOLESs project aims to provide the most comprehensive compilation and critical analysis of excited states of molecular systems in all phases of matter.

References

1. Melvin Robin 'Higher Excited States of Polyatomic Molecules' Academic Press, New York, 1974-75 and 1985

2. https://www.moless-spectroscopy.org/

CHARGE TRANSFER IN ORGANIC MOLECULES PROBED BY X-RAY SPECTROSCOPY

Tatiana Marchenko

Sorbonne Université, CNRS, Laboratoire de Chimie Physique-Matière et Rayonnement, LCPMR, F-75005 Paris, France

tatiana.marchenko@sorbonne-universite.fr

Charge transfer (CT) processes, governed by the interplay between electronic and nuclear motion, continue to attract significant attention due to their critical role in a broad spectrum of chemical, biological, and material-related phenomena. In complex systems, steering electronic dynamics with high spatial and temporal resolution demands the initiation of CT at a specific site. This level of selectivity can be achieved through X-ray excitation, which enables atomic-level targeting via core-shell electron transitions.

When a system undergoes dynamic relaxation via emission of Auger electrons or X-ray photons occurring within the lifetime of the core-excited state, typically ranging from a few femtoseconds to the attosecond regime, it becomes possible to probe the underlying electron dynamics of CT processes. Using resonant Auger electron spectroscopy (RAES) and resonant inelastic X-ray scattering (RIXS) in sulphur-containing systems, we gain insight into electron dynamics unfolding on ultrafast timescales defined by the ~1 femtosecond lifetime of the sulphur 1s core hole.

I will demonstrate two applications of these techniques. First, using RAES, we have revealed the CT mechanisms in organic conjugated thiophene-based polymers induced by resonant hard X-ray excitation at the sulfur K-edge, see Velasquez *et al*. 2024. We have established that intra-chain electron delocalisation is the dominant mechanism of CT, whereas inter-chain electron delocalisation is negligible in the studied systems (Fig. 1). Furthermore, I will discuss application of a conventional core-hole-clock (CHC) method for estimating the CT time scale and the newly developed quantum-mechanical Fano-based framework for timing ultrafast CT, which accounts for Fano interference in the core-excited state and goes beyond the conventional CHC method, see Liu *et al*. 2026.

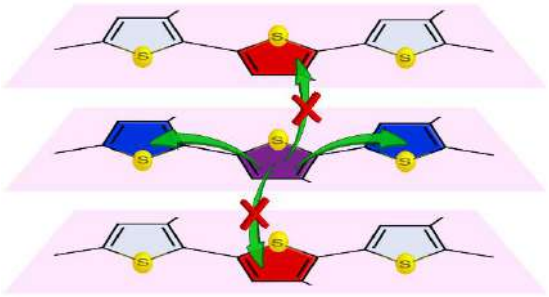

Figure 1: Sketch of the excited thiophene ring (purple) and its nearest neighbours along the chain (blue) and in the layers above and below (red) in P3HT film. The green arrows show that only the intra-chain CT is possible.

In a second example, we applied RIXS for observation of charge transfer to solvent in aqueous amino acid solutions. Taking the proteinogenic amino acid l-cysteine as a model system, we have shown that the efficiency of charge transfer from the core-excited sulphur site to the surrounding water molecules can be efficiently controlled by the pH of the solution, see Sarkar *et al*. 2026.

References

Liu *et al.* (2026) Timing ultrafast charge transfer via Fano interference beyond the Core-Hole Clock, *Phys. Rev. Lett*. accepted, DOI: https://doi.org/10.1103/h6h9-j83r

Sarkar S *et al.* (2026) Manuscript submitted

Velasquez N *et al*. (2024) X-ray induced ultrafast charge transfer in thiophene-based conjugated polymers controlled by core-hole clock spectroscopy, *Phys. Chem. Chem. Phys.* **26**, 1234–1244.

PROBING ULTRAFAST DYNAMICS OF CHARGE CARRIERS AND VALENCE BAND STRUCTURE IN PEROVSKITE-INSPIRED MATERIALS

Radovan Dojčilović[1], Danijela Danilović[1], Dušan Božanić[1], Nevena Božinović[1], Milan Jocić[2], Aleksandar Milosavljević[3], Federico Grandi[4], Eugenio Luigi Cinquanta[4], and Vladimir Djoković[1]

[1] *Center of Excellence for Photoconversion, "Vinča" Institute of Nuclear Sciences - National Institute of the Republic of Serbia, University of Belgrade, P.O. Box 522, 11001 Belgrade, Serbia,*

[2]*Institute of Physics Belgrade, University of Belgrade, Pregrevica 118, 11080 Belgrade, Serbia*

[3]*Synchrotron SOLEIL, Saint-Aubin, BP 48, F-91192 Gif-sur-Yvette Cedex, France*

[4]*Istituto di Fotonica e Nanotecnologie─CNR (CNR-IFN), Milano 20133, Italy*

radovan@vinca.rs

The effective design of an advanced solar cell requires an understanding of the fundamental quantum mechanical process underlying photoexcitation, such as the alignment of the valence energy levels between the absorbing and transport layers or ultrafast relaxation processes in charge carriers. Perovskite-inspired copper-silver-bismuth-iodide (Cu-Ag-Bi-I) are a new class of solar cell absorber materials that possess advantageous optoelectronic properties and can be processed in various forms at low temperatures, with pronounced chemical stability and low toxicity. In this contribution we will present Ag-Bi-I based nanomaterials with adjustable composition, size, dimensionality, and tunable optical properties. We will focus on their valence band structure obtained in the gas phase with synchrotron X-Ray Aerosol Photoemission Spectroscopy and we will present results from exploring charge carrier mobility in the deposited samples with THz spectroscopy.

This research was supported by the Science Fund of Republic of Serbia (Grant No. 230, Aerosol4solar) and Ministry of Science, Technological Development and Innovation through Bilateral project with Italy (SR25MO03).

References

Danilović D *et al* (2020) *J. Phys. Chem. C* **124**, 23930.
Danilović D *et al* (2022) *J. Phys. Chem. C* **126**, 13739.
Danilović D *et al* (2024) *ChemPhysChem* **25 (17)**, e202400328.
Lal S *et al* (2024) *Adv. Funct. Mater.*, **34**, 2315942.
Milosavljević A R *et al* (2018) *J. Phys. Chem. Lett.* **9**, 3604.
Moon T (2025) *Small*, **e10252**.

FROM IONISATION TO DETECTION: COMPUTATIONAL PREDICTIONS OF MOLECULAR IONS IN ASTROCHEMICAL ENVIRONMENTS

Felipe Fantuzzi[1]

[1]*School of Natural Sciences, University of Kent, Park Wood Rd, Canterbury CT2 7NH, UK*

f.fantuzzi@kent.ac.uk

Astrochemical molecules are exposed to ultraviolet and X-ray photons, cosmic rays, energetic electrons, and ions. Ionisation by these processes can trigger structural rearrangement, fragmentation, and ion-molecule reactions, affecting chemical evolution in molecular clouds, planetary atmospheres, and circumstellar environments (McGuire *et al.* 2020). Molecular ions are particularly relevant because they often exhibit structures, reactivity, and spectroscopic signatures distinct from those of their neutral counterparts (Mason *et al.* 2026). Here, quantum-chemical studies of ions formed under high-energy astrochemical conditions are presented. Potential-energy-surface exploration, density functional theory, coupled-cluster methods, multireference calculations, and Born-Oppenheimer molecular dynamics (BOMD) are employed to predict structures, stability, bonding, fragmentation pathways, and spectroscopic observables. The $C_2H_4O_2^+$ and $C_2H_4O_2^{2+}$ systems illustrate how ionisation can favour structures unrelated to the corresponding neutral isomers. The lowest-energy cationic structures are enolic, whereas the dications include H_2O^+ and $C{\equiv}O^+$ terminal groups (Fantuzzi *et al.* 2011; Fantuzzi *et al.* 2012). Double ionisation of benzene leads to a pentagonal-pyramidal global minimum, while multiply charged chlorobenzene species exhibit unusual carbon-chlorine multiple-bond character (Fantuzzi *et al.* 2017; Fantuzzi *et al.* 2018). Calculations on $HNCO^{2+}$ and multiply charged naphthalene further demonstrate the importance of structural rearrangement in interpreting ionisation experiments and fragmentation processes (Gerlach *et al.* 2021; Santos *et al.* 2022). Finally, BOMD simulations show that ionisation of saturated interstellar molecules can form persistent cations that have not yet been detected in space. These include CH_2NH_2+, $HCOH^+$, H_2NCOH^+, $HCCNH^+$, and a series of unsaturated $C_3H_2N^+$ and $C_4H_2N^+$ ions, which represent attractive targets for laboratory spectroscopy and astronomical searches. Their

predicted structures and spectroscopic properties provide a basis for expanding molecular-ion inventories and refining astrochemical models of high-energy environments (Londoño-Restrepo *et al.* 2025; Quitián-Lara *et al.* 2025).

References

Fantuzzi F, Pilling S, Santos ACF, Baptista L, Rocha AB and Boechat-Roberty HM (2011) *Mon. Not. R. Astron. Soc.*, **417**, 2631.

Fantuzzi F, Baptista L, Rocha AB and Boechat-Roberty HM (2012) *Int. J. Quantum Chem.*, **112**, 3303.

Fantuzzi F, de Sousa DWO and Nascimento MAC (2017) *Comput. Theor. Chem.*, **1116**, 225.

Fantuzzi F, Rudek B, Wolff W and Nascimento MAC (2018) *J. Am. Chem. Soc.*, **140**, 4288.

Gerlach M, Fantuzzi F, Wohlfart L, Kopp K, Engels B, Bozek J, Nicolas C, Mayer D, Gühr M, Holzmeier F and Fischer I (2021) J. Chem. Phys., 154, 114302.

Londoño-Restrepo J, Gómez S, Quitián-Lara HM, Fantuzzi F and Restrepo A (2025) Chem. Sci., 16, 3051.

Mason NJ, Ioppolo S, Quitián-Lara HM, Fantuzzi F, Mifsud DV and Bocková J (2026) *Foundations of Astrochemistry II: Photon- and Radical-Induced Processes in Ices, Computational Approaches, and Biomolecular Chirality.* In: *Advances in Atomic and Molecular Physics at the Interfaces with the Natural Sciences, Technology and Medicine*, World Scientific, 623.

McGuire BA, Asvany O, Brünken S and Schlemmer S (2020) *Nat. Rev. Phys.*, **2**, 402.

Quitián-Lara HM, Londoño-Restrepo J, Gómez S, García-González KV, Restrepo A, Mason NJ, Caselli P, Boechat-Roberty HM and Fantuzzi F (2025) *Mon. Not. R. Astron. Soc.*, **539**, 3778.

Santos JC, Fantuzzi F, Quitián-Lara HM, Martins-Franco Y, Menéndez-Delmestre K, Boechat-Roberty HM and Oliveira RR (2022) *Mon. Not. R. Astron. Soc.*, **512**, 4669.

PE(AE)PIPICO SPECTROSCOPY AT PLEIADES – EXPERIMENTAL METHODS AND DATA PROCESSING ENABLING STATE-RESOLVED STUDIES OF UNIMOLECULAR DECOMPOSITION IN THE SOFT X-RAY RANGE

Aleksandar R. Milosavljević, Christophe Nicolas, Emmanuel Robert and John Bozek

Synchrotron SOLEIL, L'Orme des Merisiers, Départementale 128, St Aubin, France

aleksandar.milosavljevic@synchrotron-soleil.fr

The permanent experimental station EPICEA at the soft X-ray PLEIADES beamline of Synchrotron SOLEIL (France) allows for photoelectron (or Auger electron)–photoion–photoion coincidence (PE(AE)PIPICO) spectroscopy of neutral molecular targets isolated in the gas phase (Liu *et al.* 2017). This presentation will describe in detail the beamline characteristics, the EPICEA experimental technique, as well as the procedure for data processing, including the statistical treatment of false coincidences.

EPICEA consists of a double toroidal electron analyzer (DTA) (Miron *et al.* 1997) and a linear time-of-flight (TOF) mass spectrometer with 3D focusing capabilities (Miron *et al.* 1997; Seccombe and Reddish 2001). The detection of an electron triggers a voltage pulse that is applied to the extraction grids, pushing the photoions toward a delay-line position-sensitive ion detector (HEX75, RoentDek GmbH) placed at the end of the TOF drift tube. Additionally, we use a pulse generator to produce regular "virtual" triggers, which also extract ions to the detector, without a coincident electron event, thereby allowing for statistical subtraction of false coincidences based on the procedure proposed by Prümper and Ueda (Prümper and Ueda 2007). The DTA can accept photoelectrons (or Auger electrons) emitted at the magic angle, which are focused into the analyzer by a system of lenses (Liu *et al.* 2013) and are selected according to a defined DTA pass energy (E_p). The detection window of the electron kinetic energy is approximately 12% of the defined E_p. The spectral resolution, as defined by the DTA, is about 1% of E_p. After passing the DTA, the selected electrons are recorded by a delay-line position-sensitive detector (DLD40, RoentDek GmbH).

The distance of the electron position from the center of the detector is inversely proportional to its kinetic energy.

In this presentation, we will discuss, as examples, several recently studied molecular targets, such as formic acid (Gloroid *et al.* 2026), benzonitrile (Rodrigues *et al.* 2026) and betaine (Rousseau *et al.* 2021), particularly electronic state-resolved fragmentation upon valence ionization or resonant Auger decay following carbon K-shell excitation. We will also discuss technical limitations, improvements, and perspectives.

References

Gloroid A *et al.* (2026) *J. Chem. Phys.* **164** 174313.

Liu X-J *et al.* (2017) *Sci. Rep.* **7** 2898.

Liu X-J *et al*. (2013) *Rev. Sci. Instrum.* **84** 033105.

Miron C *et al.* (1997) *Rev. Sci. Instrum.* **68** 3728.

Prümper G and Ueda K (2007) *Nucl. Instrum. Methods Phys. Res.* A **574** 350.

Rodrigues R *et al*. (2026) *ChemPhysChem* **27** e202500206.

Rousseau P *et al.* (2021) *Sci. Adv.* **7** eabg9080.

Seccombe D P and Reddish T J (2001) *Rev. Sci. Instrum.* **72** 1330.

ELECTRON-DRIVEN REACTIVITY OF MOLECULAR CATIONS IN COLD PLASMAS

Mezei Jànos Zsolt[1], Riyad Hassaine[2], Rawand Mezlini[3], Flore Iffly[3], Nicolina Pop[4], Kalyan Chakrabarti[5], Mehdi Ayouz[6], Khalid Hassouni[7], Arnaud Bultel[8], Asa Larson[9], Jonathan Tennyson[10], and Ioan F. Schneider[3]

[1]*HUN-REN Institute for Nuclear Research (ATOMKI), H-4001 Debrecen, Hungary*

[2]*Dept. of Physics and Astronomy, Purdue Univ., 47907 West Lafayette IN, USA*

[3]*LOMC, CNRS-Univ. Le Havre Normandy, 76600 Le Havre, France*

[4]*Dept. of Phys. Found. Eng., Politehnica Univ. of Timisoara, 300223 Timisoara, Romania*

[5]*Dept. of Mathematics, Scottish Church College, 700006 Kolkata, India*

[6]*LGPM, CentraleSupelec, Univ. Paris-Saclay, F-91190 Gif-sur-Yvette, France*

[7]*LSPM, CNRS-Univ. Sorbonne Paris Nord, 93430 Villetaneuse, France*

[8]*CORIA, CNRS-Univ. Rouen Normandy, 76800 Saint-Etienne du Rouvray, France*

[9]*Dept. of Physics, Stockholm Univ. 10691 Stockholm, Sweden*

[10]*Dept. of Physics and Astronomy, Univ. College London, WC1E6BT London, UK*

mezei.zsolt@atomki.hu

The cold plasmas produced in various contexts - hypersonic entry of spacecrafts in planetary atmospheres, at the wall of the magnetic fusion devices, industrial processes, discharge-assisted combustion - are the seat of a very rich physical chemistry, mainly due to the presence of electrons, photons and excited molecular species. The successful modelling of the kinetics of these environments - highly non-linear - relies in a critical manner on the accuracy of the rate coefficients for the governing collisional and/or radiative elementary processes [1].

Among them, electron impact recombination, (ro-)vibrational, electronic and dissociative excitation of molecular cations are in the heart of the molecular reactivity, being major destruction paths for the charged species and producing often atoms in metastable states, inaccessible through optical excitations. They involve superexcited molecular states undergoing predissociation and

autoionization, having thus strong resonant character. They are subject to beyond-Born-Oppenheimer approximation modeling within the quasi-diabatic representation, and they require special treatment due to the superposition of many continua and infinite series of Rydberg states.

The methods based on the Multichannel Quantum Defect Theory (MQDT) [2] are the most suitable approaches for these processes, capable to account the strong mixing between ionization and dissociative channels, open - direct mechanism - and closed - indirect mechanism, via capture into prominent Rydberg resonances correlating to the ground and excited ionic states, and the rotational effects.

New results on H_2^+ [3], N_2^+ [4], NeH^+ [5] BeH^+ [6], BH^+ [7], N_2H^+ [8], and C_2H^+ [9] as well as advancement in the theoretical treatment - as the inclusion of new dissociative pathways, the isotopic effects, etc.… will be presented.

References

[1] Schneider I F, Dulieu O and Robert J, *eds*. (2015) *EPJ Web of Conferences,* **84**.

[2] Mezei J Zs *et al.* (2019) *ACS Earth Space Chem*, **3**, 2376.

[3] Hassaine R *et al.* (2025) *A&A*, **703**, A220.

[4] Abdoulanziz A *et al.* (2021) *J. Appl. Phys.*, **129**, 053303.

[5] Hassaine R *et al.* (2026) *Phys. Rev. A*, **113**, 032820.

[6] Djuissi E *et al.* (2024) *PCCP*, **26**, 18311.

[7] Mezlini R *et al.* (2026) to be submitted to *J. Chem. Phys.*

[8] Mezei J Zs *et al.* (2023) *Eur. Phys. J. Spec. Top.*, **232**, 1967.

[9] Mezei J Zs *et al.* (2026) to be submitted to *Atoms.*

ELECTRON COLLISION CROSS SECTION SETS FOR C-C_4F_8 AND 1,3-C_4F_6

Satoru Kawaguchi[1], Yuto Sugai[1], Kazuhiro Takahashi[1], and Kohki Satoh[1]

[1]*Muroran Institute of Technology*

skawaguchi@muroran-it.ac.jp

Plasma simulation is an indispensable tool for understanding complex chemistry and transport phenomena in plasmas. An accurate description of electron kinetics is particularly important because the electron energy distribution and spatial distribution determine the production of radicals, excited species, and ions through electron-impact reactions. Such a description requires reliable electron swarm parameters, reaction rate coefficients, and probabilities, all of which are derived from electron collision cross sections. Therefore, reliable plasma simulations require a cross section set that is both complete and self-consistent. A complete set is a set that includes the fundamental processes governing electron transport in plasmas, whereas a self-consistent set is a set that is able to reproduce experimental electron swarm parameters over a wide range of reduced electric fields. In this study, we constructed complete and self-consistent electron collision cross section sets for c-C_4F_8 and 1,3-C_4F_6.

The cross section sets are constructed in the following manner. An initial cross section set is constructed from experimental and theoretical data reported in the literature. Electron swarm parameters calculated using Monte Carlo simulations (MCS) are compared with experimental data, and the cross sections are iteratively adjusted to reproduce the measured swarm parameters. During this procedure, the available experimental and theoretical cross sections are respected as far as possible to avoid arbitrary modifications. Particular attention is paid to the correspondence between measured and calculated electron drift velocities because the value of the electron drift velocity can depend on how it is measured and calculated [e.g., Satoh et al. (1994)].

Figure 1 shows the electron collision cross section sets for c-C_4F_8 and 1,3-C_4F_6 developed in this study. The cross section set for c-C_4F_8 includes a total neutral dissociation cross section, five electron attachment cross sections, and 13 ionization cross sections. The electron attachment and ionization cross sections

are based on Feil et al. (2008) and Jiao et al. (1998), respectively, and correspond to the formation of $C_4F_8^-$, $C_3F_5^-$, $C_2F_3^-$, CF_3^-, F^-, F^+, CF^+, C_2F^+, CF_2^+, C_3F^+, $C_2F_2^+$, CF_3^+, $C_3F_2^+$, $C_2F_3^+$, $C_3F_3^+$, $C_2F_4^+$, $C_3F_4^+$, and $C_3F_5^+$. The cross section set for 1,3-C_4F_6 includes seven electron attachment cross sections and seven ionization cross sections. They are based on Feil et al. (2008) and Bull et al. (2013), respectively, and correspond to the formation of $C_4F_6^-$, F^-, F_2^-, $C_3F_3^-$, $C_3F_4^-$, $C_4F_4^-$, $C_3F_5^-$, $C_4F_5^+$, $C_3F_4^+$, $C_4F_6^+$, $C_3F_3^+$, CF_3^+, $C_3F_2^+$, and CF^+.

We calculated electron swarm parameters, including the mean-arrival-time drift velocity W_m, center-of-mass drift velocity W_r, electron drift velocity $W=(W_m + W_r)/2$, reduced longitudinal diffusion coefficient, reduced ionization coefficient, reduced electron attachment coefficient, and reduced effective ionization coefficient. The self-consistency of the cross section sets developed in this study was demonstrated by comparing the calculated electron swarm parameters with experimental data for c-C_4F_8, c-C_4F_8/Ar mixtures, 1,3-C_4F_6, and 1,3-C_4F_6/Ar mixtures.

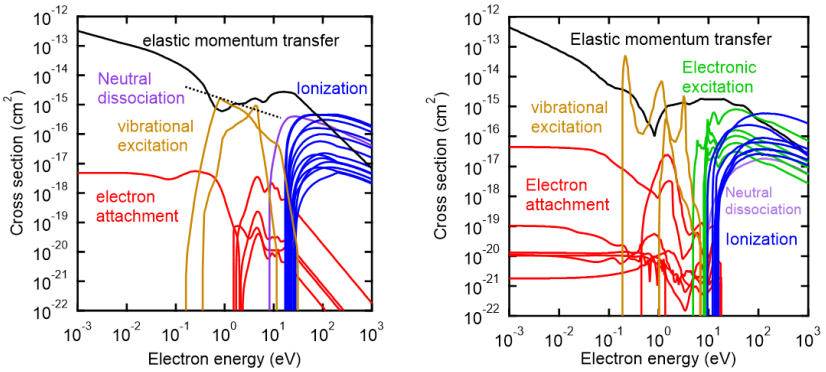

(a) c-C_4F_8 gas (b) 1,3-C_4F_6 gas

Figure 1: Electron collision cross section sets determined in this study

Acknowledgement: This work was partly supported by Tokyo Electron Miyagi Ltd.

References

Bull J N, Bart M, Vallance C, and Harland P W (2013) *Phys. Rev. A* **88**, 062710.

Feil S, Märk T D, Mauracher A, Scheier P, and Mayhew C A (2008) *Int. J. Mass Spectrom.* **277**, 41.

Jiao C Q, Garscadden A, and Haaland P D (1998) *Chem. Phys. Lett.* **297**, 121.

Satoh K, Hataguchi M, Itoh H, Sakai Y, and Tagashira H (1994) *J. Phys. D: Appl. Phys.* **27**, 1480.

ELECTRON TRANSPORT IN NOBLE LIQUIDS: FROM SWARM PHYSICS TO NEXT-GEN PARTICLE DETECTORS

G.J. Boyle[1], D.L. Muccignat[1], R.D. White[1], N. Garland[2], D. Belča[3], I. Simonović[3], D. Bošnjaković[3] and S. Dujko[3]

[1]*James Cook University, Townsville, Australia*

[2] *Griffith University, Nathan, Australia*

[3]*Institute of Physics Belgrade, Pregrevica 118, 11080 Belgrade, Serbia*

gregory.boyle@jcu.edu.au

The transport of low-energy electrons through liquid noble gases lies at the intersection of plasma physics, atomic collisions, condensed matter physics and particle detection. Accurate descriptions of electron mobility, diffusion and energy relaxation underpin the operation of modern liquid argon and liquid xenon time projection chambers used in dark matter and neutrino experiments (ECFA 2021, Boyle *et al.* 2025). As detector technologies advance towards the detection of single ionisation electrons and scintillation quanta, existing empirical transport models are reaching the limits of their predictive capability, creating an urgent need for first-principles descriptions of electron transport in dense media (ECFA 2021).

This presentation outlines a roadmap for developing predictive electron transport models in noble liquids. Recent swarm measurements are reviewed together with advances in *ab initio* kinetic theory, including the roles of coherent scattering, polarisation screening, liquid structure and medium-induced modifications of the electron-atom interaction potential. Together, these developments have enabled quantitative predictions of elastic transport properties across a wide range of conditions and provide a firm foundation for next-generation transport models (Boyle *et al.* 2025).

Outstanding challenges and future opportunities are then discussed, including the potential for *ab initio* descriptions of inelastic electron scattering in liquids, transport in doped and mixed noble-liquid systems, electron transport across liquid-gas interfaces, and the incorporation of first-principles transport models into detector simulation frameworks. The combination of precision swarm

experiments, advanced kinetic theory, Monte Carlo simulations and machine-learning approaches for scattering cross-section determination offers a pathway towards predictive simulations of future particle detectors operating at ultra-low energies.

References

Boyle G J, Garland N A, Muccignat D L, Simonović I, Bošnjaković D, Dujko S and White R D (2025) *Front. Detect. Sci. Technol.*, **3**, 1616204.

ECFA Detector R&D Roadmap Process Group, The 2021 ECFA Detector Research and Development Roadmap, CERN-ESU-017, CERN (2021).

RADIATION DAMAGE OF NUCLEOTIDES-THE STORY REVEALED BY X-RAY ACTION SPECTROSCOPY

Aarathi Nair[1], Rebecca Boll[2,3], Christine Bülow[4], May Constabel[5], Panagiotis Katechis[2], Tobias Lau[4,6], Juliette Leroux[1], Rebecka Lindblad[4,7,10], Jesus Lucia-Tamudo[8], Carlos Ortiz-Mahecha[9], Bart Oostenrijk[1,2], Laura Pille[2], Lucas Schwob[2], Sergio Diaz-tendero Victoria[11], Vicente Zamudio-Bayer[4], Sadia Bari[2,12]

[1]*The Hamburg Centre for Ultrafast Imaging, Hamburg, Germany;*

[2]*Deutsches Elektronen-Synchrotron DESY, Germany;*

[3]*European XFEL, Schenefeld, Germany;*

[4]*Abteilung für Hochempfindliche Röntgenspektroskopie, Helmholtz-Zentrum Berlin für Materialien und Energie, Berlin, Germany;*

[5]*Division of BioAnalytical Chemistry (MS-LaserLab), Department of Chemistry and Pharmaceutical Sciences, Amsterdam Institute of Molecular and Life Sciences AIMMS, Vrije Universiteit Amsterdam, Amsterdam, The Netherlands;*

[6]*Physikalisches Institut, Albert-Ludwigs-Universität Freiburg, Freiburg, Germany;*
[7]*Department of Physics, Lund University, Lund, Sweden;*

[8]*Universität Regensburg, Regensburg, Germany*

[9]*Hamburg University of Technology, Hamburg, Germany*;

[10]*Inorganic Chemistry, Department of Chemistry – Ångstrom Laboratory, Uppsala University, SE-75121 Uppsala, Sweden;*

[11]*Universidad Autónoma de Madrid, Spain*

[12]*Zernike Institute for Advanced Materials, University of Groningen, Groningen, The Netherlands*

aarathi.nair@desy.de

The combination of soft-ionisation techniques, such as electrospray ionisation, with mass spectrometric techniques, including radiofrequency ion filtering and trapping, is a powerful tool for studying biomolecules like proteins and DNA in the gas phase, free from solvent interference. Activating these isolated biomolecules with UV, VUV or X-rays from synchrotron sources helps us to gain

more insight into their intrinsic properties. A detailed understanding of DNA nucleotides, and the different dissociation mechanisms involved in radiation damage can help explain the photoprotection mechanisms in DNA. In this context, soft X-ray absorption being element specific makes it particularly ideal to explore the resonant photo-absorption at the C, N and O inner-shell edges. Moreover, to obtain a full picture, it is crucial to investigate the role of the sugar and phosphate moieties and whether their presence near the nucleobases affects the photoabsorption and the stability of the system.

In this study, near-edge X-ray absorption mass spectrometry experiments were performed at the UE52_PGM Ion Trap end station at the BESSY II synchrotron (HZB, Berlin, Germany) and using our home-built ion-trap mass spectrometer at the P04 soft X-ray beamline at the PETRA III synchrotron (DESY, Hamburg, Germany). Measurements were taken at the C, N and O K-edges on a protonated oligonucleotide containing all four DNA bases—guanine, cytosine, adenine and thymine—linked via a sugar- phosphate backbone. The resulting data offer insights into protonation effects, fragmentation mechanisms and resonant electronic transitions within the nucleotides, contributing to a deeper understanding of DNA's radiation response at the molecular level.

LATEST THEORETICAL INVESTIGATIONS OF THE INTERPARTICLE COULOMBIC ELECTRON CAPTURE

Jan Šenk[1,2], Vincent Graves[3], Jimena D. Gorfinkiel[3], Přemysl Kolorenč[2], and Nicolas Sisourat[1]

[1]*Sorbonne Université, CNRS, Laboratoire de Chimie Physique Matière et Rayonnement, UMR 7614, F-75005 Paris, France*

[2]*Institute of Theoretical Physics, Faculty of Mathematics and Physics, Charles University, V Holešovičkách 2, 180 00 Prague, Czech Republic*

[3]*School of Physical Sciences, The Open University, Walton Hall, Milton Keynes MK7 6AA, United Kingdom*

jan.senk@sorbonne-universite.fr

Interparticle Coulombic electron capture (ICEC) is an environment-enabled electron capture process where the excess energy is released by ionization of a neighboring particle. Both the capturing particle and the neighbor can be atoms, molecules, or ions. It is one of the many electron capture (or electron attachment) processes that are relevant to astrophysics and plasma physics. ICEC was predicted theoretically using scattering theory, see Gokhberg *et al.* 2009, and is expected to be significantly more efficient than the competing photorecombination. To date, it has been studied using analytical approximations, e.g. Molle *et al.* 2023, theoretical models, e.g. Pont *et al.* 2016, and *ab initio* calculations, e.g. Sisourat *et al.* 2018. It has yet to be experimentally observed.

The asymptotic approximation, see Gokhberg *et al.* 2010, has been shown to severely underestimate the ICEC cross section when the distance between the two particles is comparable to their size. It treats the whole process as two independent events – virtual photorecombination at the capturing particle and virtual photoionization of the neighbor – linked by the transfer of the excess energy. This separation into two isolated events neglects the possibility of an electron transfer from the neighbor to the capturing particle. We have proposed a semiempirical model of the electron transfer mechanism of ICEC, and benchmarked it with *ab initio* electron scattering calculations for several systems, see Šenk *et al.* 2024.

In comparison to the original asymptotic approximation, our model improved the agreement with the *ab initio* results at relevant inter-particle distances while remaining simple – the model ICEC cross sections can be evaluated with an analytical formula using tabulated properties of the participating particles, avoiding expensive *ab initio* calculations.

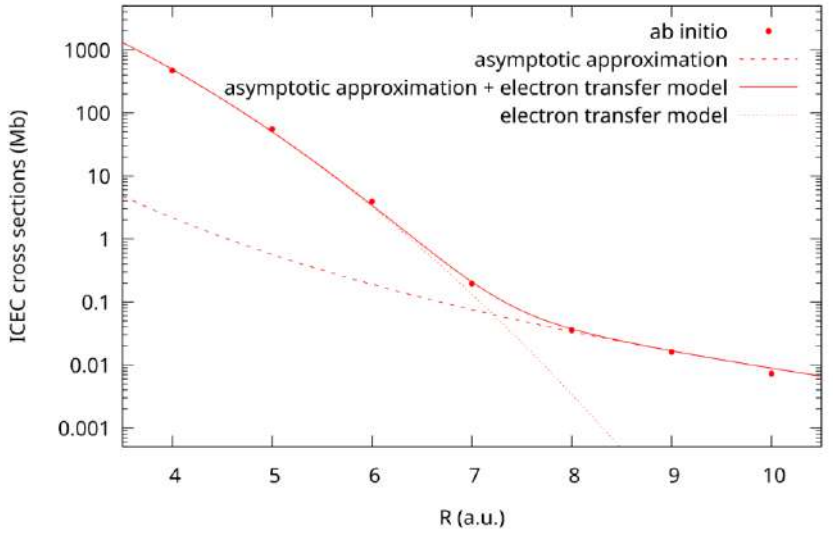

Figure 1: ICEC $e^- + He^+Ne \rightarrow HeNe^+ + e^-$, i.e. the electron is captured by He^+, and neighboring Ne is ionized. The outgoing electron energy is 8 eV. By including the electron transfer term, the agreement with *ab initio* is greatly improved.

References

Gokhberg K and Cederbaum L S (2009) *J. Phys. B: At. Mol. Opt. Phys.*, **42**, 231001.

Gokhberg K and Cederbaum L S (2010) *Phys. Rev. A*, **82**, 052707.

Molle A, Zatsarinny O, Jagau T, Dubois A, and Sisourat N (2023) *J. Chem. Phys.*, **158**, 134306.

Pont F M, Bande A, and Cederbaum L S (2016) *J. Phys.: Condens. Matter*, **28**, 075301.

Sisourat N, Miteva T, Gorfinkiel J D, Gokhberg K, and Cederbaum L S (2018) *Phys. Rev. A*, **98**, 020701.

Šenk J, Graves V, Gorfinkiel J D, Kolorenč P, and Sisourat N (2024) *J. Chem. Phys.*, **161**, 174113.

PHOTOELECTRON CIRCULAR DICHROISM IN HELICAL CHIRALITY SHOWCASE: THE *HELICENES* FAMILY

Sanket Sen[1,2], Etienne Rouquet[1,2], Darius Lebeau[2], Gustavo A. Garcia[1], Valeria Lepere[2], Yohan Gisbert[3], Chengshuo Shen[4], Nicolas Vanthuyne[5], Anne Zehnacker[2], Jeanne Crassous[3] and Laurent Nahon[1]

[1]*Synchrotron SOLEIL, L'Orme des Merisiers, Départementale 128, St Aubin, France*

[2]*Institut des Sciences Moléculaires d'Orsay (ISMO), CNRS, Université Paris-Saclay, Orsay, France*

[3]*Institut des Sciences Chimiques de Rennes, Univ Rennes, CNRS, Rennes Cedex, France*

[4]*School of Chemistry and Chemical Engineering, Zhejiang Sci-Tech University, Hangzhou, China*

[5]*Aix Marseille University, CNRS, Centrale Marseille, iSm2, Marseille, France*

sanket.sen@synchrotron-soleil.fr

Helicenes attracted a lot of interest for both fundamental and applied studies as their chiral helical structure exhibit intriguing chemical and photophysical properties, see Crassous *et al*. (eds) 2022. Besides, Photoelectron circular dichroism (PECD) manifests itself as an intense forward-backward asymmetry in a chiral target's photoelectron angular distribution when ionised by circularly polarised radiation, and as such is particularly well-suited for studies of dilute chiral matter, see Nahon *et al*. 2015 and Sparling *et al*. 2025. So far, this chiroptical effect has been observed on samples exhibiting central and axial chirality, as well as D3 propeller type of chirality, see Darquie *et al*. 2021.

In the present work, we probed the helical chirality of custom synthesised enantiomers of [6]helicene, first member of the helicene family to complete one flight of "benzene-like" rings causing an effect akin to steric hindrance, preventing racemisation. We employed a double imaging particle coincidence spectrometer, see Garcia *et al*. 2013 and circularly polarised VUV synchrotron radiation, see Nahon *et al*. 2012 to record mass-selected electron orbital/band correlated PECD. We report the first, intense (~25%), orbital/band specific PECD on a sample exhibiting helical chirality (left, Fig. 1).

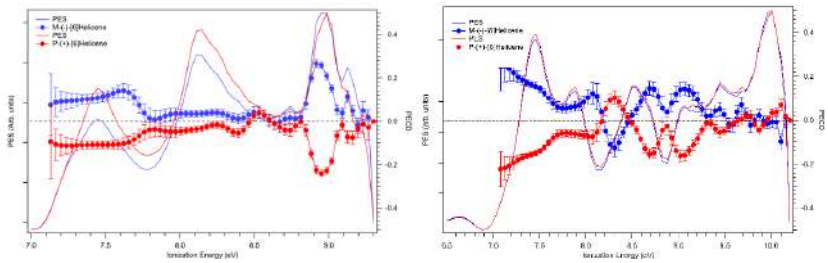

Figure 1: PES (solid line) and PECD (dots with error bars) corresponding to enantiomers P-(+)- (red) and M-(-)- (blue) of [6]helicene recorded at 9.3 eV (left) and [8]helicene recorded at 10.2 eV (right).

We further explored the effect of pitch and length of the helicene "staircase" on the PECD, as Electronic Circular Dichroism of [n]helicenes in solution unveils a clear trend of anisotropy factor (g) increasing with the size(n) of helicene, see Nakai *et al*. 2012. PECD from [7]helicene and [8]helicene, is similar in magnitude as of [6]helicene. Moreover, rich and oscillating PECD is observed for [8]helicene, quickly changing sign across the photoelectron spectra (PES) (right, Fig. 1) showing the presence of several electronic states non-totally resolved in the PES.

In addition, we recently investigated PECD from the clusters of [8]helicenes, as it is of relevance to astrochemistry. PECD has been suggested as a symmetry breaking process, see Hadidi *et al*. 2018 and helicenes are considered as models of icy nanograins, a probable chiral substrate, on which non-racemic elementary bricks of life could have been formed, see Kaiser *et al*. 2022, leading to life's homochirality.

References

Crassous J *et al*. (eds) (2022) *Helicenes*, Wiley-VCH.

Darquie B *et al*. (2021) *Phys. Chem. Chem. Phys.*, **23**, 24140.

Garcia G A *et al*. (2013) *Rev. Sci. Instrum.*, **84**, 053112.

Hadidi R *et al*. (2018) *Advances in Physics: X*, **3**, 1477530.

Kaiser R I *et al*. (2022) *Phys. Chem. Chem. Phys.*, **24**, 25077.

Nahon L *et al*. (2015) *J. of Elec. Spec. and Rel. Phenomena*, **204**, 322.

Nahon L *et al*. (2012) *J. Synchrotron Rad*., **19**, 508.

Nakai Y *et al*. (2012) *J. Phys. Chem. A*, **116**, 7372.

Sparling C *et al*. (2025) *Phys. Chem. Chem. Phys.*, **27**, 2888.

RADIATION EFFECTS ON C/N-RICH ORGANIC ICES: IMPLICATIONS FOR TITAN'S STRATOSPHERIC CHEMISTRY

R. Sreeja[1], A. L. F de Barros[1,2], T. Nguyen Trung[1], C. A. P da Costa[3], D. Dubois[1], H. Rothard[1] and A. Domaracka[1]

[1]*Centre de Recherche sur les Ions, les Matériaux et la Photonique, Université Caen-Normandie, ENSICAEN, CNRS, CEA, Normandie Univ., CIMAP UMR 6252, 14000 Caen, France*

[2]*Departamento de Física, Centro Federal de Educação Tecnológica Celso Suckow da Fonseca, Rio de Janeiro, Rio de Janeiro 20271-110, Brazil*

[3]*Aix Marseille Univ, CNRS, Institut Origines, PIIM, Marseille, France*

sreeja.raghunandanan@ganil.fr

Organic molecules observed in space raise fundamental questions about their origin and potential role in the emergence of life on Earth. In cold planetary and astrophysical environments, icy layers are continuously exposed to radiation including UV and X-ray photons, electrons, and keV to GeV ions from solar winds, planetary magnetospheres, and cosmic rays, see Rothard *et al.* 2017, leading to the formation of complex organic compounds such as polycyclic aromatic hydrocarbons (PAHs). Among these, ion irradiation is particularly significant as energetic ions penetrate deeply into icy mantles, driving a radiation-induced chemistry through nuclear and electronic energy deposition, see Boduch *et al.* 2015.

Titan, the largest moon of Saturn, has a dense carbon and nitrogen rich atmosphere often regarded as a natural prebiotic chemistry laboratory. In the stratosphere, benzene (C_6H_6) and propionitrile (C_2H_5CN) condense onto aerosol particles forming icy mantles, see Anderson *et al.* 2018, where cosmic ray processing is thought to drive complex chemistry contributing to the molecular complexity of Titan's organic haze. Crystalline benzene and propionitrile ices were irradiated with heavy ion beams (from keV to MeV energies) as space radiation analogues at the ARIBE and IRRSUD beamlines at CIMAP-GANIL. The IGLIAS setup which combines in-situ infrared spectroscopy and quadrupole mass spectrometry, see Augé *et al.* 2018, allowed to study ice-phase chemical pathways in Titan's stratosphere.

The results presented here also serve as a benchmark reference for the new unique MIRRPLA (Multiple IRRadiation PLAtform) experimental set-up, currently under development at CIMAP-GANIL, which will integrate UV photons, keV electrons, and keV to GeV ions for simultaneous and sequential ice irradiation, see Domaracka *et al.* 2024. This capability will enable direct investigation of synergistic effects between different radiation types, a critical step towards realistic astrophysical simulations. MIRRPLA also incorporates a gas chromatograph coupled to a high-resolution Orbitrap mass spectrometer, enabling unprecedented molecular-level identification of irradiation products.

References

Anderson, C. M., Samuelson, R. E., & Nna-Mvondo, D. (2018). Organic ices in Titan's stratosphere. *Space Science Reviews*, ***214*****(8)**, 125.

Augé, B., Been, T., Boduch, P., Chabot, M., Dartois, E., Madi, T., ... & Voivenel, P. (2018). IGLIAS: A new experimental set-up for low temperature irradiation studies at large irradiation facilities. *Review of Scientific Instruments*, **89(7)**.

Boduch, P., Dartois, E., de Barros, A. L., da Silveira, E. F., Domaracka, A., Lv, X. Y., ... & Strazzulla, G. (2015, June). Radiation effects in astrophysical ices. In *Journal of Physics: Conference Series* (Vol. **629**, No. 1, p. 012008). IOP Publishing.

Domaracka, A., & Danger, G. (2023). Multiple Beam Irradiation Platform MIRRPLA: Origin and Evolution of Organic Matter in the Solar System. *Nuclear Physics News*, **33(4)**, 36–37. https://doi.org/10.1080/10619127.2023.2265772.

Rothard, H., Domaracka, A., Boduch, P., Palumbo, M. E., Strazzulla, G., Da Silveira, E. F., & Dartois, E. (2017). Modification of ices by cosmic rays and solar wind. *Journal of Physics B: Atomic, Molecular and Optical Physics*, **50(6),** 062001.

ION-INDUCED INTRACLUSTER REACTIVITY IN GAS PHASE CARBONACEOUS MOLECULES CLUSTERS

S Srivastav[1], P Eng-Jonhsson[2], R Feifel[3], A Domaracka[1], P Rousseau[1], S Díaz-Tendero[4], D G. Piekarski[5] and S Maclot[1]

[1]*Université Caen Normandie, ENSICAEN, CNRS, CEA, Normandie Univ, CIMAP UMR6252, F-14000 Caen, France*

[2]*Department of Physics, Lund University, P.O. Box 118, 22100, Lund, Sweden*

[3]*Department of Physics, University of Gothenburg, Origovägen 6 B, 41296 Gothenburg, Sweden*

[4]*Departamento de Química, Módulo 13, Universidad Autónoma de Madrid, 28049 Madrid, Spain*

[5] *Institute of Physical Chemistry, Polish Academy of Sciences, Kasprzaka 44/52, 01-224, Warsaw, Poland*

sumitsrivastav2708@gmail.com

Recent investigations have revealed the importance of various carbonaceous molecules, such as polycyclic aromatic hydrocarbon (PAH), fullerenes (C_{60}) and diamondoids in fields of environmental science and astrochemistry. It is now established that nanodiamonds are the most abundant component of presolar grains, and nanodiamonds (size of 2-3 nm) have been extracted from primitive meteorites (Jones *et al.* 2004). Diamondoids are yet to be conclusively identified in the interstellar medium (ISM). However, two broad emission bands at 3.43 and 3.53 μm, observed in the spectra of circumstellar disks around the stars HD 97048 and Elias 1, have been attributed to large (about 50 nm) nanodiamond particles (Habart *et al.* 2004). On the other hand, PAHs and their derivatives are well known for their presence in ISM and planetary atmosphere (Nixon 2024). It has been a key question whether these hydrocarbon molecules are formed through bottom-up chemical pathways, or whether they originate from the fragmentation of larger species in astrophysical environments. Recently, we reported the dissociation channels of simplest PAH, naphthalene, and its simplest nitrogenated derivatives, quinoline and isoquinoline, and observed that their cations emit various hydrocarbon and hydrocarbon-nitriles fragments that are also present in Titan's atmosphere (Srivastav *et al.* 2025).

In the conference, I will present our recent experimental results, performed at CIMAP-GANIL Caen, based on keV energy ions interacting with clusters of two type of molecules, simplest diamondoid, adamantane (see Fig (a)), and a PAH molecule, anthracene (see Fig (b)). Employing a coincidence mass spectrometry, we observed that keV ions can induce intracluster reactivity leading to the formation of new covalently bound species with masses larger than that of the parent molecule. Moreover, we also investigated how the hydrated and ammoniated environments affect the growth processes in the clusters of aforementioned molecules under ionizing radiation. These results are relevant not only to astrochemistry but also highlight how ion-induced molecular growth in a diamond-like saturated hydrocarbon framework can differ from that in planar PAH systems.

(a) (b)

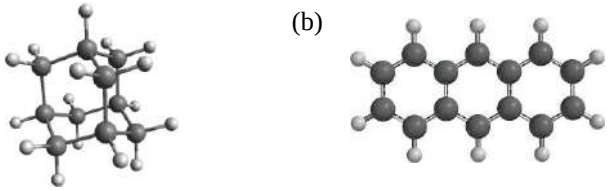

Figure: Structures of (a) adamantane ($C_{10}H_{16}$) and (b) anthracene ($C_{14}H_{10}$).

References

Habart et al., (2004) *The Astrophysical Journal* **614**, L129.

Jones et al., (2004) *A&A* **416**, 235.

Nixon C A, (2024) *ACS Earth Space Chem.* **8**, 406.

Srivastav et al., (2025) *J. Chem. Phys.* **163**, 224305.

INVERSE PROBLEMS IN ELECTRON SCATTERING: LIQUID MICROJET AND e-H_2

Dale L. Muccignat[1], Gregory J. Boyle[1], Nathan A. Garland[1], Ronald D. White[1],

[1]*College of Science and Engineering, James Cook University, Townsville, Queensland, Australia*

dale.muccignat@my.jcu.edu.au

Electron-scattering cross sections enable predictive modelling in critical applications such as plasma medicine, environmental remediation and advanced manufacturing. They describe how electrons exchange energy and momentum with matter and form the fundamental inputs to kinetic models. Experimental techniques, such as the crossed-beam and swarm experiments, have been extensively used to determine cross-section data for many target species in the gas phase. In this work, we present progress on two simulation-driven approaches to resolving outstanding problems in electron-scattering cross-section determination: the long-standing e-H_2 vibrational cross-section discrepancy, and the interpretation of direct electron-liquid scattering measurements under vacuum conditions.

For over 50 years, a disagreement of as much as 50% has existed between crossed-beam and swarm-derived values of the e-H_2 $v = 0 \rightarrow 1$ vibrational excitation cross section. This problem has recently been revisited using improved ab initio calculations, which are in good agreement with the swarm measurements (Scarlett *et al.* 2026). Here we present progress on a machine-learning approach to quantify the uncertainty in the $v = 0 \rightarrow 1$ cross section retrieved via inversion of experimental swarm transport data.

Electron-liquid scattering from a liquid microjet presents additional challenges relative to the dilute gas phase, including the liquid-vacuum interface, multiple scattering within the liquid, and an evaporative vapour layer surrounding the target, all of which complicate the extraction of cross-section data from measured spectra. Recent work investigated the feasibility of determining cross-section data from electron energy-loss spectra measured using a new liquid microjet experiment at Flinders University (Muccignat *et al.* 2022), followed by

preliminary measurements (Muccignat *et al.* 2024). In this work, we use Monte Carlo simulations of electron transport through the microjet to conduct a sensitivity analysis with respect to the underlying cross sections, jet geometry, and surface/vapour effects, in order to aid in the interpretation and validation of the measured spectra.

References

Boyle G. J. *et al.* (2025) Review of the experimental and theoretical landscape of electron transport in noble liquids. *Front. Detect. Sci. Technol.* **3**, 1616204.

Muccignat, D. L. *et al.* (2022) Simulating the Feasibility of Using Liquid Micro-Jets for Determining Electron–Liquid Scattering Cross-Sections, *International Journal of Molecular Sciences* **23**, 3354.

Muccignat, D. L. *et al.* Direct electron-liquid energy loss spectra measurements using a liquid micro-jet. in *Contributed papers & abstracts of invited lectures, topical invited lectures and progress reports: 32nd Summer School and International Symposium on the Physics of Ionized Gases* 53–56 (Astronomical Observatory Belgrade, Volgina 7, 11060 Belgrade 38, Serbia, 2024).

Scarlett, L. H. *et al.* (2026) Unified treatment of direct and resonant scattering in low-energy electron - H 2 vibrational excitation: boomerang oscillations and the $\upsilon = 0 \rightarrow 1$ excitation. *Phys. Rev.* A **113**, 62803.

ANALYTICAL CROSS SECTION SETS FOR COLLISIONS OF SUPRA-THERMAL ELECTRONS WITH MOLECULES

Anthony Jeseněk[1] and Sébastien Célestin[1] and Alejandro Luque[2]

[1]*Laboratoire de Physique et de Chimie de l'Environnement et de l'Espace (LPC2E), OSUC, Université d'Orléans, CNRS*

[2]*Instituto de Astrofísica de Andalucía (IAA), CSIC*

anthony.schmalzried@cnrs-orleans.fr

The endeavour of producing complete sets of cross sections describing the interaction of electrons in gaseous media has been at the core interest of the plasma community concerned with modelling electron swarms. Historically, there have long been two major sources of cross sections each serving the purposes of two distinct communities:

1) Low-energy electrons $\lesssim$10 eV, colliding in low-temperature plasmas mainly characterised from swarm and scattering **experiments**

2) (Near-)relativistic electrons $\gtrsim$100 keV in particle/nuclear/high-energy physics obtained from the Born-Bethe **theory**.

Later on, the contact between these two opposite regimes would be outlined by:

3) Supra-thermal electrons [100 eV to 10 keV] in transient events of fast electrons energy degradation, or conversely: electron thermal runaway.

Although numerical values of cross sections can be calculated with quantum models, calculations are complicated and modelling required advanced knowledge. However, a simple analytical semi-empirical method, generically known as scaled plane-wave Born-Bethe approximations (Kim et al. 2000, 2007), showed remarkable flexibility in accurately representing cross sections for impact electronic excitation and ionisation of molecules by electrons.

It is in this context that the IAA database on LXCat sought to generate reliable, yet simple and traceable cross sections, covering the full range of electron energies, based on scaled plane-wave Born-Bethe approximations and Kawaguchi et al. 2021's in-depth testing of the validity of cross sections. An example is shown in the figure below for electronic impact excitation of N_2 with a set of fully analytical cross sections, which is asymptotically complete in the

sense of the Bethe sum rule of dipole oscillator strengths characterising the amplitude of optically allowed excitations.

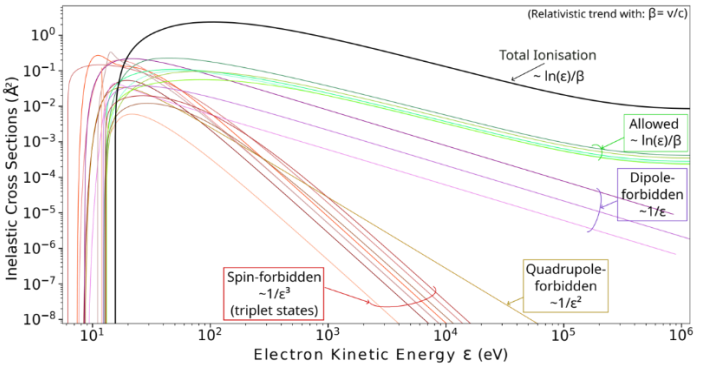

Figure: Analytical cross section set of impact ionisation and electronic excitations for N_2

From the asymptotic behaviour of the curves with respect to the electron kinetic energy ε (relativistic velocity β), impact excitations can be easily identified as:

0 - optically allowed ~ ln(ε)/β, 2 - quadrupole forbidden ~ 1/ε²,
1 - dipole forbidden ~ 1/ε, 3 - spin-forbidden ~ 1/ε³.

Optically allowed excitations (and ionisation) are further constrained by the values of the corresponding dipole oscillator strengths (f_i) obtained from photoelectron spectroscopy. Their generalised sum amounts to the total number of electrons (Inokuti 1971) : $\sum f_i = Z$. The total ionisation cross section is determined by an adaptation of the RBEQ model (Kim at al. 2000), where the contribution to the (generalised) dipole oscillator strength is encapsulated in the parameter Q. Finally, the asymptotic trend of the elastic momentum-transfer cross section can be similarly determined from a plane-wave Born scaling method.

Details of the construction are expounded in chapters 11.4 and 11.5 of A. Jeseněk's doctoral thesis: "Electron Thermal Runaway in Atmospheric Electrified Gases: a microscopic approach", https://digital.csic.es/handle/10261/338079

References

Inokuti M. (1971) *Rev. Mod. Phys*., **43**, 314 eq. (3.19).

Kim Y.-K. *et al*. (2000) *Phys. Rev. A*, **62**, 52710.

Kim Y.-K. (2007) *J. Chem. Phys.*, **126**, 064305.

Kawaguchi K. *et al*. (2021) *Plasma Sources Sci. Technol.*, **30**, 035006.

STUDIES OF AUTOIONIZING STATES IN MOLECULAR NITROGEN AT 302.25 eV OF ELECTRON INCIDENT ENERGY

Bratislav P. Marinković, Jelena B. Maljković and Jozo J. Jureta

Institute of Physics Belgrade, Pregrevica 118, 110080 Belgrade, Serbia

bratislav.marinkovic@ipb.ac.rs

We study autoionizing states in N_2 by using a high-resolution hemispherical analyzer equipped with 7 channeltrons and non-monochromatic electron beam with high electron current. The apparatus has been used in the past in studies of autoionizing states in He, Ne, Ar, Kr and Xe (Jureta *et al*. 2016; Marinković et al. 2026) at low and high incident electron energies. We noticed very low signal to background ratio in N_2 in comparison with measurements in atoms.

The molecular nitrogen (N_2) has been a subject of investigation since the inception of atomic and molecular physics. Given its biological significance and its prominence as a major constituent of the Earth's atmosphere, it has been studied extensively through both experimental and theoretical approaches. All research until 1977 has been summarized in review by Lofthus and Krupenie. In new generation of synchrotron experiments, Yencha *et al*. (2014) studied N_2 in the photon energy region 15.0 – 52.7 eV. They applied threshold photoelectron and photoion spectroscopy technique with high resolution.

The analyzer operates at pass energy mode of 1 eV with defined retarding ratio and defined magnification determined by the two stage 11 elements lens system. The background pressure in the vacuum chamber was $5x10^{-8}$ mbar, while the working pressure with nitrogen was $2.2x10^{-6}$ mbar. The accumulation time was 2 x 15 min for the spectrum in Fig. 1. The kinetic energy scale has been calibrated via the energy $3s3p^6 3d(^1D)$ state at 11.72 eV. Calibration of the incident electron energy scale was performed using the elastic scattering channel, with an energy resolution characterized by a FWHM of approximately 0.80 eV.

Features in the 1.6–6.1 eV energy range were assigned by comparing their energy separations with the vibrational spacings of the ionic states to which they decay. The binding energy (BE) of each state was calculated as the sum of the measured kinetic energy (KE) and the ionization potential of the corresponding ionic state.

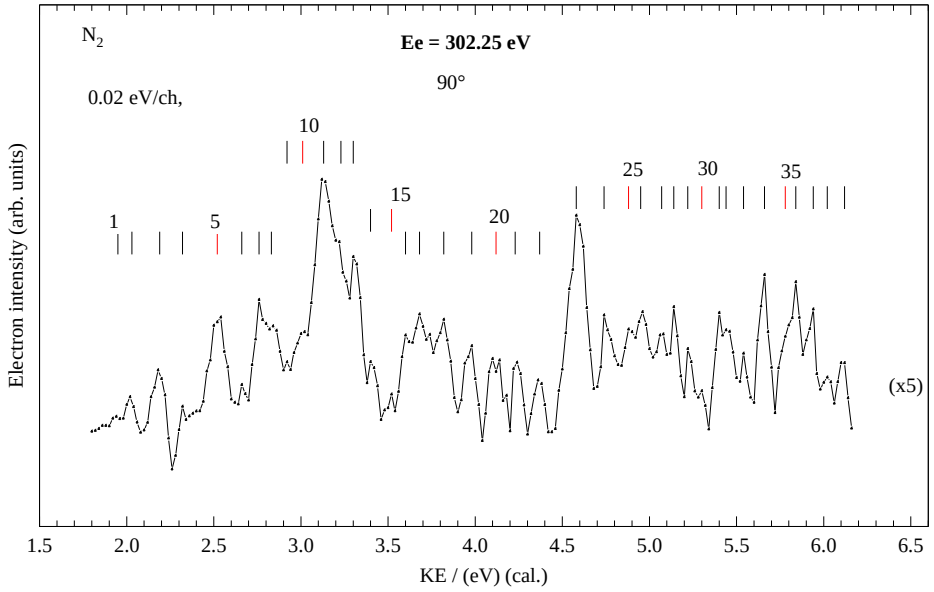

Figure 1: Autoionizing spectrum of N_2 taken at electron incident energy of 302.25 eV, kinetic energy region 1.6 to 6.1 eV and ejection angle of 90°. The spectrum is presented in linear subtraction mode with energy step of 0.020 eV/ch and a smooth mode of 3 points due to large number of closely spaced features.

We identified pairs of features that result from the decay from the ground $X\ ^2\sum_g^+$ sate of $N_2^{+\cdot}$ as well as Rydberg state (v'=n, v'' = 0) of the $B\ ^2\sum_u^+$ ion state.

Acknowledgement: This research was supported by the Science Fund of the Republic Serbia, Grant No. 6821, ATMOLCOL.

References

Jureta J J; Marinković B P and Avaldi L (2016) *Eur. Phys. J. D,* **70**, 199.

Lofthus H and Krupenie H (1977) *J. Phys. Chem. Ref. Data,* **6**, 113.

Marinković B P; Avaldi L and Jureta J J (2026) *Atoms,* **14**, 9.

Yencha A J; Ellis K and King G C (2014) *J. El. Spec. Rel. Phenom*., **195**, 160-173.

ION GENERATION IN ELECTRON CYCLOTRON RESONANCE ION SOURCES (ECRIS)

Bogdan Popović[1], Tiberiu Minea[1], Thomas Thuillier[2], and Adrien Revel[1]

[1]*Université Paris-Saclay, CNRS, Laboratoire de Physique des Gaz et des Plasmas (LPGP), 91405, Orsay, France*

[2]*Lawrence Berkeley National Laboratory (LBNL), Berkeley, CA 94720, USA*

bogdan.popovic@universite-paris-saclay.fr

Electron cyclotron resonance ion sources (ECRIS) are typically used to produce multiply charged ions for high-energy accelerators among other applications. These sources need to operate at very low pressures to avoid neutral pollution, while also ensuring the plasma density remains high enough to generate multiple ionized species. Such conditions are achieved through electron cyclotron resonance (ECR) heating, which can sustain plasmas at significantly reduced gas pressure. Therefore, energetic electrons can efficiently ionize the background gas, whereas the low collision frequency reduces the probability of recombination.

PHOENIX V2 is an ECRIS source designed to produce high-intensity beams of multiply charged ions and has demonstrated stable extraction of O^{6+} ion beams with currents up to 1.3 mA of ions (Thuillier et al., 2012). To better understand the effect of the operation parameters on the beam formation, we are developing a Monte Carlo simulation of the ion source. Helium was selected as the working gas due to its simple atomic structure and an abundance of cross-section measurements in the literature.

The simulation tracks both electrons and ions. Particle movement is calculated using the relativistic implementation of the Boris pusher (Birdsall and Langdon 1991), while the collision processes are modeled with the null-collision Monte Carlo method (Vahedi and Surendra 1995). Another important aspect of the simulation is the ECR heating effect. To quantify it, we analyze electron and ion energy distributions, ionization location, charge-density maps, and particle confinement times.

ECR description is quite challenging. Working with a realistic ECRIS geometry prevents us from assuming a constant angle and phase between the electric and magnetic field vectors. The electromagnetic field experienced by a particle varies massively along its trajectory due to strong magnetic field gradients, up to 50 T/m in PHOENIX V2. Therefore, resolving the full-time-dependent electromagnetic interaction for every particle becomes unfeasible. A common solution is to implement an ECR zone. In this model, only electrons crossing the resonance region interact with the microwave field. The ECR zone is defined by the resonance condition where the local electron cyclotron frequency matches the applied microwave frequency. In this case, electrons can efficiently absorb energy from the electromagnetic field and therefore perform ionizations.

The described Monte Carlo model can be used to study ion production in the PHOENIX V2 ion source. With particle tracking, collisions, and ECR heating, the model enables us to study the effect of the microwave field on the plasma properties. By implementing the ECR zone, we can work with arbitrary magnetic field configurations, not limited to the one in the PHOENIX V2 setup. Additionally, generating charge-density maps will help us better understand the resulting ion-beam parameters.

References

Thuillier T, Angot J and Lamy T (2012) *20th International Workshop on Electron Cyclotron Resonance Ion Sources* (*ECRIS)*, Sydney, p. 59.

Birdsall C K and Langdon A B (1991) *Plasma Physics via Computer Simulation*. Adam Hilger, Bristol.

Vahedi V and Surendra M (1995) *Comput. Phys. Commun.*, **87**, 179–198.

RELATIVE PARTIAL CROSS-SECTIONS FOR ELECTRON IMPACT IONIZATION OF CO_2

Nikoleta Vojinović and Goran B. Poparić

University of Belgrade, Faculty of Physics, Studentski trg 12, P.O. Box 44, 11000 Belgrade, Serbia

goran.poparic@ff.bg.ac.rs

The relative cross-sections for partial ionization of CO_2 molecules by electron impact were measured for incident electron energies in a range from the threshold up to 200 eV. Measurements were performed using a linear electron-molecule collision spectrometer. This hybrid spectrometer consists of a trochoidal electron monochromator and a time-of-flight mass spectrometer arranged in a linear configuration along an external magnetic field, which enables total ion collection. The details of the spectrometer design, its measurement operation and preliminary test measurements for nitrogen molecule are given in ref. Vojnović *et al.* 2026.

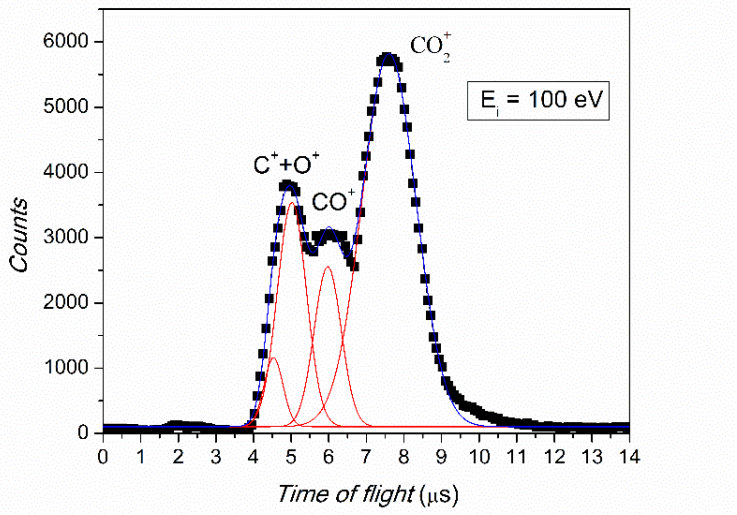

Figure 1: Time-of-flight spectra of CO_2 positive ions and positive ion fragments arisen after electron-molecule collisions at an incident electron energy of 100 eV. Red lines represent Gaussian fits.

Measurement of the time-of-flight spectrum, for ions arisen during electron-molecule collisions, extracted and accelerated (by applying a short voltage pulse of 100 V) from the interaction region to the detector, is presented in Figure 1. As can be seen from the spectrum, three peaks can be identified. The first peak belongs to C^+ and O^+ ions which reach the detector first due to their low masses, after about 5 microseconds. The second peak belongs to CO^+ ions, whose arrival times are about 6 microseconds. The CO_2^+ ions, having the largest mass, arrive last, after about 7-8 microseconds. This time of flight spectrum enables the determination of relative partial cross-sections for ionization and dissociative ionization of CO_2, by deconvoluting their peaks and integrating the areas under these deconvoluted peaks. The preliminary results for relative partial cross-sections show significant agreement with results obtained earlier in the measurements by King and Price (2008).

Acknowledgments: This work was supported in part by the Ministry of Science, Technological Development and Innovation of the Republic of Serbia under contract Nos. 451-03-34/2026-03/200162.

References

Vojnović M M, Ristić M M, Stanković Mališ V V, Belić D S and Poparić G B (2026) *Rev. Sci. Instrum.* **97**, 000000. doi: 10.1063/5.0325169

King S J and Price S D (2008) *International Journal of Mass Spectrometry*, **272,** 154. doi:10.1016/j.ijms.2008.02.008

A SET OF CROSS SECTIONS, FOR H_3O^+ IONS IN H_2O

Zoran Lj. Petrović[1,2], Vladimir Stojanović†[3], Ilija Stefanović[4], Ivan Petraš[4], Jasmina Jovanović[5], Dragana Marić[3]

[1]*Serbian Academy of Sciences and Arts, Kneza Mihaila 35, 11001 Belgrade, Serbia*

[2]*School of Engineering, Ulster University, Jordanstown, County Antrim BT37 0QB, UK*

[3]*Institute of Physics, University of Belgrade, Pregrevica 118, 11080 Belgrade, Serbia*

[4]*Institute of Technical Sci., Serbian Academy of Sciences and Arts, 11000 Belgrade, Serbia*

[5]*Faculty of Mechanical Engineering, University of Belgrade, 11000 Belgrade, Serbia*

zoran@ipb.ac.rs

A cross-section set for H_3O^+ ions in H_2O has been derived based on the compiled mobility data and on a model for inelastic processes. We have tried to work in the low-pressure limit where one may expect the simplest spectrum of ions. Transport and rate coefficients in a DC electric field at gas temperature of T = 300 K and low pressures were calculated as a function of the reduced electric fields E/N (where E - electric field, N - gas number density) using a well-tested and verified Monte Carlo simulation code.

In our previous paper on this topic (Stojanović *et al.* 2016) we have presented a first iteration towards developing cross sections for H_3O^+ ions in H_2O. This paper has a new iteration with a more extensive set of experimental data (Lange 1981, Ryzko 1965, Gazda 1986). The fit of the mobilities at low and moderately high E/N is shown in Figure 1. The cross sections were established by considering induced polarizability at low energies (Lange 1981) and inelastic processes based on the Denpoh and Nanbu theory (1998). The data are for the low-pressure limit or for a small addition of water vapour to the buffer gas. At higher water vapour pressures, one would have to include some representation of the kinetics of formation, breakdown and transport of ions with water clusters (Gazda 1986). Data for ion transport and modelling of low temperature plasmas (Petrović *et al.* 2007) are lacking, so, having in mind a broad range of applications of the plasmas with water vapour in the mixture, the effort in this direction is well justified.

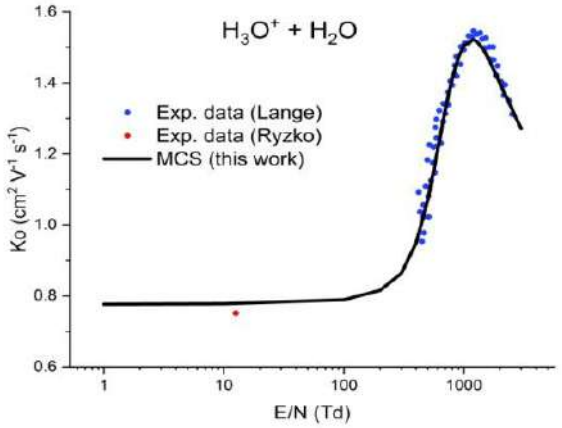

Figure 1. Mobilities of H_3O^+ ions in H_2O, predictions based on our cross-section set, are provided by the solid line.

ZLjP and IP acknowledge project SANU F155 for partial support. IS and JJ acknowledge financial support from the Ministry of Science, Technological Development and Innovations RS, contracts No. 451-03-33/2026-03/200175 and contract No. 451-03-34/2026-03/200105, respectively.

References

Denpoh K and Nanbu K (1998) *J. Vac. Sci. Technol.* A **16** 1201.

Gazda E (1986) *J. Phys.* B*: At. Mol. Phys.* **19** 2973.

Lange F D (1981) *Int. J. Mass. Spectrosc. Ion Phys.* **37** 341.

Petrović Z Lj, Raspopović Z, Stojanović V D, Jovanović J V, Malović G, Makabe T and de Urquijo J (2007) *Appl. Surf. Sci.* **253** 6619.

Ryzko H (1965) *Proc. Phys. Soc.* **85** 1283

Stojanović V, Jovanović J, Marić D, and Petrović Z Lj (2016) *Proceedings of the 28th Summer School and International Symposium on the Physics of Ionized Gases* (SPIG 2016). University of Belgrade Faculty of Physics, pp. 128-131.

ELECTRON DIFFRACTION FROM THE METHANE MOLECULE

Jelena Vukalović[1,2], Jelena Maljković[2], Nenad Simonović[1,2], Shruti Sarswat[3], Jobin Jose[3], and Himadri S. Chakraborty[4]

[1]*Faculty of Science, University of Banja Luka, Mladena Stojanovića 2, 78000 Banja Luka, Republic of Srpska, Bosnia and Herzegovina*

[2]*Institute of Physics Belgrade, Pregrevica 118, 11080 Belgrade, Serbia*

[3]*Department of Physics, Indian Institute of Technology Patna, Bihar 801103, India*

[4]*School of Natural Sciences, D.L. Hubbard Center for Innovation, Northwest Missouri State University, Maryville, Missouri 64468, USA*

jelena.vukovic@pmf.unibl.org

Differential cross section (DSC) for elastic scattering of electrons on atomic and molecular targets in many cases shows a diffraction pattern superimposed on the steady decay background. While this background is always present, even for structureless targets, the diffraction pattern is a fingerprint of the target's structure. The DSC is usually given as a function of the incident electron energy E and the scattering angle θ, but for studying diffraction phenomena it is convenient to represent it as a function of E and the magnitude of the transferred electron momentum

$$q = |\mathbf{k} - \mathbf{k}'| = 2k \sin \theta/2, \quad (1)$$

where $\mathbf{k}$ and $\mathbf{k}'$ are momenta of the incident and scattered electrons, respectively, and $k = |\mathbf{k}| = |\mathbf{k}'| = (2m_e E)^{1/2}$. By removing the decay background from the overall DSC at a fixed value of E, a pure diffraction signal as a function of the q variable at this energy is obtained. Its Fourier transform reveals structural information about the target particle, which is more complete if more values of E are considered. This analysis was first applied to electron diffraction on the fullerene molecule (Aiswarya *et al.* 2024) and recently on atomic targets (Aiswarya *et al.* 2026).

Here we study diffraction patterns in the DSC for elastic scattering of electrons from the methane molecule (CH_4). This molecule has a symmetric structure with the H atoms located at the tetrahedron vertices and the C atom in its center. Here,

the CH (bond) and HH separations are $d_{\mathrm{CH}} = 2.1$ au and $d_{\mathrm{HH}} = 3.4$ au. We used experimental data for DSC in the incident electron energy range from 50 to 300 eV and for scattering angles from 0° to 180° determined by Vukalović *et al.* 2021. Figure 1 shows: (a) the q-dependence of DSC at energy $E = 100$ eV (full line), the fitted decay background (dotted line) and the diffraction signal obtained as their difference (dashed line); (b) the power spectrum of the diffraction signal. It can be seen that the position of the main peak in the spectrum for this energy matches well with the HH separation. It was found, however, that using higher incident electron energies ($E > 200$ eV) this analysis reveals more details about the molecular structure.

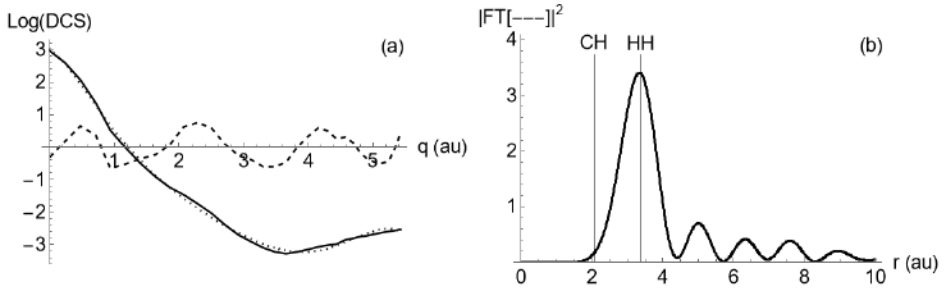

Figure 1: (a) The q-dependence of DSC at the incident electron energy $E = 100$ eV (full line), the fitted decay background (dotted line) and the diffraction signal obtained as their difference (magnified 5 times, dashed line). (b) The power spectrum of the diffraction signal and the CH and HH separations in the CH_4 molecule.

The research is supported by: Science Fund of the Republic of Serbia, grant No. 6821 ATMOLCOL; CRG/2022/000191, India; US National Science Foundation Nos. PHY-2110318 and PHY-2512850.

References

Aiswarya R, Jose J, Simonović N, Marinković BP, and Chakraborty HS (2026) *Phys. Rev. A*, **113**, L010801.

Aiswarya R, Shaik R, Jose J, Varma HR, and Chakraborty HS (2024) *Phys. Rev. Lett.*, **133**, 033002.

Vukalović J, Maljković JB, Tökési K, Predojević B, Marinković BP (2021) *Int. J. Mol. Sci.*, **22**, 647.

HYDROGEN MIGRATION AND METASTABLE DYNAMICS IN ELECTRONICALLY EXCITED METHANIMINE

Sanja Tošić[1], Vladimir A. Srećković[1] and Veljko Vujčić[2]

[1]*Institute of Physics Belgrade, University of Belgrade, Pregrevica 118, Belgrade, Serbia*

[2]*Astronomical Observatory, Volgina 7, 1100 Belgrade, Serbia*

seka@ipb.ac.rs

Hydrogen migration represents an important intramolecular rearrangement process that can strongly influence fragmentation dynamics in electronically excited molecules. In the present work, we investigate the relationship between hydrogen migration, metastable behavior, and fragmentation dynamics in electronically excited methanimine (CH_2NH), an astrochemically relevant molecule that has been investigated in recent studies of molecular excitation and destruction processes (Bouallagui *et al*. 2023), using classical reactive molecular-dynamics simulations.

Large ensembles of statistically independent trajectories were propagated on a reactive model potential-energy surface for internal excitation energies between 3 and 9 eV. For each energy, up to 200 trajectories were generated, allowing statistical characterization of migration processes, dissociation pathways, and fragmentation time scales.

Hydrogen migration remains prevalent throughout the investigated energy range, occurring in approximately 96% of trajectories at 3 eV and 62% at 9 eV. Repeated hydrogen transfer between carbon and nitrogen centers constitutes the most common rearrangement pattern, particularly at lower excitation energies where extensive intramolecular energy redistribution occurs consistent with the important role of hydrogen-transfer dynamics in molecular rearrangement processes (Garrett *et al*. 1986).

Figure 1 compares mean dissociation times for trajectories with and without hydrogen migration. Trajectories involving hydrogen migration exhibit substantially longer dissociation times over the entire investigated energy range, indicating a strong connection between intramolecular rearrangement and metastable molecular evolution.

Delayed fragmentation is closely associated with hydrogen migration. Nearly all delayed dissociation events (97–100%) involve hydrogen migration, whereas trajectories without migration dissociate substantially faster. Migration-assisted trajectories exhibit mean dissociation times between approximately 350 and 590 fs, compared with only 100–175 fs for trajectories without migration. These results suggest that transient hydrogen rearrangements contribute to the formation of long-lived metastable states prior to dissociation. Similar long-lived dynamical behavior has been associated with metastable regions of phase space in previous studies of molecular reaction dynamics (Krajňák and Waalkens 2018).

The present results identify hydrogen migration as a key dynamical mechanism governing metastable behavior in electronically excited CH_2NH. The results highlight the close connection between hydrogen migration, energy redistribution, and fragmentation dynamics in electronically excited CH_2NH.

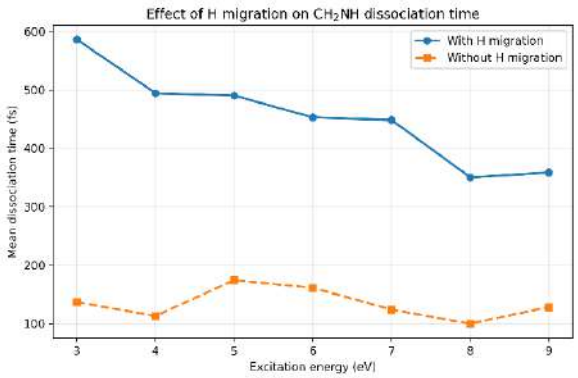

Figure 1: Effect of hydrogen migration on CH_2NH dissociation times.

Acknowledgments: This research was supported by the Science Fund of the Republic Serbia, Grant No. 6821, ATMOLCOL.

References

Bouallagui A. et al. (2023) *Astrophys J*., **956**, 22.
Garrett B. et al. (1986) *J. Am. Chem. Soc*., **108**, 3515.
Krajňák V. and Waalkens H. (2018) *J. Math. Chem*., **56**, 2341.

ENERGY-DEPENDENT REARRANGEMENT PATHWAYS IN EXCITED CH_2NH

Sanja Tošić[1], Vladimir A. Srećković[1] and Veljko Vujčić[2]

[1]*Institute of Physics Belgrade, University of Belgrade, Pregrevica 118, Belgrade, Serbia*

[2]*Astronomical Observatory, Volgina 7, 1100 Belgrade, Serbia*

seka@ipb.ac.rs

Hydrogen transfer is one of the most common intramolecular rearrangement mechanisms in electronically excited molecules and can strongly influence subsequent fragmentation dynamics. In small astrochemically relevant systems, such processes provide efficient pathways for energy redistribution and may compete with direct bond cleavage channels (Garrett *et al*. 1986). However, the influence of excitation energy on the complexity of hydrogen-transfer pathways remains insufficiently characterized.

In the present work, hydrogen-transfer dynamics in electronically excited methanimine (CH_2NH) were investigated using classical reactive molecular-dynamics simulations. Methanimine is a nitrogen-bearing organic molecule detected in a variety of astrophysical environments and considered a potential precursor of more complex prebiotic species (Bouallagui *et al*. 2023). Large ensembles of statistically independent trajectories were propagated on a reactive model potential-energy surface for excitation energies between 3 and 9 eV, with 200 trajectories generated for each energy.

The simulations reveal a pronounced evolution of rearrangement dynamics across the investigated energy range. At low excitation energies, the dynamics are dominated by repeated hydrogen-transfer cycles. The most common sequence is C→N, C→N, N→C, accounting for approximately 69% of trajectories at 3 eV. As the excitation energy increases, the contribution of this multi-step rearrangement pathway decreases systematically, indicating a reduced role of extensive intramolecular reorganization.

To characterize the complexity of hydrogen-transfer dynamics, trajectories were classified according to the total number of migration events occurring during the simulation. Figure 1 shows the fractions of trajectories exhibiting zero, one, two,

or three hydrogen-transfer events as functions of excitation energy. Near the fragmentation threshold, trajectories with three migration events strongly dominate the dynamics. With increasing excitation energy, the fraction of such trajectories decreases, while trajectories involving fewer or no migration events become progressively more important.

The decrease in migration multiplicity with increasing excitation energy indicates a gradual transition from extensive hydrogen-transfer dynamics toward more direct fragmentation pathways. Similar transitions between complex rearrangement dynamics and more direct reaction mechanisms have been reported in previous studies of molecular reaction dynamics (Zhou and Schlegel 2009). At lower energies, multiple migration events facilitate energy redistribution prior to dissociation, while at higher energies fragmentation becomes increasingly direct.

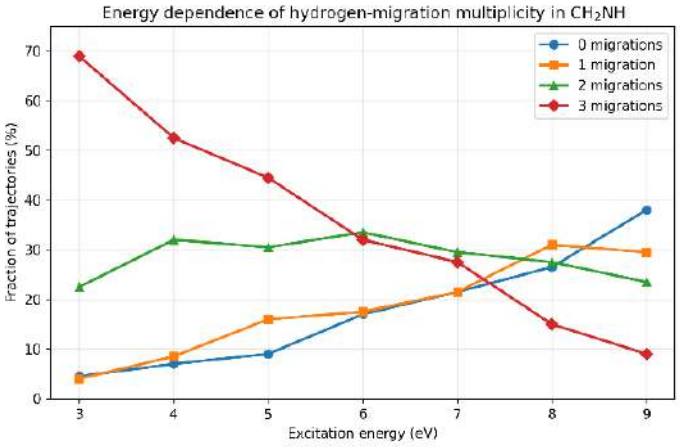

Figure 1: Energy-dependent distribution of hydrogen-transfer events in excited CH_2NH.

Acknowledgments: This research was supported by the Science Fund of the Republic Serbia, Grant No. 6821, ATMOLCOL.

References

Bouallagui A. *et al*. (2023) *Astrophys J*., **956**, 22.
Garrett B. *et al*. (1986) *J. Am. Chem. Soc*., **108**, 3515.
Zhou J and Schlegel H B (2009) *J. Phys. Chem. A*, **113**, 9958.

FUNDAMENTAL COLLISION PROCESSES IN ATOMIC AND MOLECULAR SYSTEMS: INTEGRATING EXPERIMENT, THEORY, AND NUMERICAL MODELLING WITHIN THE ATMOLCOL PROJECT

Jelena B. Maljković[1], Jelena Vukalović[1,2], Bratislav P. Marinković[1], Vladimir Srećković[1], Hristina Delibašić-Marković[3], Sanja Tošić[1] and Violeta Petrović[3]

[1]*Institute of Physics Belgrade, University of Belgrade, 11080 Belgrade, Pregrevica 118, Serbia*

[2]*Faculty of Science, University of Banja Luka, Mladena Stojanovića 2, 78000 Banja Luka, Republic of Srpska, Bosnia and Herzegovina*

[2]*University of Kragujevac, Faculty of Science, Radoja Domanovića 12, 34000 Kragujevac, Serbia*

jelenam@ipb.ac.rs

Understanding the interactions of electrons, photons, and ions with atoms and molecules is essential for describing processes relevant to plasma physics, astrophysics, atmospheric chemistry, radiation physics, and biophysics. The ATMOLCOL project brings together complementary experimental, theoretical, and computational approaches to investigate collision-driven phenomena occurring on ultrashort time scales and to provide reliable cross-section data for a wide range of atomic and molecular targets.

The project addresses fundamental processes including elastic electron scattering (Vukalović *et al.* 2026), ionization (Srećković *et al.* 2025), photoionization (Delibašić *et al.* 2024) autoionization (Jureta *et al.* 2024), electron autodetachment, and dissociative electron attachment (Kopyra *et al.* 2025). Experimental investigations are primarily based on crossed-beam techniques, enabling well-defined binary collision conditions and high-precision measurements of collision observables. Theoretical studies employ first- and second-order formalisms together with advanced numerical modelling, including the Independent Atom Model with the Screening Corrected Additivity Rule and

interference corrections (IAM-SCAR+I), providing accurate descriptions of electron scattering from complex molecular systems.

By integrating experimental measurements with predictive theoretical models, ATMOLCOL contributes to a deeper understanding of charged-particle and photon interactions with matter and to the development of comprehensive databases of collision parameters. The synergy between experiment and theory enables systematic studies of atoms and biologically relevant molecules and supports applications in radiation damage modelling, environmental science, plasma technologies, and biomedical research. The project therefore provides an interdisciplinary framework for advancing both fundamental atomic and molecular physics and its broader scientific and technological applications.

Acknowledgement: Acknowledge support of the Science Fund of the Republic of Serbia, Grant No. 6821, 'Atoms and (bio)molecules-dynamics and collisional processes on short time scale ATMOLCOL'.

References

Delibašić H. *et al.* (2024) *Laser Phys. Lett.* **21**, 033001.
Jureta J. *et al.* (2024) *Atoms* **12**, 6.
Kopyra J. *et al.* (2025) *Eur. Phys. J. D* **79**, 97.
Srećković V. *et al.* (2025) *Results in Phys.* **77**, 108455.
Vukalović J. *et al.* (2026) *Phys. Chem. Chem. Phys.* **28,** 13496.

ELASTIC ELECTRON SCATTERING FROM GAS-PHASE INHALATION ANAESTHETIC MOLECULES

Jelena Vukalović[1,2], Bratislav P. Marinković[1], Francisco Blanco[3], Gustavo García[4] and Jelena B. Maljković[1]

[1]*Institute of Physics Belgrade, University of Belgrade, 11080 Belgrade, Pregrevica 118, Serbia*

[2]*Faculty of Science, University of Banja Luka, Mladena Stojanovića 2, 78000 Banja Luka, Republic of Srpska, Bosnia and Herzegovina*

[3]*Departamento de Física Atómica Molecular y Nuclear, Facultad de Ciencias Físicas, Universidad Complutense, Avda. Complutense s/n, E-28040 Madrid, Spain*

[4]*Instituto de Física Fundamental, Consejo Superior de Investigaciones Científicas, Serrano 121, 28006 Madrid, Spain*

jelena.vukovic@pmf.unibl.org

Electron interactions with biologically relevant molecules play an important role in radiation physics, plasma medicine, and electron-driven chemical processes. In this work, we investigate elastic electron scattering from the gas-phase inhalation anaesthetics halothane (Maljković *et al.* 2023), sevoflurane (Vukalović *et al.* 2022), isoflurane (Vukalović *et al.* 2024), and desflurane (Vukalović *et al.* 2026), which are widely used in clinical practice and represent structurally complex halogenated molecules. Besides their medical relevance, these compounds are also potent greenhouse gases with high global warming potentials (GWPs), motivating studies of their electron-induced processes and collision dynamics in the context of atmospheric chemistry and environmental modelling.

Elastic electron scattering is studied using a crossed electron–molecular beam apparatus operating under single-collision conditions. Differential cross sections are determined by the relative flow method over a broad range of incident electron energies and scattering angles. The experimental measurements are complemented by theoretical calculations based on the Independent Atom Model with the Screening Corrected Additivity Rule and interference corrections (IAM-SCAR+I), providing a comprehensive description of electron scattering from these polyatomic molecular targets.

The measured and calculated differential cross sections show overall good agreement, demonstrating the reliability of the combined experimental and theoretical approach for describing electron collisions with fluorinated inhalation anaesthetics. The new cross-section data contribute to the limited database available for these medically and environmentally important molecules, supporting the modelling of low-energy electron transport and collision-induced processes in complex molecular systems.

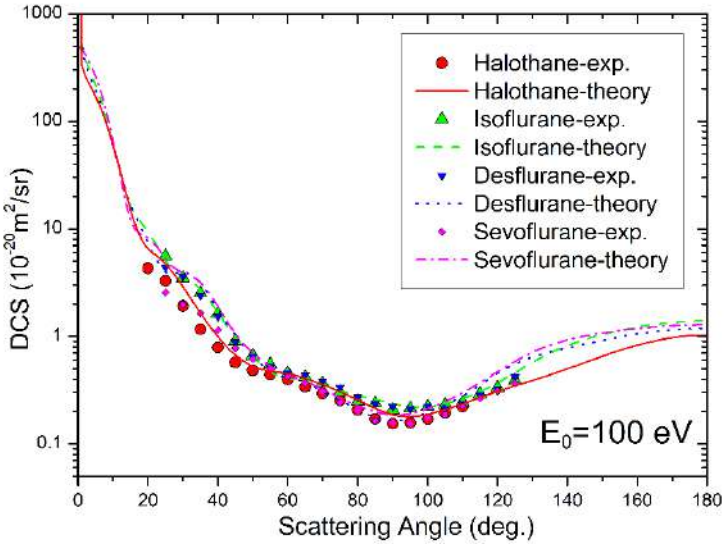

Figure 1: Experimental and IAM-SCAR+I differential cross sections (DCSs) for elastic scattering of 100 eV electrons by gas-phase inhalation anaesthetics.

References

Maljković, J.B. *et al*. (2023) *Eur. Phys. J. Plus*, **138**, 349

Vukalović J. *et al.* (2022) *Int. J. Mol. Sci.* **23**, 21

Vukalović J. et al. (2024) *Phys. Chem. Chem. Phys.* **26**, 985

Vukalović J. *et al.* (2026) *Phys. Chem. Chem. Phys.* **28,** 13496.

VIBRATIONAL EXCITATION OF CO UNDER CONDITIONS OF ELECTRON CYCLOTRON RESONANCE

M. Ristić[1] and M. Vojnović[2]

[1] *University of Belgrade, Faculty of Physical Chemistry, Studentski Trg 12, 11158 Belgrade, Serbia*

[2] *University of Belgrade, Faculty of Physics, Studentski Trg 12, 11158 Belgrade, Serbia*

mvojnovic@ff.bg.ac.rs

Vibrational excitation from $v = 0$ to $v = 1$ state of the CO molecule by electron impact is investigated considering the presence of a microwave electric field crossed at right angles to a uniform magnetic field. Electron cyclotron resonance (ECR) conditions were set in the Monte Carlo simulation developed earlier (Vojnović and Ristić 2025), which is modified to treat electron motion in the atmosphere of the CO gas.

Electrons move in the atmosphere of CO at gas pressure of 1 Torr, which corresponds to the gas number density of $N = 3.2 \cdot 10^{22}\,\mathrm{m}^{-3}$. All relevant processes that can occur during electron-CO collisions were taken into account by introducing the relevant cross sections database into the Monte Carlo simulation. These are: elastic collisions, rotational and vibrational excitations, electronic excitations into singlet and triplet states and ionization. The Treanor vibrational distribution is assumed for a vibrational temperature of 4000 K and a gas temperature of 300 K.

The simulation generates electron energy distribution functions $f(\varepsilon, t)$ within one full period of the oscillating electric field. These distribution functions are used to obtain rate coefficient values for vibrational excitation ($v = 0 \rightarrow 1$) of the CO molecule:

$$K(t) = \sqrt{2/\mathrm{m}} \int_{\varepsilon_{\mathrm{th}}}^{\infty} \sigma(\varepsilon) \sqrt{\varepsilon} f(\varepsilon, t) d\varepsilon. \qquad (1)$$

where m is the electron mass, ε is the electron energy, $\sigma(\varepsilon)$ is the cross section for the given vibrational excitation and $\varepsilon_{\mathrm{th}}$ is threshold energy of this excitation (~0.26 eV). We used the cross-section values that were measured in our

laboratory (Ristić *et al.* 2007). The simulation was performed for electric field frequency, *f*, of 2.45 GHz. The point of electron cyclotron resonance for this frequency is reached at *B*=87.5 mT, which is fulfilled for the given *N* at the reduced magnetic field value of *B*/*N*=2720 Hx. The reduced electric field value was set to *E*/*N* = 100 Td. The temporal variation of the calculated rate coefficient within one period of the electric field can be seen in Fig. 1.

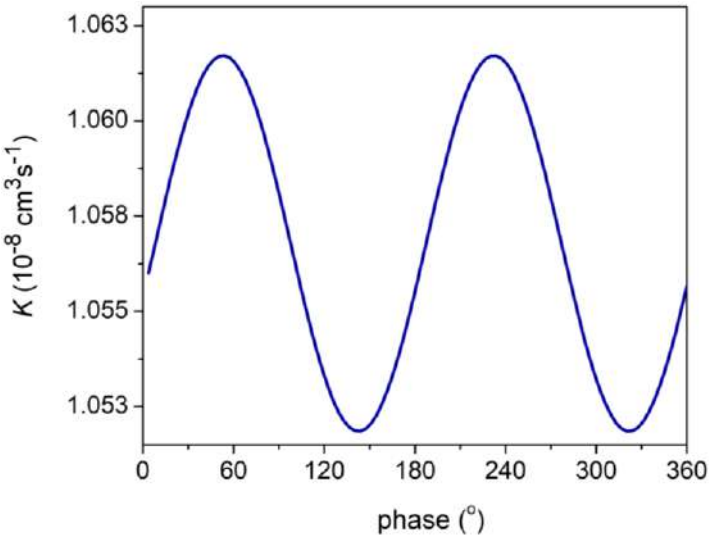

Figure 1: Rate coefficient for electron-impact vibrational excitation $v = 0 \rightarrow 1$ of CO at *B*/*N* = 2720 Hx (*ECR* conditions) versus phase of the electric field (*f* = 2.45 GHz).

Acknowledgments: The research was funded by the Ministry of Education, Science and Technological Development of Serbia, Contract Nos: 451-03-34/2026-03/200146 and 451-03-33/2026-03/200162.

References

Vojnović M and Ristić M (2025) *Plasma Sources Sci. Technol.* **34**, 055014.

Ristić M, Poparić G and Belić D (2007) *Chem. Phys*, **336**, 58.

ULTRAFAST CHARGE-TRANSFER-TO-SOLVENT IN AQUEOUS L-CYSTEINE

N Velasquez[1], A Nyborg[2], H Kaur[1], O Travnikova[3], D Céolin[4], B Winter[1], M Iannuzzi[2], E Muchová[5], F Trinter[1], and T Marchenko[3]

[1]*Fritz-Haber-Institut der Max-Planck-Gesellschaft, Faradayweg 4-6, 14195 Berlin, Germany*

[2]*Department of Chemistry, University of Zurich, Zurich 8057, Switzerland*

[3]*Sorbonne Université, CNRS, Laboratoire de Chimie Physique - Matière et Rayonnement, LCPMR, 75005 Paris, France*

[4]*Synchrotron SOLEIL, L'Orme des Merisiers, Saint-Aubin, BP 48 91192 Gif-sur-Yvette Cedex Paris, France*

[5]*Department of Physical Chemistry, University of Chemistry and Technology, Prague, Technická 5, 166 28 Prague, Czech Republic*

velasquez@fhi-berlin.mpg.de

Charge-transfer-to-solvent (CTTS) processes provide a route by which electronic excitation in a solute can delocalize into the surrounding aqueous environment. In biomolecular systems, such processes are expected to depend sensitively on protonation state and local solvation, but their ultrafast timescales make them difficult to access directly. Here, we use sulfur KLL resonant Auger-Meitner spectroscopy to investigate CTTS dynamics in aqueous l-cysteine as a function of pH.

Auger-Meitner spectra reveal a strong dependence of the decay pattern on protonation state. At pH 5, where cysteine is dominated by the zwitterionic thiol form, resonant excitation leads primarily to localized spectator decay. At pH 12, where cysteine is deprotonated to the thiolate form, additional decay contributions appear at kinetic energies close to that of the normal Auger-Meitner line. The spectral separation between the localized spectator components and the CT contribution is shown in Figure 1, where the pH 12 resonant Auger spectrum is compared with the corresponding pH 5 spectrum. These features are assigned to CTTS-related decay channels because delocalization of the resonantly

promoted electron into the solvent reduces spectator screening of the two-hole final state.

The spectator shift therefore provides a direct spectral handle for separating localized spectator decay from solvent-delocalized CT decay. By combining the extracted spectator/CT intensity ratios with a Fano-based core-hole-clock formalism, we estimate the characteristic timescale of electron delocalization within the S 1s core-hole lifetime. Complementary electronic-structure calculations support the assignment, showing that deprotonated cysteine supports solvent-delocalized CT character, whereas the zwitterionic form remains dominated by localized thiol-centered excitations. These results establish resonant Auger-Meitner spectroscopy as a sensitive probe of ultrafast electronic relaxation and CTTS dynamics in aqueous biomolecular systems.

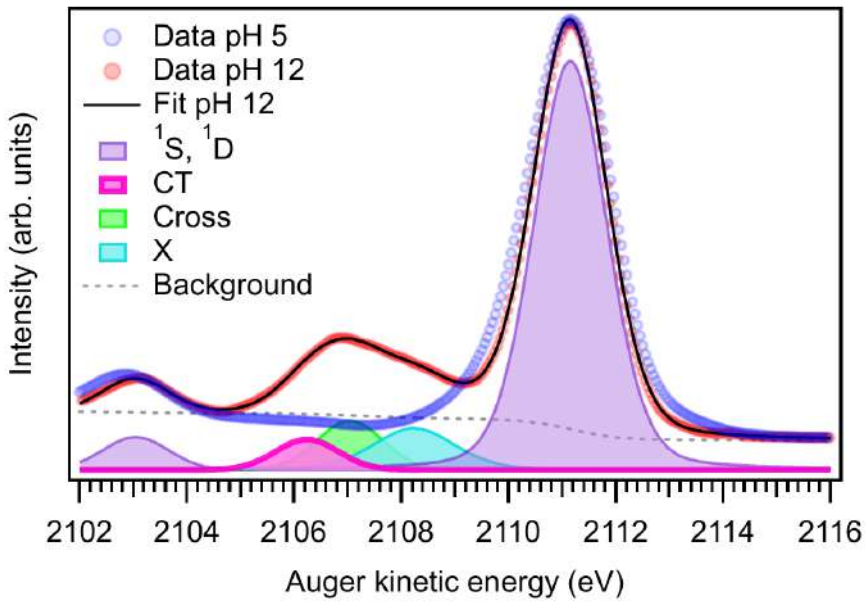

Figure 1: Experimental S $KL_{2,3}L_{2,3}$ Auger spectrum of aqueous l-cysteine at pH 12, measured at the S $1s^{-1}\sigma^*$ resonance, with normalized and offset pH 5 data shown for comparison. The fit separates localized spectator Auger decay (^{1}S, ^{1}D) from a CT contribution near the normal Auger kinetic energy. The absence of a comparable CT feature at pH 5 highlights the localized spectator character of the zwitterionic form.

ANGULAR DISTRIBUTIONS FOR SINGLE-ELECTRON CAPTURE IN COLLISIONS OF FAST PROTONS WITH NEON

Nenad Milojević[1], Danilo Delibašić[1], Ivan Mančev[1], Miloš Milenković[2] and Jelena Arsenijević[3]

[1]*Faculty of Sciences and Mathematics, University of Niš, Višegradska 33, 18000 Niš, Serbia*

[2]*Faculty of Technology, University of Niš, Bulevar Oslobodjenja 124,*

16000 Leskovac, Serbia

[3]*Faculty of Sciences and Mathematics, University of Priština in Kosovska Mitrovica, Lole Ribara 29, 38220, Kosovska Mitrovica, Serbia*

nenad.milojevic@pmf.edu.rs

The process of single-electron capture from the K shell of a neon atom by fast protons has been investigated using perturbative theoretical methods. Two second-order methods were employed: the three-body boundary-corrected continuum-intermediate-states (BCIS-3B) method, see Milojević *et al.* 2020, and the four-body boundary-corrected continuum-intermediate-states (BCIS-4B) method, see Milojević *et al.* 2023, together with two first-order methods: the three-body boundary-corrected first-Born approximation (CB1-3B), see Belkić *et al.* 1987, and the four-body boundary-corrected first-Born approximation (CB1-4B), see Mančev *et al.* 2012. Unlike the first-order methods, the second-order methods include intermediate electron continuum states in one of the collision channels. All applied methods are formulated in the prior form; consequently, in the case of the BCIS methods, electron continuum states are included only in the final channel. In this way, the BCIS methods predict the Thomas double-scattering mechanism (Thomas peak), which becomes dominant at high projectile incident energies. Differential cross sections for electron capture into specific hydrogenic states, $\left(\frac{dQ}{d\Omega}\right)_{n,l,m}$, as well as the state-summed cross sections $\left(\frac{dQ}{d\Omega}\right)_{n,l} = \sum_{m=-l}^{l}\left(\frac{dQ}{d\Omega}\right)_{n,l,m}$ and $\left(\frac{dQ}{d\Omega}\right)_{n} = \sum_{l=0}^{n-1}\left(\frac{dQ}{d\Omega}\right)_{n,l}$, were calculated. The maximum principal quantum number for which the differential cross sections were calculated explicitly is n_{max}=4, while the contribution of higher excited states to electron capture into any projectile state was taken into account using

the Oppenheimer scaling law, see Oppenheimer 1928. The frozen-core approximation and the independent-particle model were employed. In the frozen-core approximation, the non-captured (passive) electron is assumed to occupy the same orbital before and after the capture of the active electron, whereas in the independent-particle model, the passive electron is taken into account only through its screening of the original nuclear charge of the target. The obtained theoretical results were compared with the available experimental measurements, see Horsdal-Pedersen *et al.* 1982.

References

Belkić Dž and Taylor H S (1987) *Phys. Rev. A,* **35**, 1991.

Horsdal-Pedersen E, Folkmann F, Pedersen N H (1982) *J. Phys. B*, **15**, 739.

Mančev I, Milojević N and Belkić Dž (2012) *Phys. Rev. A*, **86**, 022704.

Milojević N, Mančev I, Delibašić D and Belkić Dž (2020) *Phys. Rev. A*, **102**, 012816.

Milojević N, Mančev I, Delibašić D and Belkić Dž (2023) *Phys. Rev. A*, **107**, 052806.

Oppenheimer J R (1928) *Phys. Rev.*, **31**, 349.

IMPACT OF INITIAL AND BOUNDARY CONDITIONS ON CURRENT WAVEFORM ANALYSIS IN AN IDEALIZED PULSED-TOWNSEND EXPERIMENT

D. Bošnjaković[1], I. Simonović[1] and S. Dujko[1]

[1]*Institute of Physics, University of Belgrade, Pregrevica 118, 11080 Belgrade, Serbia*

danko.bosnjakovic@ipb.ac.rs

The pulsed-Townsend (PT) experiment is commonly employed to measure electron transport properties in gases, including the drift velocity, longitudinal diffusion coefficient and ionization rate. These data can serve as input for plasma modelling and for swarm inversion procedure used to derive the cross-sections for electron scattering (Šašić *et al*. 2025). The interpretation of PT measurements, however, and their relation to transport properties obtained from kinetic theory and Monte Carlo (MC) calculations, remains debated (Vemulapalli *et al*. 2026, Casey *et al*. 2021). The present work aims to contribute to this discussion by analyzing current waveform signals generated by our MC simulation of an idealized PT experiment.

Our MC PT experiment simulation follows the trajectories of individual electrons and their collisions with the background gas in a region bounded by the cathode and anode (Bošnjaković *et al*. 2014). The resulting current waveforms, obtained via Ramo's theorem, are analyzed using a Levenberg-Marquardt fitting procedure with several analytical expressions derived from the advection-diffusion-reaction equation. The extracted transport data are compared with the corresponding hydrodynamic transport properties, obtained using the same MC code and cross-section set under steady-state conditions in free space. Particular attention is given to the influence of the initial electron velocity distribution, steady-state relaxation, and cathode boundary conditions. Overall, good agreement is found between the fitted and bulk transport coefficients. However, under certain experimental conditions, the fitted values show pronounced sensitivity to the finite steady-state relaxation time.

References

Šašić O *et al.* (2025) *Plasma Sources Sci. Technol.*, **34**, 045011.

Vemulapalli H *et al.* (2026) *Plasma Sources Sci. Technol.*, **35**, 015014.
Casey M *et al.* (2021) *Plasma Sources Sci. Technol.*, **30**, 035017.
Bošnjaković D *et al.* (2014) *J. Instrum.*, **9**, P09012.

POSITRON TRANSPORT IN NEON, ARGON, KRYPTON AND XENON

Dušan Belča[1], Ilija Simonović[1], Danko Bošnjaković[1] and Saša Dujko[1]

[1]*Institute of Physics Belgrade, Pregrevica 118, 11080 Belgrade, Serbia*

dbelca@ipb.ac.rs

Investigations of positron transport in noble gases provide valuable insights into the fundamental interactions between matter and antimatter. Furthermore, a precise kinetic description of low-energy positrons under the influence of electric fields is of practical significance for the modelling and optimisation of positron traps (Marjanović *et al.*, 2016).

In this work, we calculate the transport properties, including the third-order transport coefficient tensor, of positron swarms in neon, argon, krypton and xenon over a wide range of reduced electric fields (E/N). For our calculations, we use a multi-term solution of Boltzmann's equation and independently validate the results with Monte Carlo simulations, following the methodology benchmarked in Dujko et al. (2010). The scattering cross sections are taken from established datasets: convergent close-coupling calculations for neon and argon (Mori *et al.*, 2024) and relativistic optical-potential calculations for krypton and xenon (Machacek and McEachran, 2024). Direct annihilation is treated separately and computed using the Z_{EFF} data of Green *et al.* (2014). The evaluated swarm parameters include the mean energy, bulk and flux drift velocities, bulk and flux longitudinal and transverse diffusion coefficients, skewness tensor components, and rate coefficients for the individual collision channels.

Our results show that positrons remain in thermal equilibrium with the gas at low electric fields. As the field strength increases, the mean positron energy rises rapidly due to enhanced swarm heating. The onset of inelastic processes then moderates this trend, resulting in a more gradual increase in the mean energy. The influence of annihilation on the drift velocity becomes noticeable for krypton and xenon, manifesting as an increase in the bulk component, consistent with the behaviour reported for heavier systems such as radon (Boyle *et al.*, 2026). At higher fields, a marked drop in the bulk drift velocity is found for all gases, leading to NDC in the bulk component only. As an illustrative example, Figure 1

displays the bulk and flux drift velocities for positrons in Neon. Calculations were performed using a numerical multi-term solution of Boltzmann's equation. The transverse diffusion coefficient ND_T shows little difference between bulk and flux, whereas the longitudinal coefficient ND_L is the most sensitive to positronium formation, with the bulk component suppressed by several orders of magnitude at intermediate fields. The annihilation rate coefficients vary only weakly with E/N, while the positronium formation rate displays a sharp threshold-driven rise. The skewness tensor components are even more sensitive to these reactive processes and represent a promising direction for future analysis.

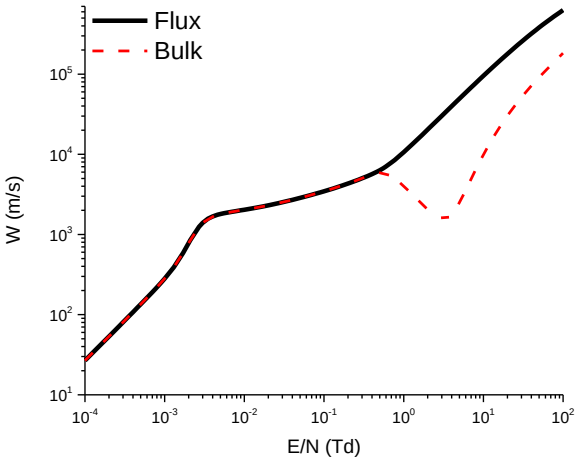

Figure 1: Variation of the bulk and flux drift velocities with E/N for positrons in neon.

References

Boyle G J, Muccignat D L, Machacek J R and McEachran R P (2026) *Atoms*, **14**, 34.

Green D G, Ludlow J A and Gribakin G F (2014) *Phys. Rev. A*, **90**, 032712.

Dujko S, White R D and Petrović Z Lj (2010) *Phys. Rev. E*, **81**, 046403

Machacek J R and McEachran R P (2024) *Eur. Phys. J. D*, **78**, 17.

Marjanović S, Banković A, Cassidy D, Cooper B, Deller A, Dujko S and Petrović Z Lj (2016) *J. Phys. B.: At. Mol. Opt. Phys.*, **49**, 215001.

Mori N A, Scarlett L H, Bray I and Fursa D V (2024) *Eur. Phys. J. D*, **78**, 19.

ELECTRON TRANSPORT IN LIQUID ARGON AND XENON DOPED WITH HYDROGEN AND DEUTERIUM

Dušan Belča[1], Ilija Simonović[1], Danko Bošnjaković[1] and Saša Dujko[1]

[1]*Institute of Physics Belgrade, Pregrevica 118, 11080 Belgrade, Serbia*

dbelca@ipb.ac.rs

The introduction of light-element dopants into liquid noble-gas time-projection chambers (TPCs) has recently been proposed to enhance detector sensitivity to low-mass particles (Lippincott *et al.*, 2025). In this context, a detailed investigation of the impact of such dopants on electron transport is of great importance and naturally extends previous transport modelling studies in pure noble liquids (Simonović *et al.*, 2019).

In this work, we study electron transport in liquid argon (LAr) and liquid xenon (LXe) doped with small fractions of molecular hydrogen (H_2) and deuterium (D_2). As a first approximation, Monte Carlo simulations are performed using a hybrid cross-section approach that combines gas-phase cross sections for the dopant molecules with liquid-phase cross sections for the pure liquids. Ongoing work aims to incorporate the structural effects of the liquid environment into the dopant molecules' scattering cross sections. The Monte Carlo code used in this work has been benchmarked against the multi-term Boltzmann equation results of Dujko *et al.* (2010). The liquid-phase cross sections for pure xenon are taken from Simonović *et al.* (2019), and those for pure argon from Simonović (2020), while the gas-phase cross sections for H_2 and D_2 are taken from MAGBOLTZ, with the rotational excitation cross sections adjusted to the liquid temperature by rescaling the rotational level populations according to the partition function. Transport coefficients, including mean electron energy, drift velocity, transverse and longitudinal diffusion coefficients, and relevant rate coefficients, are calculated over a wide range of reduced electric fields (10^{-3}–10^{3} Td) and compared with the corresponding values in pure liquids and across different dopant concentrations.

Our results show that the addition of H_2 and D_2 leads to a significant reduction in mean electron energy and a strong suppression of transverse diffusion at low reduced fields, reflecting efficient energy loss via rotational excitation of the dopant molecules. As an illustrative example, in Figure 1, we show the variation

of the mean energy with the reduced electric field E/N for pure LXe and LXe doped with 1% H_2 and 1% D_2. The drift velocity, in contrast, generally increases upon doping, with the magnitude of the effect depending on the host liquid. At higher reduced fields, where electrons access the inelastic channels of the host liquid, transport coefficients for the doped and pure systems converge. While suppressed diffusion benefits the spatial resolution of electron swarms, the reduced mean electron energy may hinder electron extraction across the liquid–gas interface in dual-phase detectors (Xu and Pereverzev, 2014), highlighting a trade-off between improved swarm confinement and efficient electron extraction.

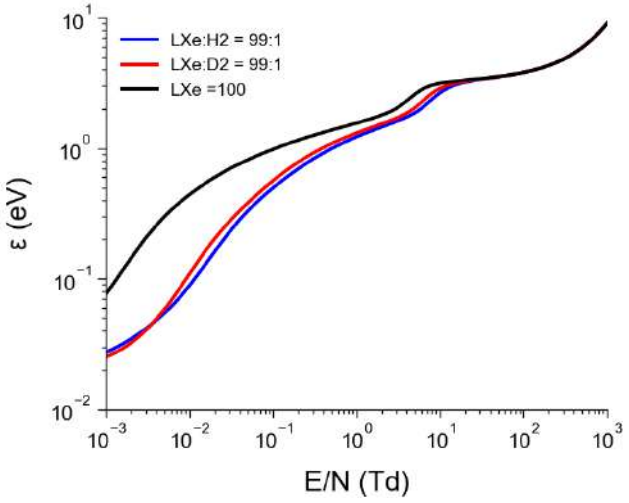

Figure 1: Mean electron energy as a function of reduced electric field in pure liquid xenon and in liquid xenon doped with 1% H_2 and 1% D_2.

References

Dujko S, White R D and Petrović Z Lj (2010) *Phys. Rev. E*, **81**, 046403.
Lippincott W H, Nelson H N, Akerib D S et al. (2025) *Commun. Phys.*, **8**, 244.
Simonović I (2020), PhD thesis, University of Belgrade.
Simonović I, Garland N, Bošnjaković D, Petrović Z Lj, White R D and Dujko S (2019) *Plasma Sources Sci. Technol.*, **28**, 015006.

MONTE CARLO AND DRIFT-DIFFUSION ANALYSIS OF THE SCANNING DRIFT TUBE EXPERIMENT

J. Gardnir[1], G. J. Boyle[1], D. L. Muccignat[1], and R. D. White[1]

[1] *James Cook University, Townsville, Australia*

gregory.boyle@jcu.edu.au

The scanning drift-tube experiment (SDT) [Korolov *et al.* 2016] provides a unique capability for measuring the full spatio-temporal evolution of electron swarms under uniform electric fields. By recording electron swarm maps with high spatial and temporal resolution, the technique offers considerably more information than conventional swarm experiments and has become an important tool for studying electron transport and equilibration processes. Analytical interpretations of SDT measurements generally assume that, once equilibration is achieved, the swarm evolution is described by the hydrodynamic drift–diffusion equation, from which transport coefficients are obtained via the measured swarm map (Donko *et al.* 2019, Kawaguchi *et al.* 2023).

We investigate the validity of these assumptions using Monte Carlo simulations of electron swarms over a range of reduced electric fields and gas conditions. Synthetic swarm maps are generated under controlled conditions and analyzed using both conventional drift–diffusion descriptions and higher-order continuity equations. By comparing transport coefficients extracted from the simulations with the corresponding ground truth values, we can comment on the regimes in which the standard analysis is appropriate, and those where modifications to the theory become important.

References

Donko Z, Hartmann P, Korolov I, Jeges V, Bosnjaković D, Dujko S (2019) *Plasma Sources Sci. Technol.*, **28**, 095007.

Kawaguchi S, Takahashi K, Satoh K (2023) *J. Phys. D: Appl. Phys*., **56**, 244003.

Korolov I, Vass M, Bastykova N Kh, Donko Z (2016) *Rev. Sci. Intrum*., **87**, 063102.

ELECTRON TRANSPORT IN CROSSED ELECTRIC AND MAGNETIC FIELDS IN $C_2H_2F_4$

Saša Dujko[1], Snježana Dupljanin[2], and Zoran Lj. Petrović[3]

[1]*Institute of Physics Belgrade, Pregrevica 118, 11080 Belgrade, Serbia*

[2]*Faculty of Natural Sciences and Mathematics, University of Banja Luka, M. Stojanovića 2, 78000 Banja Luka, Bosnia and Herzegovina*

[3]*Serbian Academy of Sciences and Arts, Kneza Mihaila 35, 11001 Belgrade, Serbia*

sasa.dujko@ipb.ac.rs

Understanding collisional and transport properties of electrons in electric and magnetic fields in neutral gases is essential for accurate modelling of non-equilibrium plasmas. The gas $C_2H_2F_4$ is widely used in the fabrication of integrated circuits and plays a central role as a working medium in modern gaseous particle detectors (Šašić *et al.* 2025).

In this work, electron transport in crossed electric and magnetic fields is investigated using Monte Carlo simulations and numerical multi-term solutions of the Boltzmann equation (Dujko *et al.* 2010). The electron–molecule collision cross section set for $C_2H_2F_4$, developed and discussed in Šašić *et al.* (2025), is used as the input dataset for all simulations presented in this work.

We first analyse transport in dc crossed fields, where an increasing reduced magnetic field leads to pronounced magnetic cooling of the electron swarm, manifested through reductions in drift velocity, diffusion coefficients, and ionisation rate. Based on simulations of electron transport in arbitrary configurations of electric and magnetic fields, these effects were found to be most pronounced in the orthogonal field configuration.

We then examine electron transport in radio-frequency electric and magnetic fields, systematically exploring the influence of field frequency, electric and magnetic field amplitudes, phase difference, and field orientation. The results reveal clear signatures of cyclotron resonance, magnetic field-induced electron heating, oscillatory behaviour in time-resolved transport properties, and transient negative diffusivity. Electron energy and velocity distribution functions are

computed, and the validity limits of the quasi-stationary approximation and the effective field approximation are critically assessed.

As an illustrative example, in Figure 1, we show the velocity distribution function for a parallel-field orientation and a crossed-field configuration. The electric and magnetic field amplitudes are 270 Td and 10 000 Hx, respectively, and the field frequency is 1 GHz. In the parallel-field configuration (left panel), the distribution remains elongated along v_x, reflecting field-aligned acceleration. In the orthogonal configuration (middle panel), the magnetic field induces cyclotron motion that broadens the distribution in the transverse plane, producing a pronounced extension toward larger radial velocities v_r. The difference plot (right panel) highlights this effect.

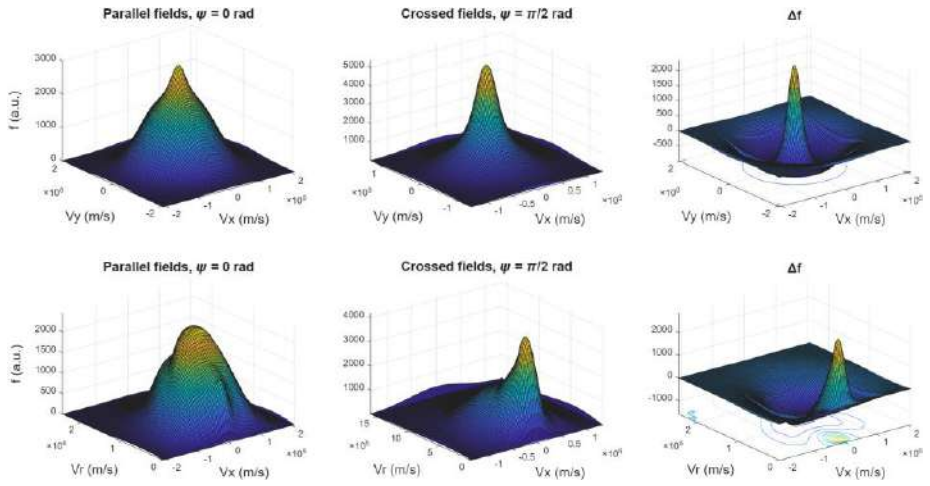

Figure 1: Electron velocity distribution functions in $C_2H_2F_4$ for parallel (left) and orthogonal (middle) electric–magnetic field configurations, and their difference (right).

References

Dujko S, White R D, Petrović Z Lj, and Robson R E (2010) *Phys. Rev. E*, **81**, 046403.

Šašić O, Dupljanin S. Dujko S and Petrović Z Lj (2025) *Plasma Sources. Sci. Technol.*, **34**, 045011.

TRANSPORT AND SPATIAL RELAXATION OF ELECTRONS IN AN IDEALIZED STEADY-STATE TOWNSEND EXPERIMENT IN BERYLLIUM AND MAGNESIUM VAPOURS

Žarko Mažić[1], Danko Bošnjaković[1], Ilija Simonović[1] and Saša Dujko[2]

[1]*Institute of Physics Belgrade, Pregrevica 118, 11080 Belgrade, Serbia*

maziczarko@gmail.com

Understanding electron transport and the associated spatial non-locality under non-hydrodynamic conditions is essential for accurate modelling of non-equilibrium plasmas, particularly in situations where strong gradients, rapid energy exchange, and non-Maxwellian electron energy distributions dominate the physics. Such conditions arise in numerous plasma-based technologies, including plasma processing, gas discharges, and radiation-detection systems. Beryllium and magnesium vapours are of particular interest due to their highly structured, strongly energy-dependent electron-scattering cross sections, which give rise to pronounced non-local transport effects and make them ideal test beds for studying deviations from hydrodynamic behaviour.

Electron transport is investigated using Monte Carlo simulations and numerical multi-term solutions of the Boltzmann equation. The computational tools based on these methodologies have been rigorously benchmarked against a wide range of conservative and non-conservative model gases and standard test problems (Dujko *et al.* 2010). For beryllium vapour, the electron–atom collision cross-section sets of McEachran *et al.* (2018a) and Zatsarinny *et al.* (2016) are employed. For magnesium vapour, we use the cross sections of McEachran *et al.* (2018b) together with a dataset from the Phelps-LXCat database, comprising both theoretical calculations and experimental measurements. Calculations are performed for vapour temperatures of 2750 K (Be) and 750 K (Mg), assuming that all atoms are in the ground state and neglecting the influence of metastable and excited states on transport properties.

Transport coefficients and velocity distribution functions are first obtained in the hydrodynamic regime for reduced electric fields ranging from 1 to 10 000 Td. In the low-field limit, electrons are in thermal equilibrium with the vapour. As the field increases, the mean energy, drift velocity, and diffusion coefficients rise

monotonically. Once ionisation becomes sufficiently frequent, bulk values of the drift velocity and diffusion coefficients exceed their flux counterparts. At high fields, an interesting reversal occurs: the flux drift velocity exceeds the bulk drift velocity, a behaviour that can be understood by analysing the energy dependence of the ionisation cross section. The validity of the two-term approximation to the Boltzmann equation is examined and shown to deteriorate at higher fields, as illustrated by the behaviour of the first two Legendre components of the velocity distribution function.

In the second part of this work, the spatial relaxation of electrons in an idealised steady-state Townsend experiment is analysed. For both vapours, oscillatory behaviour in the profiles of mean energy and average velocity emerges at fields above ~10 Td, when electrons acquire sufficient energy to excite atomic levels. These oscillations are analogous to those observed in the Franck–Hertz experiment (Robson et al. 2000, Dujko et al. 2008), with their damping occurring at approximately 1500 Td in magnesium and 1000 Td in beryllium. Owing to weaker energy exchange in collisions, magnesium exhibits noticeably longer relaxation lengths than beryllium. Differences between conservative and non-conservative transport models are examined, showing that once ionisation becomes significant (several hundred Td and above), the conservative model yields higher mean energies and excitation/ionization rates, reduced elastic collision rates, and systematically longer relaxation lengths. Finally, we compare models of post-ionisation energy sharing, distinguishing between asymmetric and equal-partition schemes. For fields above ~1000 Td, asymmetric-sharing models yield higher mean energies and lower excitation and elastic collision rates, while the ionisation coefficient remains only weakly sensitive to the chosen energy-sharing approach.

References

Dujko S, White R D and Petrović Z Lj (2008) *J. Phys. D: Appl. Phys*., **41**, 245205.

Dujko S, White R D, Petrović Z Lj, and Robson R E (2010) *Phys. Rev. E*, **81**, 046403.

McEachran R, Blanco F, García G, and Brunger M J (2018a) *J. Phys. And Chem. Ref. Data*, **47**, 033103.

McEachran R, Blanco F, García G, Stokes P W, White R D, and Brunger M J (2018b) *J. Phys. And Chem. Ref. Data*, **47**, 043104.

Robson R E, Li B and White R D (2000) *J. Phys. B: At. Mol. Opt. Phys.*, **33**, 507.

Zatsarinny O, Bartschat K, Fursa D V, and Bray I (2016), *J. Phys. B: At. Mol. Opt. Phys.*, **49**, 235701.

Section 2.

PARTICLE AND LASER BEAM INTERACTIONS WITH SOLIDS

ADVANCED CHANNELING TO GUIDE CHARGED & NEUTRAL BEAMS

Sultan B. Dabagov

INFN Laboratori Nazionali di Frascati, Italy

sultan.dabagov@lnf.infn.it

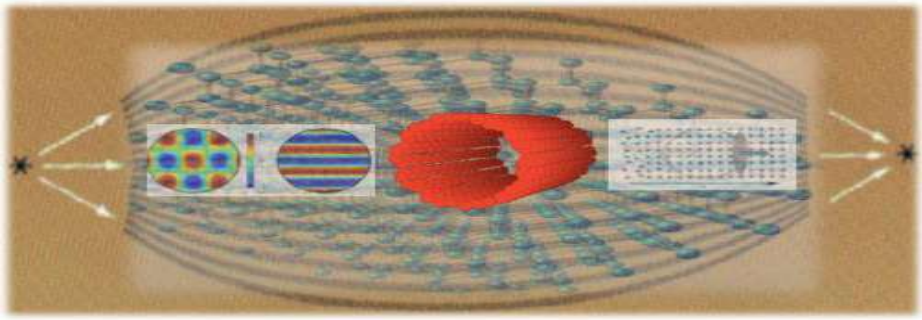

Channeling is well-known phenomenon in the physics mostly related to the motion of the beams of charged particles in aligned crystals. Since the beginning of 1970s channeling of high-energy leptons (electrons/positrons of several MeV up to hundreds of GeV energies) and hadrons (protons/ions of tens GeV up to several TeV energies) has been applied at various famous world research centers within several national/international projects that aims in shaping, effective deflecting beams as well as in producing high power x-ray and γ radiation sources.

Recent studies have shown the feasibility of channeling phenomenology for describing other mechanisms of interaction of beams, both charged and neutral particles ones, in solids, plasmas and in various electromagnetic fields, in the research for crystal/laser/plasma based undulators and collimators, as well as for channel-based x-ray and neutron optical elements.

This review talk is devoted to actual channeling related projects that have been realising since so-called renaissance of channeling studies started in the end of

last century. The future possible developments in channeling physics will be analysed within the presentation.

References

Dabagov S B (2023) *Physics Uspekhi*, **46** (10), 1053.

Dabagov S B (2018) *European Physical Journal Web Confs*., **167,** 01002.

Dabagov S B and Gladkikh Yu P (2019) *Radiation Physics and Chemistry*, **154**, 3-16.

Dabagov S B and Dik A V (2022) *Quantum Beam Sci*., **6**(1), 8 doi: 10.3390/qubs6010008 (on volume cover).

FROM IONIZATION TO STRUCTURAL TRANSFORMATION: MECHANISMS OF SWIFT HEAVY ION TRACK FORMATION IN SOLIDS

R. A. Rymzhanov[1,2], J. H. O'Connell[3], M. Ćosić[4], V. A. Skuratov[1,5,6], A. E. Volkov[1,7]

[1]*Joint Institute for Nuclear Research, Joliot-Curie 6, 141980 Dubna, Russia*

[2]*The Institute of Nuclear Physics, Ibragimov St. 1, 050032 Almaty, Kazakhstan*

[3]*Nelson Mandela University, University Way, 6001 Port Elizabeth, South Africa*

[4]*Vinča Institute of Nuclear Sciences, University of Belgrade, P. O. Box 522, 11001 Belgrade, Serbia*

[5]*Dubna State University, Universitetskaya St. 19, 141980 Dubna, Russia*

[6]*National Research Nuclear University MEPhI, Kashirskoye sh 31, Moscow, Russia*

[7]*P.N. Lebedev Physical Institute of the RAS, Leninskij pr., 53,119991 Moscow, Russia*

rymzhanov@jinr.ru

When energetic heavy ions penetrate a solid, they lose most of their energy through intense ionization of the target material. The resulting extreme excitation of the electronic subsystem relaxes through energy transfer to the lattice, leading to the formation of localized damage zones known as ion tracks. Owing to these unique features, swift heavy ions are widely employed in three principal research areas: (i) simulation of fission fragment effects in structural materials for nuclear energy, (ii) assessment of radiation tolerance in electronic components exposed to cosmic radiation, and (iii) nanoscale modification and structuring of materials.

This work presents recent and most relevant results on the morphology of radiation-induced damage in materials used for nuclear and electronic applications, as a function of irradiation parameters such as ion mass, energy, fluence, and temperature. The structural response of functional materials to swift heavy ion irradiation was investigated using transmission electron microscopy in combination with numerical modeling, coupling the Monte Carlo code TREKIS (see Medvedev *et al.* 2015) with molecular dynamics simulations (see Rymzhanov *et al.* 2024; Rymzhanov, Volkov, Skuratov 2024). We discuss the stages and

mechanisms of single-track formation, track overlap, and surface modification processes in various amorphizable and non-amorphizable solids subjected to SHI irradiation.

Acknowledgements: The work was funded by the Russian Science Foundation (grant No 25-72-10101, https://rscf.ru/project/25-72-10101/).

References

Medvedev N A, Rymzhanov R A, Volkov A E (2015) Time-resolved electron kinetics in swift heavy ion irradiated solids, *J. Phys. D*, **48**, 355303.

Rymzhanov R A, Ćosić M, N. Medvedev N A, Volkov A E (2024) From groove to hillocks – Atomic-scale simulations of swift heavy ion grazing impacts on CaF_2, *Appl. Surf. Sci.*, **652**, 159310.

Rymzhanov R A, Volkov A E, Skuratov V A (2024) Bulk, overlap and surface effects of swift heavy ions in CeO_2, *J. Nucl. Mater*., **604**, 155480.

CRYSTAL RAINBOW CHANNELING AND THE SUPERFOCUSING EFFECT

Srdjan Petrović[1]

[1]*Laboratory of Physics, Vinča Institute of Nuclear Sciences, University of Belgrade,*

P. O. Box 522, 11001 Belgrade, Serbia

petrovs@vin.bg.ac.rs

Since its first theoretical introduction (Demkov and Mayer, 2004), the concept of superfocusing ion channeling has emerged as a promising pathway toward the realization of a truly sub-atomic beam microscope, enabling manipulation of ion beams at the picometer scale. The spatial distributions of channeled protons in the two-dimensional representation at the superfocusing point for the tilted angle $\varphi = 0, \pm 0.1\psi_c, , \pm 0.1\psi_c, , \pm 0.1\psi_c$, where ψ_c is the critical angle for channeling is presented in Fig. 1 (Petrović et al., 2012).

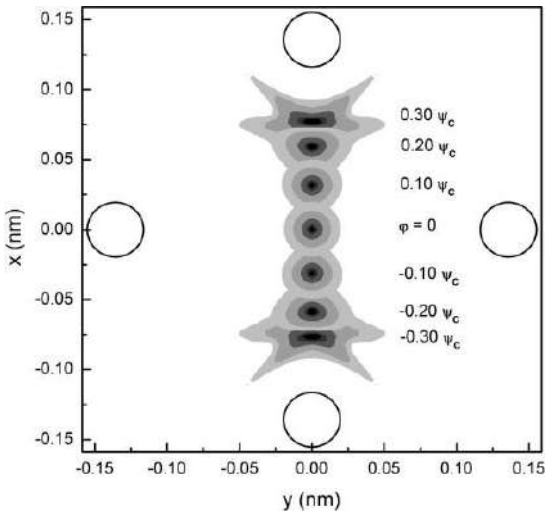

Figure 1: The spatial distributions of channeled protons at the superfocusing point for the tilted angle $\varphi = 0, \pm 0.1\psi_c, , \pm 0.1\psi_c, , \pm 0.1\psi_c$. The atomic strings defining the channel are represented by the circles lying on the *x* and *y* axes.

At first glance, focusing a particle beam to a size smaller than the atomic lattice elements may appear unfeasible. However, in the case of channeling, the periodic arrangement of atoms in the crystal lattice allows the beam to interact coherently with a large number of atoms. This collective interaction effectively compensates for the individual atomic positional uncertainties, making superfocusing possible.

In this talk, we present the theory of crystal rainbow channeling as the physical foundation underlying the singular nature of the superfocusing effect (Nešković et al. 2009, Petrović et al., 2000). It is supplemented by a discussion of its indirect experimental verification (Motapothula et al., 2016). Furthermore, we explore the prospective applications of the superfocusing ion crystal lens within emerging picobeam technologies.

References

Demkov Yu N and Meyer J D (2004) *The European Physical Journal B* **42**, 361.

Motapothula M, Petrović S, Nešković N and Breese M B H (2016) *Physical Review B* **94**, 075415.

Nešković N, Petrović S And Borka D (2009) *Nuclear Instruments and Methods in Physics Research B* **267**, 2616.

Petrović S, Nešković N, Berec V, Ćosić M (2012) *Physical Review A* **85**, 032901.

Petrović S, Miletić L and Nešković N (2000) *Physical Review B* **61**, 184.

PLASMA ASSISTED FABRICATION AND MODIFICATION OF COMPOSITIONALLY COMPLEX NANOMATERIALS IN LIQUID: CAPABILITIES AND CHALLENGES

Nikolai Tarasenko, Anton Radomtsev, Natalie Tarasenka, Alena Nevar, Mikhail Nedelko

B.I. Stepanov Institute of Physics, National Academy of Sciences of Belarus, 68-2 Nezalezhnasti Ave., 220072 Minsk, Belarus

n.tarasenko@ifanbel.bas-net.by

High-entropy alloys (HEAs), as a subclass of compositionally complex materials (CCM), are multicomponent solid solutions containing five or more elements in near-equiatomic proportions with the ability to stabilize their structure by maximizing configurational entropy (Miracle *et al.* 2017). HEAs represent a promising class of materials with significant potential in a variety of applications, including heterogeneous catalysis, energy, photovoltaics, etc. However, the production of such materials imposes a number of requirements on their synthesis, including compositional control, synthesis efficiency, cost, environmental friendliness. These requirements can be particularly satisfied using plasma-laser methods, which have proven successful in recent years for producing nanoparticles (NPs) of various compositions (Stucker *et al.* 2025).

In this paper, we propose an approach for synthesis of multicomponent NPs based on the use of a nonequilibrium plasma in contact with a liquid, and additional laser modification of the resulting NPs. A distinctive feature of this approach is simultaneous anodic dissolution of several solid metal plates immersed in a liquid and their reduction by plasma-produced reactive species. The plasma was ignited near the liquid surface by applying a high voltage of 1–3 kV (current of 4 mA) to a capillary with a gas (Ar) passing through it. Unfocused beam from a Nd:YAG laser (532 nm, pulse duration of 10 ns) was used for additional modification of the resulting nanostructures. The proposed approach was applied to the production of a nanomaterial consisting of Zn, Fe, Mo (Ni), Cu, and Mn and can be extended to nanomaterials of other compositions. The study focused on optimizing experimental conditions to produce compositionally complex nanostructures of controlled size and shape and establishing the parameters important for their application in catalysis.

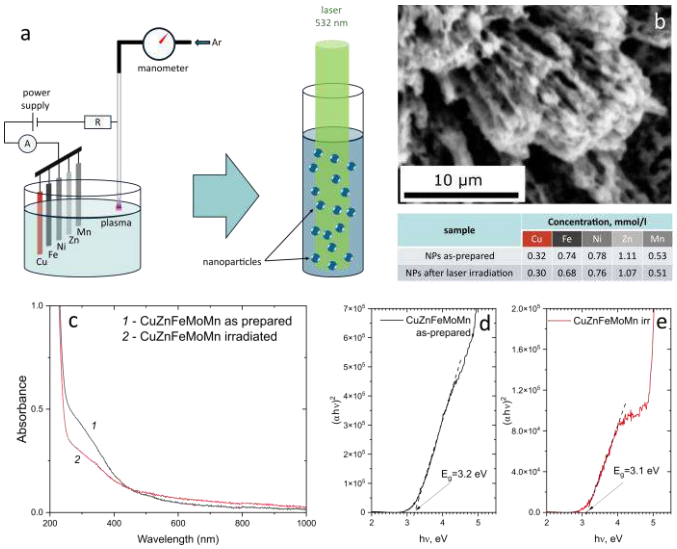

Figure 1: Approach for CCM synthesis (a) and the results of the CuZnFeMo(Ni)Mn NPs characterization: SEM (b), absorption spectra (c), Tauc plots before (c) and after laser irradiation (e). The table shows the composition of the synthesized CuZnFeNiMn NPs.

A suggested mechanism for formation of CCM NPs in the developed approach starts with the dissolution of the anode, followed by metal ions reduction involving reactions with electrons and radicals generated by plasma-liquid interaction. The high reactivity and short lifetime of the reactive species limit the reaction zone to the near-surface region, therefore increasing the possibility of simultaneous presence of all elements in the reaction zone. Additional laser modification of the resulting colloid is proposed as a further way for controlling the morphology and internal structure of the synthesized NPs. The established relationship between the structure and catalytic activity of the resulting structures will be used to design improved catalysts with enhanced performance.

The work was supported by the National Academy of Sciences of Belarus under project Convergence 2.2.07 and by the Belarusian Foundation for Fundamental Research under Grant F25INDA-005.

References

Miracle D and Senkov O (2017) *Acta Materialia* **122**, 448.

Stucker R *et al.* (2025), *Beilstein J. Nanotechnol*. **16**, 1141.

NUMERICAL CODE FOR CALCULATING THE IONIZATION EVENTS OCCURING ON SHORT TIME SCALES IN LASER INDUCED BREAKDOWN OF GASES

Jasna Stevanović[1], Violeta Petrović[1], Hristina Delibašić Marković[1] and Ivan Petrović[2]

[1]*University of Kragujevac, Faculty of Science, Kragujevac, Serbia*
[2]*Academy of Professional Studies Šumadija, Department in Kragujevac, Serbia*

jasna.stevanovic@pmf.kg.ac.rs

The development of powerful laser systems has opened the door to a wide range of applications. Among them, laser-induced breakdown (hereinafter referred to as LIB) has an important place in numerous fields, including medicine and industry, see Manrique *et al.* 2024, Palleschi *et al.* 2025. Therefore, understanding the physical mechanisms underlying this phenomenon remains a relevant research topic. Numerous papers about different aspects of LIB can be found. Both aspects, theoretical and experimental are equally represented in literature, see Fikry *et al.* 2026, Palleschi *et al.* 2025. In this paper, we analyzed the LIB process as a physical phenomenon with respect to its potential applications, depending on the laser parameters. To achieve this, numerical code for calculation the key parameter of LIB, the free electrons density, was developed.

The initial free electrons are assumed to originate from photo-ionization process (PI). Depending on the pressure and pulse duration, two processes can be expected to occur. The low pressures and the case of short pulses (sub-nanosecond) create the conditions for the multiphoton ionization (MPI), whereas tunnel ionization (TI) is much less likely to occur. The classical diffusion theory is taken as a theoretical framework, that assumed that initially created free electron population has been accelerated by inverse bremsstrahlung until they have sufficient energy to ionize neutral gas atoms through impact ionization. This process is referred to as avalanche ionization (AI). This is in accordance with the early theoretical predictions, later confirmed by numerical and experimental findings, as it was shown by Mühlberger *et al.* 2004 and Rapp *et al.* 2014.

Based on previous research results we incorporate diffusion and recombination as loss processes, see Petrović *et al*. 2026. It is shown that these kinds of processes generally play role, but importance varies depending on the gas considered, and all circumstances (pressure, geometry).

The common approach for LIB description starts from the temporal evolution of free electron density, ρ(t):

$$\frac{\partial \rho(t)}{\partial t} = \sum_1^n a_i \rho_i^n(t) - \sum_1^m b_j \rho_j^m(t), \quad (1)$$

where the first sum denotes all contributing processes, while the second corresponds to the processes leading to the electron loss. The coefficients a_i and b_j represent the rates of the corresponding processes, while $\rho_i^n(t)$ denotes the reciprocal degree of the electron density.

To develop the code for obtaining the abovementioned numerical values, we used Python and Wolfram Mathematica.

Acknowledgements. Authors would like to acknowledge the support received from the Science Fund of the Republic of Serbia, #GRANT 6821, Atoms and (bio)molecules-dynamics and collisional processes on short time scale - ATMOLCOL. Our appreciation also goes to the Serbian Ministry of Education, Science and Technological Development (Agreement No. 451-03-34/2026-03/ 200122).

References

Fikry M, Mohammed A, Aboulfotouh A and Omar M (2026) *Eur. Phys. J. Plus*, **141**, 318.

Manrique J, Garrido P and Velasco J (2024) *Atoms*, **12**, 21.

Mühlberger M, Schneidenbach M, Braun A, Schittenhelm H and Kautek W (2004) *Appl. Phys. A*, **79**, 1161.

Palleschi V, Legnaioli S, Poggialini F, Bredice F O, Urbina I A, Lellouche N and Aberkane S M (2025) *Nat. Rev. Methods Primers*, **5**.

Petrović V, Delibašić-Marković H and Srećković V (2026) *Laser Phys.*, **36**.

Rapp L, Haberl B, Bradby J E, Gamaly E G, Williams J S and Rode A V (2014) *Appl. Phys. A*, **114**, 33.

METAL-ORGANIC INTERFACE OF ISOLATED LIGAND COATED SILVER NANOPARTICLES IN THE GAS PHASE

Namitha Deepak[1], Aleksandar R. Milosavljevic[2], Anahita Heraji Esfahani[1], Sufian Rasheed[1], Matthias Hartlieb[1], Sergio Kogikoski Jr.[1] and Ilko Bald[1]

[1]*Institute of Chemistry, University of Potsdam, Potsdam, 14476, Germany*

[2]*Synchrotron SOLEIL, L'Orme des Merisiers Départementale 128, 91190 Saint-Aubin, France*

namitha.deepak@uni-potsdam.de

Plasmonic metal nanoparticles have emerged as a versatile platform for light-driven chemical transformations. Upon photoexcitation at the Localized Surface Plasmon Resonance (LSPR), noble metal nanoparticles can drive reactions via several mechanisms, i.e., enhanced electromagnetic field, hot charge carriers, heat, etc.

A complete description of the electronic structure of the metal molecule interface provides a fundamental understanding of the underlying pathways. In this work, we investigate the electronic structure of silver nanoparticles functionalized with halogenated thiophenols (4-XTP, X = Cl, Br, I), which serve as model systems relevant to Suzuki–Miyaura coupling reactions. Identifying the occupied states, unoccupied states, and the Fermi level at the metal-molecule interface reveals the exact energetics for the chemical transformations.

Using the state-of-the-art experimental setup at the PLEIADES beamline at SOLEIL, France, we carried out X-ray photoelectron spectroscopy (XPS) and Near-edge X-ray absorption fine structure (NEXAFS) spectroscopy to probe the occupied and unoccupied electronic states in the gas phase, where a nanoparticle beam was generated from a colloidal solution. Further surface-enhanced Raman scattering (SERS) measurements were done to monitor reactions *in-situ*. The nature of the halogen substituents significantly influences the electronic density distribution, metal–molecule coupling, and energy-level alignment at the interface.

Our findings provide insight into plasmon-driven reactions by correlating electronic structure with hot carrier energetics.

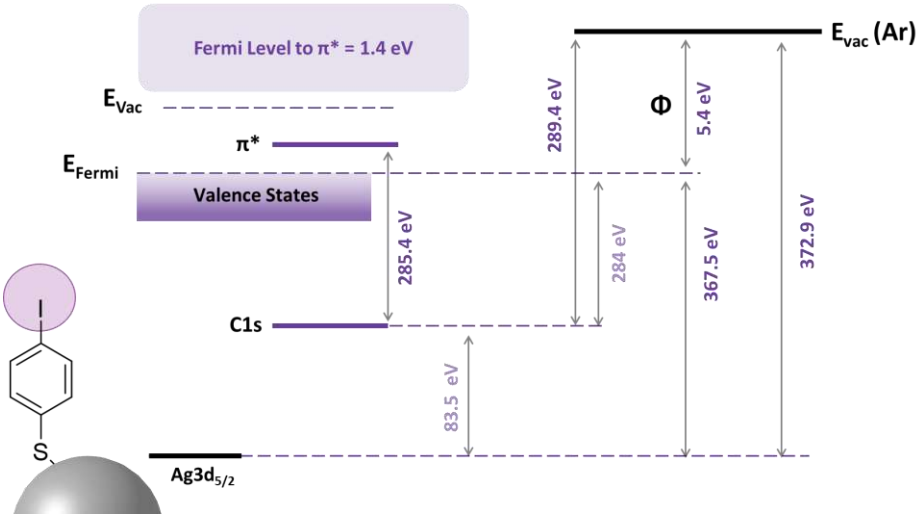

Figure 1: Complete energy landscape for the plasmonic system of Ag nanoparticles modified with 4-iodothiophenol derived from NEXAFS and XPS measurements.

References

Danilović D, Božanić D K, Dojčilović R, Vukmirović N, Sapkota P, Vukašinović I, Djoković V, Bozek J, Nicolas C, Ptasinska S, Milosavljević A R (2020) *J. Phys. Chem. C*, **124,** 43, 23930.

Jiang P, Dong Y, Yang, L, Zhao and Xie W (2019) *J. Phys. Chem. C*, **123** ,27 16741.

Schürmann R, Dutta A, Ebel K, Tapio K, Milosavljević A R and Bald I (2022) *J. Chem. Phys.*, **157**, 8, 84708.

ION BEAM MODIFIED GRAPHENE OXIDE SENSORS FOR MONITORING CO, NO_2, AND SO_2

Željko Mravik[1], Marko Jelić[1], Marija Milićević[1], Predrag Stolić[2], Sonja Jovanović[1], Zoltán Száraz[3], Zoran Jovanović[1]

[1]*Laboratory of Physics, Vinča Institute of Nuclear Sciences, University of Belgrade, Belgrade, Serbia*

[2]*Technical faculty in Bor, University of Belgrade, Bor, Serbia*

[3]*Slovak University of Technology in Bratislava, Faculty of Materials Science and Technology in Trnava, Advanced Technologies Research Institute, Trnava, Slovakia*

mravik@vin.bg.ac.rs

Graphene oxide (GO) and GO-based composites have attracted considerable attention for gas sensing applications due to their large specific surface area, abundance of oxygen-containing functional groups, and tunable electronic properties. The presence of oxygen groups provides numerous active sites for gas adsorption, while the balance between oxidized and graphitic domains governs charge transport through the material. Tailoring structural and chemical features is therefore essential for optimizing sensor sensitivity, selectivity, and response dynamics. Ion beam irradiation represents a versatile approach for controlled modification of GO and GO-based composites. Energetic ions interact with the material inducing bond breaking, defect formation, local atomic rearrangements, and the removal of oxygen-containing functional groups. As a result, irradiation can promote partial reduction of GO, increase electrical conductivity through restoration of sp^2 domains, and modify the density and nature of adsorption sites available for gas–surface interactions.

In this work, thin films of GO, GO/12-tungstophosphoric acid (GO/WPA), and GO/ hydrothermally treated cobalt ferrite (GO/CFO_HT) were deposited on interdigitated electrode arrays and irradiated with 2 MeV carbon ions at a fluences of 1×10^{13}, 1×10^{14} and 1×10^{15} ions cm^{-2}. The effects of irradiation on electrical properties of the materials were investigated using electrochemical impedance spectroscopy (EIS). Ion irradiation enhanced electrical conductivity and altered charge transport mechanisms probably through partial reduction of GO (see Jovanović et al. 2022). The gas sensing performance of irradiated samples was

evaluated toward CO, NO_2, and SO_2 under controlled environmental conditions. Figure 1 shows impedance vs. CO concentration curves for irradiated GO, GO/CFO_HT and GO/WPA. The results show that all three irradiated samples are sensitive to CO gas, where HT treatment and addition of CFO lowered the values of impedance while addition of WPA increased the linearity of the response. The results demonstrate that ion beam irradiation is an effective tool for engineering GO-based sensing materials and provide insight into the relationship between irradiation-induced structural changes (see also Mravik, *et al.* (2021) and Mravik, *et al.* (2022)) and gas sensing behavior.

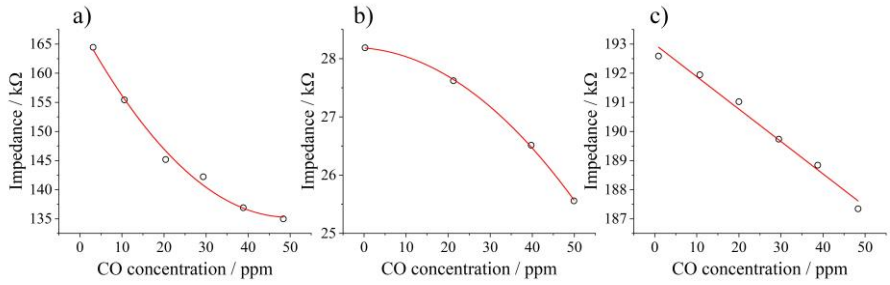

Figure 1: Impedance vs. CO concentration dependance of a) GO irradiated with 1×10^{14} ions cm^{-2} recorded at RH 70% and 30°C, b) GO/CFO_HT irradiated with 1×10^{15} ions cm^{-2} recorded at RH 47% and 30°C and c) GO/WPA irradiated with 1×10^{14} ions cm^{-2} recorded at RH 45% and 30°C.

Acknowledgment: This research was supported by the Science Fund of the Republic of Serbia, grant No. 6706, "Low-dimensional nanomaterials for energy storage and sensing applications: Innovation through synergy of action"- ASPIRE and Serbian-Slovak Bilateral project, grant No. 337-00-3/2024-05/05.

References

Jovanović *et al.* (2022) *Radiation Physics and Chemistry*, **199**, 110355.

Mravik, *et al.* (2021) *Radiation Physics and Chemistry*, **183**, 109422.

Mravik *et al.* (2022) *Journal of Raman Spectroscopy*, **53**, 1974.

A STUDY OF TWISTED BILAYER GRAPHENE VIA PROTON RAINBOW SCATTERING

Milivoje Hadžijojić and Marko Ćosić

Laboratory of Physics, Vinča Institute of Nuclear Sciences, University of Belgrade,

P. O. Box 522, 11001 Belgrade, Serbia

mcosic@vinca.rs

In this work, we investigate the rainbow scattering of 5 keV protons transmitted through twisted bilayer graphene (TBG). The theoretical modeling of the transmission process is performed using the momentum approximation. To account for temperature effects, the thermal vibrations of the target atoms are determined using molecular dynamics simulations. Our study specifically focuses on the twist angles that generate commensurate Moiré supercells. We analyze the specific singularities in the mapping from the impact parameter plane to the scattering angle plane. The findings indicate that the resulting proton rainbow patterns are highly sensitive to the atomic arrangement of the target. Based on these observations, we demonstrate that the rainbow scattering pattern effectively reflects the structural properties of twisted bilayer grapheme.

NON-LINEAR PHENOMENA OF THE ELECTRON STATE EVOLUTION IN THE ION-SURFACE SYSTEM

S. M. D. Galijaš, V. Milosavljević and G. B. Poparić

University of Belgrade, Faculty of Physics, Studentski trg 12, P. O. Box 44, 11000 Belgrade, Serbia

galijas@ff.bg.ac.rs

A well developed two state vector model enables us to consider the electron capture process as a type of a synergetic problem using two independent modes of the mixed flux *I*. From a time perspective, the phase point (Re*I*, Im*I*) starting from expected chaos and finally reaches a self-organization around stationary point which can be connected to the ion-surface neutralization distance R_S.

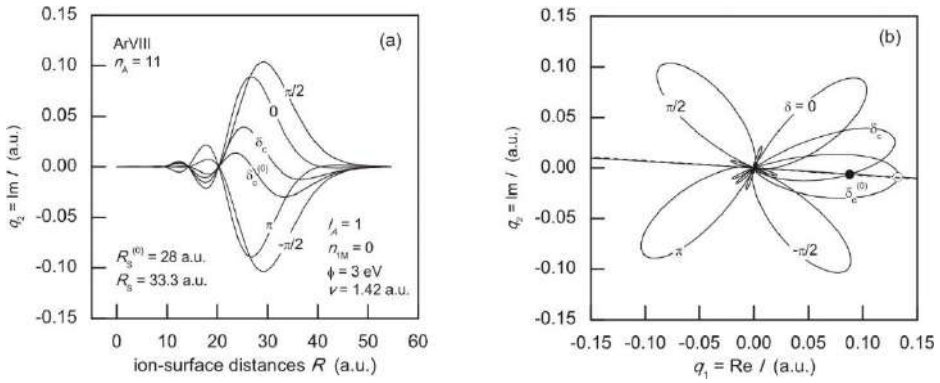

Figure 1: Phase trajectories of the mixed flux *I* for different values of the phase factor δ.

Taking into account that the mixed flux (see Galijaš *et al.* 2019, 2026) as the central quantity of the two state vector model is a complex function, it is possible to introduce two generalized modes (Re*I*, Im*I*) of the self-organizing dynamics.

If we start from the nonlinear model of the time derivative of the mixed flux $\dot{I}(t) = a_1 I(t) + a_2 I^2(t)$, the following initial system of equations is obtained: $\dot{q}_1 = L_{11} q_1 + L_{12} q_2 + N_1(q_1, q_2)$ and $\dot{q}_2 = L_{21} q_1 + L_{22} q_2 + N_2(q_1, q_2)$, where $L_{11} = L_{22} = \mathrm{Re} a_1$ and $L_{21} = -L_{12} = \mathrm{Im} a_1$ with $q_1(t) = \mathrm{Re} I(t)$ and $q_2(t) =$

$\mathrm{Im}I(t)$; $\varepsilon = L_{21}/L_{22} = -L_{12}/L_{11}$. In order to find the expansion coefficients a_1 and a_2, we will use the analytical form $I(t) \approx I_0 \exp(i\delta)\exp(iwt + (\tilde{\gamma}_M - \gamma_{A0})gR - \tilde{\gamma}_M R)$, see Galijaš *et al*. (2011).

In order to fixed the phase trajectory, i.e. to eliminate uncertainty due to the phase factor δ, we shall use an iterative procedure. First, we use the condition $\dot{q}_2/_{R=R_{S,\delta}^{(0)}} = 0$ for $\delta = 0, \pm\pi/2$ and π to determine the ion-surface distance $R_S^{(0)} = \langle R_{S,\delta}^{(0)} \rangle$ as a corresponding mean; simultaneously we determine the value $\varepsilon^{(0)} = \varepsilon/_{R=R_S^{(0)}}$. From the condition that the stationary point $\left(q_{1S}^{(0)}, q_{2S}^{(0)}\right)$ for $R = R_S^{(0)}$ is the intersection of the line $q_2 = -\varepsilon^{(0)} q_1$ and the phase trajectory $q_2 = \mathcal{F}(q_1)$ for the phase factor $\delta = \delta_c^{(0)}$, we specify the value $\delta_c^{(0)}$. In the next iterative step we calculate the ion-surface distance $R_S^{(1)} = \max\left\{R_S; \dot{q}_2/_{R=R_S} = 0, \delta = \delta_c^{(0)}\right\}$. Following the procedure, we calculate the value $\varepsilon^{(1)} = \varepsilon/_{R=R_S^{(1)}}$ and from the condition that the stationary point $\left(q_{1S}^{(1)}, q_{2S}^{(1)}\right)$ for $R = R_S^{(1)}$ is in the intersection of the line $q_2 = -\varepsilon^{(1)} q_1$ and the phase trajectory $q_2 = \mathcal{F}(q_1)$ for $\delta = \delta_c^{(1)}$, we specify the phase factor $\delta = \delta_c^{(1)}$, etc. The mentioned procedure leads to the delta factor δ_c that defines the stationary point (q_{1S}, q_{2S}). In the first approximation, we can take that $(q_{1S}, q_{2S}) \approx \left(q_{1S}^{(1)}, q_{2S}^{(1)}\right)$ for $\varepsilon = \varepsilon^{(1)}$ and $R_S = R_S^{(1)}$.

Acknowledgments: This work is supported by the Ministry of Science, Technological Development and Innovation of the Republic of Serbia through project No. 451-03-34/2026-03/200162.

References

Galijaš S M D and Poparić G B (2026) *Rom. Rep. Phys.* **78** 1

Galijaš S M D and Poparić G B (2019) *Phys, Scr.* **94**, 025401.

Galijaš S M D, Nedeljković N N and Majkić M D (2011) *Surf. Sci*. **605**, 723.

PHONON-INDUCED WAKE POTENTIAL IN A GRAPHENE-HBN-GRAPHENE HETEROSTRUCTURE

Ivan Radović[1], Lazar Karbunar[2], Vito Despoja[3] and Zoran L. Mišković[4]

[1]*Department of Atomic Physics, Vinča Institute of Nuclear Sciences - National Institute of the Republic of Serbia, University of Belgrade, P.O. Box 522, 11001 Belgrade, Serbia*

[2]*School of Computing, Union University, Knez Mihailova 6, 11000 Belgrade, Serbia*

[3]*Centre for Advanced Laser Techniques, Institute of Physics, Bijenička 46, 10000 Zagreb, Croatia*

[4]*Department of Applied Mathematics, and Waterloo Institute for Nanotechnology, University of Waterloo, Waterloo, Ontario, Canada N2L 3G1*

iradovic@vin.bg.ac.rs

In our previous publications (Despoja *et al.* 2019, Kalinić *et al.* 2021 and 2024), we studied the wake effect in a sandwich-like structure consisting of two doped graphene sheets, separated by an insulating layer (Al_2O_3, SiO_2, and HfO_2), which is induced by an external charged particle moving parallel to the mentioned structure. In all those publications, we considered only isotropic insulators between two graphene sheets. We also assumed a zero gap between graphene and insulator to simplify calculations.

In this work, we investigate for the first time the wake effect generated by an external charged particle moving parallel to the heterostructure composed by two graphene layers separated by an insulating slab that exhibits anisotropy of a uniaxial crystal. We choose an anisotropic layer of hexagonal boron nitride (hBN) because van der Waals heterostructures based on graphene and hBN layers with different stacking modes currently attract a great deal of interest owing to their potential applications (Kalinić *et al.* 2026, Song *et al.* 2026 and Wang *et al.* 2026).

We evaluate the wake potential (the total potential in the plane of the upper graphene sheet) for a charged particle moving at the sub-threshold speed for the wake effect in a single, free graphene. The response function of each graphene is obtained using the dynamic polarization function of doped graphene within the random phase approximation for its π electrons described as Dirac's fermions (Allison *et al.* 2009). The response of the anisotropic hBN layer is described by a

diagonal dielectric tensor consisting of the in-plane and out-of-plane components (Caldwell *et al.* 2014).

The first objective is to explore the effects of anisotropy of hBN on the wake potential in a graphene-insulator-graphene composite system. In particular, we examine the plasmon-phonon hybridization in the range of frequencies corresponding to the Reststrahlen bands of hBN, where the phonon modes of this material exhibit hyperbolic dispersion. We compare the results for the wake potential in the cases of the anisotropic and fictitious isotropic (with the dielectric functions equal to the in-plane or out-of-plane components) hBN layers.

The second objective is to explore the effects of the graphene-insulator distance on the wake potential in a graphene-hBN-graphene nanostructure. The results for the wake potential are compared in the cases of the zero and non-zero gaps between graphene and hBN surface.

References

Allison K F, Borka D, Radović I, Hadžievski Lj and Mišković Z L (2009) *Phys. Rev. B*, **80**, 195405.

Caldwell J D, Kretinin A V, Chen Y, Giannini V, Fogler M M, Francescato Y, Ellis C T, Tischler J G, Woods C R, Giles A J, Hong M, Watanabe K, Taniguchi T, Maier S A and Novoselov K S (2014) *Nat. Commun.*, **5**, 5221.

Despoja V, Radović I, Karbunar L, Kalinić A and Mišković Z L (2019) *Phys. Rev. B*, **100**, 035443.

Kalinić A, Radović I, Karbunar L, Despoja V and Mišković Z L (2021) *Phys. E*, **126**, 114447.

Kalinić A, Radović I, Karbunar L, Despoja V and Mišković Z L (2024) *Nanomaterials*, **14**, 1951.

Kalinić A, Despoja V, Radović I, Karbunar L and Mišković Z L (2026) *Phys. Rev. B*, **113**, 155408.

Song G, Chen Y, Wu C, Zhang Z, Deng S and Chen J (2026) *IEEE Electron Device Lett.*, **47**, 164.

Wang R, Wang W, Zhou H, Zhang Q, Liang L, Luo X, Li W and Liu F (2026) *Mater. Sci. Eng. B*, **328**, 119389.

ION BEAM ANALYSIS USING RAINBOW SCATTERING IN CHANNELING

Nikola Starčević and Srđan Petrović

Vinča Institute of Nuclear Sciences

nikolas@vin.bg.ac.rs

We present a novel ion beam analysis approach based on rainbow scattering in channeling through very thin crystals. The method relies on the morphological analysis of rainbow lines generated in the angular distributions of MeV protons transmitted through crystalline channels. Using crystal rainbow theory and numerical simulations, we investigated proton channeling through cubic crystals with body-centered cubic, face-centered cubic, and diamond cubic structures in their major crystallographic orientations. The analysis demonstrates that the morphology of the primary rainbow line is uniquely determined by the geometry of the crystal channel, enabling reliable identification of crystal orientation. In addition, the angular position of the secondary rainbow line exhibits strong dependence on the crystal atomic number and channel geometry, providing a criterion for distinguishing between different crystal types. By combining the information carried by the inner and outer rainbow lines, simultaneous determination of crystallographic orientation and crystal structure becomes possible. The obtained results show that rainbow scattering in channeling can serve as an efficient ion beam analysis technique for characterization of very thin crystals, while also providing a framework for future experimental investigations of crystal structures and ion–crystal interaction phenomena.

OPTICAL AND ELECTRICAL PROPERTIES $LaMnO_3$+1%Er_2O_3 FILMS

N. A. Bosak[1]*, A. N. Chumakov[1], L. V. Baran[2], V. V. Malyutina-Bronskaya[3], A. A. Shevchenok[4], A. V. Buka[5], A. S. Kuzmitskaya[3], N. V. Podvitsky[6]

[1] *B.I. Stepanov Institute of Physics of the National Academy of Sciences of Belarus, Minsk*

[2] *Belarusian State University, Minsk*
[3] *State Scientific and Production Association "Optics, Optoelectronics, and Laser Technology", Minsk*

[4] *Belarusian State Agrarian Technical University, Minsk*

[5] *Belarusian State Technological University, Minsk*

[6] *JSC "Peleng", Minsk*

n.bosak@ifanbel.bas-net.by

Currently, a relevant topic remains the investigations of the properties of thin films based on the $LaMnO_3$ compound obtained by various methods, which have properties close to bulk ceramic materials, since the structural, electrical and optical properties of thin films are determined by the technological modes of the synthesis method.

Experimental. $LaMn_4O_3$+1%Er_2O_3 thin films were deposited by high-frequency laser sputtering of ceramic targets in vacuum (p = $2.2 \cdot 10^{-2}$ mm Hg) on an experimental neodymium glass laser setup (wavelength λ = 1.06 μm, laser pulse duration at the half-height τ ~ 85 ns) on glass and silicon substrates. To obtain macroscopically homogeneous films, the laser radiation power was q = 77 MW/cm^2 with a pulse repetition rate f ~ 10-12 kHz [1]. The current-voltage characteristics of the $LaMn_4O_3$+0.5%Er_2O_3/Si structures have been measured using a Keithly 2450 set-up under laser radiation (with wavelengths from 405 to 1064 nm) with a common fiber optic output and a calibrated radiation power of about 2 mW.

Results and Discussion. $LaMn_4O_3$+1%Er_2O_3 thin films have a developed surface. The average height of the surface relief of the films on Si is 65 nm. A significant number of formations in the form of drops with a diameter of 0.2-5.0 μm and a height of up to 800 nm were observed (Fig. 1, a). The transmittance T of the laser-

deposited $LaMn_4O_3$+1%Er_2O_3 film on Si in the near IR region of the spectrum (Fig. 1, b) sharply increases from 0.8% at a wavelength of λ = 968 nm to 58% at a wavelength of λ = 1227 nm. The dependence of the reflectivity *R* of the film on wavelength has an oscillatory nature and reaches a maximum value of R_{max} = 24.3% at λ = 929 nm. When exposed to laser radiation with wavelengths from 405 nm to 1064 nm, photoconductivity is observed for all wavelengths. The maximum photoelectric effect is detected at an applied voltage of -20 V and +20 V. A positive value of spectral sensitivity is realized at a voltage of -20 V and a negative value of spectral sensitivity is observed at a voltage of +20 V.

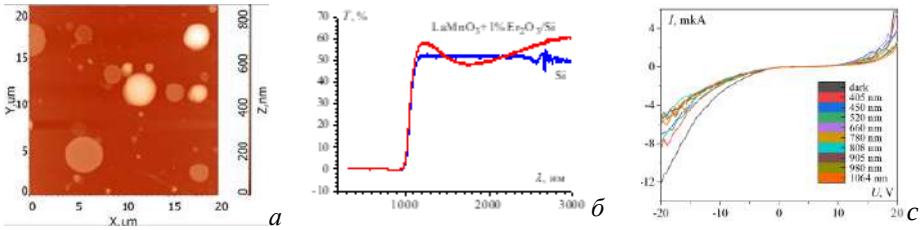

Figure 1: Atomic force microscopy images of the morphology (a), transmission spectra in the visible and near-IR regions (b), and the current-voltage characteristics in the dark and under laser radiation with different wavelengths of the $LaMnO_3$+1%Er_2O_3/Si structure (c).

The maximum value of the spectral sensitivity $S(\lambda)$ was 7 mA/W at a wavelength of 405 nm with a bias voltage of - 20 V. A small maximum of the $S(\lambda)$ dependence is also observed in the wavelength range from 600 to 1064 nm, which may be due to the presence of impurity states in the $LaMnO_3$ film, including Er^{3+} ions. The photoconductivity of the $LaMnO_3$+1%Er_2O_3/Si structure is due to the mechanisms of capture and recombination of minority charge carriers at impurity levels in the $LaMnO_3$+1%Er_2O_3 film.

Conclusions. $LaMn_4O_3$+1%Er_2O_3 thin films produced by high-frequency laser sputtering exhibit a developed surface structure and high transmittance (over 58%) in the infrared range. The $LaMnO_3$+1%Er_2O_3/Si structure exhibits a maximum spectral sensitivity of 7 mA/W at a wavelength of 405 nm and a bias voltage of - 20 V.

References

Chumakov A N, Avramenko V B and Bosak N A (2012) *Journal of Applied Spectroscopy*, **79**(2), 261.

BICHROMATIC LASER IMPACT ACTION ON OXYGEN-FREE COPPER IN AQUEOUS MEDIUM

Viacheslav Lychkouski[1], Alexander Chumakov[1], Vladimir Rogalin[2], Yury Khomich[2], Sergey Mikolutskiy[2], Viacheslav Zheleznov[2]

[1]*B. I. Stepanov Institute of Physics NASB, 220072, Nezavisimosti Ave. 68, Minsk, Belarus*

[2]*Institute for Electrophysics and Electric Power of the Russian Academy of Sciences, 191186, Dvortsovaya nab. 18, Saint Petersburg, Russia*

v.luchkouski@dragon.bas-net.by

In the context of searching for methods to improve the efficiency of laser impact action (laser shock peening), the possibility of laser impact treatment of materials (see Rogalin et. al. 2024, Sadhu et. al. 2022), using double nanosecond pulses with different wavelengths (see Min'ko et. al. 1994, Chumakov et. al. 2022) in aqueous medium was investigated. The experiments were conducted using an experimental setup consisting of two nanosecond Nd:YAG lasers generating pulses λ = 355 and 532 nm with durations of 18 ns and 15 ns, respectively, that were focused to 125 μm diameter spot with energy density ≈200 J/cm^2. A noticeable effect of water layer thickness and order of pulses with different wavelengths on size of laser craters on the copper surface was revealed. The proposed methods can be used to strengthen structural materials to improve the reliability of different machinery parts.

The effect of bichromatic (λ = 355 and 532 nm) nanosecond laser radiation on the oxygen-free copper sample under a layer of deionized water was studied with and without a protective coating. Without protective coating, a noticeable influence of bichromatic laser radiation pulses order on depth of craters on the copper sample's surface was established. The greatest depth was observed for 532 + 355 nm pulses order and 2 mm water layer (up to 16.5 μm against ~4.2 μm for different order). It is assumed that such strong influence of the pulses order for bichromatic laser irradiation can be caused by the highest transmission coefficient near the range of wavelengths, that 532 nm pulses belong. Considering the fairly high removal of material in the described method, it can be used for perforating metal layers or drilling micro-holes on the surface of structural materials.

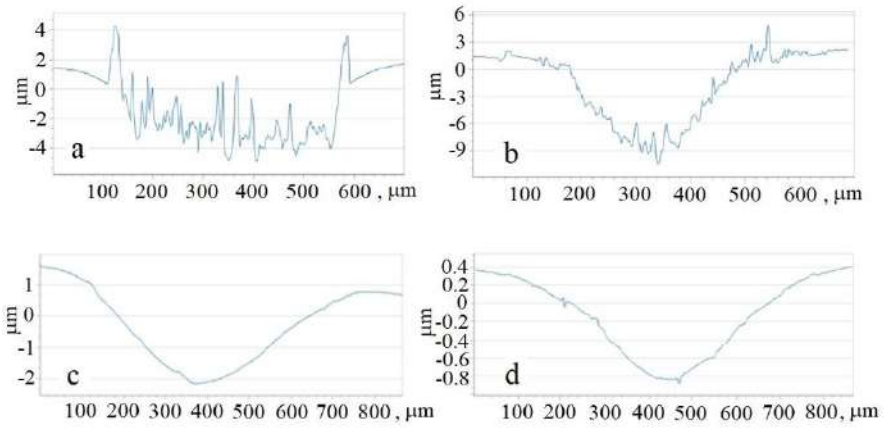

Figure 1: Profilometry of craters produced by 355+532 nm bichromatic laser irradiation (≈200 J/cm^2) of copper in 2 mm thick layer of water with (c, d) and without (a, b) protective coating. a, c – leading action of 355 nm laser pulses of bichromatic laser radiation; b, d – leading action of 532 nm laser pulses.

When vinyl tape was used as protective coating, the obtained results also shows that thickness of water layer and pulses order for bichromatic irradiation have effect on magnitude of the resulting impact action. The greatest obtained depth of a crater (about 3.7 μm) was observed with leading action of 355 nm pulses of bichromatic laser radiation and water layer thickness of 2 mm. It is worth noting that the applied technique is a development of the so-called laser shock peening – a popular promising technology used to strengthen the surface of structural materials and protect them from cracking. Moreover, unlike the classical method, the presented method involves the use of nanosecond pulses with relatively low energy (25 mJ per pulse).

References

Chumakov A N *et al.* (2022) *Technical Physics*, **67**(1), 16.

Min'ko L *et al.* (1994) *J. Appl. Spectrosc.*, **61**, 805.

Rogalin V E (2024) *Acta Astranautica*, **225**, 307.

Sadhu A *et al.* (2022) *Materials Science & Engineering*, **A 831**, 142238.

LIBS-BASED EVALUATION OF THERMAL ALTERATION IN PIG BONE VIA C/P EMISSION LINE RATIO: IMPLICATIONS FOR FORENSIC ANALYSIS

Milica Marković[1], Aleksandra Šajić[1], Dušan Dimić[1], Aleksandar Joksimović[1], Miroslav Kuzmanović[1]

[1] *Faculty of Physical Chemistry, University of Belgrade, Studentski trg 12 - 16, 11158 Belgrade, Serbia.*

milica.markovic@ffh.bg.ac.rs

Thermal alteration of bone is of considerable importance in forensic investigations because exposure to elevated temperatures induces physicochemical changes that can provide valuable information about burning conditions and postmortem events. Bone is a hierarchical composite material consisting of an organic matrix, primarily collagen, and an inorganic mineral phase dominated by carbonated hydroxyapatite. Since these components exhibit different thermal stabilities, heating may significantly modify their structural organization and elemental distribution, thereby affecting their spectroscopic signatures.

In this study, pig shoulder bone, a well-established analogue of human bone due to its similar composition and microstructure, was subjected to controlled thermal treatment at 100 °C and 200 °C for 5, 10, and 15 min. The samples were analyzed using laser-induced breakdown spectroscopy (LIBS) employing a Nd:YAG laser operating at 1064 nm with a pulse energy of 90 mJ. The analysis was focused on the C I 247.86 nm and P I 255.33 nm emission lines, which are associated with the organic and mineral fractions of bone, respectively. Their intensity ratio (C/P) was used as a spectroscopic indicator of thermally induced changes in the collagen–apatite system.

A systematic increase in the C/P ratio was observed with increasing temperature and exposure time, from 1.85 in the untreated sample to 17.70 after heating at 200 °C for 15 min (Fig. 1). Such behavior indicates progressive modification of the bone matrix resulting from dehydration, collagen degradation, lipid redistribution, and changes in the local environment of phosphate-containing

mineral components. Since phosphate species within hydroxyapatite are generally more thermally resistant than the organic constituents, the observed changes reflect disruption of the native collagen–apatite composite structure. The use of emission line intensity ratios minimizes fluctuations associated with laser–plasma interactions and improves the robustness and reproducibility of LIBS-based evaluation.

These findings demonstrate that the C/P ratio represents a sensitive spectroscopic marker of early thermal alterations in bone. The established correlation between thermal exposure conditions and LIBS response highlights the potential of this technique as a rapid, minimally destructive tool for the forensic characterization of thermally altered skeletal remains.

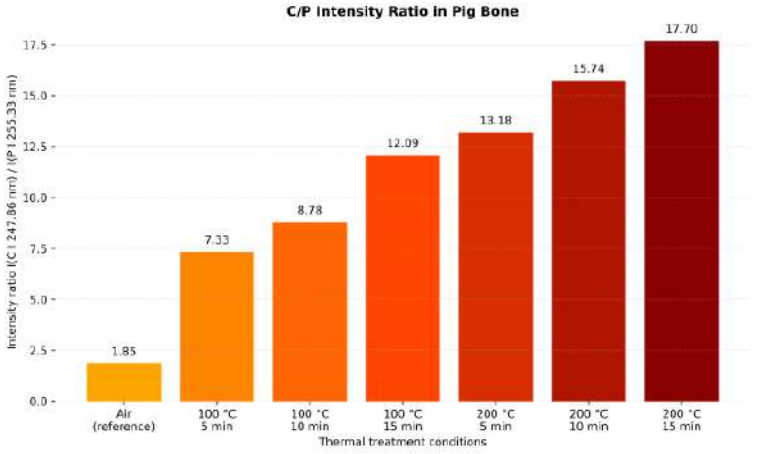

Figure 1: C/P intensity ratio in thermally treated pig bone (100–200 °C, 5–15 min).

References

Sullivan C H and Krueger H W (1981) *Nature*, **292**, 333.

Younesi M *et al.*(2011) *J. Mater. Eng. Perform*, **20**, 1484.

FABRICATION OF SnO_2/Si HETEROSTRUCTURES USING THE LASER-PLASMA DEPOSITION METHOD: OPTICAL AND ELECTRONIC PROPERTIES

M. V. Puzyrev, F.F. Komarov, O.V. Milchanin, I.S. Rogovaya, I. N. Parkhomenko

A.N. Sevchenko Institute of Applied Physical Problems of Belarusian State University, Minsk, Belarus

puzyrev@bsu.by

Recently, heterojunctions based on metal-oxide nanostructures and silicon have attracted significant scientific interest due to their potential wide range of applications in photosensors, telecommunication systems, robotics, and biomedical devices. Among oxide semiconductors, particular attention is devoted to SnO_2 (n-type, Eg ~ 3.6 eV, high chemical stability in contact with silicon).

For the deposition of tin films (10–30 nm) onto silicon wafers, a pulsed YAG:Nd^{3+} laser (model LS-2137, manufactured by Lotis–TII, Belarus–Japan) with a wavelength $\lambda = 1064$ nm and a pulse duration $\tau \sim 20$ ns (full width at half maximum) was employed. The laser pulse repetition rate was 5 Hz, and the power density of the incident laser radiation on the target was 3.8×10^8 W/cm². The experiments were conducted under vacuum conditions with a residual gas pressure of $\sim 10^{-4}$ Pa. Temporal current variations on the substrate were monitored using a Tektronix TDS 2022B oscilloscope. A detailed schematic of the experimental setup is presented in our previous work (see Komarov F et al. 2024). Subsequently, the deposited tin films on silicon wafers were annealed in air using two-step thermal treatment. The first annealing step at 200 °C ensured oxygen saturation of the tin film and the formation of oxide phases. The second step at 500 °C was employed to crystallize the oxidized layers.

Based on the results of structural investigations, it was established that after the two-step thermal treatments, a crystalline SnO_2 phase with tetragonal symmetry and space group $P4_2/mnm$ is formed. The lattice parameters were found to be a = 4.716 Å and c = 3.155 Å.

Figure 1a shows the photoluminescence spectra of ultrathin (20 nm) SnO_2 layers on silicon. The spectra consist of a set of narrow bands in the ultraviolet (UV) region (365–400 nm) and a broad band with a maximum in the blue-green region (500 nm), which is attributed to defect states. The luminescence of this broad band is observable even at room temperature. The narrow UV bands exhibit energies lower than the bandgap width of SnO_2 (Eg = 3.596 eV), indicating an impurity-related nature of the luminescence—namely, conduction-band-to-acceptor and/or donor-to-valence-band transitions. (see Li Y*et al.* 2012).

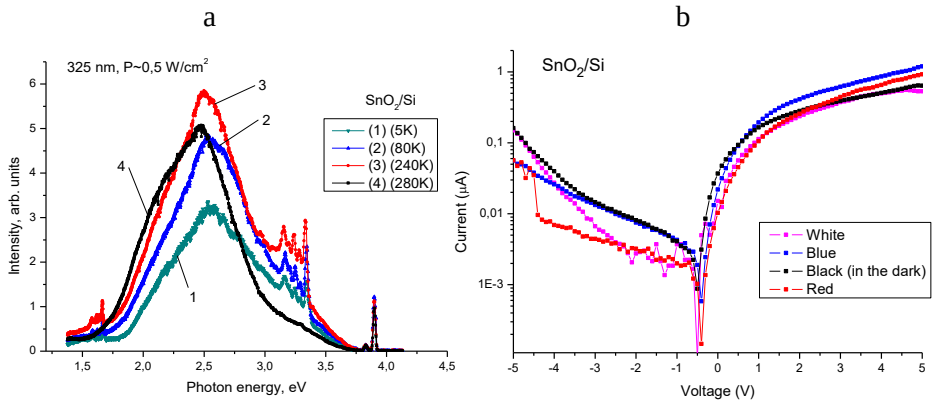

Figure 1: Photoluminescence spectra (a) measured at various recording temperatures and current–voltage characteristics (b) for the SnO_2/Si heterostructure.

From electrophysical measurements, it follows that the current–voltage characteristics of the SnO_2/Si heterostructure (Figure 1b) exhibit a pronounced diode-like behavior, which is consistent with the n-type conductivity of the SnO_2 film on p-type silicon. The current–voltage dependence across the SnO_2 layer surface between metal contacts is nearly linear in the range from –5 V to +5 V. The average sheet resistance was found to be 245.27 kΩ. The electrical conductivity of the SnO_2 film is 54.36 S/cm, which corresponds to a charge carrier concentration on the order of 10^{16}–10^{17} cm^{-3}, depending on their mobility.

References

Komarov F *et al.* (2024) *SPIG 2024*, 103, 81.

Li Y, Yin W *et al.* (2012) *NPG Asia Mater*, **4**, 1.

HEAVY-PARTICLE AVERAGED PSEUDOPOTENTIAL FOR BUFFER-GAS-DOMINATED HIGH INTENSITY LASER GENERATED PLASMAS: LASER-ENERGY SCALING AND COULOMB TAIL ANALYSIS

Nenad M. Sakan[1], Biljana Stankov[1], Vladimir A. Srećković[1], Veljko Vujčić[2], and Zoran Simić[2]

[1]*University of Belgrade, Institute of Physics Belgrade, PO Box 57, 11001 Belgrade, Serbia*

[2]*Astronomical Observatory, Volgina 7, 11060 Belgrade, Serbia*

nsakan@ipb.ac.rs

Laser-induced breakdown spectroscopy (LIBS) could be used for the analysis of organic-rich soils, it produces a transient plasma plume whose early-time expansion is dominated by the ambient buffer gas - helium or argon - with trace contributions from soil-derived light elements (H, C, N, O) (Sakan *et al.* 2023, Stankov *et al.* 2022). This has led to the conclusion to investigate a high intensity laser generated plasma behavior under similar compositions. A realistic electron-heavy-particle scattering potential for quantitative Stark broadening and transport diagnostics requires going beyond the simple Debye-screened Coulomb form to account for the norm-conserving pseudopotential core, angular-momentum-dependent nonlocal corrections, and temperature-dependent valence-electron screening.

We apply the pseudopotential averaging method of Sakan *et al.* 2023 to five-component plasma mixtures (buffer gas at 85% by number, with H 10%, C 3%, N 1%, O 1%), at high intensity laser generated plasma conditions T_e = 50 kK (4.31 eV) and $n_e = 5\ 10^{19}$ cm^{-3}. For each element, angular momentum channel potentials (l = 0 - 3) are reconstructed from UPF Kleinman-Bylander projectors (Hamann *et al.* 1979) and Boltzmann-averaged at the plasma temperature. Saha ionisation equilibrium determines the per-species populations, and the valence-electron Hartree screening correction is computed via the Numerov-Schrödinger-Poisson chain. The number-density weighted average over all heavy-particle species yields the effective single-species potential $V_{\mathrm{avg}}^{\mathrm{heavy}}(r)$.

A laser-pulse-energy scaling model is introduced, linking E_{pulse} to (T_e, n_e) through power-law relations $T_e \propto E^{0.4}, n_e \propto E^{0.8}$ with a reference point at $= 100\ mJ$. This enables the prediction of $\langle Z \rangle$ and $V_{\text{avg}}^{\text{heavy}}(r)$ across $= 10 - 200\ mJ$. Free-electron Debye screening is applied to $V_{\text{avg}}^{\text{heavy}}$, giving the externally screened potential $V_{\text{Debye}}(r) = V_{\text{avg}}^{\text{heavy}}(r) exp(-\kappa_D r)$. The Debye length at nominal conditions is $\lambda_D \approx 41 a_0$, large compared to the pseudopotential well scale ($\sim 1 - 2 a_0$), confirming that intrinsic Hartree valence-electron screening dominates over classical free-electron screening.

An automated Coulomb-tail fitting algorithm extracts the effective charge Z_{eff} from the asymptotic behaviour $V(r) \to -2\, Z_{\text{eff}}/r$ (Rydberg units). The Saha-derived mean charge $\langle Z \rangle_{\text{Saha}}$ serves as the convergence target for the automated detection of the asymptotic region. The tail-fitted Z_{eff} matches $\langle Z \rangle_{\text{Saha}}$ within 1% at the nominal 100 mJ , and the Pearson correlation across all pulse energies is r = 0.986.

The computed $V_{\text{avg}}^{\text{heavy}}(r)$ and $V_{\text{Debye}}(r)$ provide realistic scattering centres for electrontransport, Stark-broadening, and line-shape calculations across the full LIBS operating range. All computations are performed with the D_plas_V code (Hamann *et al.* 1979, Sakan *et al.* 2023).

References

Hamann D R, Schlüter M and Chiang C (1979) *Phys. Rev. Lett.*, **43**, 1494.

Sakan, N M, Srećković V A, Stankov B and Simić Z (2023) *Contrib. Astron. Obs. Skalnaté Pleso*, **53**, 101.

Stankov B, Ivković M and Kuzmanović M (2022) *Publ. Astron. Obs. Belgrade*, **102**, 239.

GRAPHENE PROPERTIES INFLUENCE ON LIBS

Nataša Simić[1] and Milivoje Ivković[2]

[1]*Department of Physics, University of Novi Sad, Trg Dositeja Obradovića 4, 21000 Novi Sad, Serbia*

[2]*Institute of Physics, University of Belgrade, P.O.Box 56, 11080 Belgrade, Serbia*

natasa.simic@df.uns.ac.rs

The importance of graphene properties is clearly illustrated by the fact that the authors obtained the Nobel Prize in 2010 for this subject. The properties of graphene are important in photonics applications also. In areas like Surface Enhanced Raman Scattering (SERS) and Graphene-Enhanced Fluorescence (GEF), the enhancement relies heavily on near-field electromagnetic effects and efficient charge transfer at the 2D interface. On the contrary, applications of graphene in Laser Induced Breakdown Spectroscopy (LIBS) are very rare. The graphene oxide, GO, is used for the Dispersive Micro Solid Phase Extraction DμSPE with LIBS for detecting trace metal ions in water samples. In this method, after adsorption, the GO (with the retained analytes) is isolated and then analyzed by LIBS, see Cardoso et al, 2024. In another application, Stefanuk et al. reported sensitivity gains by transferring ~ 6 – 14 graphene layers onto glass before using 355 nm LIBS, see Stefanuk et al., 2020.

In this work, we analyzed requirements for possible LIBS signal enhancement by comparing spectra emitted from the same oil type positioned on the surface of the silicon wafer with and without a few layers of graphene. For analysis of the composition of the different oil types (sunflower, olive, machine...) we used LIBS with the various wavelength ns lasers. Having in mind that spectral line intensities depend on oil film thickness, special care was taken to obtain the same oil film thickness on the bare wafer and on the graphene layers. Various parameters influencing LIBS performance, such as graphene's high thermal conductivity, low absorption and fragility, as well as surface plasmon resonances, are studied.

References

Cardoso AT *et al.* (2024) *Molecules*, **29**, 3661.

Stefanuk B *et al*. (2020) *Spectrochimica Acta Part B*, **167**, 105823.

Section 3.

LOW TEMPERATURE PLASMAS

QUANTIFICATION OF GASEOUS SPECIES: RELEVANT SPECTROSCOPIC TECHNIQUES AND THEIR APPLICATION TO PLASMA-BASED GAS CONVERSION

Nikolay Britun

Centre for Low-temperature Plasma Sciences (cLPS), Nagoya University, Japan

britun@plasma.engg.nagoya-u.ac.jp

The methods of plasma diagnostics, especially those relying on optical spectroscopy, provide flexible possibilities for determination of the various plasma parameters or monitoring of the important plasma processes in both fundamental research and applications (see Britun 2026). Some of the widespread plasma parameters accessible by optical spectroscopy are: the electron density (see Nikiforov *et al.*, 2015) and energy distribution, the electron temperature (see Zhu and Pu 2010), the electric field (see Gavrilenko *et al.*, 2006) the density of the ground and metastable states of heavy species (such as atomic and molecular neutrals and ions, see Britun *et al.*, 2015 and Hnilica *et al.*, 2020), the velocity distribution function of these species, the ro-vibrational excitation of molecules, etc. Optical spectroscopy is a powerful tool which can be used for widening our understanding of the related plasma processes, for providing the plasma modelling with required input parameters, as well as for improving various plasma processes, such as film deposition, dry etching, gas conversion, and others.

This talk overviews the non-intrusive spectroscopy methods suitable for quantitative measurements of the density of heavy gaseous species in various discharges. A special attention is given to the techniques relying on optical emission spectroscopy (namely line ratio methods) and laser-based spectroscopy (namely single- and two- photon absorption techniques). It is shown that using these groups of techniques a reliable diagnostics of ground state and metastable species in plasma can be performed, especially when the number of suitable absorption transitions is limited by the dipole selection rules. The typical calibration methods for particle density determination, such as those based on single-photon (emitted by lasers or low-current light sources) and two-photon (emitted by lasers) absorption are also discussed.

The multiple examples given in the talk serve for a better understanding of non-intrusive optical diagnostic methods. These examples are mainly related to the greenhouse gas conversion in low-temperature plasmas, involving the microwave (see Chen *et al*., 2021), spark (see Britun *et al*., 2021), arc as well as He-based (see Mathieu *et al.*, 2026) and water-contacting (see Gromov *et al.*, 2021) nanosecond repetitive discharges. For a wider understanding of the topic, the results also illustrate the possibilities for quantitative measurements of the ground state density of F, H, O atoms (see Ribeiro *et al.*, 2026) as well as Cl and P atoms, selected metal neutrals and ions (such as Ti, Ti^+, W, W^+, etc., see Britun *et al.*, 2015 and Hnilica *et al.*, 2020) and some molecular species.

References

Britun N (2026) *J. Phys. D: Appl. Phys.*, **59**, 053002.
Nikiforov A, Leys C, Gonzalez M, Walsh J (2015) *Plasma Sourse Sci. Technol*., **24**, 034001.
Zhu X M and Pu Y K (2010) *J. Phys. D: Appl. Phys*., **43**, 403001.
Gavrilenko V (2006) *Instrum. Exp. Tech*., **49**, 149.
Britun N, Palmucci M, Konstantinidis S, Snyders R (2015) *J. Appl. Phys*., **117**, 163302.
Britun N, Palmucci M, Konstantinidis S, Snyders R (2015) *J. Appl. Phys*., **117**, 163303.
Hnilica J, Klein P, Vašina P, Snyders R, Britun N (2020) *J. Appl. Phys*., **128**, 043303.
Hnilica J, Klein P, Vašina P, Snyders R, Britun N (2020) *J. Appl. Phys*., **128**, 043304.
Chen G, Snyders R and Britun N (2021) *Journal of CO_2 Utilization*, **49**, 101557.
Britun N, Gamaleev V, Hori M (2021) *Plasma Sources Sci. Technol*., **30**, 08LT02.
Mathieu P, Mo M K T, Hori M *et al.* (2026) *Plasma Sources Sci. Technol*., (submitted).
Gromov M, Leonova K, De Geyter N *et al.* (2021) *Plasma Sources Sci. Technol*., **30**, 065024.
Ribeiro M, Mo M K T, Hori M, Silva T *et al.* (2026) *Plasma Sources Sci. Technol*, (submitted).

A MAGNETIC FIELD INFLUENCE ON STRUCTURE OF VOLUMETRIC AND SURFACE GAS DISCHARGES

Yu. Akishev[1], N. Dyatko[1], I. Kochetov[1], A. Petryakov[1],C. Zhang[2], T. Shao[2]

[1]*State Research Center of Russian Federation - Troitsk Institute for Innovative and Fusion Research, Joint-Stock Company, Moscow, Troitsk, Russia*

[2]*Institute of Electrical Engineering, Chinese Academy of Sciences, Beijing, China*

akishev@triniti.ru

The spatial structure of gas discharge affects the spatial distribution of energy release into the plasma and, consequently, the uniformity of the outcome plasma parameters.

For many applications using plasma to condition surfaces or volumes, uniformity of the final treatment is a key factor. Thus, the development of methods ensuring both the retention of plasma in a diffuse form as well as an effective impact on its constricted form aimed to smooth out the plasma parameters in the treatment area is a demanded task.

One of the promising ways to solve this problem is the using a magnetic field. The influence of a magnetic field on the discharge plasma can occur in two ways:

1) force action on the plasma as a whole like on a conductor with current due to Ampere force;

2) the effect of the Lorentz force on electrons, which leads to the Larmor rotation of electrons and therefore limits the energy got by them from an electric field.

The Larmor rotation dramatically changes the electron energy distribution function and, consequently, the transport and kinetic processes involving electrons. Insight in behavior of plasma properties under magnetic field helps to find out the optimal regimes for specific plasma processing.

This report provides an overview of the experimental and theoretical works devoted to the influence of longitudinal and transverse magnetic fields on volumetric and surface discharges at pressure from 10 Torr up to 1 atmosphere.

The information can be of interest for scientists dealing with plasma chemistry application.

This report was prepared within the framework of international cooperation between the Russian Science Foundation (grant No. 25-49-00039) and the National Foundation for Natural Sciences of China (grant No. W2412070)

PLASMA PHYSICS ACROSS SCALES: FROM STREAMER PHYSICS TO TERRESTRIAL GAMMA-RAY FLASHES

Christoph Köhn[1,2], Pierre Gourbin[2], Saša Dujko[3], Mathias Gammelmark[4], Sven Karlsson[4], Angel Ricardo Jara Jimenez[5], Morten Westermann[2], Hannah van Gemert[2] and Elloise Fangel-Lloyd[2,5]

[1]*Department of Physics, Technical University of Dortmund*

[2]*Department of Space Research and Technology, Technical University of Denmark*

[3]*Institute of Physics, University of Belgrade*

[4]*Department of Applied Mathematics and Computer Science, Technical University of Denmark*

[5]*Danish Meteorological Institute*

christoph.koehn@tu-dortmund.de

Lightning is a multiscale phenomenon bridging several length and time scales, from the nanoscale motion of electrons to the kilometer-long and millisecond-lasting lightning channels. It is associated with the emission of terrestrial gamma-ray flashes (TGFs), gamma-ray glows (GRGs) and flickering gamma-ray flashes (FGFs), beams of energetic X- and gamma-rays with energies of up to 40 MeV, making them the highest natural phenomena from Earth with energies beyond those of radioactive decay chains, see Marisaldi *et al.* 2024 and Köhn *et al.* 2025 and for more details.

In this presentation, we will provide an overview of the various stages of lightning, from streamer discharges as the first stage (Fig. 1) to the production of high-energy particles in TGFs, GRGs, and FGFs (Fig. 2), as well as the current state of our research. We will discuss our recent effort on developing numerical tools to study discharges in various planetary environments (see Fangel-Lloyd *et al.* 2026a), the production of high-energy beams, their relation to lightning, as well as their effect on nature (e.g. atmospheric chemistry) and technology.

In the end, we will provide an overview of future projects and introduce the Horizon Europe Doctoral Network GRAIL (Gamma Radiation from the

Atmosphere for Investigation and Learning), which will study lightning and associated phenomena in more detail.

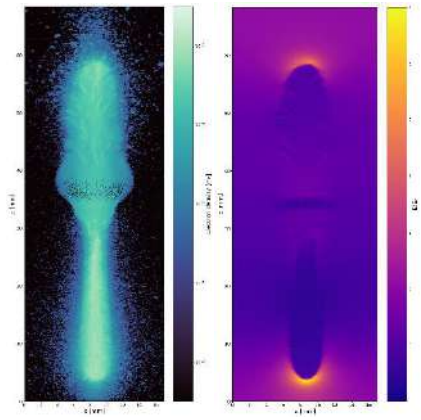

Figure 1: The electron density (left) and the electric field (right) after 2.676 ns of a streamer at ground pressure in an ambient electric field of 4.8 MV/m [Fangel-Lloyd *et al.* 2026b].

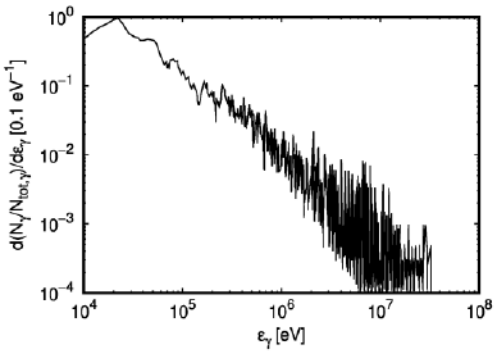

Figure 2: The typical energy distribution of a TGF from a lightning leader (simulated). Reproduced from Köhn *et al.* 2020 and Köhn *et al.* 2025.

References

Fangel-Lloyd E *et al*. (2026a) *Nature Scientific Reports*, In Press.

Fangel-Lloyd E *et al*. (2026b) *Comp. Phys. Comm.*, submitted.

Horizon Europe Doctoral Network GRAIL: https://grail.physik.tu-dortmund.de/

Köhn C *et al*. (2020) *Geophys. Res. Lett.*, **47**, e2020GL089749.

Köhn C *et al*. (2025) *Surv. Geophys.*, **46**, 753–821.

Marisaldi M *et al*. (2024) *Nature*, **634**, 57–60.

PLASMAS FOR THE GENERATION OF ION BEAMS: THEORY AND TECHNOLOGY

S. Gammino[1], G. Castro[1], L. Celona[1], and O. Leonardi[1]

[1]*Istituto Nazionale di Fisica Nucleare - Laboratori Nazionali del Sud, Via S. Sofia, 62, 95123 Catania, Italy*

gammino@lns.infn.it

High-current ion beams are gaining increasing attention as a key enabling resource for next-generation hadron therapy, medical isotope production, experimental nuclear physics, and radiation-damage studies in materials. While the achievable intensity of both continuous-wave (CW) and pulsed ion beams has steadily improved through advances in source design, RF/microwave coupling, magnetic confinement, and a more refined understanding of plasma parameters (electron temperature, density, ion confinement time), progress in predictive physics modeling has remained comparatively limited. In particular, self-consistent modeling of plasma kinetics, ionization balance, and transport processes in strongly magnetized, nonequilibrium plasmas is still an open challenge. For this reason, substantial effort is devoted to the development of advanced diagnostics, including Langmuir probes, optical emission spectroscopy, X-ray spectroscopy, and beam emittance and current measurements, since the extracted beam current and charge-state distribution are critically determined by plasma density, electron energy distribution function (EEDF), and confinement efficiency inside the ion source.

In this context, we focus on the development of Electron Cyclotron Resonance Ion Sources (ECRIS) and Microwave Discharge Ion Sources (MDIS). ECRIS devices exploit resonant electron heating at the cyclotron frequency in high magnetic fields (typically employing minimum-B configurations, according the so-called “High B mode” concept proposed by the INFN-LNS Ion Source Team in 1990 and demonstrated three years later) to produce high-density plasmas with hot electron populations, enabling efficient stepwise ionization and the generation of highly charged ions across a wide range of species. In contrast, MDIS operate at lower magnetic fields and power densities, favoring high-current extraction of low-charge-state beams with excellent stability, making them particularly suitable for proton and singly charged light-ion production. Finally, we outline

optimized operating regimes and design strategies—such as magnetic field topology, microwave frequency tuning, gas pressure control, and extraction optics—that enable the generation of intense, low-emittance, and stable ion beams.

MEASUREMENT OF PLASMA PARAMETERS DURING THE FORMATION OF THE LASER-INDUCED BREAKDOWN

M. Skočić, N. Nedić, L. Rajačić, D. Dojić and S. Bukvić

University of Belgrade, Faculty of Physics, Serbia

skocic@ff.bg.ac.rs

This paper presents a technique for measuring the temperature of a target material surface at the beginning of a Laser Induced Breakdown experiment, before the creation of plasma, see Fig 1. The experiment was conducted using a Nd:YAG laser at three different irradiances: 1.4×10^9, 3.2×10^{11}, and 3.7×10^{12} W/cm^2, at a residual atmosphere of 0.05 mbar.

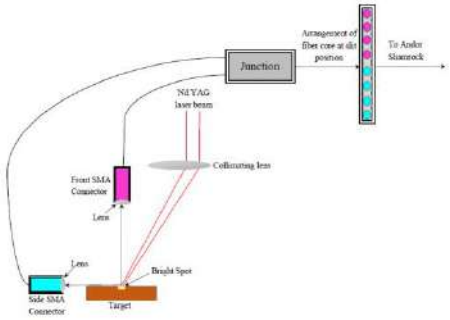

Figure 1: The experimental setup involved illuminating the target with the 1064 nm Nd:YAG harmonic while monitoring the bright area using two legs of a bifurcated optical cable. The purple leg is used to measure the surface temperature, while the blue one is used to monitor the creation of the plasma.

The results show that the temperature of the copper surface is in the range of 7400-11200 K (Skočić *et al.* 2022), which is consistent with the most data available in the literature for the critical temperature of copper (Horvath 1973). The relaxation time of electron and ion temperature necessary to achieve equilibrium via elastic collisions is estimated to be less than 1 ns, while the relaxation time among the internal electronic degrees of freedom via inelastic collisions is estimated to be below 10 ps. Following the creation of the plasma,

the temperature significantly increases, reaching values over 50000 K (Skočić *et al.* 2022). It is worth noting that all temperature measurements were obtained by analyzing the continuous spectra emitted from the bright spot illuminated by the laser, see Fig 2.

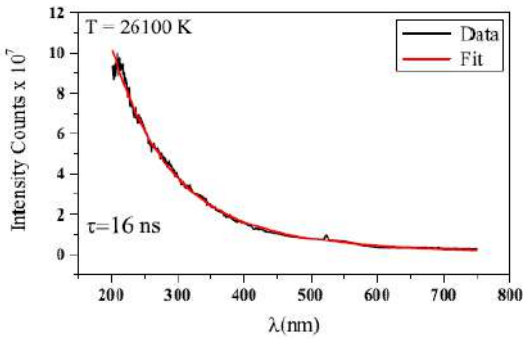

Figure 2: Plasma temperature obtained from the Planck's spectrum.

Additionally, electron number density and temperature were measured inside the plasma measuring attenuation of the two lasers HeNe at 633 nm and the diode laser at 400 nm wavelength, applied side on. Assuming that inverse bremsstrahlung is the dominant absorption mechanism (Dalgarno and Lane 1966) and comparing absorption coefficients for the two lasers, we derived values for electron density and electron temperature inside the plasma. Electron density and temperature at 150 μm from the target are 3.5x1025 m-3 and 19000 K (Nedić *et al.* 2022), respectively.

References

Dalgarno A and Lane N F (1966) *Astrophysical Journal*, **145**, 623.

Horvath A L (1973) *Journal of Chemical Education*, **50**, 335-336.

Nedić N V, Bukvić S, Dojić D, Rajačić L and Skočić M (2022) *Plasma Sources Science and Technology*, **10**, 31.

Skočić M, Dojić D and Bukvić S (2022) *Physical Review E*, **4**, 105.

MODELING PERSPECTIVES ON NON-THERMAL PLASMAS FOR IN-ATMOSPHERE PROPULSION AND ACTIVE FLOW CONTROL

Arturo Popoli, Fabio Ragazzi, Giorgio Mongaretto, Andrea Cristofolini

Department of Electrical, Electronic and Information Engineering "Guglielmo Marconi", University of Bologna, 40136, Bologna, Italy

arturo.popoli@unibo.it

Non-thermal atmospheric-pressure plasmas are increasingly investigated for aerospace applications, including electrohydrodynamic (EHD) propulsion and plasma actuators for active flow control. In both cases, the macroscopic effect of the device results from a strongly coupled sequence of mechanisms: electron-impact ionization, charged-particle transport, plasma chemistry, space-charge distortion of the electric field, surface charging and electrohydrodynamic momentum transfer.

This contribution discusses modeling strategies for corona and dielectric barrier discharges relevant to in-atmosphere propulsion and active flow control. Starting from the hierarchy of plasma models, the contribution reviews the role of kinetic, fluid and hybrid approaches, with emphasis on drift-diffusion plasma fluid models for atmospheric-pressure devices. In this framework, charged species are described by continuity equations coupled to electrostatics,

$$\begin{cases} \frac{\partial n_s}{\partial t} + \nabla \cdot \mathbf{\Gamma}_s = \Omega_s + S_{ph}, \\ \nabla \cdot (\varepsilon_r \mathbf{E}) = \frac{\rho}{\varepsilon_0}, \\ \nabla_\Sigma \cdot (\varepsilon_r \mathbf{E}) = \frac{\sigma}{\varepsilon_0}, \ \frac{\partial \sigma}{\partial t} = \mathbf{J} \cdot \hat{\mathbf{n}}. \end{cases} \quad (1)$$

Although compact in form, this system is numerically challenging because of stiffness, nonlinear chemistry, and the global coupling introduced by Poisson's equation. The open-source plasma solver Merlino2D (https://github.com/PTL-Unibo/Merlino2D), developed by the Plasma Technology Laboratory of the University of Bologna, is introduced.

Merlino2D solves two-dimensional drift-diffusion-reaction problems on triangular meshes, coupled to Poisson's equation and, when needed, to surface-charge and photoionization models. The governing equations are formulated as a monolithic differential-algebraic system. Merlino2D is also coupled with the open-source LisbOn KInetics Boltzmann solver (LoKI-B) (Tejero-del-Caz A et al. 2019).

Focusing on recent applications, corona discharges in wire-grid (see Fig. 1) and blade-collector configurations are discussed as examples where simulations help interpret current plateaus, collector shielding and the onset of back discharge. For active flow control, dielectric-barrier-discharge (DBD) actuators are considered, where AC excitation, surface charging and near-wall plasma dynamics determine the spatial and temporal structure of the electrohydrodynamic forcing.

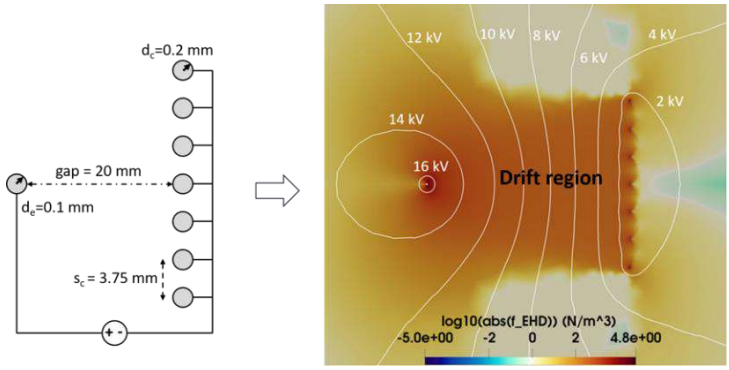

Figure 1: Simulation of the EHD force produced by a gridded-collector corona thruster.

Acknowledgements

Funded by the European Union

Funded by the European Union under Grant Agreement No. 101098900 — IPROP. Views and opinions expressed are however those of the author(s) only and do not necessarily reflect those of the European Union or the granting authority. Neither the European Union nor the granting authority can be held responsible for them.

References

Tejero-del-Caz A *et al*. (2019) *Plasma Sources Science and Technology*, **28**, 043001.

ATMOSPHERIC PRESSURE PLASMA JET – FROM DISCHARGE PROCESSES TO CONTROLLED BIOLOGICAL RESPONSE

Aliaksandra Kazak[1] and Leanid Simonchik[1]

[1]*Institute of Physics of NAS of Belarus*

a.pavlova@ifanbel.bas-net.by

Atmospheric pressure plasma jets (APPJs) represent a versatile tool of plasma physics, chemistry, and medicine. This work provides an overview of plasma-induced effects, spanning from the fundamental physics of non-equilibrium discharge generation to the controlled biological responses observed in microbiological systems. APPJs operating in inert gases or ambient air, generate highly non-equilibrium conditions where the electron temperature (T_e ~1-5 eV) vastly exceeds the gas temperature (T_g). This separation allows the production of reactive particles without causing thermal damage to sensitive biological objects or living tissue. However, achieving high reproducibility in plasma treatment remains a significant challenge due to the complex, non-linear coupling between the discharge electrical parameters, ambient air diffusion, and the target's electrical impedance. Understanding the physical basis of plasma treatment dosing requires deep insights into the plasma chemistry and self-sustaining mechanisms of both DC and pulsed discharges.

The device (see Kazak & Simonchik, 2024) utilizes a non-thermal atmospheric pressure plasma jet generate from an atmospheric pressure glow microdischarge (APGD) operating in a DC mode. The discharge burns in an ambient air flow at rate of 3–5 l/min. The interelectrode gap of 0.5–1.0 mm at typical discharge currents of 20–40 mA and a discharge voltage of ~650 V. High-resolution optical emission spectroscopy combined with spectrum fitting (using SpecAir 3.0) shows that the electron temperature (T_e ~1 eV) significantly exceeds the vibrational (T_{vib}) and rotational (T_{rot}) temperatures, validating the highly non-equilibrium thermodynamic state (see Arkhipenko *et al,* 2012).

The gas-dynamic transport of the air plasma effluent into the environment triggers a gas-phase reaction cascade. While conventional barrier discharges are known to generate significant amounts of ozone, FTIR and UV absorption spectroscopies

confirms that air APGD operates in a strictly non-ozone regime. In the high-temperature zone of the discharge (Tg~2000 K), atomic oxygen rapidly reacts with nitrogen via non-thermal plasma-chemical pathways to prioritize the generation of nitric oxide (NO). In the low-temperature zone (<700K) of the jet, fast three-body reactions preferentially consume oxygen atoms to oxidize NO into nitrogen dioxide (NO_2), effectively suppressing O_3 formation. As the jet propagates and cools down to ambient temperatures, the coexistence of these primary nitrogen oxides with water vapor from the humid air flow drives the on-the-fly synthesis of stable gaseous nitrous acid (HNO_2) (see Kazak *et al,* 2024). Quantitative FTIR/UV establishes a robust chemical composition where reactive nitrogen species (RNS) dominate the active effluent, yielding concentrations of NO 500 ppm, NO_2 250 ppm, and HNO_2 50 ppm in out-put discharge cell. This specific kinetic route totally avoids the accumulation of aggressive nitric acid (HNO_3). The controlled composition of the RNS allows for the introduction of a definition of the plasma exposure dose as the number of RNS particles arriving at an object per unit of time (see Kazak & Simonchik, 2024).

On a molecular level, the biological response is mediated by biochemical inhibition of respiration rather than non-specific thermal or aggressive oxidative destruction. As detailed in the discussed mechanisms, the gas-phase flux of NOx rapidly diffuses through the cell envelope, displacing O2 from vital respiratory enzymes and halting bacterial energy metabolism (see Poole & Cook, 2000). This metabolic shutdown leads to rapid biofilm disruption and a multi-fold reduction in bacterial load. Concurrently, the tissue-protective and regenerative effects align with the well-established role of nitric oxide at physiological doses, which mitigates inflammatory cascades and promotes endothelial signaling pathways essential for accelerated epithelialization (see Pacher *et al*., 2007). This explains the different effect of the device on different biological objects.

References

Arkhipenko V I *et al*. (2012) *Eur. Phys. J. D,* **66**, 252.
Kazak A V *et al*. (2024) *Journal of Applied Spectroscopy,* **91**(3), 511-519.
Kazak A V & Simonchik L V (2024) *Plasma Medicine,* **14**, 45–54.
Pacher P, Beckman J S, Liaudet L (2007) *Physiol Rev.,* **87**(1), 315–424.
Poole R K, Cook G M (2000) *Adv. Microb. Physiol.,* **43**, 165-224.

APPLICATION OF ATMOSPHERIC PRESSURE PLASMA IN AGRICULTURE: WATER DECONTAMINATION AND ACTIVATION

Nikola Škoro[1], Olivera Jovanović[1], Desanka Topalović[1] and Nevena Puač[1]

[1]*Institute of Physics, University of Belgrade, Pregrevica 118, Belgrade, Serbia*

nskoro@ipb.ac.rs

Plasma treated liquids (PTL) have gained attention due to many possible applications that were investigated mostly at a laboratory level so far. This led to understanding most of the fundamental reactions and chemistry behind the plasma-liquid interaction and creation of Reactive Oxygen and Nitrogen species (RONS). Although recent results point the way towards possible use in water treatment and agriculture (e.g. Puač and Škoro 2025, Kumar *et al.* 2021) the potential for successful plasma application is inevitably linked to the ability of plasma systems to treat larger amounts of liquids along with production of suitable reactive chemistry. Such scaling-up of the plasma systems is usually foreseen through increase of the volume of produced PTL, but approaches to this could be different – e.g. it could be achieved by maximizing through recirculation of the liquid or by increasing flux of reactive species to minimize the treatment time per volume unit. As each application and plasma system requires specific approach, in this study we will evaluate the potential of the plasma system that could be used for agricultural applications – pesticide decontamination from agriculture outflow water and treatment of water for plant growth.

In our experiment the plasma source for water treatment is a multi-pin electrode atmospheric pressure plasma jet operating with Ar as a working gas. The pin-type electrodes are connected to a 350 kHz sine wave signal while grounded electrode is the liquid. The excitation signal enables creation of streamers that operate in contact with water surface. In order to characterize the plasma, we performed optical emission spectroscopy, plasma imaging and electrical characterization of the system. The diagnostics provided us information on plasma chemistry and power delivered to the sample. This also allowed us to study the stability of plasma operation and the properties of created PTL. Regarding decontamination of pesticides, we used 2 different insecticides and followed degradation kinetics.

In order to investigate different scaling-up approaches we treated the sample volumes from 15 ml up to 2 l, also adding a sample recirculation system.

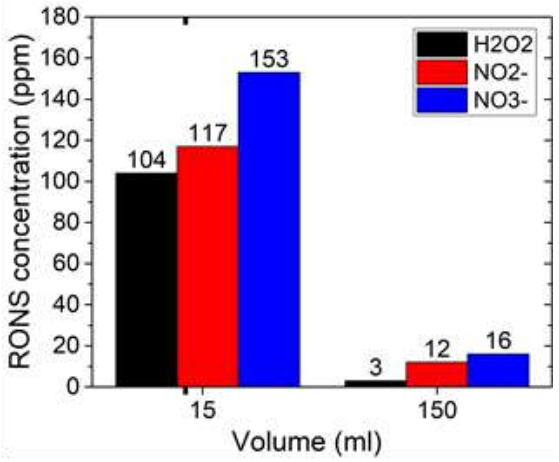

Figure 1: Concentrations of RONS after 20 minutes treatment in 2 different volumes of the sample vessel: 15 ml and 150 ml.

In Fig.1 we present RONS concentrations obtained for volumes of 15 ml and 150 ml using the same plasma parameters and the treatment time. The results show that the increase of the sample volume is not simply reducing the total amount of reactive species created but also influences the ratio between concentrations of different species. This illustrates the fact that the further approaches regarding scaling-up of the plasma systems are multiple due to the complexity of the system and the interaction with the liquid target. To obtain relevant conclusions about the potential of the plasma system and possible ways for scaling up, several key parameters of the plasma and PTL should be assessed.

Acknowledgement: This work was supported by MSTDI Republic of Serbia grant 451-03-68/2025-14/200024, the Science Fund of the Republic of Serbia, grant No. 3114/2021 - Project APPerTAin-BIOM and grant No.14916/2024 – Project PoWeRCAP-EGARDEN.

References

Puač N and Škoro N (2025) *Plasma Proc. Polym.*, **22**, e2400208.

Kumar A, Škoro N, Gernjak W, Puač N (2021) *Eur. Phys. J. D*, **75**, 283.

ELECTRON SWARM ANALYSIS AND ITERATIVE ACTINOMETRY FOR IMPROVED CF_4 PLASMA DIAGNOSTICS

M. Ribeiro[1], M. K. T. Mo[2], M. Hori[2], T. Silva[1], V. Guerra[1], N. Britun[2]

[1]*Instituto de Plasmas e Fusão Nuclear, Instituto Superior Técnico, Universidade de Lisboa, Portugal*

[2]*Center for Low-Temperature Plasma Sciences (CLPS), Nagoya University*

mariana.silva.ribeiro@tecnico.ulisboa.pt

Introduction: CF_4 plasmas are widely used in semiconductor applications. Accurate diagnostic techniques, such as Optical Emission Spectroscopy (OES) and actinometry (Coburn and Chen 1980), are essential for monitoring reactive species, but their reliability depends on the underlying electron kinetics governed by the electron energy distribution function (EEDF). In this work, electron swarm analysis was used to assess available CF_4 electron-collision cross-section sets, and a self-consistent iterative actinometry framework was developed to remove the common assumption of a Maxwellian EEDF (Kim et al. 2024).

Electron Swarm Analysis: Several CF_4 electron-collision cross-section sets were evaluated by comparing electron transport parameters with experimental swarm data over a range of reduced electric fields using the LisbOn KInetics Boltzmann (LoKI-B) and Monte Carlo (LoKI-MC) solvers (Tejero-del-Caz et al. 2019; Dias et al. 2023). The cross-section set of Kurihara et al. (2000) provides the best overall agreement with experimentally measured drift velocity (Fig.1(a)). Using this set, LoKI-B systematically overestimates the characteristic energy relative to LoKI-MC and experiment, reflecting the limitations of the Two-Term Approximation (TTA) in CF_4 (Fig. 1b). These discrepancies arise from anisotropic electron velocity distributions in CF_4 (Dujko et al. 2008), showing the importance of advanced kinetic treatments for this gas.

Iterative Actinometry: An iterative actinometric framework was developed by coupling OES measurements from CF_4-containing discharges with LoKI-B EEDF calculations. A line-ratio method determined an effective reduced electric field (E/N), which was used to calculate the EEDF, update electron-impact rate coefficients and plasma composition, and recalculate species densities until convergence, ensuring self-consistency between the EEDF, electron kinetics, and actinometric analysis. The F, H and O atom densities (Fig.2) differ only slightly

between conventional Maxwellian and iterative actinometry, indicating limited sensitivity to non-Maxwellian effects under the investigated conditions. Both approaches show good agreement with independent Two-Photon Absorption Laser-Induced Fluorescence (TALIF) measurements.

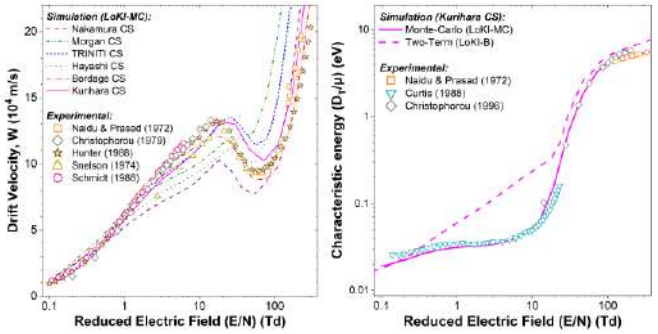

Figure 1: Drift velocity in pure CF_4 as a function of E/N. (a) Comparison of LoKI-MC simulations using different cross-section sets with experimental data. (b) Comparison between LoKI-MC and LoKI-B using the Kurihara cross-section set.

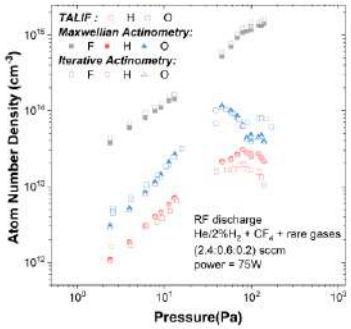

Figure 2: Absolute atom number densities of F, O, and H atoms in an RF discharge with a He/2%H_2 + CF_4 + rare gases mixture (2.4:0.6:0.2 sccm), comparing conventional Maxwellian actinometry, the proposed iterative actinometry workflow, and TALIF measurements (O and H).

Acknowledgments: IPFN activities were supported by FCT - Fundação para a Ciência e Tecnologia, I.P. by project references UID/50010/2025, UID/PRR/50010/2025, UID/PRR2/50010/2025 and LA/P/0061/2020. This work was also supported by Japan Science and Technology Agency (JST)'s ASPIRE Project JPMJAP2321.

References

Coburn J and Chen M (1980) *J. Appl. Phys.*, **51**, 3134.

Dias T *et al*. (2023) *Comput. Phys. Commun.*, **282**, 108532.

Dujko S *et al*. (2008) *Facta Univ. Ser. Phys. Chem. Technol.*, **6**, 61.

Kim J W *et al.* (2024) *Phys. Plasmas*, **31**, 103510.

Kurihara M *et al.* (2000) *J. Phys. D: Appl. Phys.*, **33**, 2146.

Tejero-del-Caz A *et al*. (2019) *Plasma Sources Sci. Technol.*, **28**, 043001.

OPTICAL DIAGNOSTICS DEVELOPMENT FOR MICROWAVE-PLASMA BASED GAS CONVERSION

Lex Kuijpers[1,2], Qinghao Shen[1], Cas van Deursen[1], Waldo Bongers[1] and Richard van de Sanden[1,2]

[1] *Dutch Institute For Fundamental Energy Research (DIFFER), De Zaale 20, 5612 AJ Eindhoven*

[2] *Eindhoven Institute of Renewable Energy Systems (EIRES), Eindhoven University of Technology, Eindhoven, The Netherlands*

l.kuijpers@differ.nl

Plasma-based gas conversion is a promising technology for the electrification of chemical processing. An example is the dry reforming of methane (DRM). In DRM, methane is reacted with CO_2 to produce synthesis gas. It has potential uses in the context of methane valorisation, carbon capture and utilisation, and biogas reforming. Especially warm plasmas (i.e. microwave, gliding arc) have shown promising results in terms of energy efficiency and conversion (Wang *et al* 2024). In warm plasmas the chemistry is driven by the high temperature of the gas. Accurate measurements of the gas temperature are thus indispensable in the development of these applications. In this work, optical emission spectroscopy (OES) methods are applied to determine the gas temperature and investigate the in-situ chemistry.

DRM discharges containing significant fractions of methane typically show characteristics similar to that of fuel rich flames, meaning that excess methane will pyrolyse into larger hydrocarbons and eventually solid carbon (in flames: *soot*). Like in flames, the emission spectrum consists mainly out of chemiluminescent molecular emissions, and thermal radiation from solid carbon particles. The thermal radiation of the particles can be used to determine the particles' temperature and volume fraction. To do so technique called Spectral Soot Emission (SSE) (see Snelling 2002) is adapted from combustion literature. In this technique the soot emission is modelled using the assumption of Kirchoff's radiation law and the Rayleigh-Debye-Gans approximation for absorption by fractal aggregates. The technique relies heavily on the knowledge of the absorptive properties of the carbon particles, and thus on the absorption function

of the refractive index, which is generally unknown. A power-law wavelength dependence of the absorption and thus emissivity is assumed: $\varepsilon_\lambda \propto \lambda^{-\xi}$, with ξ the dispersion exponent. Temperatures from the SSE technique are benchmarked against the rotational temperature of C_2 Swan band emissions, indirectly giving information on the optical properties of carbon material entrained in the plasma. Since broadband radiation is probed, the spectral resolution requirement for the technique is low, allowing for implementation of the technique in 2D using a CCD and different band-pass filters.

Methods: A vortex-stabilized microwave (2.45 GHz) discharge is operated at 150 mbar, 10-20 SLM and 1.0-1.5 kW. The chemistry is changed through adding CO_2 and H_2 to CH_4 discharges. Optical emissions are mapped by fitting a USB spectrometer on translation stages to allow for spatially and spectrally resolving the light emitted by the plasma. Additionally, the plasma is imaged using a CCD camera with different band pass filters ranging from the 700-900 nm.

Results and conclusions: C_2 Swan rotational temperatures for pure methane discharges and discharges of methane with hydrogen are found to be close to 3000 K in the conditions tested. Addition of CO_2 increases the gas temperature due to the changing thermodynamic characteristics of the gas mixture. Temperatures acquired using SSE show good agreement for low dispersion exponents ($\xi = 0 - 0.5$). This is contradictory to combustion literature, where the dispersion exponent is usually close to unity, stemming from a λ^{-1} factor in the RDG absorption cross section. We hypothesize that the difference in dispersion exponent stems from temperature-dependence of the material- and optical properties of the carbon.

2D SSE is applied to DRM discharges with excess CO_2. It is found that in 'lean' (low CH_4) DRM discharges, locally there is still (partial) pyrolysis of methane due to the temperature gradient and the lower activation energies of methane.

Acknowledgements: This work is partially funded by NXTGEN HT under the Energy domain, project 03: Plasma conversion of methane.

References

Wang K *et al*. (2024) *Curr. Opin. Green Sustain. Chem.*, **50**, 100981.
Snelling R R (2002) *AIAA Journal*, **40**(9), 1789–1795.

PIEZOELECTRIC TRANSFORMER-BASED ATMOSPHERIC-PRESSURE PLASMA SOURCES: TYPES, PARAMETERS, OPERATIONAL FEATURES AND APPLICATIONS

Nikolai N. Bogachev[1], Evgeny M. Konchekov[1], Leonid V. Kolik[1], Evgeny I. Grudiev[2], Vyacheslav P. Stepin[1], Alexander S. Bakshaev[3], Tatiana I. Pavlik[1], Ismail R. Seriev[1], Dmitry V. Malakhov[1] and Namik G. Gusein-zade[1]

[1]*Prokhorov General Physics Institute of the Russian Academy of Sciences, Moscow, Russia*

[2]*Institute of Physical Research and Technology, RUDN University, Moscow, Russia*

[3]*MIREA – Russian Technological University, Moscow, Russia*

bgniknik@yandex.ru

Piezoelectric-transformer (PT)-based atmospheric-pressure plasma sources are a compact, low-power alternative to high-voltage systems, as the high voltage forms directly at the discharge tip. Earlier work demonstrated piezoelectric direct discharge (PDD) devices and prototypes for plasma medicine, decontamination and plasma-activated liquids (PAL) (Korzec *et al*. 2021; Artemev *et al*. 2020), and recent roadmaps stress the need for compact, tunable low-temperature sources (Adamovich *et al*. 2022; Laroussi *et al*. 2022). This report reviews our PT-based sources, from single-mode systems to a multimode platform and two fourth-generation power architectures driving several PTs in parallel.

The current multimode source uses a resonant PT driven by a digitally controlled Class-E amplifier with adaptive frequency tuning (10–100 kHz) and autonomous supply from three 18650 Li-ion cells. The output reaches about 5 kV peak-to-peak, and the same electronics operate in three configurations by replacing only the discharge head: spark discharge in air, dielectric barrier discharge, and argon plasma jet. Digital interfaces (CAN/RS-485) enable synchronized multichannel operation and scale-up.

In spark mode the current pulse lasts about 20 ns, with peak current ~0.34 A and energy per pulse ~2×10^{-5} J; four sparks occur per driving period (Artemev *et al.* 2025). Optical emission spectroscopy shows the air spark is dominated by the N_2 second positive system, while barrier and argon-jet modes show intense Ar I lines

with N_2 and N_2^+ bands. For argon-flow treatment of liquids and DMEM medium, the rotational temperature from OH emission is about 700 K, the excitation temperature from Ar I lines about 0.46 eV, and the electron density estimated from Hα Stark broadening ~10^{16} cm^{-3}, which is consistent with typical PDD sources (Konchekov *et al*. 2026).

The PT-based source efficiently produces long-lived reactive oxygen and nitrogen species in liquids. For distilled water treated in argon mode, measured concentrations are H_2O_2 20–80 μM, NO_2^- 10–20 μM, NO_3^- 40–70 μM, pH 4.5–6.5, consistent with our earlier PDD-activated water (Konchekov *et al*. 2021). Spark treatment of deionised water in air gives much higher nitrite/nitrate, up to ~10^3 μM after 60 s. Biomedical potential was shown on HEp-2 cells treated by PT-based argon discharge: metabolic activity (MTT) drops ~50% after 20 s and viability (PI/Hoechst) after 150 s, correlating with H_2O_2 (~50 μM) and NO_2^- (~20 μM) accumulation in the medium (Konchekov *et al*. 2026).

Two fourth-generation supplies are under development. Variant I is a high-frequency Class-E architecture for autonomous low-power systems, driving one to several PTs through matched resonant channels with high efficiency, soft switching and precise digital frequency control, suited to portable jets and low-power DBD arrays. Variant II is a bridge topology (half-/full-bridge) from a boosted 100–150 V bus for higher output power, lower harmonic distortion at the PT input and stable operation of several PTs in parallel or in modular arrays for large-area treatment and high-throughput liquid activation. Both use combined current/voltage feedback and CAN/RS-485 sync. Thus the PT platform evolves from a compact multimode source into a scalable family of atmospheric-pressure plasma generators with flexible mode selection, adaptive resonance control and coordinated multi-PT operation.

References

Adamovich I *et al*. (2022) *J. Phys. D: Appl. Phys.* **55**, 373001.
Artemev K V *et al.* (2020) *Russ. Phys. J.* **62**, 2073–2080.
Artemev K V *et al*. (2025) *Phys. Plasmas* **32**, 063502.
Korzec D *et al*. (2021) *Plasma* **4**, 1–41.
Konchekov E M *et al*. (2021) *Front. Phys.* **8**, 616385.
Konchekov E M *et al*. (2026) *Inventions* **11**, 38.
Laroussi M *et al*. (2022) *IEEE Trans. Radiat. Plasma Med. Sci.* **6**, 127–157.

ATMOSPHERIC PRESSURE PLASMA PIN-JET: DIAGNOSTICS AND APPLICATIONS IN WATER TREATMENT

Olivera Jovanović[1], Nevena Puač[1], and Nikola Škoro[1]

[1]*Institute of Physics, University of Belgrade, Pregrevica 118, Belgrade, Serbia*

olivera@ipb.ac.rs

Atmospheric pressure plasma sources have emerged as promising tools in plasma agriculture and water purification technology. Their efficacy relies on the generation of Reactive Oxygen and Nitrogen Species (RONS) in the gas phase and their subsequent transfer into the liquid phase. The type and concentration of reactive species generated, together with the energy input, determine reactions occurring in both gas and liquid phases (Bruggeman *et al*. 2016, Ng *et al*. 2021). Controlling discharge parameters like working gas composition, flow rate, and deposited power directly governs reactive species formation, resulting in destruction of water pollutants or generation of plasma-activated water (PAW). For water decontamination, dissolved RONS drive the degradation of persistent pollutants not efficiently removed by conventional methods (Kumar *et al*. 2023, Topolovec *et al*. 2024). Plasma parameters can also be tuned to produce PAW rich in nitrates that is relevant for applications in plasma agriculture (Puač and Škoro 2025). Detailed plasma diagnostics are therefore required to relate discharge parameters to reactive species formation and liquid-phase chemistry.

In this work, a pin-type plasma jet generating streamer discharge at atmospheric pressure is characterized and applied to liquid sample treatment. The discharge is driven by a sinusoidal voltage at 330–350 kHz using argon and helium as working gases, with streamers propagating from the powered electrode towards the liquid surface. Voltage and current waveforms were monitored at the plasma source and in the ground line, enabling precise determination of deposited power and reproducibility of treatment conditions. Optical Emission Spectroscopy (OES) was employed to follow reactive species formation in the gas phase as a function of deposited power. Gas temperature was determined from OES measurements, while liquid temperature was monitored by using an immersed probe. Figure 1 shows changes in emission intensity in (a) He and (b) Ar plasma as a function of deposited power.

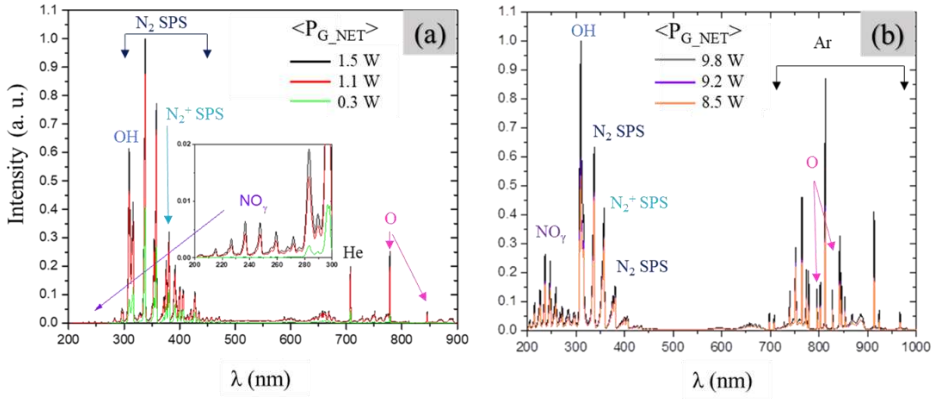

Figure 1: Optical emission spectra of (a) He and (b) Ar plasma as a function of deposited power $\langle P_{G\_NET} \rangle$. Spectra are normalized to the most intense line in each individual spectrum.

Spectra are normalized to the most intense line in each spectrum. In both discharges, emission from NO, OH, and O — reactive species critical for long-lived RONS formation in PAW — were identified, with intensities increasing with the power deposited in the target. Compared to He, in Ar plasma more energy is deposited into the water target and there is more excitation of NO and OH in the UV region — species directly responsible for modifications of liquid-phase properties. These results emphasize the role of systematic discharge diagnostics in linking operational parameters to gas-phase chemistry and, consequently, to the properties of the treated liquid.

Acknowledgement: This work was supported by MSTDI Republic of Serbia grant 451-03-68/2025-14/200024, the Science Fund of the Republic of Serbia, grant No. 3114/2021 - Project APPerTAin-BIOM.

References

Bruggeman P J *et al*. (2016) *Plasma Sourc. Sci. Techn*., **25**, 053002.
Kumar A *et al*. (2023) *Sci. Total Environ*., **864**, 161194.
Ng S W *et al*. (2021) *J. Appl. Phys*., **129**, 123303.
Puač N and Škoro N (2025) *Plasma Proc. Polym*., **22**, e2400208.
Topolovec B *et al*. (2024) *J. Environ. Chem. Eng*., **12**, 112979.

DIAGNOSTICS OF LOW-TEMPERATURE PLASMA OF FLUORINE-CONTAINING GASES FOR OPTIMIZATION OF PLASMA ETCHING PROCESSES OF DIELECTRICS IN MICROELECTRONICS

Vitaly Kuzmenko[1]

[1]*Moscow Institute of Physics and Technology (MIPT)*

kuzmenko.vo@phystech.edu

The study of plasma parameters and determination the mechanisms of physical and chemical processes occurring on surfaces allows for the optimization of precision plasma etching processes, which is important for fabrication of modern microelectronics devices. We focus on the etching processes of low-k and high-k dielectrics as accuracy of the etching process significantly affects the characteristics of the manufactured microelectronic structures.

The first part of the study is devoted to the investigation of the plasma composition of fluorobromine-containing gases and the interaction of plasma with the surface of a porous low-k dielectric, used in metallization system of modern integrated circuits, see Hoofman *et al.* 2005, to optimize the etching process. It was found that, unlike capacitively coupled plasma (CCP) discharges of fluorobromocarbon gases at high pressures (30–75 mTorr), in inductively coupled plasma (ICP) discharge at pressures of 5–20 mTorr, the concentration of fluorine radicals in the plasma ($\sim 10^{13}$ cm^{-3}) exceeds the concentration of bromine radicals ($\sim 10^{12}$ cm^{-3}). This fact explains the degradation of a dielectric with ultra-low permittivity during etching in CF_3Br gas plasma, previously observed by other authors. Studies of the low-damage cryogenic etching process for a low-k dielectrics have shown that, despite qualitatively similar trends in particle fluxes onto the surface from $C_2F_4Br_2$ gas plasma and CF_3Br gas plasma, etching in a $C_2F_4Br_2$ gas discharge results in less degradation of films with low permittivity, expressed in a smaller depth of the damaged layer and a smaller change in the refractive index, which is associated with a greater molecular mass and better protection of the dielectric surface from the effects of fluorine and bromine radicals.

The second part of the study of atomic layer etching (ALE) process of high-k dielectrics used as gate dielectrics in modern transistors, see Park *et al.* (2009). ICP of $Ar/CF_4/H_2$ gas mixture was used for surface modification in the process (Fig. 1).

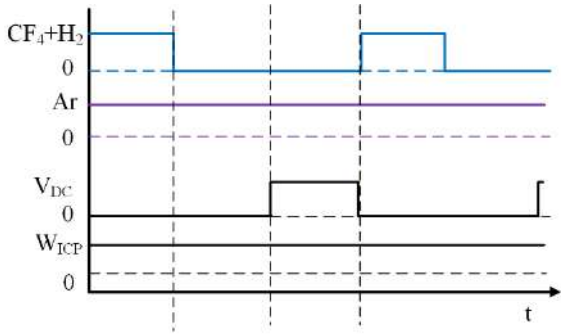

Figure 1: ALE process diagram

In a study of the interaction of an $Ar/CF_4/H_2$ gas mixture with surfaces, it was found that as the CF_4/H_2 flow ratio in the plasma-forming gas mixture increased from 0.25 to 4, with a constant Ar fraction, the balance between processes on various surfaces changed significantly from film deposition to etching. This is due to a twofold increase in the fluorine concentration in both the plasma and the deposited fluorocarbon film. The mechanism of HfO_2 etching during the ALE process was studied. It was found that during the modification step, the HfO_2 surface is significantly fluorinated, and a fluorocarbon film with a low fluorine content is deposited on the surface. This is consistent with the dominant concentration of F radicals in the plasma compared to other fluorocarbon radicals. During the reaction activation step, the fluorocarbon film is initially etched. Then, when the film is sufficiently thinned, accelerated ions etch both the film and the fluorinated hafnium oxide layer. The sputtering rate of pure HfO_2 is significantly lower (4 times) than the etching rate of fluorinated hafnium oxide. The results of the study of the mechanisms occurring at each step of ALE and the optimization of plasma parameters made it possible to develop an ALE process for Al_2O_3, HfO_2 and AlN_x that is selective with respect to TiN.

References

Hoofman R.J.O.M. *et al.* (2005) *Microelectronic Engineering*, **80**, 337-344.
Park J.B. *et al.* (2009) *J. Phys. D Appl. Phys.*, **42**, 055202.

MAGNETOPLASMA COMPRESSOR AS A SOURCE OF PLASMA FOR MATERIAL TREATMENT PURPOSES

Nora Trklja Boca[1], Ivan B. Krstić[1], Bratislav M. Obradović[1] and Milorad M. Kuraica[1]

[1]*Faculty of Physics, University of Belgrade, Studentski trg 12, 11001 Belgrade, Serbia*

nora@ff.bg.ac.rs

Magnetoplasma compressor devices have been used as plasma sources for several decades in leading research laboratories worldwide. Although individual devices differ in their design characteristics, they exhibit similar operational dynamics. The present study focuses on the magnetoplasma compressor installed at the Laboratory for Fusion Plasma Physics, Faculty of Physics, University of Belgrade (Figure 1). The objective of this research was to adapt the magnetoplasma compressor as a plasma flow source for material surface modification applications.

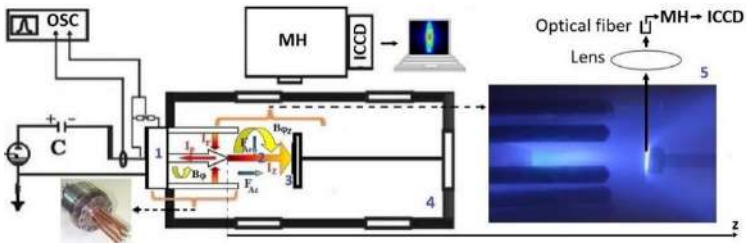

Figure 1: Magnetoplasma accelerator - 1 , Compressed plasma flow - 2, Sample (optional) - 3, Vacuum chamber - 4, Surface (steel 16MnCrS) treatment by CPF -5.

The distribution of energy flux density along the plasma flow was determined using the calorimetric method for three different working gases: hydrogen, argon, and hydrogen with a 5% helium admixture (Figure 2), see Trklja *et al.* 2019.

Various materials were exposed to plasma pulse treatment, including different types of steel, steel substrates coated with thin titanium nitride (TiN) layers, silicon samples with multilayer surface structures (Al–Ti and Ni–Ti), tungsten, and tungsten coated with a titanium layer.

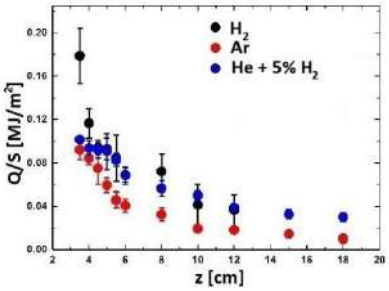

Figure 2: Energy transferred to the target surface

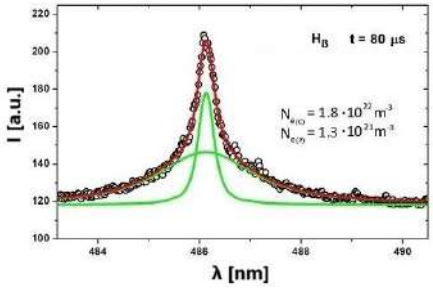

Figure 3: Analysis of H_β line

Surface modification under high thermal loads was investigated, see Trklja Boca *et al.* 2021. Morphological changes in the samples were examined using several diagnostic techniques. Before and after plasma treatment, the samples were analyzed by optical microscopy, scanning electron microscopy (SEM), atomic force microscopy (AFM), and X-ray diffraction (XRD). Surface hardness and roughness were also measured and evaluated. In addition, the plasma–material interaction was investigated using optical emission spectroscopy. Analysis of the recorded spectra enabled the determination of plasma parameters and composition, as well as the identification of species originating from material sputtering in the plasma layer adjacent to the treated surface.

A significant increase in the hardness of the treated steel samples was achieved, demonstrating the potential of this approach for industrial applications. Furthermore, the results obtained from the interaction of plasma flows generated by the magnetoplasma compressor with different materials contribute to the fundamental understanding of material behavior under conditions of high thermal loading.

References

Trklja N, Iskrenović P S, Mišković Ž Z, Krstić I B, Obradović B M, Mitrović R M, Kuraica M M and Purić J (2019) *JINST*, **12**, CO9041.

Trklja Boca N, Mišković Ž Z, Mitrović R M, Obradović B M and Kuraica M M (2021) *Surface and Coatings Technology*, **416**, 127157.

STREAMER DISCHARGES ASSISTED BY FEMTOSECOND LASER FILAMENTATION IN AIR

Thomas Clark[1], Quentin Gutierrez[1], Leonid Arantchouk[1] and Aurelien Houard[1]

[1]*Laboratoire d'Optique Appliquée, ENSTA, Ecole Polytechnique, CNRS, Institut Polytechnique de Paris, 828 Boulevard des Maréchaux, 91762 Palaiseau Cedex, France*

Thomas.clark@ensta.fr

The advent of intense ultrashort laser systems ($P > 5$ GW, $\tau < 1$ ps) has demonstrated their ability to generate weakly ionized plasma columns in the atmosphere [A. Couairon *et al.* 2007]. This phenomenon, known as femtosecond laser filamentation, has opened new possibilities for controlling high-voltage (HV) discharges. Laser filamentation has been extensively studied for triggering HV devices [H. Pepin *et al*. 2001, M. Rodriguez *et al*. 2002, L. Arantchouk *et al*. 2014], generating plasma antennas [Y. Brelet *et al*, 2012] and even controlling lightning [J.-C. Diels *et al*. 1997, A. Houard, *et al*. 2023]. In recent years, major steps forward have been taken at LOA, notably with the lightning-guiding experiments carried out in 2021 at the summit of Säntis Mountain. However, the possibility of reliably triggering lightning remains an open question.

To answer this question, we performed laboratory experiments to analyze the propagation of guided discharges, using a high intensity ultrashort laser system paired with various high-voltage generators. Our goal was to understand the effect of the laser on the formation of the precursors of the guided spark, known as streamers [L. Arantchouk *et al*. (in preparation)].

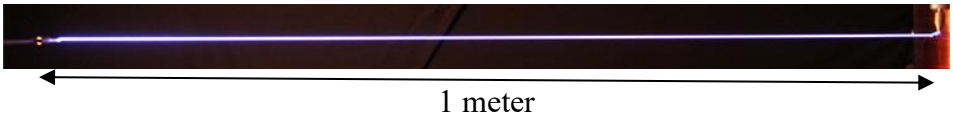

Figure 1: Example of a meter-scale guided discharge experiment produced with our high-voltage Tesla coil.

Here, we present a laboratory experiment featuring a custom-built Tesla coil developed by the FILM group, which is capable of delivering up to 300 kV.

First, we will present an experiment featuring a custom-built Tesla coil developed by our group. This coil is capable of delivering voltage pulses of up to 300 kV. Using a fast camera and electrical diagnostics, we observed that, in the presence of the filament, the streamer produced by the Tesla coil transformed into a leader, increasing its length and current tenfold.

Then, we implemented additional diagnostics—such as optical emission spectroscopy and X-ray measurements—to monitor the propagation phase of these guided discharges, in order to determine the plasma's characteristics and analyze how they are affected by the laser filament. In parallel, a numerical study has been initiated to simulate the creation of the streamer discharge in the presence of a laser filament.

References

Arantchouk L *et al.* (2014) *Appl. Phys. Letters*, **104**, 103506.

Arantchouk L *et al*. (In preparation).

Brelet Y *et al.* (2012) *Applied Physics Letters*, **101**(26), 264106.

Couairon A and Mysyrowicz A (2007) *Phys. Rep.,* **441**, 47.

Diels J C *et al*. (1997*) Sci. Am*., **277**, 50–55.

Houard A *et al.* (2023) *Nat. Photon*., **17**, 231–235.

Pépin H *et al*. (2001) *Phys. Plasmas*, **8**, 2532.

Rodriguez M *et al*. (2002) *Opt. Lett*., **27**, 772.

PHOTOELECTRON ATTENUATION CIRCULAR DICHROISM OBSERVED ON ISOLATED TRYPTOPHAN-FUNCTIONALIZED GOLD NANOPARTICLES

Dušan K. Božanić[1], Gustavo A. Garcia[2], Jelena Pajović[3], Željko Šljivančanin[1], Vladimir Djoković[1] and Laurent Nahon[2]

[1] *Vinča Institute of Nuclear Sciences - National Institute of the Republic of Serbia, University of Belgrade, P.O. Box 522, 11001 Belgrade, Serbia*

[2] *Synchrotron SOLEIL, l'Orme des Merisiers, St. Aubin, BP48, 91192 Gif sur Yvette Cedex, France*

[3] *Faculty of Physics, University of Belgrade, P.O. Box 368. 11001 Belgrade, Serbia*

bozanic@vin.bg.ac.rs

Sensitive detection and quantification of chiral molecular species is of paramount importance for different analytical, biomedical or environmental applications. Conventional methods for detection of chirality in dense targets, like circular dichroism (CD) spectroscopy, measure the difference between total absorption cross sections of circularly polarized light (CPL) for two optical isomers (enantiomers). These techniques produce dichroic signals of about 0.01% of the absorption, which is usually insufficient for quantitative determination of enantiomeric excess, particularly in diluted matter. Photoelectron circular dichroism (PECD) is an angle-resolved technique that relies on a forward-backward asymmetry in the photoemission from chiral molecules irradiated with CPL (Ritchie 1976, Powis 2000, Bowering *et al.* 2001). Unlike conventional approaches, PECD can be fully described within the electric dipole approximation that can result in dichroic signals well above 10% on randomly oriented molecules in gas-phase, see for example Hadidi *et al*. 2018. In addition to the studies on free molecules and molecular clusters, PECD can be also used for evaluation of circular dichroism in photoemission in condensed chiral nanosystems – isolated in high-vacuum conditions in the form of aerosols (Hartweg *et al.* 2021, Hartweg *et al.* 2026). In this case, the observed electron energy and angle-resolved dichroism is usually suppressed due to outgoing electron scattering, but the total photoemission yield may show few percent chiral asymmetry due to the combined light absorption and PECD effects.

Here we present the results of the PECD experiments on aerosols 100 – 150 nm in size comprised of 8 nm spherical gold nanoparticles functionalized by L- or D-tryptophan, performed at DESIRS beamline of Synchrotron SOLEIL using 10.2 eV circularly polarized radiation. The investigated hybrid nanosystem showed clear asymmetry between the NP functionalized by opposite enantiomers, reaching PECD of up to ~3%. The obtained value is comparable to the results for free gas-phase Trp molecules (~5%) and notably higher than the PECD of condensed Trp aerosol particles (~0.5%). Furthermore, for a given enantiomer, the photoelectron emission in functionalized nanoparticles was of the opposite sign than for free tryptophan molecules and pure tryptophan aerosol particles under the same conditions. These observations are explained using aerosol photoemission model (Božanić et al., 2020) in terms of angle-resolved attenuation of spin-polarized photoelectrons emerging from Au NP due to enantiomer-sensitive scattering on tryptophan layers

References

Božanić DK, Garcia GA, Sublemontier O, Pajović J, Djoković V, and Nahon L (2020) *J.Phys. Chem. C,* **124**, 24500.

Bowering N, Lischke T, Schmidtke B, Müller N, Khalil T, and Heinzmann U (2001) *Phys. Rev. Lett.*, **86**, 1187.

Hadidi R, Božanić DK, Garcia GA, and Nahon L (2018) *Adv. Phys. X*, **3**, 1477530.

Hartweg S, Garcia GA, Božanić DK, and Nahon L (2021) *J. Phys. Chem. Lett*, **12**, 2385.

Hartweg S, Božanić DK, Garcia GA, and Nahon L (2026) *Nat. Commun.*, **17**, 2792.

Powis I (2020) *J. Chem. Phys*, **112**, 301.

Ritchie B (1976) *Phys. Rev. A*, **13**, 1411.

ELECTRIC FIELD BEHAVIOUR IN THE BURST REGIME OF A REPEATABLE NANOSECOND He-BASED ATMOSPHERIC DISCHARGE

Pierre Mathieu[1], Michael K. T. Mo[2], Masaru Hori[2], Nikolay Britun[2*]

[1] *Chimie des Interactions Plasma-Surface (ChIPS), University of Mons*

[2] *Centre for Low-Temperature Plasma Sciences (cLPS), Nagoya University*

britun@plasma.engg.nagoya-u.ac.jp

Fundamental physical processes occurring in the atmospheric low-temperature flowing gas discharges, are in focus of the modern research because of the wide applicability of these plasmas for surface treatment, plasma medicine and agriculture, etc. (Fridman 2008). In particular, a precise control and optimization of electric field, electron density and radical production are crucial, requiring advanced non-intrusive diagnostic approaches (Britun 2026).

In this contribution a He-driven repetitive nanosecond atmospheric jet discharge has been studied, which is based on a single thyristor circuitry (Gamaleev et al. 2022) and shown in Fig. 1(a). The time-resolved behaviour of the characteristic temperatures, propagation of ionization waves (Britun et al. 2023), the evolution of electron density (measured by Stark spectroscopy of H lines and electric field (Stark spectroscopy of He lines (Britun 2023)), the dynamics of He $^3S_1$ metastable states (measured by laser- collisions- induced fluorescence, LCIF (Britun and Hori 2025) and H atom ground states (two-photon absorption laser-induced fluorescence, TALIF (Mathieu et al.2026)) were studied.

Special attention is given to the discharge operation in the burst regime, namely the time-resolved evolution of the electric field in the discharge gap. It was shown that the electric field strength may experience an abrupt jump in the late burst pulses at certain time delays (e.g. after the 7th pulse, compared to the 1st pulse in the burst), as revealed by the analysis of the forbidden-to-allowed emission component separation in the He 447.15 nm emission line, shown in Fig. 1(b). From this figure one can see that the mentioned line profile clearly evolves with time, demonstrating a large broadening during the 7th burst pulse (which is much larger than that found after the first pulse) and which corresponds to a larger increase in the electric field.

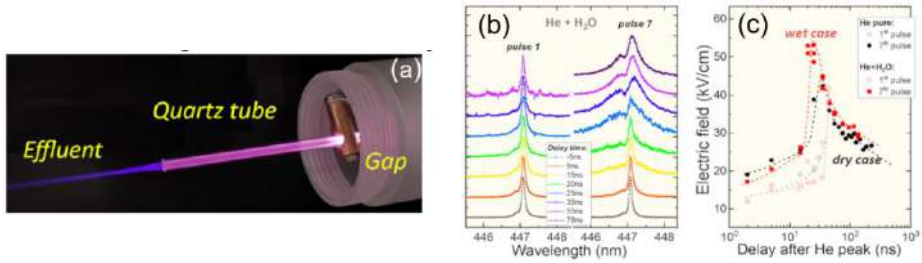

Figure 1: A photograph of the ns-discharge (a) along with He 447 nm emission profiles measured at different time delays (b) and the evolution of E-field in the gap in the wet and dry cases (c).

Such a field jump is especially pronounced in the wet He case (i.e. when He was mixed with water vapour), see Fig.1(c). The effect is nearly negligible after the 1st burst pulse and is likely related to an enhanced ioni-zation developed at the end of the burst sequence. The additional ionization may be caused by the presence of vibrationally excited molecules favouring stepwise ionization. The measurements of the H_β profile performed in our case revealed few linewidth oscillations signifying the propagation of multiple streamers in the volume at the end of the burst sequence (not shown here).

The density of H atoms produced in the burst regime may be enhanced by a factor of ten, based on either H_2O or CH_4 dissociation, corresponding to the energy cost of ~ 50 eV/H atom. As the burst evolves, this effect is also accompanied by a significant elevation in electron density during the plasma-on time. The found effects confirm that in the strongly non-equilibrium ns- discharges operating in burst regime the dissociation of molecular species might be significantly facilitated as a result of enhanced ionization, likely caused by accumulation of vibrationally excited species and stronger electric field, associated with streamers.

References

Britun N (2026) *J. Phys. D: Appl. Phys.*, **59**, 053002.
Britun N *et al*. (2023) *PSST,* **31**, 125012.
Britun N (2023) *J. Appl. Phys.* **133**, 183303.
Britun N and Hori M (2025) *PSST* **34**, 01LT02.
Fridman A *Plasma chemistry* (2008, Cambridge University Press).
Gamaleev V *et al*. (2022) *Rev. Sci. Instrum*., **93**, 053503.
Mathieu P *et al*. (2026) *PSST Submitted.*

TEMPORAL EVOLUTION OF SPECTRAL LINES IN TEA CO2 LASER-INDUCED GRAPHITE PLASMA

Vladimir Gavrilović[1], Biljana D. Stankov[1] and Miroslav Kuzmanović[2]

[1]*Institute of Physics Belgrade - National Institute of the Republic of Serbia, Pregrevica 118, Belgrade, 11080, Serbia*

[2] *Faculty of Physical Chemistry, University of Belgrade, 11158 Belgrade, Serbia*

vgavrilovic@ipb.ac.rs

Nanosecond Nd:YAG lasers are most commonly used in laser-induced breakdown spectroscopy (LIBS). However, TEA CO_2 lasers operating at a wavelength of 10.6 μm have some specific advantages, such as reduced destructiveness, enhanced coupling with softer targets, and inherent eye safety. TEA CO_2 also has a much longer pulse duration. The laser pulse has a sharp initial spike (FWHM ~ 100 ns) with slowly decaying tail (~ 2 μs), see Savovic et al. 2016. While there is a significant number of publications in the literature describing the successful application of the TEA CO_2 lasers for LIBS analysis of various samples, investigations of the plasma time evolution are lacking. Understanding the temporal and spatial evolution of plasma is important for the optimization of detection parameters in LIBS measurements.

The aim of this work was to investigate the temporal evolution of different spectral lines in graphite plasma (atomic and ionic lines of metallic and non-metallic elements, air-related species, molecular bands, etc.) with partially spatially resolved measurements. The plasma was generated by focusing a TEA CO_2 laser beam orthogonally on the surface of the graphite target in ambient air. The resulting plasma was then focused onto the entrance slit of the imaging spectrograph using a quartz lens, with its axis oriented parallel to the vertical axis of the ICCD chip and perpendicular to the optical axis of the spectrograph. This experimental setup enables the investigation of the temporal evolution of spectral emissions at different distances from the target.

The experimental results reveal significantly prolonged emission lifetimes compared to typical Nd:YAG-induced plasmas, a direct consequence of the extended laser pulse tail, see Cremers and Radziemski 2013. Ion line spectra, as

well as lines with higher excitation energies, appear in earlier stages of plasma evolution, closer to the target. At later delay times, the plasma cools down, leading to the decay of ionic species and the emergence of molecular bands. Specifically, the C_2 and CN molecular bands appear at the later stage of the plasma evolution, with their emission maxima located farther from the target.

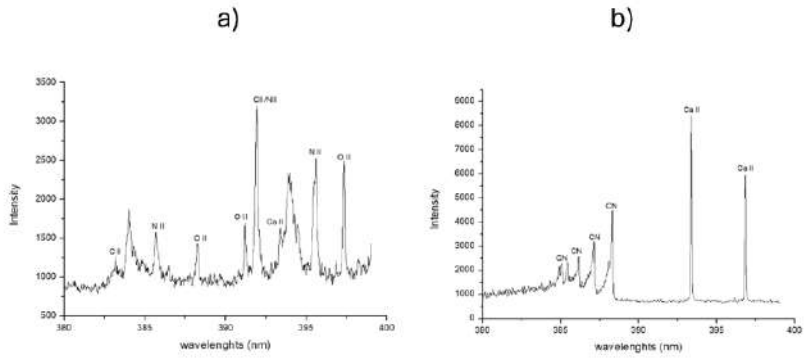

Figure 1: Graphite plasma spectrum around 390 nm recorded at a ICCD camera delay of a) 1.2 μs and b) 5 μs.

References

Cremers D and Radziemski L (2013) *Handbook of Laser-Induced Breakdown Spectroscopy, Second edition*, Cambridge.

Savovic J, Stoiljkovic M, Kuzmanovic M, Momcilovic M, Ciganovic J, Rankovic D, Zivkovic S and Trtica M (2016) *Spectrochimica Acta Part B*, **118**, 127–136.

THE SPECTROSCOPIC DIAGNOSTICS OF LOW PRESSURE PULSED DISCHARGE: A REVIEW

Jovica Jovović

University of Belgrade, Faculty of Physics, Studentski trg 12-16, 11000 Belgrade

jjovica@ff.bg.ac.rs

In this paper, a review of spectroscopic results obtained from several experimental campaigns with low pressure pulsed plasma source and cylindrical cathode will be presented. In the first part, the results of fast hydrogen atoms (H_f) study in hydrogen-containing gases with copper, aluminum, stainless steel and graphite cathodes will be shown. The spectral line shape of H I 656.28 nm line recorded by means of the CCD camera imaging mode using Side-On alignment is described by 2-Gaussian or 3-Gaussian model function (Jovović 2025). The area (A_f), averaged energy (E_f) and maximum energy related to H_f are deduced from the fitting function. The broadest part of H I (i.e. the pedestal) is related to Excessive Doppler Broadening (EDB) of excited hydrogen atoms in plasma which occurs when strong electric field as well as hydrogen ions (H^+, H_2^+, H_3^+) exist in studied gas discharge. In our case, Ar+3% H_2, H_2+5% Ar, N_2+5% H_2 and Ne+0.8% H_2 served as the source of hydrogen atoms and the difference in H I spectral line shape is evident. The maximum H_f energy up to 400 eV is detected while the maximum A_f of 97 % is found in Ar-H_2 gas mixture.

In the second part of this paper, the molecular bands belonging to $N_2^+(B^2\Sigma_u^+$-$X^2\Sigma_g^+)$, $CN(B^2\Sigma^+$-$X^2\Sigma^+)$ and $AlO(B^2\Sigma^+$-$X^2\Sigma^+)$ transitions will be presented. The synthetic bands created by means of homemade procedure will be used to fit the studied molecular bands, to determine the rotational temperature T_{rot} and consequently to estimate the plasma gas temperature T_g. Also, the spatial alteration in $N_2^+(B^2\Sigma_u^+$-$X^2\Sigma_g^+)$ rotational distribution will be shown in relation to relaxation processes. In this study, the cylindrical cathodes made of graphite and aluminum are used and working gases N_2+1% H_2 and Ar+1% O_2 employed. The T_{rot} in the range 650-850 K is measured. A detailed study on diatomic molecules spectra emitted from versatile plasma sources is given elsewhere (Jovović and Majstorović 2025).

In the third part, the change in Ne I 503.775 nm and Ne I 520.39 nm line and He I 492.2 nm spectral line shape with spatial coordinate will be given as well for the measurement of electric field strength *E*(kV/cm) in the cathode sheath of studied plasma source. It was noticed that Stark shifting and splitting occurs in the presence of DC electric field and the wavelength separation can be used for electric field strength diagnostics, see e.g., Nedić *et al*. 2022, Ivanović *et al*. 2023. For that purpose, the imaging mode of the CCD camera is employed as well. The unshifted line is present in the cathode sheath spectra due to plasma envelope surrounding the cathode sheath area of the plasma source. The electric field strength of 9-10 kV/cm was determined from Ne I while 12.5-13.5 kV/cm is estimated from He I line.

References

Jovović J (2025) *Spectrochim. Acta Part B*, **226**, 107156.

Jovović J and Majstorović G Lj (2025) *Vacuum*, **244**, 114927.

Nedić N V, Ivanović N V, Videnović I R, Spasojević Dj and Konjević N (2022) *J. Anal. At. Spectrom.*, **37**, 1318.

Ivanović N V, Nedić N V, Videnović I R, Spasojević Dj and Konjević N (2023) *Spectrochim. Acta Part B*, **208**, 106775.

DETECTION OF EXPLOSIVES IN TRACES BY LASER INDUCED SHOCKWAVES AND PLASMA SPECTROSCOPY

Violeta Lazic[1] and Biljana Stankov[2]

[1]*Italian National Agency for New Technologies, Energy and Sustainable Economic Development (ENEA), 00044 Frascati, Italy*

[2]*Institute of Physics Belgrade, University of Belgrade, 11080 Belgrade, Serbia*

Violeta.lazic@enea.it

Detection of trace amounts of explosives remains a subject of great interest in security and forensic applications. Among various techniques suitable for in-field measurements, Laser Induced Breakdown Spectroscopy (LIBS) in combination of various algorithms or chemometric approaches, showed a capability to reach low detection limits, in order of ng or less. In this work we present the results of simultaneous LIBS measurements and time-resolved detection of the plasma generated acoustic signal on traces of various substances (inert, flammable or explosive) placed on silica wafer. The experimental set-up is based on a compact LIBS instrument developed by ENEA for forensic examinations on a crime scene [Lazic et al. 2024] to which a unidirectional microphone was added at distance of 30 mm from the plasma point.

From the laser induced acoustic signal itself, it was possible to classify explosives, combustibles, and inert substances for sample masses in order of 10 ng [Lazic et al. 2026]. Compared to the clean substrate, in presence of explosives the acoustic signal showed acceleration and intensification due to rapid release of chemical energy into plasma, opposite to the case of inert substances; in case of combustion, the amplitude increase was delayed. Behavior of the laser induced shockwaves, leaving a low-pressure region behind the shock front, affects the LIBS spectra, particularly in if the integration time is relatively long (here 30 μs), as characteristic for the compact spectrometers. High explosives contain C, H, N and O where the last two elements are main components of the surrounding air and H is also present due to air humidity. The additional air rarefaction caused by the energy release through micro-explosion or combustion was observed in the LIBS spectra through increased ratios of H/N and H/O spectral peaks compared to inert materials, thus further explaining the role of these parameters in LIBS

detection of explosives, as well as the missing plasma stoichiometry [Lazic *et al.* 2011]. On the other hand, the line intensities from H and C reflected their content in sample although their ratio was dependent on the plasma parameters, also influenced by the trace sample amount and its distribution on substrate inside the laser spot.

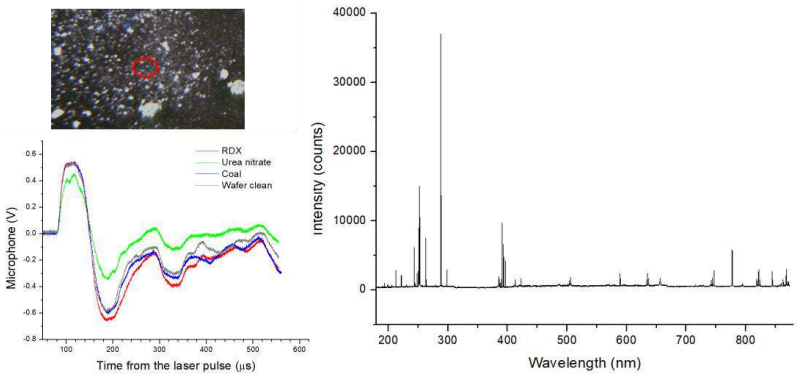

Figure 1: Examples of a photo of particles (laser spot of diameter 0.3 mm is encircled), the microphone signals and a LIBS spectrum from trace explosive on wafer.

Based on the findings from above, we built and implemented an algorithm for detection of explosives in traces by LIBS, which produced excellent results during the successive in-field validation campaign. Among the important achievements, ANFO was correctly classified as an explosive while the measurements on its main components (ammonium nitrate and diesel) did not produce false positives; also, different origins of the same types of explosives were distinguished from the impurities. The estimated detection limit by the portable compact LIBS sensor and for particles of explosives placed on wafer, was in order of 1 ng.

References

Lazic V, Palucci A, Jovicevic S, Carpanese M, (2011) *Spectrochimica Acta Part B*, **66**, 644.

Lazic V, Andreoli F, Almaviva S, Pistilli M, Menicucci I, Ulrich C, Schnürer F, Chirico R, (2024) *Sensors*, **24**, 1469.

Lazic V, Stankov B, Andreoli F, Pistilli M, Menicucci I, Ulrich C, Schnürer F, Chirico R, Gaudio P, (2026) *Sensors*, **26**, 672.

SIGNAL ENHANCEMENT IN LIBS ANALYSIS OF GLASS USING COPPER THIN FILM COATING

Aleksandra Šajić[1], Dragan Ranković[2], Miroslav Ristić[1], Milica Marković[1] and Miroslav Kuzmanović[1]

[1] *University of Belgrade, Faculty of Physical Chemistry, Studentski Trg 12-16, 11158 Belgrade, Serbia*

[2] *University of Belgrade, Vinca Institute of Nuclear Sciences, Mike Alasa 12-14, 11001 Belgrade, Serbia*

aleksandra.sajic@ffh.bg.ac.rs

Laser-induced breakdown spectroscopy (LIBS) analysis of transparent materials using a nanosecond Nd:YAG laser at 1064 nm is often limited by weak plasma formation, low emission intensity, and laser-induced surface damage (Barnett *et al*. 2008). In this work, thin copper films deposited on glass surfaces were used to enhance plasma generation and improve the analytical performance of LIBS. The influence of copper deposition time on signal enhancement and plasma stability was systematically investigated, and the greatest enhancement was observed when the samples were coated for 20 s. At this deposition time, the thickness of the metallic layer on the sample surface was below 10 nm. The presence of the copper coating significantly increased the intensity of emission lines (Fig. 1), thereby improving the detection of trace elements in both colored and transparent glass samples while reducing the risk of cracking and other surface damage.

Enhanced signal reproducibility also enabled quantitative analysis of selected elements through calibration curves with high linearity. Detection limits in the ppm range were achieved for several elements, demonstrating improved analytical sensitivity compared to uncoated glass samples. Plasma diagnostics were performed using Boltzmann plots and Stark broadening measurements to characterize plasma temperature and electron density under optimized experimental conditions. The results indicate that the copper coating promotes the formation of a denser, more stable plasma, leading to improved signal quality and analytical reliability.

The observed enhancement effects are consistent with previous studies involving gold nanoparticles and graphene-assisted NELIBS approaches (Sánchez-Aké *et al*. 2018). However, the use of thin copper films offers a simpler and more reproducible alternative to conventional NELIBS approaches that rely on droplet deposition of nanoparticles, in which non-uniform distribution and coffee-ring effects can significantly degrade signal repeatability and analytical performance. Overall, the results demonstrate that thin copper films offer an efficient and practical approach to enhancing LIBS analysis of glass using the fundamental wavelength of the Nd:YAG laser.

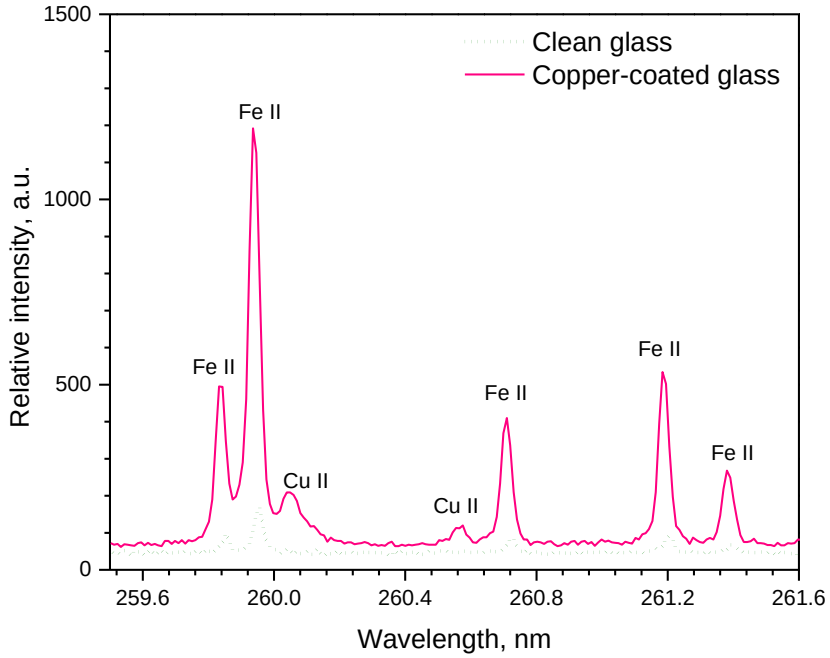

Figure 1: Comparison of LIBS spectra from uncoated and copper-coated glass samples.

References

Barnett C, Cahoon E and Almiral J R (2008) *Spectrochim. Acta Part B: At. Spectrosc.*, **63**, 1016–1023.

Sánchez-Aké C, García-Fernández T, Benítez J L, De La Mora M B and Villagrán-Muniz M (2018) *Spectrochim. Acta Part B: At. Spectrosc*. **146**, 77–83.

DIFFERENT MODELS FOR IONIZATION POTENTIAL LOWERING IN ARGON PLASMA

N. Krstevski, A. Šajić, M. Marković, S. Tomić, M. Ristić and M. Kuzmanović

University of Belgrade, Faculty of Physical Chemistry, Studentski trg 12, 11158 Belgrade, Serbia

aleksandra.sajic@ffh.bg.ac.rs

It is known that under plasma conditions each atom and ion is subjected to the Coulomb potential of all other charged particles in its surroundings, causing the ionization potential lowering (IPL) or continuum lowering, compared to the case of an isolated atom or ion. Several models that describe IPL were developed during the 20th century, but most used in modern-day literature are Stewart-Pyatt (Stewart and Pyatt 1966), Debye-Huckel (Debye and Huckel 1923) and Ecker-Kroll (Ecker and Kroll 1963) model. In the present study these three models are compared for the case of pure argon plasma, considered to be in LTE on constant pressure of 1 bar, across temperature range from 5,000 to 30,000 K. Details of calculation procedure can be found in our recent publication (Ristic *et al.* 2024).

IPL by Stewart-Pyatt model is represented by the following expression:

$$\Delta E_j^{\mathrm{SP}} = \frac{3}{2}\frac{je^2}{4\pi\varepsilon_0\lambda_D}\frac{\left[\left(\frac{r_{\mathrm{IS}}}{\lambda_D}\right)^3+1\right]^{2/3}-1}{\left(\frac{r_{\mathrm{IS}}}{\lambda_D}\right)^3} \tag{1}$$

where r_{IS} is the ion-sphere radius, N_e is electron's number density, j is the ionization stage of particle (j=1 for the neutral atom), λ_{D} is the Debye length, ε_0 is vacuum permittivity, while e is the elementary charge. The Debye-Huckel model for IPL is accounted with the following equation:

$$\Delta E_j^{\mathrm{DH}} = \frac{je^2}{4\pi\varepsilon_0\lambda_D} \tag{2}$$

The Ecker-Kroll model, derived for dense or solid-density plasmas is calculated from the expression (assuming the constant C to be equal to 1):

$$\Delta E_j^{\mathrm{EK}} = C\frac{je^2}{4\pi\varepsilon_0 r_0} \tag{3}$$

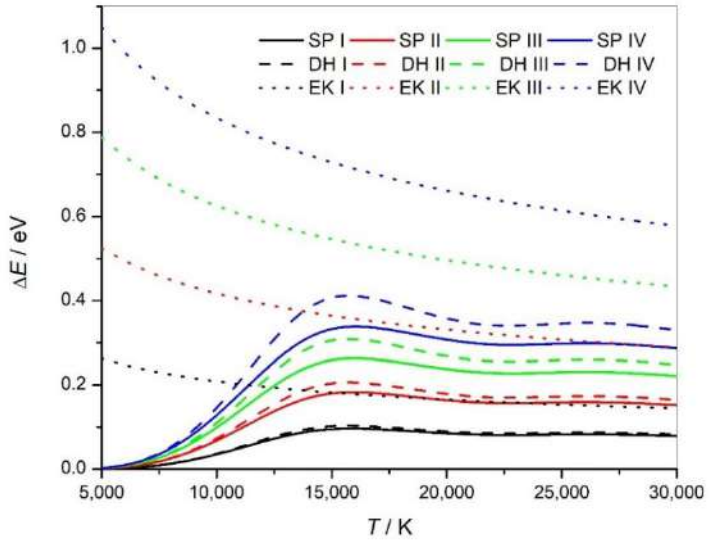

Figure 1: IPL values for pure Ar plasma at P = 1 bar for Stewart-Pyatt (SP, solid line), Debye-Huckel (DH, dashed line) and Ecker-Kroll (EK, dotted line) model for the first four ionization stages of Ar (I – black, II – red, III – green, IV – blue line).

Obtained results are presented in Fig 1. for all three models for the first four ionization stages of argon. It is noticeable that Stewart-Pyatt and Debye-Huckel model predict very similar results, the latter showing somewhat higher values of IPL. The Ecker-Kroll model predicts significantly higher IPL values than other two models.

Acknowledgments: The research was funded by the Ministry of Education, Science and Technological Development of Serbia, Contract Nos: 451-03-34/2026-03/200146 and 451-03-33/2026-03/200146.

References

Stewart J C and Pyatt Jr KD (1966) *Astrophys. J,* **144,** 1203.

Debye P and Huckel E (1923) *Phys. Z,* **24**, 185.

Ecker G and Kroll W (1963) *Phys. Fluids,* **6**, 62.

Ristic M, Krstevski N, Rankovic D, Markovic M, Sajic A and Kuzmanovic M (2024) *Plasma Phys. Control. Fusion,* **66**, 125014.

SPECTROSCOPIC STUDY OF A PLASMA CHANNEL PRODUCED BY A FEMTOSECOND LASER IN ARGON

Goran B. Sretenović[1], Vesna V. Kovačević[1], Ognjen Grkinić[1], Bratislav M. Obradović[1], Ivan B. Krstić[1], Milorad M. Kuraica[1] and Predrag Ranitović[1]

[1]*University of Belgrade – Faculty of Physics, Belgrade, Serbia*

sretenovic@ff.bg.ac.rs

In the process of strong-field-ionization (SFI), an intense femtosecond laser pulse propagates through a gas with a rapidly oscillating electric field, that can strip electrons from neutral atoms through tunnel ionization – a purely quantum-mechanical process in which the electron penetrates the Coulomb barrier suppressed by the laser field. This occurs when the laser electric field is high enough to match the atomic Coulomb force. This SFI regime is typically defined by the Keldysh parameter $\gamma < 1$, placing the interaction in the tunnelling ionization regime. The liberated electrons are accelerated and driven by the laser field. The fraction of the accelerated electron wave packet can recombine with their parent ions, emitting high-energy photons – the basis of high-harmonic generation (HHG) and attosecond pulse synthesis, see Ammosov *et al.* 1986 and Weissenbilder *et al.* 2022.

Macroscopically, as the laser-pulse propagates through the gas Kerr self-focusing confines the beam until on-axis ionization becomes strong enough for plasma defocusing to take place. This plasma dynamic balance locks the peak intensity at a clamped value determined by the plasma properties. The resulting plasma channel directly governs HHG efficiency: the clamped intensity sets the maximum photon energy attainable, the electron density controls phase matching between the driving field and the emitted harmonics, and the plasma lifetime determines whether the medium fully recovers between successive pulses at kilohertz repetition rates. Despite their importance in the HHG process, spatially resolved in situ measurements of these quantities are not well studied for Yb-based laser systems near 1030 nm, see Couairon and Mysyrowicz 2007.

In our experiment, we optimize the HHG process, and characterize the plasma parameters using spatio-temporally resolved optical emission spectroscopy of an argon filament driven by a femtosecond Yb:KGW laser at 1030 nm. The Stark broadening and red-shift of the Ar I 696.5 nm emission line, elaborated by

Sretenović *et al.* 2025, recovered via Abel inversion of the laterally resolved spectra, provide radial profiles of the electron density and ionization degree with micrometer-scale spatial resolution. Inverting the measured ionization degree through the Ammosov–Delone–Krainov (ADK) tunnel ionisation model then yields the local peak laser intensity—a direct, non-intrusive in situ measurement. We find that the plasma core contains electron densities in the low $10^{17}\,\mathrm{cm}^{-3}$ range, with a few per cent of atoms ionized. The retrieved clamped intensity is spatially uniform across the filament core at all studied pressures, which is a direct spectroscopic confirmation of the intensity-clamping mechanism. Its value is roughly half the vacuum-focus intensity, reflecting the efficiency with which plasma defocusing arrests self-focusing. Strikingly, the radial emissivity profiles exhibit a double-ring structure—an inner bright core surrounded by an outer reservoir—exactly as predicted by Couairon and Mysyrowicz 2007 for a filament in which plasma defocusing continuously redistributes energy from the axis outward. The measured clamped intensity places the theoretical single-atom HHG cutoff well into the XUV spectral domain; in practice the observable cutoff is lower because phase matching in the tight-focus geometry limits coherent harmonic build-up to lower photon energies as shown by Constant *et al.* 1999.
The extended temporal measurement reveals that the plasma decays in two distinct phases. In the first few hundred nanoseconds, electrons are rapidly lost through three-body recombination - a collision between a free electron, an ion, and a neutral atom that captures the electron back into an excited atomic state. This process is most efficient at high electron and neutral densities and becomes negligible as the plasma decays. On longer timescales, from hundreds of nanoseconds to several microseconds, the dominant loss mechanism shifts to ambipolar diffusion: the electron pressure gradient drives electrons outward, and the resulting charge separation creates an electric field that drags the heavier ions along, spreading the plasma column radially until it is too dilute to detect. Higher gas pressure slows this diffusion, which is why the plasma persists longer at higher pressure. Plasma emission is detectable for nearly 12 μs — yet at 1 kHz repetition rate the gas recovers completely before the next shot, ruling out any cumulative plasma build-up that might otherwise degrade HHG performance

References

Ammosov M V, Delone N B and Krainov V P (1986) *Sov. Phys. JETP*, **64**, 1191.
Constant E *et al.* (1999) *Phys. Rev. Lett.*, **82**, 1668.
Couairon A and Mysyrowicz A (2007) *Phys. Rep.*, **441**, 47.
Sretenović G B *et al.* (2025) *Plasma Sources Sci. Technol.*, **34**, 055013.
Weissenbilder R *et al.* (2022) *Nat. Rev. Phys.* **4**, 713.

DETERMINATION OF ELECTRON CONCENTRATION IN PULSED DISCHARGES USING MICROWAVE RADIATION TRANSMISSION THROUGH WAVEGUIDES WITH PERIODIC STRUCTURES.

Leanid Simonchik and Maxim Usachonak

Institute of Physics of NAS of Belarus, Minsk, Belarus

l.simonchik@ifanbel.bas-net.by

Determination of the electron density in the range below 10^{13} cm^{-3} in atmospheric-pressure plasmas with low gas temperature faces a number of challenges. These include insufficient sensitivity and the inability to track dynamic processes in non-stationary discharges at using a laser scattering, as well as the need for a very detailed analysis of line broadening mechanisms when using the Stark broadening method. The use of microwaves for diagnosing low-density plasma requires significant plasma size. A significant amount of work has been performed on low-pressure gas-discharge plasmas (ionospheric, tokamak, etc.) using radio waves in different frequency ranges. However, to date, there has been little research using microwave methods to study atmospheric-pressure plasma, particularly plasma jets and streamer discharges, which are characterized by small dimensions compared to the microwave emission wavelength.

The resonator method is most suitable for diagnosing small-scale discharges at atmospheric pressure. It is known from the theory and practice of resonator measurements [Golant V] that introducing plasma into a resonator tuned to one of its natural frequencies leads to a shift in its resonant frequency proportional to the relative change in plasma concentration if the electron collision frequency νe in the plasma is much lower than the resonant frequency ω_0. In the case of atmospheric-pressure plasma, the collision frequency $\nu_e >> \omega_0$, and the shift in the resonant frequency and the resonator transmission will depend on both the electron concentration ne and the collision frequency ν_e.

The 1D EBG plasma structure formed by long low-pressure discharges integrated in a waveguide was investigated in [Arkhipenko V et all]. In this work, the dependencies of microwave transmission through waveguide on plasma inhomogeneities diameters, electron concentration and electron collision frequency are traced numerically and experimentally. This approach we try to use

for diagnostics of thin pulse discharges at atmospheric pressure. Since the electron concentration in different gas-discharge sources varied widely in the experiments, waveguide filters in different wavelength ranges were used: 10, 3 and 1 cm.

To test the waveguide filter method, studies were initially conducted using a low-pressure, direct-current gas-discharge plasma source with more or less definable plasma parameters. This same source also enabled the implementation of a traveling striation mode and the determination of the electron concentration at the striation maximum and between striations. The method was then applied to a pulsed discharge in argon. In this experiment, the electron concentration was also determined from the broadening of the hydrogen lines. A comparison of the obtained concentration values was performed. Revealing significant discrepancies in the determined values at the very beginning of the applied voltage pulse. It may be related to the field in the final stage of the streamer head.

Changes in the electron concentration in the argon jet of a dielectric barrier discharge operating at a frequency of approximately 100 kHz were determined. For this, we used the waveguide filter in 10-cm wave region. It was fabricated using a rectangular waveguide section with a cross-section of 90 x 10 mm^2 and a length of 500 mm. Six rod diaphragms were positioned in the waveguide cross-sections at distances of approximately one wavelength, forming five coupled resonators. Argon plasma jet was passed through central resonator. The dynamics of electron density changes during the applied voltage period of 10 μs were traced. Four maxima in the average density were observed, each at approximately 10^{13} cm^{-3}. Electron concentration in the minima between peaks is more the 1 order of magnitude less.

Finally, the estimation of electron concentration in strimer discharge in air was made an attemp using 10-cm filter. The main difficulty in this experiment is the very thin discharge column, which is a few tenths of a millimeter.

The presented diagnosis method for determination of electron concentration in pulsed gas discharges has good time resolution and can serve as a complement to optical methods, and can also be used to determine the electron density in plasma jets enclosed in opaque dielectric tubes.

References

Golant V (1968) *Microwave methods for plasma investigation*, Moscow, Nauka.

Arkhipenko V et al (2014) *J. Appl. Phys.*, **116** (12), 123302.

APPLICATION OF MICROWAVE-INDUCED PLASMA FOR HYDROGEN ISOTOPE DETECTION STUDIES

Nikola Vujadinović[1], Ivan Traparić[1], Biljana D. Stankov[1], Dragan Ranković[2], Alexandru Anghel[3], Corneliu Porosnicu[3], Ion Mihailescu[3], Miroslav Kuzmanović[4] & Milivoje Ivković[1]

[1]*Institute of Physics Belgrade - National Institute of the Republic of Serbia, Pregrevica 118, Belgrade, 11080, Serbia*

[2]*Vinča Institute of Nuclear Sciences - National Institute of the Republic of Serbia, University of Belgrade, 11001 Belgrade, Serbia*

[3]*National Institute for Laser, Plasma and Radiation Physics, 77125, Magurele, Bucharest, Romania*

[4]*Faculty of Physical Chemistry, University of Belgrade, 11158 Belgrade, Serbia*

nikolav@ipb.ac.rs

The analysis of tritium retention in plasma-facing components (PFCs) in fusion devices is of utmost importance for ensuring safe and efficient operation. When performing optical emission spectroscopic analysis of PFC content, resolving the deuterium and tritium Balmer alpha lines (D_α and T_α) presents a major challenge. Most research so far has focused on laser-induced breakdown spectroscopy (LIBS), however, its usefulness is limited by excessive Stark broadening due to the high electron densities of LIBS plasmas.

We present the use of microwave-induced plasma (MIP), generated in a custom-designed low-pressure chamber, as a solution to this problem. Material from the target was introduced into the MIP at low argon pressure via laser-induced desorption (LID) (see Vujadinovic *et al*. 2025) and laser ablation (LA) (see Vujadinović *et al*. 2026). The light emitted from the MIP was collected and guided to a high-resolution spectrometer equipped with an ICCD camera. The target sample used for the D_α and H_α detection with LID-MIP coupling was a graphite pill with D_2O and H_2O, whereas for the LA-MIP method, a Si-based target coated with C and D was used. The resulting spectra are shown in Figure 1, where Figure 1(a) represents D_α and H_α lines obtained with LID-MIP as the target was cooling down, and Figure 1(b) represents D_α and H_α lines recorded with the LA-MIP

method, with added T_α lines of varying intensity ratios to D_α using CS tables (see Gigosos *et al*. 2003). The FWHMs of the most intense pair of lines from Figure 1(a) are 0.033 nm for the D_α line and 0.038 nm for the H_α line, when fitted with a Voigt function. For the spectrum in Figure 1(b), the Gaussian fits matched the experimental results better and the FWHMs are 0.039 nm for the D_α line and 0.048 nm for the H_α line.

The results indicate that the lowest detectable tritium level would correspond to a T_α line intensity of around 20% of the D_α line intensity (or vice versa) when using LID-MIP method, and between 30% and 50% of the D_α line intensity (or vice versa) for the LA-MIP method. These results demonstrate that both MIP-based setups are promising tools for hydrogen isotope detection studies.

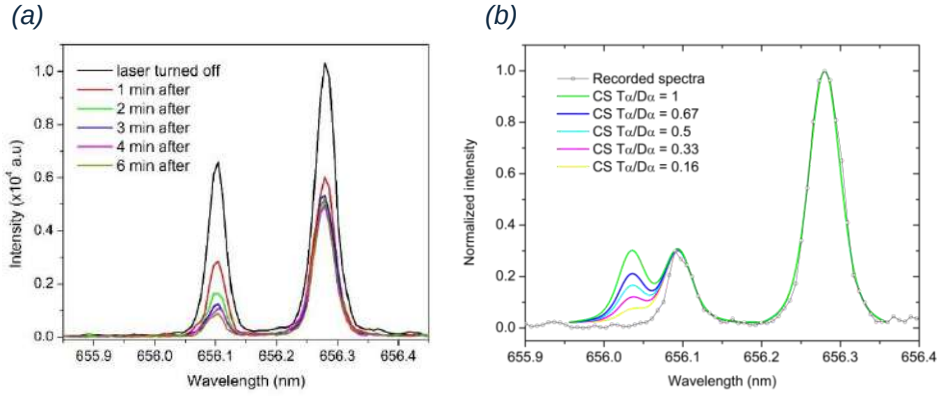

Figure 1: Hydrogen isotope detection using (a) LID-MIP coupling and (b) LA-MIP coupling, with added CS theory estimation of T_α resolving.

References

Gigosos M A, Gonzalez M A and Cardenoso V (2003) *Spectrochim. Acta Part B,* **58**(8), 1489-1504.

Vujadinović N, Traparić I, Ivković M, Ciganović J, Anghel A, Porosnicu C and Mihailescu I (2026) *Eur. Phys. J. Plus*, **141**(2), 157.

Vujadinovic N, Traparic I, Stankov B D, Rankovic D, Kuzmanovic M and Ivkovic M (2025) *Sci. Rep*. **15**(1), 12589.

ANALYSIS OF INDIUM LIBS STREAK IMAGES USING DIMENSIONALITY REDUCTION TECHNIQUES

Maja S. Rabasovic[1], Dragana M. Pavlovic[1,2], Dragutin Sevic[1] and Bratislav M. Obradovic[2]

[1]*Institute of Physics Belgrade, University of Belgrade, Serbia, Pregrevica 118, 11080 Zemun*

[2]*Faculty of Physics, University of Belgrade, Serbia, Studentski trg 12, 11001 Belgrade*

majap@ipb.ac.rs

In this work the obtained LIBS data are analyzed by using data dimension reduction techniques: principal component analysis (PCA), t-distributed stochastic neighbor embedding (t-SNE), and uniform manifold approximation and projection (UMAP) to estimate plasma electron temperature. For machine learning approach to data analysis we use Solo+Mia software package (Version 9.0, Eigenvector Research Inc, USA). The experimental setup employed in this study has been described in detail elsewhere, see Rabasovic *et al.* 2018, Rabasovic *et al.* 2019.

The electron temperature is traditionally estimated using the Boltzmann plot method. PCA, t-SNE and UMAP machine learning (ML) techniques were trained using spectra acquired by streak camera and corresponding temperatures calculated by Boltzman plot. We have used 50 spectral profiles as X block and 5 calculated temperatures as Y block in Solo+Mia software package.

The first two principal components of indium LIBS data are shown in Figure 1. Embeddings plots for two t-SNE and UMAP components are shown in Figure 2.

All three methods successfully grouped the spectral samples. However, PCA did not produce an intuitive separation of the samples corresponding to electron temperatures of 8024 K, 6808 K, and 6605 K. In contrast, both t-SNE and UMAP, with appropriate parameter selection, yielded well-defined and intuitively meaningful groupings of the spectral data.

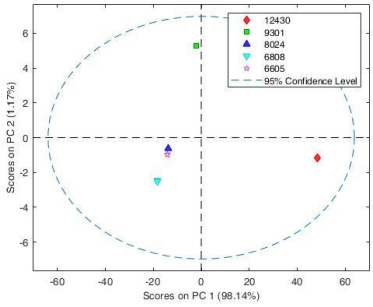

Figure 1: Scores plot of first two principal components.

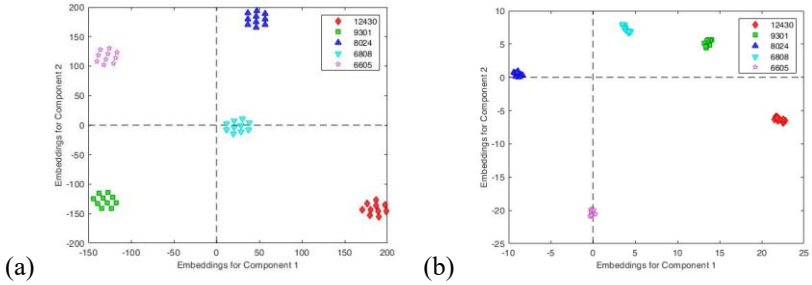

Figure 2: (a) Embeddings plot for two t-SNE components. Perplexity parameter is 10. (b) Embeddings plot for two UMAP components, using following parameters: number of neighbors is 10 and minimum distance is 0.1.

ML is a subset of AI that employs algorithms to analyze data sets and create self-learning models capable of forecasting outcomes, in our case, temperature prediction in LIBS experiments. In this way, Machine learning can be introduced into schools and colleges as part of student practice so that the next generation of students can develop more modern learning methods. Namely, this study demonstrates the possibility of providing students with experimental experience without requiring access to experimental equipment.

References

Rabasovic M S, Marinkovic B P, Sevic D (2018) *Opt. Quant. Electron,* **50**, 236.
Rabasovic M S, Marinkovic B P, Sevic D (2019) *Atoms,* **7**, 6.

INFLUENCE OF SOLAR ACTIVITY ON THE TEMPORAL AND SPATIAL DEVELOPMENT OF SPRITE STREAMERS

Saša Dujko[1], Ilija Simonović[1], Danko Bošnjaković[1], Pierre Gourbin[2] and Christoph Köhn[2,3]

[1]*Institute of Physics Belgrade, Pregrevica 118, 11080 Belgrade, Serbia*

[2] *Department of Space Research and Technology, Technical University of Denmark, Kgs. Lyngby, 2800, Denmark*

[3]*Department of Physics, Technical University of Dortmund, Dortmund, 44227, Germany*

sasa.dujko@ipb.ac.rs

Sprites are large-scale transient luminous events that occur above active thunderstorm systems, typically between 50 and 90 km altitude, where the background atmosphere is strongly shaped by space-weather conditions. They are initiated by intense quasi-electrostatic fields following lightning discharges and develop through rapidly propagating positive and negative streamers. Streamers are thin filaments of weakly ionised, highly non-stationary plasma driven by a space-charge-dominated ionisation front. Understanding their temporal and spatial evolution is essential for quantifying the electrodynamic coupling between the troposphere, mesosphere, and lower ionosphere.

In this work, we employ an axially symmetric classical fluid model for streamer inception and propagation, implemented using the AMReX adaptive-mesh-refinement framework for large-scale parallel simulations (Simonović *et al.* 2024). The model is formulated as a first-order fluid system under the local-field approximation, with time integration performed using a second-order Runge–Kutta scheme and spatial discretisation based on the finite-volume method. Photoionisation is treated using a non-local source term represented by a set of Helmholtz equations, with the Bourdon three-term parametrisation (Bourdon *et al.* 2007). The numerical implementation is verified by comparison with the Afivo-streamer code (Teunissen and Ebert 2017).

As an input to the fluid equations, we use electron transport coefficients in air obtained from Monte Carlo simulations and multi-term solutions of the

Boltzmann equation (Dujko *et al.* 2010), with careful implementation of three-body electron attachment processes relevant at mesospheric pressures. We investigate how variations in background ionisation, controlled primarily by the galactic cosmic ray (GCR) flux, which is modulated by solar activity, affect the inception of positive and negative sprite streamers. Although GCR-driven changes in atmospheric conductivity have only a minor influence on the electric fields required for streamer inception (Tonev and Velinov 2016), they significantly modify the ambient ionisation levels in which sprites evolve.

Our simulations reveal that the response of sprite streamers to changing background ionisation depends critically on the role of photoionisation. In the absence of photoionisation, increasing the background ionisation produces faster and wider streamers, while both the peak electric field and the maximum electron density decrease. When photoionisation is included, the qualitative behaviour of the electric-field and electron density maxima remains the same, but the trend in propagation speed reverses: higher background ionisation now leads to slower streamer propagation. To correctly relate laboratory-scale simulations to mesospheric conditions, we carefully apply similarity laws, modelling streamers on centimetre-scale domains at atmospheric pressure and then scaling the results to kilometre-scale sprite streamers at mesospheric densities. In addition to electron, positive-ion, and negative-ion densities, electric-field distributions, and streamer velocities, we compute streamer propagation lengths, streamer radii, and the maxima of the electric-field and charge-density profiles. Finally, we evaluate the electric field radiated by sprite streamers at large distances by computing the current moment, obtained via axial integration of the streamer current density. These results demonstrate that photoionisation plays a central role in regulating the sensitivity of sprite streamers to ambient ionisation conditions in the mesosphere.

References

Simonović I, Bošnjaković D and Dujko S (2024) *Plasma Sources Sci. Technol.*, **33**, 085012.

Bourdon A, Pasko V P, Liu N Y, Célestin S, Ségur P and Marode E (2007) *Plasma Sources Sci. Technol.*, **16**, 656.

Teunissen J and Ebert U (2017) *J. Phys. D: Appl. Phys.*, 50, 474001.

Dujko S, White R D, Petrović Z Lj, and Robson R E (2010) *Phys. Rev. E*, **81**, 046403.

Tonev P T and Velinov P I Y (2016) *J. Atmos. Solar-Terrest. Phys*., **141**, 27.

INCEPTION DYNAMICS AND ELECTRIC FIELD OF AN ELECTRODELESS DOUBLE-HEADED STREAMER AT ATMOSPHERIC PRESSURE

V. V. Kovačević[1], G. B. Sretenović[1], N. Bonifaci[2], C. Pichard[3], C. Cachoncinlle[4], A. Khacef[4] and S. Iséni[4]

[1]*Faculty of Physics, University of Belgrade, Studentski trg 12-16, 11000 Belgrade, Serbia*

[2]*G2Elab – UMR5269 CNRS / Grenoble INP / Université Grenoble Alpes, 21 rue des Martyrs, 38042 Grenoble, France*

[3]*Polytech Orléans, Université d'Orléans, Site Galilée, 12 rue de Blois, 45067 Orléans, France*

[4]*GREMI – UMR7344 CNRS / Université d'Orléans, 14 rue d'Issoudun, BP6744, 45067 Orléans, France*

vesna@ff.bg.ac.rs

Double-headed streamers (DHS) are fundamental plasma structures linked to sprite discharges and lightning inception (Kosar *et al.* 2012, Qin *et al.* 2012). Although first observed in nature in the late 1990s (Stanley *et al.* 1999), DHS have been studied mainly through numerical models, and Liu *et al.* (2012) proposed their formation from an isolated ionization column under sub-breakdown conditions. This work reports the first laboratory-scale experimental model of electrodeless DHS at atmospheric pressure (Iséni *et al.* 2025), using the Electrodeless Atmospheric Secondary Induced Ionization Jet (EASII-jet) (Iséni *et al.* 2020), which operates without solid electrodes. A noble gas (helium or neon) laminar plume expands into ambient air, a primary ionization wave seeds free charges along the plume, and a delayed secondary wave remotely ignites a DHS within this preionized column, reproducing the sub-breakdown conditions postulated by Liu *et al.* (2012).

Time-resolved iCCD images (Fig. 1) capture the simultaneous counter-propagation of positive and negative streamer fronts from the same breakdown location. The positive streamer shows a compact, intense ionization front, while the negative streamer displays a progressively widening, diffuse structure, consistent with streamer theory (Raizer 1991, Nijdam *et al.* 2020). Despite initiating growth first, the negative streamer propagates more slowly: measured

front velocities are 7.2×10^5 and 5.7×10^5 cm/s (positive, negative) in helium, and 2.8×10^6 and 1.6×10^6 cm/s in neon.

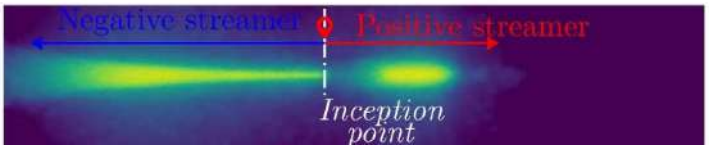

Figure 1: iCCD image of a double-headed streamer in neon at atmospheric pressure (gate width: 25 ns; 800 triggered shots; spectral range: 240–900 nm). The inception point marks the DHS origin; arrows show propagation directions.

Electric field (EF) measured via the Stark splitting and shifting of the allowed and forbidden He I lines at 492.19 nm (Sretenović *et al.* 2014), show an inflection at x = 0 mm (inception point), separating the two streamer regions and confirming their distinct nature. The local EF at x = 0 is 7.8 kV cm^{-1} in helium, below the breakdown threshold E_k = 10 kV cm^{-1}, providing direct evidence of DHS ignition under sub-breakdown conditions and supporting the model of Liu *et al.* 2012. The estimated preionization electron density prior to breakdown is ~1.5×10^{11} cm^{-3}.

In summary, this laboratory model reproduces the formation of electrodeless atmospheric DHS, enabling the first measurements of DHS velocity, gas temperature, and electric field in helium and neon, and validating the theoretical model of Liu *et al.* 2012. These results open new avenues for sprite-physics research with affordable laboratory experiments.

Acknowledgments: This research was partly supported by the French National Research Agency (ANR) with the project MIDICODE (ANR-22-CE51-0022-01) and by the Ministry of Science, Technological Development, and Innovation of Republic of Serbia (Contract No. 451-03-34/2026-03/200162).

References

Iséni S *et al*. (2020) *Phys. Plasmas*, **27**, 123504.
Iséni S *et al*. (2025) *Phys. Rev. E*, **111**, L023202.
Kosar B C *et al*. (2012) *J. Geophys. Res.*, **117**, 2012JA017632.
Liu N *et al.* (2012) *Phys. Rev. Lett.*, **109**, 025002.
Luque A *et al*. (2008) *J. Phys. D: Appl. Phys.*, **41**, 234005.
Nijdam S *et al.* (2020) *Plasma Sources Sci. Technol.*, **29**, 103001.
Qin J *et al*. (2012) *Geophys. Res. Lett.*, **39**, L05810.
Raizer Yu P (1991) *Gas Discharge Physics*, Springer-Verlag, Berlin.
Sretenović G B *et al*. (2014) *J. Phys. D: Appl. Phys.*, **47**, 102001.
Stanley M *et al*. (1999) *Geophys. Res. Lett.*, **26**, 3201.

EFFECTIVE IONIZATION COEFFICIENT AND SECONDARY ELECTRON EMISSION IN HFO-1234YF AND HFO-1234ZE(E)

Jelena Marjanović[1], Dragana Marić[1] and Zoran Lj. Petrović[2,3]

[1]*Institute of Physics, University of Belgrade, Pregrevica 118, 11080 Belgrade, Serbia*

[2]*Serbian Academy of Sciences and Arts, Kneza Mihaila 35, 11001 Belgrade, Serbia*

[3]*School of Engineering, Ulster University, Jordanstown, County Antrim BT37 0QB, UK*

sivosj@ipb.ac.rs

Non-equilibrium discharges in low-GWP (Global Warming Potential) and low-ODP (Ozone Depletion Potential) fluorocarbons are an important research topic due to their growing use as environmentally friendly alternatives to fluorinated greenhouse gases (GFGs) and SF_6 (see Bianchi *et al*. 2019; Metting van Rijn *et al.* 2026; Koch and Franck 2015; Preve *et al*. 2017; Tian *et al.* 2020; Zhang *et al*. 2020). Many applications operate under moderate or high electric fields, making it essential to obtain data relevant to these conditions. Therefore, accurate and reliable information on elementary processes, such as atomic and molecular collisions of dominant species, surface interactions, and breakdown behavior, is crucial for the development and proper functioning of these applications.

Our main objective is to gather basic data concerning DC breakdown in low-ODP and low-GWP fluorocarbon gases. The measurements are performed in a centimetre-sized plan-parallel electrode system under swarm conditions at low currents (~ 1 μA) and low pressures (~0.1 – 1 Torr). By measuring the breakdown and low-current regimes of DC discharges, we have determined coefficients for elementary processes of universal importance, such as the ionization rate and secondary electron yield. Ultimately, we may derive the corresponding effective cross sections. In this paper, we present reduced ionization coefficients determined from axial emission profiles (see Marić *et al*. 2014; Marjanović *et al*. 2024) of the low-current diffuse discharge regime (Steady-State Townsend, SST) in trans-1,3,3,3-tetrafluoropropene (HFO-1234ze(E)) and 2,3,3,3-tetrafluoropropene (HFO-1234yf). We also compare the secondary electron yields for these gases, derived from the ionization coefficients.

The ionization coefficients, together with breakdown and voltage–current measurements, provide strong constraints on the mean electron energy in the discharge. This enhanced control over mean energy facilitates the development of comprehensive and self-consistent sets of cross sections and other discharge parameters within the energy range most pertinent for plasma modeling.

Acknowledgements: This research was supported by the Science Fund of the Republic of Serbia, Grant No. 7749560, project EGWIn. Zoran Lj. Petrović is grateful to the SASA project F155.

References

Bianchi A, Delsanto S, Dupieux P, Ferretti A, Gagliardi M, Joly B, Manen S P, Marchisone M, Micheletti L, Rosano A and Vercellin E (2019) *JINST,* **14**, P1101414.

Marić D, Savić M, Sivoš J, Škoro N, Radmilović-Radjenović M, Malović G, Petrović Z Lj (2014) *Eur. Phys. J. D*, **68**, 155.

Marjanović J, Marić D, Petrović Z Lj (2024) *Eur. Phys. J.* D, **78**, 14.

Metting van Rijn M, Biagi S F, Ranković M et al (2026) J. *Phys. D: Appl. Phys*., **59**, 205205.

Koch M and Franck C M (2015) *IEEE Trans. Dielec. and Elect. Insula*., **22**, 3260.

Preve C, Piccoz D, Maladen R (2017*) CIRED Open Access Proc. J*., **1**, 42.

Tian S, Zhang X, Cressault Y, Hu J, Wang B, Xiao S, Li Y and Kabbaj N (2020) *AIP Adv.*, **10**, 050702.

Zhang B, Chen L, Li X, Guo Z, Pu Y, Tang N (2020) *IEEE Transactions on Dielectrics and Electrical Insulation*, **27**, 1187.

PASCHEN'S CURVES FOR AVALANCHE-TO-STREAMER TRANSITION AND MULTIELECTRON INITIATION

V. Lj. Marković, S. N. Stamenković and S. S. Đokić

Department of Physics, Faculty of Sciences and Mathematics, University of Niš, Serbia

vidosav@pmf.ni.ac.rs

The streamer mechanism of electrical breakdown of gases was developed in the 40s of the last century, mainly in the approximation of single-electron initiation of electron avalanches. In the present work, a generalized Paschen's law for high values of the product of pressure and interelectrode distance pd and for multielectron initiation of electron avalanches is derived. Theoretical expressions have been compared to the experimental results by varying initial number of electrons k. In the study of electrical breakdown of gases, Townsend semi-empirical formula for the electron impact ionization coefficient α is used

$$\alpha = Ap\ exp(-Bp/E), \tag{1}$$

where p is the gas pressure, E is the electric field, and constants A and B are determined by fitting the experimental data. It is well known that the breakdown condition for the Townsend breakdown mechanism is $\gamma[exp(\alpha d) - 1] = 1$, where γ is the secondary electron ionization coefficient and d is the interelectrode distance. Combining with α from (1) for the homogeneous breakdown electric field $E_T = U_T/d$, leads to the static breakdown voltage U_T at low product of gas pressure and interelectrode distance (low pd values)

$$U_T = Bpd/[\ln(Apd) - \ln\ln[(1+\gamma)/\gamma]]. \tag{2}$$

The dependence $U_T = f(pd)$ is known as Paschen law (Townsend 1915, Meek and Craggs 1978). The breakdown condition for streamer breakdown and multielectron initiation is

$$\bar{n} = ke^{\alpha d} = n_C, \tag{3}$$

where $\bar{n}$ is the mean number of electrons in the electron avalanche, k is the number of initiating electrons and n_C ($\sim 10^8$) is the critical number of electrons

for the streamer breakdown. Combining the relations (1) and (3) for the homogeneous breakdown electric field $E_S = U_S/d$, the static breakdown voltage for streamer breakdown mechanism U_S is obtained in the form

$$U_S = Bpd/[\ln(Apd) - \ln\ln[(n_C/k)]]. \quad (4)$$

By differentiating (4) over pd and equating with zero, the minimum of the streamer breakdown curve is obtained at $(pd)_{min} = e\,ln(n_C/k)/A$ and the minimum streamer breakdown voltage $(U_S)_{min} = Be\ln(n_C/k)/A$.

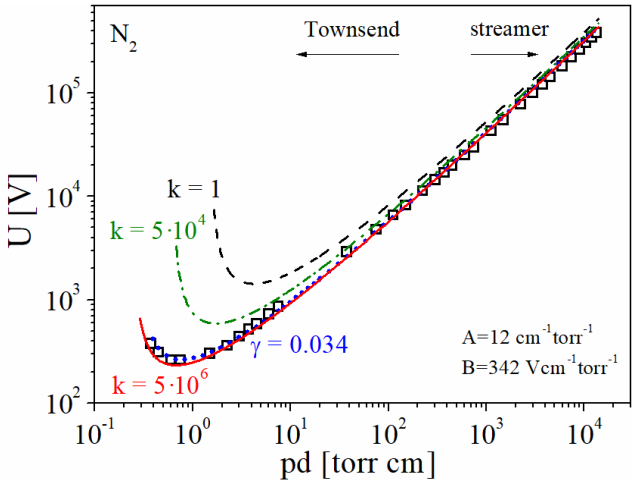

Figure 1: Paschen curves for nitrogen (Dakin *et al.* 1974), Townsend (2) and streamer breakdown mechanism (4) for $k = 1, 5 \cdot 10^4, 5 \cdot 10^6$ initiating electrons ($n_C = 10^8$).

Supported by the Ministry of Science, Technological Development and Innovation of the Republic of Serbia, contract No. 451-03-34/2026-03/200124.

References

Dakin T W, Luxa G, Oppermann G, Vigreux J, Wind G and Winkelnkemper H (1974) *Electra*, **32**, 61-82.

Meek J M and Craggs J D Ed. (1978) *Electrical Breakdown of Gases*, John Wiley and Sons, Chichester.

Townsend J S (1915) *Electricity in Gases*, Clarendon Press, Oxford.

BREAKDOWN PROBABILITY FOR STREAMER BREAKDOWN MECHANISM WITH MULTIELECTRON INITIATION

Suzana N. Stamenković, Vidosav Lj. Marković and Sanja S. Đokić

Department of Physics, Faculty of Sciences and Mathematics, University of Niš, Serbia

ssuzana@pmf.ni.ac.rs

Probability of electrical breakdown for single electron initiation P_1 is theoretically derived, based on Furry (geometrical) distribution for the number of electrons in the avalanche. We have derived the breakdown probability for multielectron initiation of avalanches P_k with k initial electrons, based on a Negative Binomial Distribution (NBD).

The electrical breakdown of a gas represents a sudden transition of a gas from a non-conductive to a conductive state. Free electrons, which can initiate breakdown, are created due to cosmic radiation and natural radioactivity of the environment. If a voltage higher than the static breakdown voltage is connected to the gas filled tube, an avalanche multiplication of electrons occurs due to ionization by electron impact. When the average number of electrons $\bar{n}$ reaches or exceeds a critical number n_c, an electric breakdown of the gas can occur by the streamer mechanism (Blair *et al*. 1978). In that case, the breakdown probability for one-electron initiation is given by relation (Blair *et al*. 1978):

$$P_k(k=1) = \int_{n_c}^{\infty} P(n,d)dn = \int_{n_c}^{\infty} \frac{1}{\bar{n}}\left(1-\frac{1}{\bar{n}}\right)^{n-1} dn, \qquad (1)$$

where $P(n,d) = 1/\bar{n}(1-1/\bar{n})^{n-1}$ represents Furry distribution for avalanche initiated by a single electron. The average number of electrons is given by:

$$\bar{n} = \sum_{n=1}^{\infty} nP(n,d) \,/\, \sum_{n=1}^{\infty} P(n,d) = \exp(\alpha d), \qquad (2)$$

where d is the inter-electrode gap distance and α is the first Townsend`s ionization coefficient. For $n \gg 1$, Furry distribution can be approximated by exponential dependence $P(n,d) = exp(-n/\bar{n})/\bar{n}$. Accordingly, the breakdown probability for single electron initiation is obtained by (Blair *et al*. 1978):

$$P_k(k=1) = \int_{n_c}^{\infty} \frac{1}{\bar{n}} exp\left(-\frac{n}{\bar{n}}\right) dn = exp\left(-\frac{n_c}{\bar{n}}\right). \qquad (3)$$

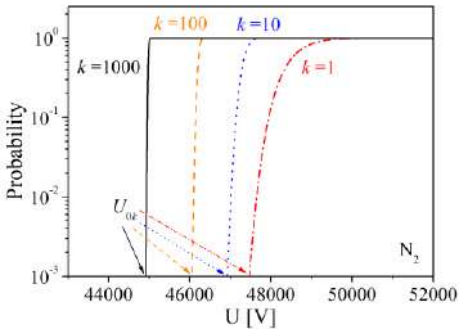

Figure 1: The breakdown probability as a function of voltage.

In the case of multi-electron initiation of an electron avalanche with k initial electrons, instead of Furry distribution, the NBD $P(n,p,k)$ should be used:

$$P_k(k>1) = \int_{n_c}^{\infty} P(n,p,k)\,dn = \int_{n_c}^{\infty} \left(\frac{k}{n}\right)^k \left(1-\frac{k}{\bar{n}}\right)^{n-k} dn, \qquad (4)$$

where the average number of electrons in the avalanche is obtained as:

$$\bar{n} = \sum_{n=1}^{\infty} nP(n,p,k) \,/\, \sum_{n=1}^{\infty} P(n,p,k) = k\,exp(\alpha d). \qquad (5)$$

For a large number of electrons in the avalanche, the Polya distribution can be used as a good approximation of the NBD (Stamenković S N *et al*. 2018):

$$P_k(k>1) \approx \frac{1}{\bar{n}} \frac{k^k}{\Gamma(k)} \int_{n_c}^{\infty} \left(\frac{n}{\bar{n}}\right)^{k-1} exp\left(-\frac{nk}{\bar{n}}\right) dn. \qquad (6)$$

The breakdown probability $P_k(U)$ grows steeper (Figure 1) compared to $P_1(U)$ and better defines the minimum breakdown voltage U_{0k} for the streamer breakdown mechanism. The breakdown voltages U_{0k} with k initial electrons decrease with increasing the number of initial electrons k.

The authors are grateful to the Ministry of Science, Technological Development and Innovation of the Republic of Serbia for partial financial support (contract number 451-03-34/2026-03/200124) and Dr. M. S. Đorđević for their assistance with the theoretical derivations

References

Blair D T A, Crichton B H, and Somerville I C (1978) *in Proc. Int. Symp. Gaseous Dielectrics*, Ed.Christophorou L G (Oak Ridge National Lab., Oak Ridge, Tenn.) 360

Stamenković S N et al. (2018) *Journal of Instrumentation* **13**, P12002.

PUMP-DOWN AND LEAK-UP CURVES OF A GLASS VACUUM CHAMBER

S. S. Đokić, V. Lj. Marković and S. N. Stamenković

Faculty of Sciences and Mathematics, University of Niš, Niš, Serbia

sanja.djokic@pmf.edu.rs

In the present work, the constant volume method was used to analyze pump-down curve of a glass vacuum chamber (for gas discharge studies in flow regime) with a turbomolecular pumping system (Suurmeier *et al.* 2015). The pressure variation p in a chamber was measured as a function of time t. For the pump-down process, the pressure decrease is described by (Kurepa *et al.* 1988):

$$p - p_{res} = (p_0 - p_{res})e^{-S_0 t/V}, \quad (1)$$

where p_0 is the initial pressure, p_{res} is the residual pressure, V is the chamber volume ($\sim 300\ cm^3$), and S_0 is the effective pumping speed at the chamber (Bello 2018).

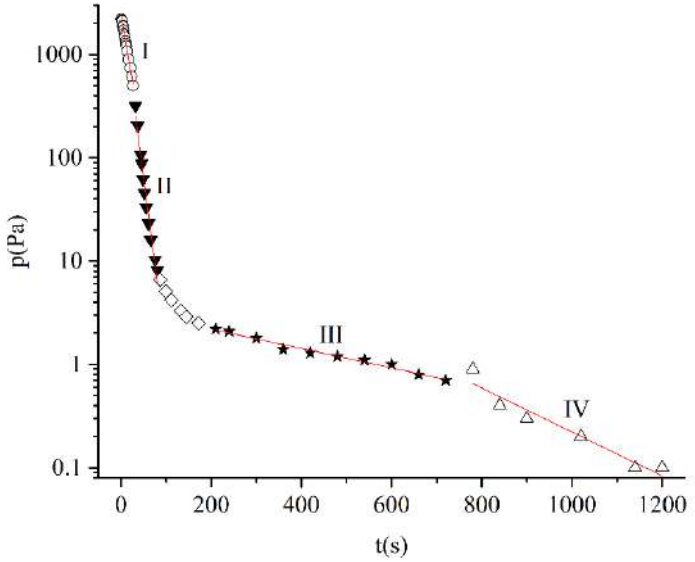

Figure 1: Pump-down pressure curve with linear fits in regions I-IV.

Assuming S_0 to be constant in each approximately linear region of the semi-logarithmic curve (Bello 2018, Suurmeier *et al.* 2015), the fitted slopes $-S_0/V$ from I-IV gave: $S_0^I = 1.72 \cdot 10^{-5}\ m^3/s$, $S_0^{II} = 2.28 \cdot 10^{-5}\ m^3/s$, $S_0^{III} = 6.47 \cdot 10^{-7}\ m^3/s$ and $S_0^{IV} = 1.47 \cdot 10^{-6}\ m^3/s$. Regions I-III correspond to pumping by the diaphragm pump, while region IV represents the transition to turbomolecular pumping observed near 1 Pa (Bello 2018).

After isolating the chamber from the pumping unit, the pressure increase was recorded as a function of time. Assuming an approximately linear pressure rise (Suurmeier *et al.* 2015) the gas throughput was determined as:

$$Q = V(\Delta p/\Delta t), \tag{2}$$

where V is the volume of the vacuum chamber and $\Delta p/\Delta t$ is the pressure rise rate (Bello 2018). The calculated value was $Q = 2.67 \cdot 10^{-6}\ Pa\ m^3/s$.

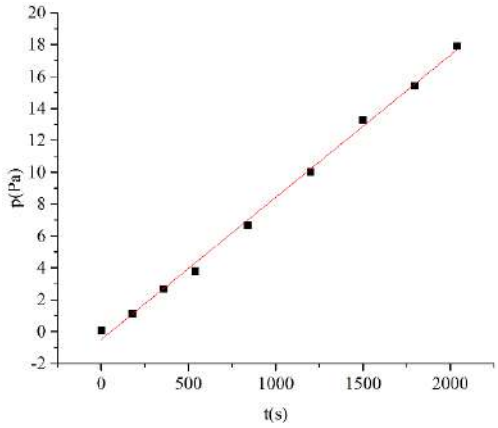

Figure 2: Pressure increase during the leak-up measurement with a linear fit.

This work was supported by the Ministry of Science, Technological Development and Innovation of the Republic of Serbia under contract 451-03-34/2026-03/200124.

References

Bello I (2018) *Vacuum and Ultravacuum: Physics and Technology*, CRC Press / Taylor & Francis Group, Boca Raton

Kurepa M i Čobić B (1988) *Fizika i tehnika vakuuma*, Naučna knjiga, Beograd.

Suurmeier B, Mulder T and Verhoeven (2015) *Vacuum Science and Technology*, The High Tech Institute and Settels Savenije van Amelsvoort, Eindhoven.

TEMPORAL DEVELOPMENT OF VIBRATIONAL DISTRIBUTION FUNCTION OF N_2 IN RF PLASMA DISCHARGES

Violeta V Stanković Mališ, Zorica Popović, Sava M D Galijaš and Goran B Poparić

[1]*University of Belgrade, Faculty of Physics, Studentski trg 12, P.O. Box 44, 11000 Belgrade, Serbia*

goran.poparic@ff.bg.ac.rs

The temporal development of the vibrational distribution function (VDF) of nitrogen molecules is calculated and tracked from the onset of radio-frequency (RF) plasma discharges at low pressure until a dynamic equilibrium is established. The calculations are performed using an extended Monte Carlo (eMC) simulation coupled with a Kinetic Module (KM). The eMC simulation includes all electron-molecule scattering processes: elastic scattering, vibrational excitations and de-excitations, electronic excitations, dissociation and ionization.

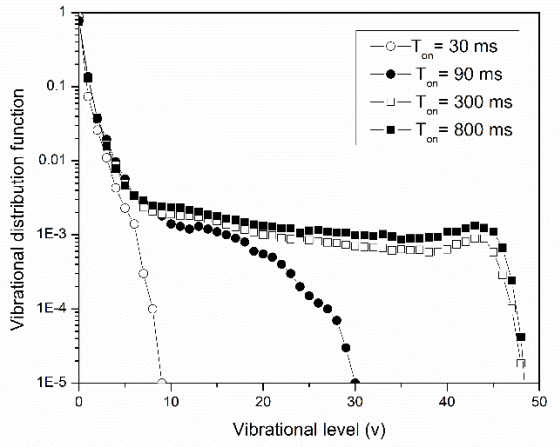

Figure 1: Temporal evolution of the vibrational distribution function of N2 in RF plasma discharges at an ionization degree of 10-7, a reduced electric field of E/N = 25 Td, a gas temperature of Tg = 300 K and a gas pressure of p = 1 Torr.

The molecule-molecule gas collisions that lead to V-V and V-T energy transfer processes are also included in the modeling through the Kinetic Module of the simulation. The simulation algorithm is described in detail in ref. Stanković Mališ *et al*. 2026, where it is applied to micro-wave plasma discharges. The temporal evolution of the vibrational distribution function of N_2 in RF plasma discharge with a standard frequency of 13.56 MHz and a reduced electric field of E/N=25 Td is shown in Figure 1 for several characteristic times following plasma ignition. The gas pressure was set to 1 Torr, while gas temperature was set to 300 K. As shown in the figure, there is a rapid increase in the population of the first few excited vibrational levels due to electron impact vibrational excitation processes. Over longer time intervals, gas molecule-molecule collision processes spread the vibrational distribution to higher vibrational levels. At the end of the temporal development, a dynamic equilibrium is achieved, and the vibrational distribution function fluctuates statistically only.

The simulation algorithm also enables tracking the coupled electron energy distribution function (EEDF). This coupled EEDF evolves simultaneously with the VDF. Along with the VDF, the EEDF also achieves dynamic equilibrium by evolving from the beginning of the plasma discharge. This dynamic equilibrium EEDF is strongly influenced by the VDF, especially its high-energy tail. In this way, the state of the VDF in RF plasma discharges, which determines the vibrational temperature of nitrogen molecules, also strongly determines the rate coefficients for excitation of highly excited electronic states of N_2 and its ionization.

Acknowledgments: This work was supported in part by the Ministry of Science, Technological Development and Innovation of the Republic of Serbia under contract Nos. 451-03-34/2026-03/200162 and 451-03-33/2026-03/200162.

References

Stanković Mališ V V, Popović Z, Galijaš S M D and Poparić G B (2026) *Plasma Sources Sci. Technol.*, **35**, 025021. https://doi.org/10.1088/1361-6595/ae42e6.

EFFECT OF RESIDUAL GAP AND PACKING MATERIAL ON DISCHARGE CHARACTERISTICS IN A SINGLE-BEAD PACKED DBD REACTOR

S. M. Radenković[1], G. B. Sretenović[1], I. B. Krstić[1], B. M. Obradović[1], M. M. Kuraica[1] and V. V. Kovačević[1]

[1]*Faculty of Physics, University of Belgrade, Studentski trg 12, 11000 Belgrade, Serbia*

simeon.radenkovic@ff.bg.ac.rs

Packed-bed dielectric barrier discharge (PB-DBD) reactors are widely used in plasma-catalytic applications such as gas conversion, VOC abatement and ozone generation, since the packing material locally enhances the electric field and provides extra surface for plasma-catalyst interaction. Two discharge regimes are typically distinguished: polar (point-to-point) microdischarges at particle contact points, and surface streamers propagating along the dielectric surface. The transition between the two regimes depends on the permittivity of the packing material and on the reactor geometry, with the residual gap between the electrode and the packing particle recently identified as a key parameter controlling streamer formation. Ozone production is a convenient probe reaction for the chemical activity of PB-DBD systems, since its yield is sensitive to the electron energy distribution, gas temperature and surface processes taking place in the discharge.

We investigate a single-bead packed DBD reactor with four dielectric materials – alumina, glass, zeolite, zirconia – as 3 mm spherical beads placed between two pin electrodes covered with flat alumina dielectrics, inside a sealed chamber with quartz windows for optical access. The bead rests on the lower dielectric above the grounded electrode; the upper high-voltage electrode is mounted on a micrometer stage allowing the residual gap to be varied from 0 to 3 mm. The discharge is generated in dry air and in argon at a constant flow rate of 3 slm and atmospheric pressure, driven by a sinusoidal high-voltage supply (700 Hz, amplitude up to 20 kV).

Figure 1 illustrates the influence of packing material and surrounding gas on discharge morphology for a 1 mm residual gap. High-permittivity zirconia favours localized, point-like microdischarges near the contact region, while

lower-permittivity glass promotes surface streamers bridging the gap; in argon the discharge is more diffuse, covering a larger bead area than in air. Current-pulse analysis yields microdischarge amplitude, duration and charge, while optical emission spectra identify the dominant excited species. Ozone concentration, discharge power (Lissajous figures) and voltage-current characteristics are recorded for each material and gas over a range of applied voltages. Increasing the residual gap enhances ozone production in air, consistent with the larger volume available for streamer development. These results link discharge electrical and optical parameters to chemical output, clarifying the role of packing material and reactor geometry.

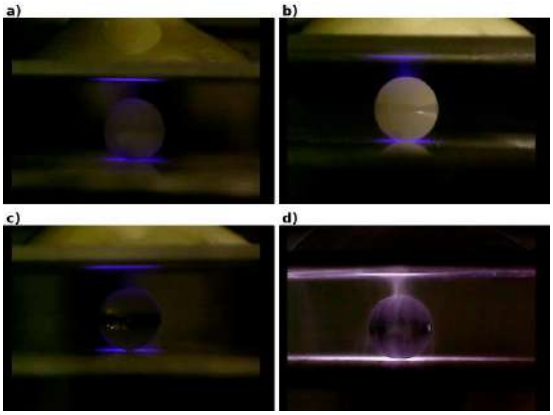

Figure 1: Discharge images with a) alumina, b) zirconia and c) glass beads in air, and d) glass bead in argon, for a residual gap of 1 mm.

Acknowledgments: This work was supported by the Ministry of Science, Technological Development and Innovation of the Republic of Serbia (Contract No. 451-03-34/2026-03/200162).

References

Butterworth T and Allen R W K (2017) *Plasma Sources Sci. Technol.*, **26**, 065008.

Kim H-H (2004) *Plasma Process. Polym.*, **1**, 91.

Kogelschatz U (2003) *Plasma Chem. Plasma Process.*, **23**, 1.

Van Laer K and Bogaerts A (2016) *Plasma Sources Sci. Technol.*, **25**, 015002.

Whitehead J C (2016) *J. Phys. D: Appl. Phys.*, **49**, 243001.

COLLISIONS OF STREAMERS IN THE MIXTURES OF N_2 AND C_3F_8 IN THE PIN-PIN ELECTRODE CONFIGURATION

Ilija Simonović[1], Danko Bošnjaković[1], and Saša Dujko[1]

[1]*Institute of Physics Belgrade, Pregrevica 118, 11080 Belgrade, Serbia*

isimonovic@ipb.ac.rs

Streamers are thin filaments of non-equilibrium plasma that form when an ionization front moves through non-ionized matter, see Teunissen and Ebert 2017. They have numerous applications in technology, including purification of polluted gases and liquids, surface processing and plasma medicine. Streamers are also the main breakdown mechanism in high-voltage insulation technology. Further optimization of these applications requires the joint effort of experimental investigations and theoretical modelling.

In this work, we have investigated streamer collisions in N_2-C_3F_8 mixtures using a pin-pin electrode configuration and an axisymmetric fluid model. Our model has been developed in the AMReX library, see Zhang et al 2019., and it has been shown in Simonović et al. 2024. and Simonović et al. 2025. Cross sections for electron scattering in N_2 and C_3F_8 were taken from the MAGBOLTZ code (Biagi 1999 and Biagi MAGBOLTZ version 11.17) and used to calculate electron swarm transport coefficients by employing Monte Carlo simulations (Mirić et al. 2016) and numerical multi-term solutions of Boltzmann's equation (Dujko et al. 2010). Electron swarm transport coefficients were then used as input to our axisymmetric fluid model. The simulations have been performed at an applied electric field equal to half the critical field of C_3F_8.

In this work, we have investigated the spatial profiles of electron number density and the resulting electric field, as well as their temporal evolution as streamers form, propagate and collide with each other. We have also investigated the temporal evolution of the maximum electric field, maximum electron number density, streamer velocity, and streamer radius. The maximum electric field, the maximum number density of electrons, and the streamer velocity of both positive and negative streamers all rise monotonically as the streamers approach each other until they collide. In contrast, the streamer radius for both positive and negative streamers decreases monotonically as the streamers approach each other.

The maximum electric field, attained before the streamers collide, increases with the percentage of C_3F_8. The same holds for the maximum electron number density. However, the value of the streamer radius before the streamers collide reduces with increasing percentage of C_3F_8.

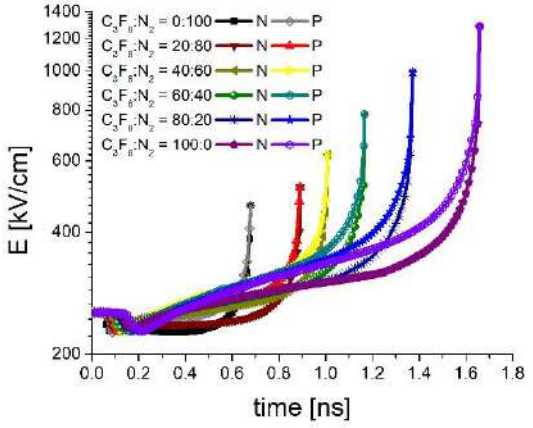

Figure 1: The comparison of the maximum electric field for streamers in all studied gases. N and P denote negative and positive streamers, respectively.

References

Biagi S F (1999) *Nucl. Instrum. Methods Phys. Res. A*, **421**, 234.

Biagi S F, *MAGBOLTZ*, version 11.17.

Dujko S *et al*. (2010) *Phys. Rev. E*, **81**, 046403.

Mirić J *et al* (2016) *Plasma Sources Sci. Technol.*, **25**, 065010.

Simonović I *et al*. (2024) *Plasma Sources Sci. Technol.*, **33**, 085012.

Simonović I *et al.* (2025) *Plasma Sources Sci. Technol.*, **34**, 125004.

Teunissen J and Ebert U (2017) *J. Phys. D: Appl. Phys.*, **50**, 474001.

Zhang W *et al*. (2019) *J. Open Source Softw.*, **4**, 1370.

SPECTROSCOPIC STUDY OF A GRIMM-TYPE GLOW DISCHARGE WITH REVERSED ORDER END-ON VIEW

Nikodin V. Nedić[1], Nikola V. Ivanović[2], Ivan R. Videnović[1] and Djordje Spasojević[1]

[1]*University of Belgrade, Faculty of Physics, P.O. Box 44, 11001 Belgrade, Serbia*

[2]*University of Belgrade, Faculty of Agriculture, Nemanjina 6, 11080 Belgrade, Serbia*

ivan.videnovic@ff.bg.ac.rs

The standard Grimm abnormal glow discharge source is the basic design used in many commercial emission instruments for analytical purposes in industry and laboratory research. The increasing use of optical emission spectroscopy for qualitative and quantitative analysis of metallic and non-metallic samples has created a need for reliable cataloguing of the wavelengths of argon and neon spectral lines, as these gases are the most widely used working gases in analytical glow discharge sources. Weiss *et al.* 2009 used Fourier transform spectroscopy to measure the wavelengths and intensities of spectral lines emitted by the standard Grimm discharge source and compared them with corresponding data obtained from other radiation sources. It was observed that some Ar I and Ne I spectral lines exhibit a spectral width at half maximum 4 to 5 times greater than the instrumental profile. In addition to the line broadening, a pronounced asymmetry on the red wing was detected. Research reported by Majstorović *et al.* 2013 argued that these neon and argon line asymmetries arise from the combined influence of the Stark effect caused by microfields in the negative glow region and the Stark effect caused by the macroscopic electric field in the cathode sheath. Further detailed investigations by Nedić *et al.* 2022 and Ivanović *et al.* 2023 correlated the asymmetries in end-on line recordings with the red-shifted Stark components in the electric macrofield in the cathode sheath. These results indicated the possibility of estimating the maximum electric field strength and cathode sheath length in a standard Grimm glow discharge with traditional end-on spectroscopy, in which the optical path first passes through the negative glow region and then through the cathode sheath, see Figure 1.

This naturally leads to the following question: would the characteristic asymmetry of Ne I spectral lines remain unchanged if the observation direction

were reversed? To enable the reversed observation direction, a 2 mm aperture was drilled through a flat copper cathode sealed with a quartz window on the observation side and a metallic mesh on the opposite (discharge) side to prevent a hollow cathode operation. This modification enabled the abnormal glow regime characteristic for the Grimm-type source.

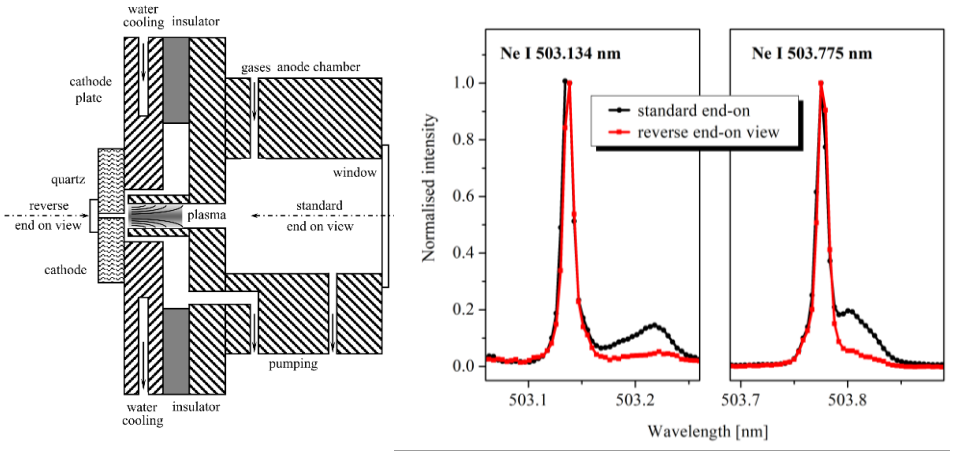

Figure 1. Spectroscopic observations of Grimm glow discharge in standard and reversed end-on view, and recorded profiles of Ne I 503.134 nm and Ne I 503.775 nm spectral lines.

End-on spectra of the neon spectral lines were recorded under identical discharge conditions in both standard and reversed directions. After intensity normalisation, the profiles exhibited similar shapes, with differences primarily in relative intensities and signal-to-noise ratio, see Figure 1. The absence of the opposite asymmetry in the end-on profiles recorded in the reversed direction provides further evidence that the structures in the red wings are not predominantly of Doppler origin, but arise from the shifted Stark components in the macroscopic electric field in the cathode sheath.

References

Ivanović N V *et al.*(2023) *Spectrochim. Acta Part B*, **208**, 106775.

Majstorović G L *et al.*(2013) *Plasma Sources Sci. Technol.*, **22**, 045015.

Nedić N V *et al.*(2022) *J. Anal. At. Spectrom.*, **37**, 1318.

Weiss Z, Steers E B M, Šmid P and Hoffmann V (2009) *J. Anal. At. Spectrom.,* **24**, 27.

STRUCTURAL DEGRADATION AND ELECTROKINETIC PROPERTY CHANGES OF SPODUMENE CRYSTALS VIA ATMOSPHERIC-PRESSURE DBD PLASMA TREATMENT

Igor Bunin[1] and Irina Khabarova[1]

[1]*N.V. Melnikov's Institute of Comprehensive Exploitation of Mineral Resources, Russian Academy of Sciences (ICEMR RAS), Moscow, Russia*

bunin_i@mail.ru

Spodumene ($LiAl[Si_2O_6]$) represents a primary lithium-bearing chain silicate. The extraction of lithium from pegmatite deposits faces significant constraints due to the physical and surface affinity between spodumene and associated gangue components, such as quartz or feldspars. Standard physical separation techniques often fail to provide high efficiency. This study explores an alternative approach based on non-equilibrium plasma-induced surface modification to alter the structural state and surface charging of the mineral. We investigate the behavior of natural spodumene crystals exposed to low-temperature atmospheric-pressure dielectric barrier discharge (LTP–DBD) plasma generated in ambient air. The investigated specimens consist of grayish-green prismatic crystals containing approximately 7.0–8.0 wt.% (Li_2O), see Morozova and Bazai 2020, featuring intergrowths of albite, muscovite, quartz, and other minor mineral phases. The plasma treatment was conducted in a plane-parallel discharge configuration featuring a single nickel mesh electrode to enhance local electric field gradients. The system was driven by microsecond periodic pulses with a voltage amplitude $U_A \approx 20$ kV and a rapid rise time of ~300 ns. The discharge energy delivery was controlled by varying the pulse width $\tau_{imp} = 4.0$ and 8.0 μs and the repetition frequency $f_{imp} = 2.0$ and 16.0 kHz. Exposure intervals t_{treat} varied between 10 and 60 s. The resulting surface variations, elemental re-distribution, microhardness profiles, and zeta potential shifts were systematically monitored using SEM–EDX, Vickers indentation, and electrophoretic light scattering. The plasma-stimulated surface degradation and the intensive propagation of induced microcracks are clearly visualized via SEM imaging (Figure 1). The pristine mineral surface exhibits typical regular cleavage steps and minor structural irregularities (Fig. 1a). In contrast, exposure to the LTP–DBD environment even under moderate settings leads to severe structural failure (Fig. 1b). The

micrograph explicitly demonstrates the explosive opening of block boundaries and thermal-shock induced fragmentation. This surface degradation is driven by several concurrent plasma-surface interaction mechanisms: localized thermal-shock and mechanical stress accumulation at the boundaries of different mineral phases due to mismatched dielectric and thermal constants under high electric fields; rapid pressure buildup within internal gas-liquid macro- and micro-inclusions, resulting in their explosive opening even at moderate bulk temperature rises ($\Delta T \approx 100$–150 ºC); and localized structural amorphization or melting, leading to the formation of altered polymorphic modifications on the treated surface. These combined factors induce intensive microcracking, resulting in a substantial mechanical weakening of the outer crystal layers. The highest relative reduction in Vickers microhardness reached 18.0% (dropping from 1085 down to 890 kgf/mm^2), observed under intense discharge conditions ($\tau_{imp} = 8.0$ µs, $f_{imp} = 16.0$ kHz), $t_{treat} = 30$–40 s. Concurrently, plasma exposure modified the surface functional groups, shifting the negative electrokinetic potential of fine particles from –18.5 mV to –33.5 mV under moderate settings ($\tau_{imp} = 4$ µs, $f_{imp} = 2$ kHz), $t_{treat} = 10$–30 s. The findings indicate that atmospheric DBD plasma parameters can be tailored to induce controlled structural damage and surface charge reorganization in complex silicates, offering a promising approach for implementation in advanced chemical processing and lithium extraction from spodumene concentrates.

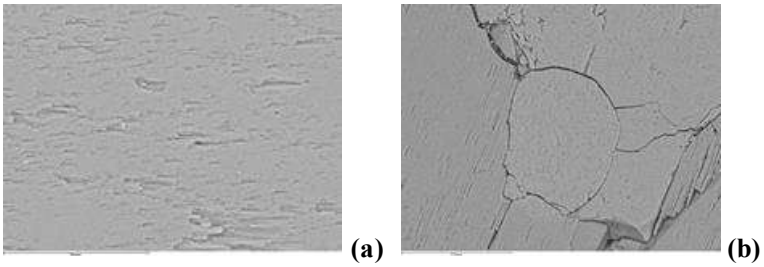

Figure 1: SEM micrographs of spodumene crystal surface: (a) pristine cleavage plane, and (b) induced microcracks and block boundaries after LTP–DBD plasma treatment. Scale bars: (a) 60 µm, (b) 100 µm.

References

Morozova L and Bazai A (2020) *Proc. Fersman Sci. Session Geol. Inst. Kola Sci. Center RAS*, **17**, 369.

GAS-DEPENDENT SURFACE MODIFICATION OF CARBON THIN FILMS IN A PULSE RESONANCE PLASMA SYSTEM

Thea Ferley[1] and Vladimir Milosavljević[1,2]

[1]*School of Physics, Clinical and Optometric Sciences, Technological University Dublin, Ireland*

[2]*Faculty of Physics, University of Belgrade, Serbia*

C20429394@mytudublin.ie

Gas-dependent surface modification of carbon thin films in a pulse resonance plasma system is strongly governed by the interaction between the working gas and the resulting plasma chemistry (Fig. 1). The choice of gas alters fundamental plasma characteristics such as ionisation energy, dominant species, and the balance between reactive and energetic processes. These differences directly translate into variations in how the plasma interacts with the carbon surface and therefore determine the nature and extent of the resulting surface modification.

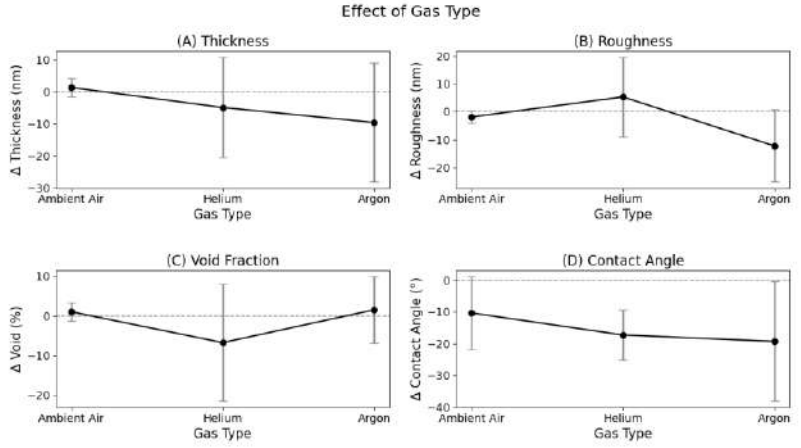

Figure 1: Change in film properties after plasma exposure, grouped by gas type (ambient air, helium, and argon). Panels show the average post–pre difference in (A) thickness, (B) roughness, (C) void fraction, and (D) water contact angle. Error bars represent one standard deviation across samples.

A key observable outcome of these interactions is the change in wettability, which can be linked to modifications in surface chemistry. The contact angle is primarily controlled by surface energy, which in turn depends on the introduction or removal of functional groups at the surface. In ambient air, the presence of reactive oxygen and nitrogen species promotes chemical functionalisation, leading to the formation of polar groups that increase surface energy and reduce the contact angle. This chemically driven pathway explains the stronger wettability changes observed under air plasma conditions.

In contrast, inert gas environments such as argon and helium influence the surface primarily through physical processes. Argon, due to its higher atomic mass, is more effective in momentum transfer during ion bombardment, enhancing sputtering and the removal of weakly bound surface material. This process increases the number of active surface sites and contributes to changes in wettability through physical restructuring. Helium, on the other hand, generates a more stable and uniform plasma with lower variability. Although it has reduced momentum transfer compared to argon, its higher population of energetic electrons and excited species still enables surface modification, albeit through a different interaction pathway.

These gas-dependent mechanisms also influence structural properties such as roughness and void fraction. Given the porous and heterogeneous nature of carbon thin films, localised plasma interactions can significantly affect the internal structure of the material. Depending on the gas environment, the dominant effect may shift between material removal, surface restructuring, or partial collapse of the porous network. This highlights the sensitivity of both chemical and structural surface properties to plasma conditions.

References

Bucalossi J (2022) *Nuclear Fusion*, **62**:042007–042007, 02.

Gulan M and Milosavljevic V (2021) *Europhysics Letters*, **133**:43002, 02.

Gulan M and Milosavljevic V (2022) *International Journal of Energy Research*, **46**(5), 6337-6350.

Singh A, Choubey A, Modi M H, Upadhyaya B N, Oak S M, Lodha G S and Deb K S (2013) *Applied Surface Science*, **283**:612–616, 10.

THERMAL RESPONSE OF ELECTRICALLY DISSIMILAR MESH SURFACES UNDER ATMOSPHERIC PRESSURE PLASMA JETS IN GASEOUS ENVIRONMENTS

James Lalor[1,2] and Vladimir Milosavljević[1,3]

[1] *School of Physics, Clinical and Optometric Sciences, Technological University Dublin, Ireland*

[2]*School of Mechanical Engineering, Technological University Dublin, Ireland*

[3]*Faculty of Physics, University of Belgrade, Serbia*

james.lalor@mytudublin.ie

This work investigates the thermal response of conductive and insulating mesh surfaces exposed to atmospheric pressure plasma jets operating in different gaseous environments. Helium/air and argon/air plasma discharges were generated within the kilohertz frequency range and examined under varying treatment times, gas flow rates and standoff distances (Figure 1). Infrared thermography was employed to characterise the surface temperature evolution during plasma exposure and to determine the influence of substrate electrical properties on heat transfer mechanisms.

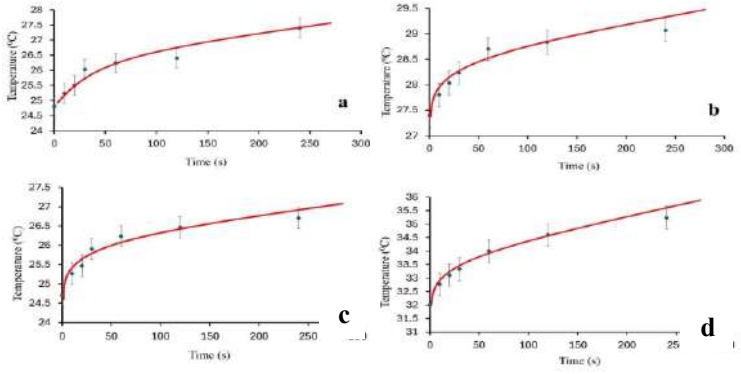

Figure 1: Heat transfer effect (°C) of the Argon (a and b) and Helium (c and d) APPJs on metal (a and c) and plastic (b and d) mesh substrates at varying treatment times in seconds (s) for a fixed standoff distance of 20mm.

The results demonstrated that conductive metallic meshes redistributed thermal energy more rapidly than insulating polymer-based meshes, resulting in lower localised surface temperature accumulation under identical operating conditions. In contrast, insulating meshes exhibited slower thermal dissipation and more pronounced temperature gradients across the treatment region. The thermal behaviour was also found to depend strongly on the gaseous environment of the plasma jet. Helium based discharges generally produced lower overall surface heating with more spatially uniform thermal profiles, whereas argon based discharges generated increased localised heating due to differences in plume structure and energy transfer characteristics.

Furthermore, the study confirmed that both treatment time and standoff distance play significant roles in determining surface temperature evolution. Shorter standoff distances increased energy deposition onto the substrate surface, leading to higher measured temperatures for both conductive and insulating meshes. Increasing treatment duration produced progressive temperature growth, although the rate of heating differed substantially depending on substrate electrical characteristics and gas composition. These observations demonstrate the importance of considering both plasma operating parameters and substrate material properties when designing plasma treatment systems for continuous or temperature sensitive applications.

The thermal behavior of plasma jets allows for an optimisation in order to enhance adhesion of coatings in manufacturing. The controlled thermal effects also provide an understanding of how to safely enhance wettability in the treatment of textiles or to ensure precise temperature control in processes involving biological tissues or biomedical devices. The findings contribute to a broader understanding of plasma–surface thermal interactions and provide insight into the engineering considerations required for scalable atmospheric pressure plasma processing technologies.

References

Lalor J, Scally L, Cullen P J and Milosavljevic V (2018) *Journal of Vacuum Science & Technology A: Vacuum, Surfaces, and Films*, **36**, 03E108.

Lalor J F, Orlic T and Milosavljevic V (2026) *Journal of Vacuum Science & Technology A: Vacuum, Surfaces, and Films*, **44**(3), 033003.

Scally L, Lalor J, Gulan M, Cullen P J and Milosavljevic V (2018) *Plasma Processes and Polymers*, **15**(6), e1800018.

EFFECT OF COLD PLASMA TREATMENT ON ENZYMATIC ACTIVITY AND MICROBIOTA OF TECHNOGENICALLY DISTURBED SOIL

Veronika Lyushkevich[1], Irina Filatova[1], Svetlana Goncharik[1], Aliaksandra Kazak[1], Igor Ovchinnikov[2], Helen Nedved [2], Anastasia Fedorenchik[3]

[1]*B.I. Stepanov Institute of Physics of the National Academy of Sciences of Belarus, Minsk, Belarus*

[2]*V. F. Kuprevich Institute of Experimental Botany of the National Academy of Sciences of Belarus, Minsk, Belarus*

[3] *Institute of Microbiology of the National Academy of Sciences of Belarus, Minsk, Belarus*

v.lyushkevich@ifanbel.bas-net.by

Soil salinization due to anthropogenic impact is a complex environmental problem causing degradation of agricultural lands and loss of biodiversity. In the last decade, the possibility of using non-thermal plasma in agriculture has been actively considered as an effective method for seed treatment, as well as for the remediation of soil containing organic pollutants such as polyaromatic hydrocarbons, phthalates and pesticides (Zhao *et al.* 2023). In this work, the effect of plasma treatment on the enzymatic activity and beneficial microbiota of soil from roadside strips of an urban highway was studied. Soil samples were treated by dielectric barrier discharge (DBD) plasma (at a peak-to-peak applied voltage of 20 kV, a frequency of 1 kHz and treatment duration of 2 min)] as well as by the air jet plasma (PJ) generated by a direct current glow discharge (at a discharge current of 30 mA, air flow rate of 1.5 l/min and treatment duration of 10 min)]. Plasma treatment generally reduced the number of microorganisms that assimilate mineral forms of nitrogen on the 1st day after treatment (fig.1), but DBD-treatment significantly contributed to an increase in their number after thirty days. On the 1rst day, the number of oligotrophic microorganisms increased significantly as a result of exposure to DBD plasma, and after 30 days this number remained above the control level. Oligotrophic microorganisms usually thrive in nutrient-poor soil and utilize scarce resources efficiently, as well as decompose stubborn, difficult-to-decompose organic matter (Wainwright *et al.* 1993*)*.

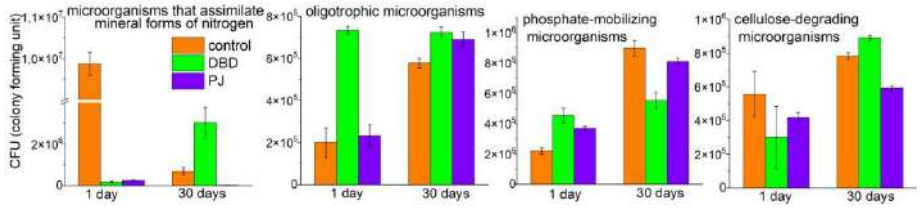

Figure 1: Changes in some microbial populations investigated as a result of treatment with direct and afterglow plasma

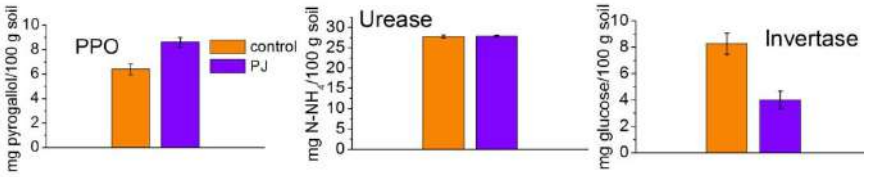

Figure 2: Activity of soil enzymes: polyphenol oxidase (A), urease (B) and invertase (B) after soil treatment with an air plasma jet

Plasma treatment also contributed to an increase in the content of phosphate-mobilizing (1st day) and cellulose-degrading (30th day) microorganisms. A decrease in the number of microorganisms that assimilate mineral forms of nitrogen and destroy cellulose on the 1st day of the study is confirmed indirectly by a decrease or absence of the activity of hydrolytic enzymes (fig. 2): urease, which catalyzes the breakdown of urea into ammonia available to plants, and invertase, which breaks down sucrose into glucose and fructose. It has been reported a close direct connection between urease and cellulase activity, indicating their interplay in soil processes (Kuzina *et al.* 2022*)*. A high content of oligotrophic microorganisms and an increase in the activity of PPO in plasma treated technogenically disturbed soil and the growth of cellulose-destroying microorganisms (on 30th day) may indicate an active humification process and the creation of favorable conditions for the growth of cellulose-destroying microorganisms (Nutt *et al.*2006).

Acknowledgements: This work was supported by the Belarusian Republican Foundation for Fundamental Research (grant No F24KITG-012).

References

Kuzina E V *et al.* (2022) *Dostizheniya nauki i tekhniki APK (Russian)*, **9**, 32-36.
Nutt A (2006), *Hydrolytic and Oxidative Mechanisms Involved in Cellulose Degradation*, Acta Universitatis Upsaliensis, Faculty of Science and Technology; **185**:51.
Wainwright *et al.* (1993) *International Biodeterioration & Biodegradation*, **31**, 1-13.
Zhao *et al.* (2023) *Chemical Engineering Journal,* **459***,* 141632.

PLASMA SYNTHESIS OF TERNARY METAL OXIDE SEMICONDUCTOR NANOSTRUCTURES FOR H_2 GENERATION BY WATER SPLITTING

Alena Nevar[1], Aleksandra Shumejko[1], Vasilii Kiris[1], Mikhail Nedel`ko[1], Srabanti Ghosh[2] and Nikolai Tarasenko[1]

[1]*B.I. Stepanov Institute of Physics of National Academy of Sciences of Belarus, 68-2 Nezalezhnasti Ave.,220072 Minsk, Belarus*

[2]*Central Glass and Ceramic Research Institute, 196, Raja S.C. Mullick Road, 700032 Kolkata, India*

a.nevar@ifanbel.bas-net.by

Recently, increased research attention has been focused on the development of clean and sustainable energy sources aimed at reducing and replacing fossil fuels. The development of "clean" hydrogen is considered one of the most realistic paths to decarbonizing industry and transportation. The development of hydrogen synthesis from water is critically important, as it is the only way to create a truly closed and environmentally friendly energy cycle. The dissociation processes occurring in photoelectrochemical cells depend on the interaction of the semiconductor material, which acts as a catalyst, with the electrolyte. Therefore, modern research is focused on finding new materials to improve cell efficiency. Metal ternary oxide semiconductors, such as $CuFe_2O_4$ and $ZnFe_2O_4$, are considered among the most successful and promising (Lin *et al*. 2024, Manohar *et al*. 2019). The combination of several metals alters the electron density on the surface, facilitating the adsorption of water molecules, while nanostructuring provides a huge number of "active sites". For the experiments, two spark discharge power sources based on alternating current generators were used. In the Table 1 under modes 1 and 2, the generators parameters (spark voltage U, current peak amplitude I_{max}, pulse duration τ, synthesis time t, and the results of studies of nanoparticles synthesized using them are indicated.

Table 1. Experimental parameters

	U, kV	I_{max}, A	τ, μs	t, min
Mode 1	3.5	60	30	2
Mode 2	8.5	10	5	30

The discharge was initiated between two metal electrodes (Cu-Fe, Cu-Cu, Fe-Fe, Zn-Fe, Zn-Zn) with 6 mm in diameter and 20–25 mm in length, immersed in 75 ml of distilled water. The synthesized samples were obtained as colloidal solutions; after evaporation of the liquid, they were obtained as nanopowders. The morphology, structure and optical properties of the formed nanostructures were evaluated using UV-Vis, Raman, FTIR spectroscopy, XRD, SEM methods. The concentrations of metals present in the synthesized samples were determined using atomic emission spectroscopy. In both cases, no stoichiometry was observed in the sample composition: for mode 1, the Cu : Fe ratio was 1 : 1.5, and for mode 2, it was 1 : 0.9. Based on the optical absorption spectra (Figure 1), the Tauc plot method was used to determine the band gap values for direct and indirect electron transitions (Semaltianos *et al*. 2010). The synthesized $CuFe_2O_4$ sample is a narrow-bandgap semiconductor (~1.9 eV) capable of absorbing visible light but subject to rapid charge recombination. The introduction of graphene oxide may solve this problem. It provides a large surface area, excellent electrical conductivity, and acts as an electron trap, reducing the rate of electron-hole pair recombination. Further research in this area is planned.

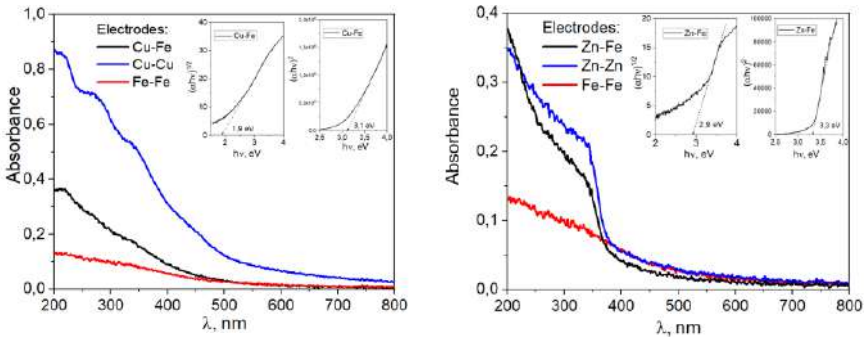

Figure 1: UV-Vis absorbance spectra of colloidal solutions synthesized in mode 1

Acknowledgements: This work was supported by the NAS of Belarus (project "Convergence 2.2.07") and the BRFFR (grant F25INDA-005).

References

Lin Z, Hao Sh, Li Zh *et al.* (2024) *Int. J. Hydrogen Energy,* **77**, 511.

Manohar A, Krishnamoorthi C, Naidu K C B *et al.* (2019) *Appl. Phys. A,* **125**, 477.

Semaltianos N G, Logothetidis S, Perrie W *et al.* (2010) *J. Nanopart. Res.,* **12**, 573.

CONSTRUCTION AND CHARACTERIZATION OF AN AIR IONIC WIND PLASMA THRUSTER

Juš Polanšek[1,2], Luka Cvelbar[3] and Uroš Cvelbar[1]

[1]*Department of Gaseous Electronics (F6), Jožef Stefan Institute, Ljubljana, Slovenia*

[2]*Jožef Stefan International Postgraduate School, Ljubljana, Slovenia*

[3]*Gimnazija Bežigrad High School, Ljubljana, Slovenia*

jus.polansek@ijs.si

A plasma thruster generates thrust without moving parts by accelerating ionized gas. Conventional plasma thrusters are mainly used in vacuum systems and rely on noble gases, whereas ionic wind thrusters operate in atmospheric air and therefore offer a simple platform for studying electrohydrodynamic propulsion and plasma-driven flow generation (Moreau *et al.* 2018; Park *et al.* 2018). In this work, we present a practical design and experimental characterization of a low-cost air ionic wind plasma thruster assembled from 3D-printed supports, copper-tape electrodes, a protective acrylic tube, and an off-the-shelf high-voltage transformer that raises a low-DC input to voltages above 10 kV.

The thruster operates by generating a corona discharge at sharp triangular emitter tips. The accelerated charged particles transfer momentum to neutral air molecules and create a directed airflow that produces measurable thrust. We investigated the influence of voltage polarity, electrode spacing, single-stage and two-stage electrode configurations, and the number of emitter teeth. Air speed was measured with an anemometer, while thrust was measured directly using an analytical balance.

The measurements show that smaller electrode spacing increases wind speed up to the onset of arcing, and that negative polarity gives about 10% higher wind speeds than positive polarity due to the more stable discharge regime. A two-stage configuration improves wind speed by about 20% compared with a single-stage design operated at the same power. Increasing the number of emitter teeth enhances performance until a plateau is reached, while too few emitters lead to a clear drop in wind speed. Direct thrust measurements yielded values of

approximately 1.0-1.6 mN, corresponding to a thrust-to-power ratio on the order of 0.1 mN/W.

These results demonstrate that an inexpensive atmospheric-pressure plasma thruster can be built from accessible components and still provide a useful experimental platform for studying corona discharges and electrohydrodynamic propulsion. Although the present device is intended primarily as a classroom and laboratory demonstrator rather than a flying prototype, the measurements identify the key design parameters that control performance and provide a practical basis for further optimization.

References

Moreau E, Audier P and Benard N (2018) *J. Electrostat.*, **93**, 85-96.
Park S, Cvelbar U, Choe W and Moon S Y (2018) *Nat. Commun.*, **9**, 371.

Section 4.

GENERAL PLASMAS

ULTRA HIGH REPETITION RATE HIGH ENERGY LASER FOR PLASMA APPLICATION

Ryo Yasuhara[1]

[1]*National Institute for Fusion Science, Japan*

yasuhara@nifs.ac.jp

With the rapid advancement of data science, the volume of available data has become a critical driver of scientific progress. High-intensity laser research is no exception, with a growing demand for statistical, data-rich approaches built on large datasets. At SLAC, for example, the X-ray free-electron laser LCLS-II raises the repetition rate of XFEL operation from the conventional 120 Hz class to as high as ~1 MHz, delivering high average brightness and coherent flux (see Walter *et al*. 2022). The same trend is now extending to visible-to-infrared laser sources: a higher repetition rate increases the throughput of laser–matter interactions, enabling the statistical evaluation and systematic parameter exploration that could reshape prevailing experimental paradigms in laser research. However, raising the repetition rate of high-intensity lasers is difficult, mainly because of the increased average thermal load, stronger nonlinear effects, and reduced optical-damage margins. One practical solution to these challenges is burst-mode operation, which delivers an MHz-equivalent pulse train within a defined temporal window while keeping the average thermal load manageable, providing a realistic route toward high-throughput laser–matter interaction studies. In this work, we report the realization of a joule-class (>1 J), nanosecond pulse-burst laser and present fusion-plasma diagnostic results obtained with it. Based on these outcomes, the prospects and enabling pathways for future MHz-class, high-intensity, high-energy laser sources are discussed.

On the Large Helical Device (LHD), the Thomson scattering (TS) system is a major diagnostic, providing high-spatial-resolution measurements (144 points across the plasma diameter) that are essential for detailed plasma studies (see Narihara *et al.* 2001). However, until recently, the acquisition rate was constrained to 30–100 Hz, primarily due to limitations of the laser system. Such repetition-rate limitations make it difficult to perform detailed measurements of various high-speed phenomena, including hydrogen pellet ablation dynamics and partial

plasma collapse events. To address these challenges, we developed a pulse-burst laser system. The laser system is a Master Oscillator Power Amplifier (MOPA) system consisting of flashlamp-pumped Nd:YAG laser rods. The oscillator and pre-amplifier each use a 9 mm diameter rod. The main amplifier is a dual-rod stage, each rod 12 mm in diameter. Q-switched laser pulses with a duration of 20 ns are produced by a DKDP Pockels cell in the laser oscillator, which consists of two planar mirrors. Amplification by the pre-amplifier and the main amplifier produces 1.2 J laser pulses. The flashlamps are driven by an IGBT-based power supply. Laser system operation is entirely computer controlled and monitored. Using this laser, we studied the fueling mechanism of the fusion plasma. When ~5% Ne was mixed into a hydrogen pellet, LHD experiments demonstrated that, for low-field-side injection, the outward expulsion of the post-ablation plasmoid is suppressed, leading to improved core particle assimilation (i.e., a larger density rise). Using high-repetition-rate burst-laser Thomson scattering, the ablation-to-mixing process can be tracked with high temporal resolution and robust multi-shot statistics, thereby accelerating mechanistic understanding and parameter optimization (see Matsuyama *et al*. 2022). Thus, pulse-burst lasers provide a practical solution for applications that require high-repetition-rate operation.

In summary, a joule-class nanosecond pulse-burst laser was developed and applied to Thomson scattering diagnostics on LHD, enabling high-temporal-resolution measurements with robust multi-shot statistics. Building on this demonstration, burst-mode operation offers a realistic pathway to MHz-class capability by combining several 100 kHz lasers scaled up from the present system (see Den Hartog *et al*. 2026), together with a transition to laser-diode pumping (see Slipchenko *et al.* 2014) and multi-beamlet combination—an application-driven route to MHz-equivalent, high-throughput laser–matter interaction studies.

References

Den Hartog D J *et al*. (2026) *JINST*, **21**, C01036.

Matsuyama A, Sakamoto R, Yasuhara R *et al*. (2022) *Phys. Rev. Lett*., **129**, 255001.

Narihara K, Yamada I, Hayashi H and Yamauchi K (2001) *Rev. Sci. Instrum*., **72**, 1122.

Slipchenko M N, Miller J D, Roy S, Meyer T R, Mance J G and Gord J R (2014) *Opt. Lett*., **39**, 4735-4738.

Walter P *et al*. (2022) "The time-resolved atomic, molecular and optical science opportunities at LCLS-II," *Phil. Trans. R. Soc. A*, **380**.

SPECTROPOLARIMETRIC PLASMA DIAGNOSTICS IN THE ATMOSPHERES OF THE SUN AND STARS

Ivan Milić[1,2,3]

[1]*Institute for Solar Physics (KIS), Freiburg, Germany*

[2]*Faculty of Mathematics, University of Belgrade, Belgrade, Serbia*

[3]*Astronomical Observatory, Belgrade, Serbia*

milic@leibniz-kis.de

The Sun is our host star, and due to its vicinity, it represents a unique natural laboratory for the study of the interaction between plasma, radiation, and magnetic field. The only layer of the Sun we can directly observe is its atmosphere, which spans more than two orders of magnitude in temperature variations, more than eight orders of magnitude in density variations, and hosts magnetic fields ranging from a few to a few thousand Gauss. To estimate the physical conditions in the solar atmosphere, in time and space, we use high cadence spectropolarimetric observations of the solar spectral lines and model the action of absorption, emission, and photon scattering processes on the shapes of the spectral lines. Additionally, we consider the action of the Zeeman and Hanle effects on the spectral line polarization, which allows us to infer the properties of the solar magnetic fields.

In this talk, we will review the current state of solar spectropolarimetric diagnostics, outlining the recent observational developments, mostly in the field of high-resolution, high-cadence spectropolarimetry, and the recent diagnostics advances, notably the so-called spectropolarimetric inversions. These are numerical techniques that fit a depth-stratified model atmosphere to the observed spectrum. Application of the inversion techniques to the spatially and spectrally resolved observations thus yields a reconstruction of the 3D structure of the solar atmosphere. Finally, we will showcase the connection between solar and stellar spectropolarimetry, as well as recent developments in techniques specifically developed to study the physical conditions in the atmospheres of other stars.

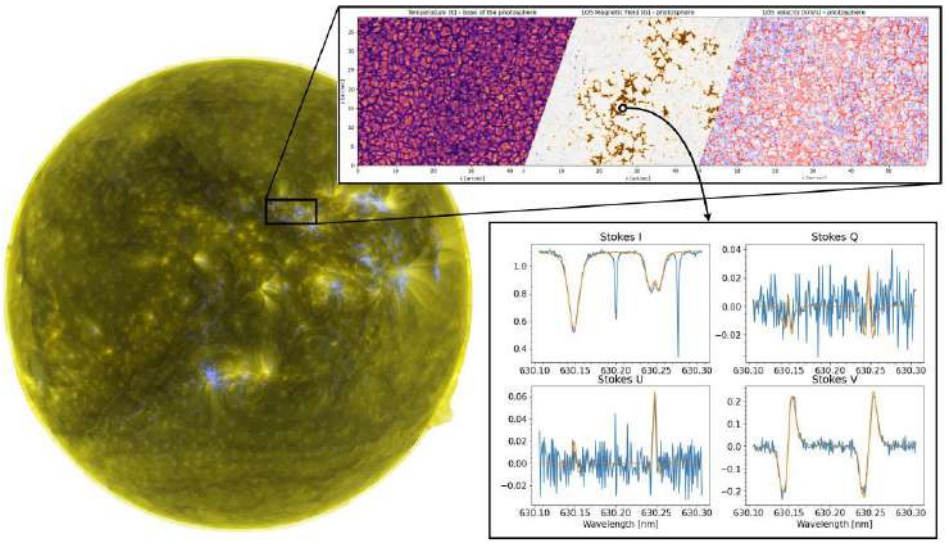

Figure 1: Overview of solar plasma diagnostics. Left: Solar corona seen in UV radiation. Top: map of the temperature, magnetic field, and velocity in a small section of the solar photosphere. Right: an example of polarized spectra of two magnetically sensitive lines of neutral iron.

COMPUTING RELIABLE NUMERICAL SOLUTIONS OF CHAOTIC DYNAMICAL SYSTEMS

Ivan Hristov

Sofia University "St. Kliment Ohridski", Bulgaria

ivanh@fmi.uni-sofia.bg

A reliable numerical solution is a solution that is expected to be numerically indistinguishable from the true solution. Computing a reliable solution for a chaotic dynamical system is a significant challenge because of the sensitivity of the true solution to the initial conditions. Due to this sensitivity and the inevitable introduction of rounding and truncation errors, standard numerical methods using double precision generally do not allow for reliable solutions to be computed.

However, for a predefined finite integration interval, such solutions can be achieved by:

1. Reducing the rounding error sufficiently by using floating-point numbers with a sufficiently long mantissa.

2. Using an arbitrarily high-order numerical method, in which the truncation error can effectively be reduced to the level of the rounding error. The Taylor series method is particularly suitable for this purpose.

The ability to choose the rounding and truncation errors to be as small as desired and to gradually reduce them allows us to calculate the so-called converged solutions. As the name suggests, a converged solution is a numerical solution that remains unchanged regardless of further increases in the mantissa's length and further reductions in the truncation error. Converged solutions are considered reliable.

The computation of converged solutions is demonstrated through the example of two famous chaotic systems: the Lorenz system and the Newtonian three-body problem. However, the proposed computational approach is much more general and can be applied to other chaotic systems arising in various fields of physics.

INVESTIGATION OF AGN VARIABILITY USING POSKI MODEL

S. Simić[1], L.Č. Popović[2,3], A. Kovačević[3], D. Ilić[3], and L. Novićević[2]

[1]*Faculty of Science, University of Kragujevac, Radoja Domanovića 12, 34000 Kragujevac*

[2]*Astronomical Observatory, Volgina 7, 11000 Belgrade*

[3]*Mathematical Faculty, University of Belgrade, Studentski trg 16, 11000 Belgrade*

ssimic@uni.kg.ac.rs

Active Galactic Nuclei (AGN) harboring binary supermassive black holes (SMBHs) at sub-parsec scales represent critical laboratories for understanding galaxy evolution and gravitational wave astrophysics. The orbital motion of these binaries around their common barycenter often induces periodic or quasi-periodic modulations in the observed flux, leaving distinct temporal signatures in the corresponding light curves. We present the PoSKI model, a comprehensive novel framework developed to simulate the photometric variability and assess the observational detectability of sub-parsec SMBH systems. By coupling empirical scaling relations with analytical orbital dynamics, the model parameterizes the binary configuration over a multi-dimensional parameter space, explicitly incorporating the primary and secondary black hole masses (*M1, M2*), mass ratio ($q = M2/M1$), orbital semi-major axis (a), eccentricity (e), inclination angle (i), and cosmological redshift (z). The output yields the time-evolving continuum flux Fn(t) spanning the ultraviolet (UV), optical, and infrared (IR) bands, alongside the profiles of prominent emission lines within these spectral regimes. To validate the framework, we generated synthetic continuum and line-emission light curves across a comprehensive grid of binary configurations, injecting realistic stochastic fluctuations characterized by power-law red noise and instrumental white noise components. Our simulations demonstrate that the PoSKI model robustly reproduces characteristic variability features across a diverse astrophysical parameter space. Furthermore, we systematically evaluate the influence of orbital parameters on the modulated signal-to-noise ratio to quantify detection efficiency. Utilizing simulated multi-band photometry, we constructed time-dependent magnitude and color-index light curves to assess the feasibility of periodogram-based periodicity recovery. Our findings confirm that

differential color-index variations constitute a powerful, extinction-resilient diagnostic strategy for identifying sub-parsec SMBH candidates within current and next-generation synoptic photometric surveys.

RELATION BETWEEN THE BRIGHTNESS AND MAGNETIC FIELD IN THE SUNSPOTS: THE SATURATION EFFECT

Ivan Živanović[1]

[1]*Astronomical Observatory of Belgrade, Volgina 7, 11060 Belgrade, Serbia*

izivanovic@aob.rs

The suppression of convection by strong magnetic fields in the solar photosphere, as proposed by Biermann [Biermann 1941], remains an important topic in solar physics. This process is primarily observed as the darkening of sunspots and pores, where the continuum intensity (I) is anti-correlated with the magnetic field strength (B).

In this progress report, we present a research with the aim to test the Biermann hypothesis that a strong magnetic field may completely suppress solar convection and to determine the magnetic field values at which a further increase in the magnetic field does not lead to a prominent decrease in continuum brightness (the saturation effect) inside sunspot umbrae and pores. For this purpose we use high-quality space data from the SDO/HMI and Hinode/SOT instruments. Our research demon-strates that upon reaching critical magnetic field values (approximately 2.6 – 2.7 kG for SDO/HMI and 3.3 – 3.5 kG for Hinode/SOT data), the umbral brightness reaches a plateau. This saturation indicates that convective suppression reaches a physical limit.

An important component of our work is the precise determination of the umbral boundary. For this purpose, we use several methods, including the gradient method [Zhivanovich *et al*. 2020], the Otsu method [Otsu 1979], and the multi-Otsu method [Liao *et al*. 2001]. This research is specifically dedicated to investigating and comparing these different boundary detection techniques across various data types and observational instruments. Such a comparative analysis is essential, as the optimal approach depends heavily on the spatial resolution and the physical parameters provided by the instrument. The intermediate results obtained from the brightness - magnetic field analysis at these transition zones have served as the starting point for our new investigation.

Furthermore, we extend our research to small-scale magnetic structures. The limitations in spatial resolution inherent to synoptic instruments like SDO often lead to filling factor ambiguities, making it difficult to distinguish between weak fields filling a resolution element and strong fields concentrated in compact structures. To resolve this, we outline a new observational strategy using the 1.5-metre GREGOR solar telescope. Our proposed campaign aims to map the transition from bright facular points (where the "hot wall" effect dominates) to dark micropores (where convective inhibition pre-vails). By combining multi-line spectropolarimetry (targeting K I 770 nm, Ca II 854.2 nm, and Si I 1082.7 nm) with high-cadence G-band imaging, we intend to establish the empirical "turnover point" of this transition. Depth-stratified inversions of the observed Stokes spectra will allow us to charac-terise the intrinsic magnetic field and temperature stratification, providing definitive constraints for contemporary 3D radiative MHD simulations.

References

Biermann L (1941) Der gegenwärtige stand der theorie der konvektiven zone im innern der sterne. *Vierteljahrsschrift der Astronomischen Gesellschaft*, **76**:194 – 200.

Liao P S, .Chen T S, and Chung P C (2001) A fast algorithm for multilevel thresholding, *J. Inf. Sci. Eng.,* **17**:713 –727.

Otsu N (1970) A threshold selection method from gray-level histograms, *IEEE Trans. Syst. Man Cybern*., **9**: 62 – 66.

Zhivanovich I, .Solov'ev A A, Efremov V I, and Miller N O (2020) Relationship between the magnetic field and brightness in sunspots, *Geomagn. Aeron*., **60**:865 – 871.

DYNAMO ACTION IN LOW DENSITY PLASMA IN EXPANDING GALACTIC DISCS

Evgeny Mikhailov[1,2], Tatiana Khasaeva[2] and Maria Frolova[2]

[1]*P.N.Lebedev Physical Institute of RAS, Moscow, Russia*

[2]*M.V.Lomonosov Moscow State University, Moscow, Russia*

e.mikhajlov@lebedev.ru

Existence of magnetic field in outer parts of galaxies is a very important question for astrophysics. Such fields should explain characteristics of the interstellar turbulence, also there is observational evidence of the field structures in these regions (Hu & Lazarian 2023). However, properties of the plasma in the outer parts of galaxies are strongly different from ones at modest distances from the galactic center. The disc expands in its peripherical parts, so the density of the interstellar plasma becomes smaller. Plasma temperature and rotation velocity decrease, too. So the classical mechanisms of the field generation such as dynamo (connected with helicity of the turbulent motions and non-uniform large-scale rotation of the object) should be suppressed. Basic estimates show that the non-dimensional number $D = \frac{9h^2\Omega^2}{u^2}$, where h is the disc half-thickness, Ω is the angular velocity and u is the turbulent velocity dispersion (Arshakian *et al.* 2009), will be smaller than critical value $D_{cr} \approx 7$, so the field should decay for large distance from the galactic center.

Numerical modeling (Mikhailov *et al.* 2014) of the magnetic field in the outer part has shown that the large-scale field unexpectedly can enlarge even for $r = 15 \ldots 20$ kpc, although the field reaches only values of $10^{-7\ldots-8}$ G (as for inner part it is usually about 10^{-6} G). This has been explained by nonlinear effects connected with saturation of the field growth. However, there are reasons to consider the field growth even on linear stage.

In our work we have studied the differential operators which take place in evolution equations for the magnetic field (Mikhailov & Khasaeva 2026). Corresponding eigenfunctions decay according to the $r^{-1/2}$ law, and it is quite enough to describe the fields which are measured in observations. They are connected with positive eigenvalues which means that these fields will grow until

the nonlinear saturations. Equipartition field is proportional to $\rho^{1/2}$, and if the density is an order of magnitude smaller than in the inner parts, we shall obtain a field which is only several times smaller.

Expansion of the disc also makes the role of the vertical flows of the plasma and diffusion in the vertical direction higher. To study this process we took the amendments related to the growth of the half-thickness and made estimates of the vertical component of the field (Mikhailov & Frolova 2023).

Another important mechanism is connected with turbulent dynamo. It is situated in small domains associated with turbulent motions (Schekochihin *et al.* 2001). Although it generates field with small length-scales, there values can be even larger than regular ones. We have made basic estimates of the fields and shown that it reaches equipartition values during times of 10^8 years (Mikhailov *et al.* 2026).

References

Arshakian T, Beck R, Krause M, Sokoloff D (2009) Astron. Astrophys., **494,** 21.

Hu Y, Lazarian A (2023) *Mon. Not. R. Astron. Soc.*, **524,** 2379.

Mikhailov E, Kasparova A, Moss D, Beck R, Sokoloff D, Zasov A (2014) *Astron. Astrophys.,* **568**, A66.

Mikhailov E, Khasaeva T (2026) *Mathematics,* **14,** 308.

Mikhailov E, Frolova M (2023) *Communications of the Byurakan Astrophysical Observatory*, **70,** 282

Mikhailov E, Khasaeva T, Zhang R, Liu X (2026) Bull. Lebedev Phys. Inst. **53,** 164.

Schekochihin A, Cowley S, Maron J, Malyshkin L (2001) Phys. Rev. E, **65,** 016305.

THE Fe II EMISSION LINES IN SPECTRA OF ACTIVE GALACTIC NUCLEI: SEARCHING FOR SIGNATURES OF ATOMIC PROCESSES

Jelena Kovačević-Dojčinović[1], Ivan Dojčinović[2] and Luka Č. Popović[1]

[1]*Astronomical Observatory, Volgina 7, 11000 Belgrade*

[2]*University of Belgrade, Faculty of Physics, Studentski trg 12, 11001 Belgrade, Serbia*

jkovacevic@aob.bg.ac.rs

The Fe II emission lines are observed in the spectra of most type 1 active galactic nuclei (AGNs). Due to the large number of Fe II transitions and large line widths, the Fe II lines are strongly blended, especially in the UV and optical range, which makes line identification and analysis difficult. In some AGNs, the Fe II emission can be surprisingly strong, contributing up to 30% of the total line-emitting energy from the broad-line region (BLR), which is unexpected given the assumed iron abundance in the BLR gas. Also, the relative intensities of the UV and optical Fe II lines, as well as those among some optical Fe II lines themselves, do not follow the theoretically expected values based on their transition probabilities. This suggests that the atomic processes responsible for the production of strong Fe II emission and the observed relative line intensities are not yet fully understood.

In order to investigate which atomic processes are responsible for the observed properties of the Fe II emission lines, we used a large sample of 1046 type 1 AGN spectra obtained from the Sloan Digital Sky Survey (SDSS) database. We divided the optical Fe II lines into two major groups referred to as "consistent" and "inconsistent" Fe II lines ($FeII_{cons}$ and $FeII_{incons}$, respectively). The inconsistent Fe II lines are those whose relative intensities are significantly stronger than theoretically expected. Namely, according to their transition probabilities, these lines should be barely visible in the spectra; however, in some sources they are observed to have fluxes of the same order of magnitude as the $FeII_{cons}$ lines. We fitted the optical ($FeII_{cons}$+$FeII_{incons}$) and UV Fe II emission lines using a flexible and complex optical Fe II model developed by Kovačević *et al.* (2010) and Kovačević-Dojčinović & Popović (2015), which decomposes the blended Fe II emission features into different Fe II line groups. In this way, we traced variations

in the relative intensities of $FeII_{cons}$ and $FeII_{incons}$ across a large sample of AGNs. We found that the flux ratio $FeII_{incons}/FeII_{cons}$ correlates with the ratio of the total optical to UV Fe II emission ($FeII_{opt}/FeII_{UV}$). Furthermore, both ratios increase with increasing Eddington ratio and decreasing Fe II line width. In terms of atomic properties, all these transitions originate from the same upper level, while their lower levels are metastable. The corresponding transition probabilities are highest for the UV FeII, lower for optical $FeII_{cons}$ and the lowest for the $FeII_{incons}$. These results suggest that both ratios may be influenced by self-absorption in the stronger FeII lines, whereby energy is redistributed toward weaker transitions: from the UV to the optical Fe II emission and, analogously, from the $FeII_{cons}$ to the $FeII_{incons}$ lines, thereby enhancing the relative strength of $FeII_{incons}$. In this scenario, a high Eddington ratio increases the optical depth of the Fe II lines, triggering the self-absorption process (see Kovačević-Dojčinović *et al.* 2025).

References

Kovačević J, Popović L Č, Dimitrijević M (2010) *ApJS*, **189**, 15.

Kovačević-Dojčinović J, Popović L Č (2015) *ApJS*, **221**, 35.

Kovačević-Dojčinović J, Dojčinović I, Lakićević M and Popović L Č (2025) *A&A*, **694**, 289.

3rd Workshop on Swarm Physics and Gaseous Dielectrics (SPGD)

MULTIPLE SCATTERING EFFECTS IN THE ELECTRON DRIFT MOBILITY IN DENSE NOBLE GASES

Armando Francesco Borghesani

[1]*Department of Physics & Astronomy, Università degli Studi di Padova and Istituto Nazionale di Fisica Nucleare, Padova unit I-35131 Padova, Italy*

armandofrancesco.borghesani@unipd.it

I review several experiments on the drift mobility of low-energy electrons in very dense noble gases (see Borghesani *et al*. 1988, Borghesani *et al*. 1992, Borghesani 2001, Borghesani 2021, Borghesani *et al*. 2025, Borghesani and Lamp 2026) to show how the classical kinetic theory is no longer valid because of the presence of multiple scattering effects. I will show that these effects can be heuristically treated within the binary collision picture of classical kinetic theory if a density dependence of the scattering cross section is introduced with no adjustable parameters, thereby obtaining a very good agreement with the experimental data. I will also present results of some more experiments [charge photoinjection (see Borghesani and Lamp 2013), Xe2 excimer infrared emission (see Borghesani *et al*. 2001, Borghesani *et al*. 2025), electron resonant attachment to O2 impurities (see Borghesani *et al*. 1991, Neri *et al*. 1997, Borghesani 2020)], apparently not related directly to electron drift, whose results can nonetheless be rationalized only if multiple scattering effects are taken into account.

References

Borghesani A F, Bruschi L, Santini M, and Torzo G (1988) *Phys. Rev. A,* **37***,* 4828.

Borghesani A F, Carugno G, and Santini M (1991) *IEEE Trans. Electr. Insul.*, **26**, 615.

Borghesani A F, Santini M, and Lamp P (1992) *Phys. Rev. A*, **46**, 7902.

Borghesani A F, Bressi G, Carugno G, Conti E, and Iannuzzi D (2001) *J. Chem. Phys.,***115**, 6042.

Borghesani A F (2001) *J. Electrostatics*, **53**, 89.

Borghesani A F and Lamp P (2013) *J. Chem. Phys.*, **138**, 034309.

Borghesani A F (2020) *Plasma Sources Sci. Technol.*, **29**, 035024.

Borghesani A F (2021) *Atoms*, **9**, 9030052.

Borghesani A F, Carugno G, Messineo G, Pazzini J (2025) *J. Chem. Phys.,* **163**, 104305.

Borghesani A F, Carugno G, Chiossi F (2025) *Front. Detect. Sci.Technol.,* **3**, 1580297.
Borghesani A F and Lamp P (2026) *J. Chem. Phys.,* **164**, 204302.
Neri D, Borghesani A F and Santini M (1997) *Phys. Rev. E,* **56**,2137.

BEYOND SIMPLE DRIFT-DIFFUSION: SKEWNESS & BOUNDARY EFFECTS IN PULSED TOWNSEND EXPERIMENTS

H. Vemulapilli[1], and C. M. Franck[1]

[1]*ETH Zurich, Zurich, Switzerland*

G. J. Boyle[2], D. L. Muccignat[2], and R. D. White[2]

[2] *James Cook University, Townsville, Australia*

gregory.boyle@jcu.edu.au

Electron swarm measurements obtained from the Pulsed Townsend (PT) experiment (van Rijn *et al.* 2024) remain a fundamental source of transport data for low-temperature plasma modelling (Petrović *et al*. 2009), and electron-scattering cross-section determination (Muccignat *et al.* 2024). Conventionally, PT waveforms are analyzed using analytic solutions of the second-order drift–diffusion equation, from which transport coefficients such as drift velocity, diffusion, and ionization or attachment rates are extracted (Crompton 1967, Casey *et al.* 2021). However, recent studies indicate that several assumptions underlying these analyses can introduce systematic errors, particularly under conditions of low gas density, small electrode spacing, and high reduced electric field (Vemulapalli *et al*. 2026).

In this work we investigate the influence of higher-order transport effects, finite source distributions, cathode boundary conditions, and experimental bandwidth limitations on the interpretation of PT measurements. Using Monte Carlo simulations benchmarked against analytic drift–diffusion models, we examine representative gases with distinct scattering behavior, such as CO2. Particular emphasis is placed on the role of the third-order transport coefficient (skewness), which produces asymmetric swarm evolution not captured by conventional analyses.

We demonstrate that neglecting skewness and boundary-layer effects can lead to significant deviations in the extracted transport coefficients and can produce apparent pressure dependencies in experimentally derived diffusion data.

Improved fitting approaches incorporating finite pulse-width effects and effective cathode boundary corrections are discussed, together with their implications for future high-accuracy swarm measurements and cross-section inversion procedures.

References

Casey M J E, Stokes P W, Cocks D G, Bosnajaković D, Simonović I, Brunger M J, Dujko S, Petrović Z Lj, Robson R E, White R D (2021) *Plasma Sources Sci. Technol*., **30**, 035017.

Crompton RW (1967) *J. Appl. Phys*., **38**, 4093.

Muccignat D L, Boyle G J, Garland N A, Stokes P W, White R D (2024) *Mach. Learn.: Sci. Technol*., **5**, 015047.

Petrović Z Lj, Dujko S, Marić D, Malović G, Nikitović Z, Sasić O, Jovanović J, Stojanović V, Radmilović-Radenović M (2009) *J. Phys. D: Appl. Phys*., **42**, 194002.

Van Rijn M M, Biagi S, Franck C M (2024) *J. Phys. D: Appl. Phy*s., **57**, 355202.

Vemulapalli H, Akbas M, Muccignat D, Boyle G, White R D, Franck C M (2026) *Plasma Sources Sci. Technol*., **35**, 015014.

COULOMB COLLISIONS IN LOW-TEMPERATURE PLASMAS

Tiago C Dias[1], Gonçalo Cardoso[2], Vasco Guerra[3], Mate Vass[4,5] and Zoltan Donko[5]

[1]*Department of Applied Physics and Science Education, Eindhoven University of Technology, Eindhoven, The Netherlands*

[2]*Department of Nuclear Engineering and Radiological Sciences, University of Michigan, Ann Arbor, USA*

[3]*Instituto de Plasmas e Fusão Nuclear, Instituto Superior Técnico, Universidade de Lisboa, Portugal*

[4]*Chair of Applied Electrodynamics and Plasma Technology, Ruhr University Bochum, Bochum, Germany*

[5]*Institute for Solid State Physics and Optics, HUN-REN Wigner Research Centre for Physics, Budapest, Hungary*

t.cunha.dias@tue.nl

Low-temperature plasmas often operate at ionization degrees from 10^{-7} to 10^{-3}. However, the long-range nature of Coulomb interactions can make charged-particle collisions relevant to electron kinetics even in plasmas dominated by neutrals (Hagelaar 2016). Here, we quantify these effects by adding electron-electron (e-e) and electron-ion (e-i) collisions to the open-source LoKI-MC Monte Carlo solver (Dias and Guerra 2025). LoKI-MC follows ensembles of electrons in prescribed fields and gas backgrounds; electron-neutral collisions are sampled stochastically, while charged-particle interactions are treated with Nanbu's cumulative small-angle scattering method (Nanbu 1997).

Figure 1 illustrates the effect of Coulomb collisions on electron mean energy for a nanosecond *E/N* pulse in argon at 100 Torr, for ionization degrees $n_e/N = 10^{-3}$ to 10^{-5}. According to the prescribed pulse, the field rises to 214 Td in 2.5 ns and then decays over ~10 ns. Comparing calculations without Coulomb collisions, adding e-e collisions only, and adding both e-e and e-i collisions, shows that charged-particle interactions modify the transient evolution of the mean electron energy. The strongest effect occurs during the afterglow, where e-e collisions accelerate energy redistribution and relaxation after the electric field pulse, while

collisions between electrons and thermal ions further decrease the mean energy at later times.

In the conference, we will discuss the mechanisms responsible for these trends and extend the analysis to other gases and to DC-field conditions. Furthermore, we will assess the validity range of the Nanbu method, based on the Landau-Fokker-Planck approximation, by benchmarking it against a more accurate treatment of electron-electron collisions based on first principles (Donko 2014).

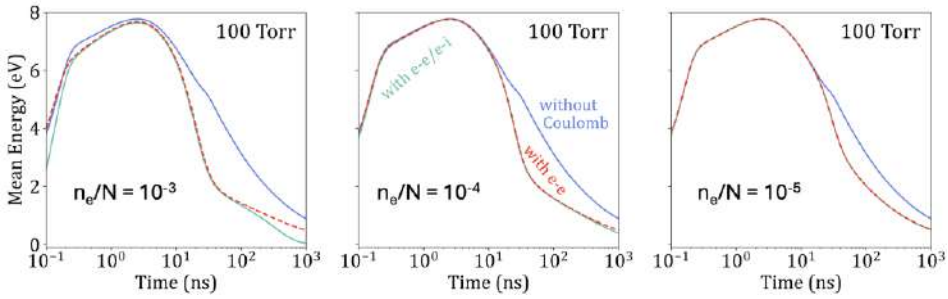

Figure 1: Electron mean energy as a function of time under a nanosecond electric field pulse in argon at 100 Torr and different ionization degrees n_e/N. The electric field pulse has an analytical formula used to mimic nanosecond-plasma conditions: $\frac{E}{N}(t) = \frac{E_0}{N}\sqrt{\frac{t}{t_{\text{pulse}}}}\exp\left(-\frac{t}{t_{\text{pulse}}}\right)$, with $\frac{E_0}{N} = 500$ Td, and $t_{\text{pulse}} = 5$ ns.

Acknowledgments: IPFN activities were supported by FCT – Fundação para a Ciência e Tecnologia, I.P. through project UID/50010/2025 (https://doi.org/10.54499/UID/50010/2025).

References

Dias T C and Guerra V (2025) *J. Phys. D*, **58**, 185204.

Donko Z (2014) *Phys. Plasmas*, **21**, 043504.

Hagelaar G (2016) *Plasma Sources Sci. Technol.*, **25**, 015015.

Nanbu K (1997) *Phys. Rev. E*, **55**, 4642.

UNDERSTANDING STRIATION FORMATION IN ATMOSPHERIC-PRESSURE DISCHARGES IN ARGON

A. P. Jovanović[1], T. Hoder[1,2], F. Sigeneger[1], D. Loffhagen[1] and M. M. Becker[1]

[1] *Leibniz Institute for Plasma Science and Technology (INP), Felix-Hausdorff-Str. 2, 17489 Greifswald, Germany*

[2] *Department of Plasma Physics and Technology, Kotlářská 2, 611 37 Brno, Czech Republic*

aleksandar.jovanovic@inp-greifswald.de

Striations, periodic bright and dark layers forming along the discharge channel, have been observed in both low-pressure (Robertson 1957) and atmospheric-pressure discharges (Hoder *et al*. 2011). They are generally understood as self-organised spatial modulations of the emission, driven by the coupling between electron transport, ionisation, and excited-state kinetics. While striations in low- and moderate-pressure discharges have been studied extensively, their origin in atmospheric-pressure plasmas remains underexplored due to their sporadic and unstable occurrence. Modelling studies aimed at finding the dominant mechanisms of striation formation in atmospheric-pressure argon indicate a strong dependence on discharge configuration and operating conditions.

This work highlights the different mechanisms of striation formation in pure argon discharges at atmospheric pressure under different conditions. The striation formation is investigated by means of a time-dependent spatially, two-dimensional fluid model. The study focuses on three cases, namely plasma jet studied in (Sigeneger and Loffhagen 2016), a single-filament dielectric barrier discharge (DBD) studied in (Jovanović *et al*. 2023b) and a transient spark in pure argon, for which modulation of the electric field has been observed during the streamer-to-spark transition. The fluid-Poisson model comprises balance equations for the particle densities of species, the electron energy balance equation, and Poisson's equation. For the description of transient spark discharge in needle-to-plane geometry, the model was extended to include the external circuit and heat equation. The equations are solved in COMSOL Multiphysics for

the plasma jet and the DBD cases and in Finite Element Discharge Modelling (FEDM) code (Jovanović *et al*. 2023a) for the transient spark discharge.

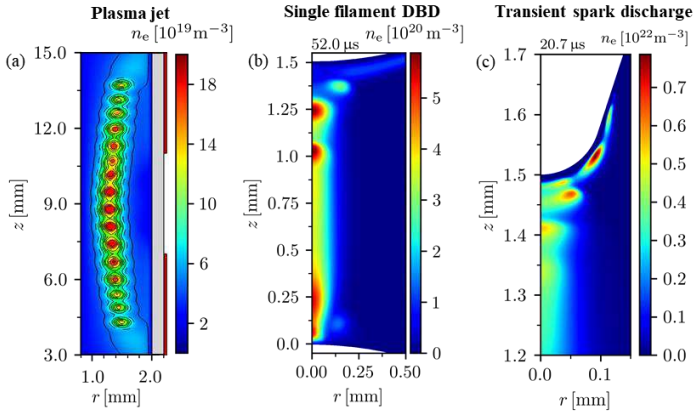

Figure 1: Spatial distribution of the electron density in argon discharges at atmospheric pressure: in a single-filament of a jet discharge (a), as well as a single-filament DBD (b) and transient spark discharge (c) at the time of strongest stratification of the column.

Figure 1 illustrates the appearance of striations in three different cases by the spatial profiles of the electron number density. In all three cases, alternating spatial maxima are observed. These maxima are more pronounced and extend along the discharge channel in the plasma jet and DBD cases, whereas in the transient spark they are localised near the needle cathode. The analysis shows that striations in the plasma jet result from the nonlinear dependence of ionisation and recombination rates on electron density, while in the DBD and transient spark discharge they are governed by stepwise ionisation of excited atoms and ionisation of excimers, which locally modulate the axial distributions of charge carriers and the electric field. These results highlight the role of excited states in generating the repetitive ionisation waves leading to the striation formation in the discharge channel.

References

Hoder T *et al*. (2011) *Phys. Rev E*, **84**, 046404.
Jovanović A P *et al*. (2023a) *Plasma Sources Sci. Technol.*, **32**, 044003.
Jovanović A P *et al*. (2023b) *Plasma Sources Sci. Technol.*, **32**, 055011.
Robertson H S (1957) *Phys. Rev.*, **105**, 368.
Sigeneger F and Loffhagen D (2016) *Plasma Sources Sci. Technol.*, **25**, 035020.

A GPU APPROACH TO STREAMER MODELLING

Christoph Köhn[1,2],Pierre Gourbin[2], Saša Dujko[3], Mathias Gammelmark[4], Sven Karlsson[4], Angel Ricardo Jara Jimenez[5], Guillermo Recuero Hinojosa[6] and Elloise Fangel-Lloyd[2,5]

[1]*Department of Physics, Technical University of Dortmund*

[2]*Department of Space Research and Technology, Technical University of Denmark*

[3]*Institute of Physics, University of Belgrade*

[4]*Department of Applied Mathematics and Computer Science, Technical University of Denmark*

[5]*Danish Meteorological Institute*

[6]*Polytechnical University of Catalonia*

christoph.koehn@tu-dortmund.de

Lightning consists of two modes, the long hot lightning leaders and the short cold streamers, as the precursors of the long lightning flashes. Streamers originate from electron avalanches in a sufficiently high ambient electric field ionizing ambient air and locally enhancing the electric field further energizing electrons. They span several orders of magnitude in space (from sub-nm to mm), time (from ps to ns) and energy (from eV to tens of keV), making their modelling complicated and time-consuming. There exist particle models that trace individual electrons, allowing for high accuracy but with large runtimes, and fluid models, faster than particle models, but losing accuracy by treating electrons and ions as fluids.

To address long runtimes, we have been developing three-dimensional GPU-based computational codes. ASTRAPÉ (Atmospheric STReamer And relativistic Particle Engine) is a particle model designed to run on local High-Performance Clusters (HPCs) and the European pre-exascale supercomputer LUMI (Large Modified Uniform Infrastructure, https://www.lumi-supercomputer.eu/about-lumi/), allowing for the simulation of unprecedentedly many electrons on a parallelised GPU system; see Fangel-Lloyd *et al.* 2026 for more details. Figure 1 shows the speed-up of large electron systems as a function of the number of GPUs, demonstrating excellent scalability.

ASTRAPÉ allows to simulate approximately 10^{10} electrons within 20 hours on 256 GPUs, faster and more accurate than any other particle code before.

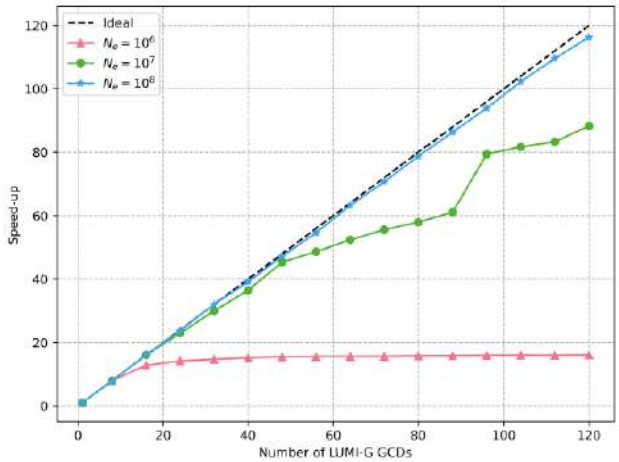

Figure 1: Speed-up of ASTRAPÉ as a function of GPU number (LUMI-G GCDs) for different electron numbers in an electron avalanche (neglecting space charge effects) in an electric field of 32 kV/cm at ground pressure.

In like manner, we are currently developing a GPU-based fluid code, based on the AMReX (Adaptive Mesh Refinement Exascale) framework, see Zhang *et al.* 2019, with the aim of simulating larger streamer systems more efficiently, see Jara Jiminez *et al.* 2026 for more details. In the end, we aim to develop a 3D GPU-based hybrid model that couples the particle and fluid models to simulate processes in thunderclouds as self-consistently and accurately as possible.

In this presentation, we will discuss streamer physics and the corresponding GPU implementation. We will present first simulation results and give an overview of the possible use cases for these new models.

References

Fangel-Lloyd E *et al*. (2026) *Comp. Phys. Comm.*, submitted.
Jara Jiminez A R *et al*. (2026) *Plasma Sour. Sci. Technol.*, In preparation.
Zhang W *et al*. (2019) *J. Open Source Software*, **4**, 1370.

BAYESIAN INFERENCE FOR DETERMINING ELECTRON SWARM PARAMETERS FROM STEADY-STATE TOWNSEND EXPERIMENTS

Satoru Kawaguchi[1], Sho Yoshita, Kazuhiro Takahashi[1], and Kohki Satoh[1]

[1]*Muroran Institute of Technology*

skawaguchi@muroran-it.ac.jp

The steady-state Townsend (SST) experiment is an electron swarm experiment that can measure the ionization coefficient α, electron attachment coefficient η, effective ionization coefficient (α - η), and secondary emission coefficient γ_T in gases. In the SST experiment, the ionization growth current is measured as a function of the electrode gap distance d under a uniform DC electric field. The measured current is described by the Townsend ionization growth equation,

$$I(d) = I_0 \frac{\frac{\alpha}{\alpha-\eta}\exp\{(\alpha-\eta)d\} - \frac{\eta}{\alpha-\eta}}{1-\gamma_T\frac{\alpha}{\alpha-\eta}[\exp\{(\alpha-\eta)d\}-1]},$$

where I_0 represents the initial current emitted from the cathode. Electron swarm parameters are conventionally determined from measured *I-d* characteristics using least-squares curve fitting. However, this deterministic approach has difficulty quantifying parameter uncertainties. In addition, the individual values of α and η are difficult to determine accurately. This is because the current growth is mainly governed by their difference, α - η. As a result, an increase in α can be offset by a corresponding increase in η, producing nearly the same *I-d* characteristics.

In this study, we apply Bayesian inference (Kruger *et al*. 2024) to analyze ionization currents measured in the SST experiment. In this approach, the model parameters, including α, η, and I_0, are estimated not as single best-fit values but as probability distributions, allowing their uncertainties and interdependencies to be quantified. A Gaussian likelihood is used to describe the scatter in the measured currents and to obtain the posterior distributions of the parameters. These distributions are sampled using a Markov chain Monte Carlo method.

We measured ionization growth currents in 1,3-C_4F_6 and determined the values of α/N, η/N, and $(\alpha - \eta)/N$ over the range E/N = 400 – 800 Td, where N represents the number density of gas molecules and E/N represents the reduced electric field (1 Td = 10^{-21} Vm^2). Figure 1(a) compares the measured currents with the Bayesian predictions at 700 Td. The Bayesian inference provides predictions as probability distributions, whereas the least-squares curve-fitting procedure provides only a best-fit curve. The resulting uncertainty ranges successfully reproduce the scatter in the measured currents. Figure 1(b) shows the posterior samples of α, η, and I_0. The off-diagonal scatter plots reveal nonlinear correlations between I_0 and α or η, as well as a strong positive correlation between α and η. This indicates that the uncertainty in I_0 is coupled with the uncertainties in α and η, and that α and η are difficult to determine independently because of multicollinearity. The diagonal panels show the marginal posterior distributions, whose widths quantify the uncertainties in I_0, α and η.

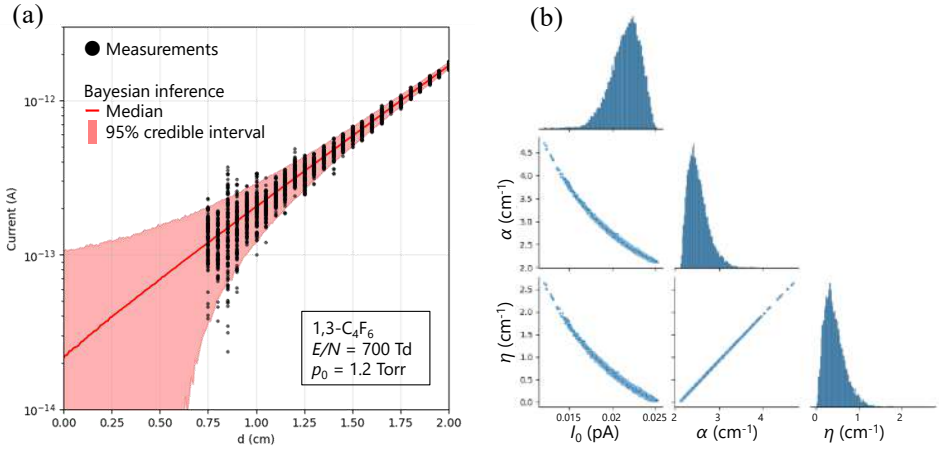

Figure 1: The ionization current and parameters obtained from Bayesian inference in 1,3-C_4F_6 at 700 Td.

Acknowledgements: This work was supported by JSPS KAKENHI Grant Number JP25K01209 and was partly supported by Tokyo Electron Miyagi Ltd.

Reference

Kruger S E, Leddy J, Howell E C, Madireddy S, Akcay C, Bechtel Amara T, McClenaghan J, Lao L L, Orozco D, Smith S P, Sun X, Samaddar A, and Pankin A-Y (2024) *Phys. Plasmas*, **31**, 050901.

DISCHARGE BEHAVIOR IN FOURTH-GENERATION FREONS UNDER SWARM-LIKE CONDITIONS

Jelena Marjanović[1], Dragana Marić[1], and Zoran Lj. Petrović[2,3]

[1]*Institute of Physics, University of Belgrade, Pregrevica 118, 11080 Belgrade, Serbia*

[2]*Serbian Academy of Sciences and Arts, Kneza Mihaila 35, 11001 Belgrade, Serbia*

[3]*School of Engineering, Ulster University, Jordanstown, County Antrim BT37 0QB, UK*

sivosj@ipb.ac.rs

Hydrofluoroolefins (HFOs) represent the fourth generation of freons, the newest class of fluorinated gases developed to replace older refrigerants while minimizing environmental impact. Their defining feature is a carbon–carbon double bond, which makes them chemically reactive and therefore short-lived in the atmosphere. As a result, HFOs exhibit extremely low Global Warming Potential (GWP), often below 1, and zero Ozone Depletion Potential (ODP). Despite the phase-down of high-GWP fluorocarbons, numerous modern technologies still rely on fluorinated gases. They remain essential in plasma etching processes used for manufacturing microchips and nanomaterials, in particle detection systems such as resistive plate chambers (RPCs), in refrigeration and air-conditioning, and in gas-filled electrical insulation (see Quaglia *et al*. 2025; Zhang *et al*. 2020; Preve *et al*. 2017). As a greener alternative, HFOs and their mixtures have been proposed to replace the current F-gas (Fluorinated Greenhouse Gas) blend, typically $C_2H_2F_4$, SF_6, and i-C_4H_{10}, used in gaseous particle-detector technologies, particularly in RPC systems (see Quaglia *et al*. 2025; Guida *et al*. 2016).

Although dielectric breakdown and swarm experiments have provided valuable insights into the electrical behavior of modern fluorinated gases, key data needed for environmentally friendly applications remain limited. This work presents elementary breakdown parameters: breakdown voltages, effective ionization coefficients, and secondary electron yields, measured under swarm-like conditions – low-current (~1 μA) and low-pressure (~0.1–1 Torr) – in a DC discharge with a plane-parallel electrode geometry. The results are obtained for discharges in trans-1,3,3,3-tetrafluoropropene and 2,3,3,3-tetrafluoropropene (HFO-1234ze(E) and HFO-1234yf). Combined with independently obtained

transport coefficients, these results support the development of reliable cross-section sets and discharge models within the energy range relevant to a wide range of gas-discharge applications.

Acknowledgements: This research was supported by the Science Fund of the Republic of Serbia, Grant No. 7749560, project EGWIn. Zoran Lj. Petrović is grateful to the SASA project F155.

References

Guida R, Capeans M, and Mandelli B (2016) *J. Instrum*., **11**, C07016.

Preve C, Piccoz D, Maladen R (2017) *CIRED Open Access Proc. J*., **1**, 42.

Quaglia L., et al. (2025) *Eur. Phys. J. Plus,* **140**, 40.

Zhang B, Chen L, Li X, Guo Z, Pu Y, Tang N (2020) *IEEE Transactions on Dielectrics and Electrical Insulation*, **27**, 1187.

SIMULATING STREAMER DISCHARGES FROM LOW TO HIGH PRESSURES WITH HIGH-PERFORMANCE COMPUTING

Robert Marskar[1]

[1]*SINTEF Energy Research*

robert.marskar@sintef.no

Streamer discharges are rapidly propagating ionized filaments, characterized by self-enhanced fields at their tips occurring as a result of electron impact ionization and charge separation. They are the most important precursors for electric breakdown at long spatial scales, and their prediction and characterization is therefore of substantial importance both in fundamental science as well as in technology.

In this talk I will provide an overview of discharge modeling work done by our group over the past decade. This talk will provide an introduction to usage of high-performance computing for simulating streamer discharges (as well as other types of discharges). Our focus will be on the usage of adaptive cut-cell meshes, with a primary focus on applications in high-voltage technology. We will discuss numerical discretizations suitable for parallelization, physics models for the charged particles, and usage of various photoionization descriptions. These advantages and drawbacks of each of these topics will be discussed in the context of both high-pressure discharges in high-voltage technology, as well as in nature in the form of ultra-low pressure sprite discharges. Finally, this talk will be summarized by my personal view of important research directions, with a main focus on physics representation, algorithms, and data reliability.

References

Marskar R (2019) *J. Comp. Phys.*, **388**, 624.
Marskar R (2026) *Plasma Sources Sci. Technol.* **35**, 035018.

REDUCED MODELS FOR STREAMERS, BASED ON TRANSPORT DATA

Thomas J.G. Smits[1], Jannis Teunissen[1,3], and Ute Ebert[1,2]

[1]*Centrum Wiskunde & Informatica, Amsterdam, The Netherlands*

[2]*Eindhoven University of Technology, Eindhoven, The Netherlands*

[3]*KU Leuven, Leuven Belgium*

thomas.smits@cwi.nl

Streamers are transient, non-stationary, filamentary phenomena with large local electric-field enhancements that often precede other types of discharges. These discharges are conventionally modelled using fluid or particle-in-cell models, which typically limits full 3D simulations to a single streamer or a small number of streamers. In nature, however, streamers form complex tree-like structures, if space and voltage are sufficiently large. Modelling these phenomena requires an efficient tree description (see Teunissen *et al.* 2025) combined with an effective streamer-head model (see Bouwman *et al.* 2025).

In this talk, we compare an effective streamer head model (see Bouwman *et al.* 2025) with a conventional fluid model. The head model takes electron transport data as input, and can be used for both positive and negative streamers. We observe good agreement between the effective and conventional model. We also investigate polarity effects by comparing, for example, relationships between streamer velocity, radius, and tip electric field, revealing interesting differences.

We also present a recently developed tree model (see Teunissen *et al.* 2025). This model uses an efficient channel model that describes the channels as cylinders with finite conductivity and finite width. The growth of streamer heads is currently described by a data-driven approach, but changes in channel conductivity are governed by the local ionization and attachment rates.

We conclude by offering a perspective on combining the effective head model, based on transport data, with the efficient tree model. The end goal is to obtain a

general tree model with a micro-physics based head model, which can be used to simulate large-scale discharges in arbitrary gases.

References

Bouwman D, Teunissen J, Ebert U (2025) *Plasma Sources Sci. Technol*., **34**, 025015.
Teunissen J, Malagón-Romero A (2025) *Computer Physics Communications*, **315**, 109773.

RELIABLE DATA DISSEMINATION WITH LXCAT AND CHEMCAT: A STATUS UPDATE

Jan van Dijk and Daan Boer

Elementary Processes in Gas Discharges, Department of Applied Physics and Science Education, Eindhoven University of Technology, The Netherlands

j.v.dijk@tue.nl, d.j.boer@tue.nl

In the 2024 edition of SPIG, the authors have reported on the development "LXCat3", a modernized version of the community-driven LXCat project (Pitchford *et al*. 2017, Carbone *et al*. 2021, also see https://lxcat.net/home/), which provides electron-impact cross sections, swarm parameters, interaction potentials and other data that are required for low-temperature plasma (LTP) modeling and simulation. LXCat hosts approximately 30 000 cross sections and entertains 60 000 visitors per year. A demo version of LXCat3 is available at https://demo.lxcat.net; it will replace the previous version once the data contributors have had a chance to verify that all data have been correctly migrated, and further testing and usability enhancements have been realized. We invite you to give LXCat3 a try and welcome your feedback at this stage.

In this contribution, the authors will first present some highlights of "LXCat3" and demonstrate that its well-defined data model and modernized software stack enable new workflows and foster the reliability and reproducibility of studies in low-temperature plasma physics.

In the second part of this contribution, the authors demonstrate how the LXCat3 data model and software stack is reused to handle plasma chemistries at large. This extension is dubbed ChemCat (Chemistry Catalog), a data platform for plasma chemistry data available at https://chemcat.net. Moreover, the authors present a suite of (online) tools built around ChemCat and they will demonstrate how the combination of the ChemCat data platform and toolset enables fully reproducible plasma chemistry simulations.

LXCat3 and ChemCat are free and open-source software, available from the GitHub repository https://github.com/LXCat-project/LXCat.

References

Carbone E A D *et al*. (2021) *Atoms*, **9**, 16, https://doi.org/10.3390/atoms9010016
Pitchford L C *et al*. (2017) *Plasma Processes and Polymers*, **14**, 1600098, https://doi.org/10.1002/ppap.201600098

FROM ELECTRON SWARMS TO BENCHMARK THEORY: REVISITING AND RESOLVING (?) THE GREAT HYDROGEN CONTROVERSY

Liam H. Scarlett[1], Nathan A. Garland[2,3], Gregory J. Boyle[4], Dale L. Muccignat[4], Mark C. Zammit[5], Igor Bray[1], Dmitry V. Fursa[1] and Ronald D. White[4]

[1]*Department of Physics and Astronomy, Curtin University, Australia*

[2]*Queensland Quantum and Advanced Technologies Research Institute, Griffith University, Queensland, Australia*

[3]*School of Environment and Science, Griffith University, Queensland, Australia*

[4]*College of Science and Engineering, James Cook University, Queensland, Australia*

[5]*Theoretical Division, Los Alamos National Laboratory, Los Alamos, New Mexico, USA*

ronald.white@jcu.edu.au

The determination of the electron-impact $v = 0 \rightarrow 1$ vibrational excitation cross section of molecular hydrogen has remained one of the defining benchmark problems in electron swarm physics and electron-molecule scattering for more than five decades. Beginning with the pioneering electron swarm measurements of Crompton and co-workers in the late 1960s and early 1970s, electron transport-derived cross sections consistently differed from those obtained from crossed-beam measurements and best available scattering calculations by almost 50%. This discrepancy became known as the Great Hydrogen Controversy and represented one of the longest-standing unresolved questions in low-energy electron collision physics. Over the ensuing decades, successive generations of researchers revisited the problem using increasingly sophisticated experimental, theoretical and computational techniques. Major advances in electron transport theory, driven by the work of Crompton, Robson, Petrović, Morrison and numerous collaborators, systematically examined the assumptions underpinning Boltzmann equation analyses of electron swarms. These developments included higher-order transport formalisms, rigorous numerical solutions of the Boltzmann equation, improved treatments of inelastic collisions, non-hydrodynamic transport and comprehensive uncertainty analyses. Collectively, this work progressively strengthened confidence in the swarm methodology while failing to identify transport-theory deficiencies capable of explaining the discrepancy.

As highlighted by White *et al.* (2007), the implications extended well beyond molecular hydrogen, influencing confidence in electron transport theory, plasma modelling and the broader electron-molecule collision database.

In this presentation we discuss how recent ab initio calculations using the vibrational-electronic Molecular Convergent Close-Coupling (VE-MCCC) method have revisited this benchmark problem. By treating electronic and vibrational motion within a fully coupled close-coupling framework, the calculations provide a unified description of direct and resonant scattering without relying on the approximations that have traditionally separated these processes. The resulting $\nu = 0 \rightarrow 1$ excitation cross section is found to be in excellent agreement with the long-standing swarm-derived values and differs from the accepted crossed-beam measurements. These benchmark calculations provide independent theoretical support for the transport methodologies developed by the electron swarm community over the past five decades and reinforce confidence in the use of swarm-derived collision cross sections. At the same time, they underscore the enduring importance of the crossed-beam experiments and motivate a renewed examination of their interpretation in light of modern benchmark theory, with the goal of achieving a fully consistent understanding of this fundamental collision process.

The presentation concludes by considering the next evolution in electron swarm analysis. While traditional swarm analyses have relied on iterative solutions of the Boltzmann equation and expert-guided optimisation, emerging machine learning approaches provide new opportunities for extracting collision cross sections directly from transport measurements. We will present recent progress in the application of machine learning techniques to swarm data inversion and highlight the current status of determining vibrational excitation cross sections using these new methodologies. Together with benchmark ab initio scattering calculations, these approaches have the potential to establish a new generation of high-confidence electron-molecule collision cross sections for increasingly complex molecular systems. This presentation acknowledges the pioneering contributions of Robert Crompton, Zoran Lj. Petrović, Robert E. Robson, Michael A. Morrison and their respective research groups on this topic.

References

Scarlett L H, Garland N A, Boyle G J, *et al.* (2026) *Phys. Rev. A*, **113**, 062803.
White R D, Robson R E, Morrison M A, *et al.* (2007) *J. Phys Conf. Series*, **71**, 012004.

5th Workshop on X-ray and VUV Interaction with Biomolecules in Gas Phase (XiBiGP)

VALENCE ELECTRONIC STRUCTURE OF HYBRID AZOBENZENE-GOLD NANOPARTICLES STUDIED BY VUV PHOTOELECTRON SPECTROSCOPY

Danijela Danilović[1], Jelena Pajović[2] Madhusree Roy Chowdhury[3], Gustavo Garcia[3], Laurent Nahon[3], Vladimir Djoković[1], Dušan K. Božanić[1]

[1]*Center of Excellence for Photoconversion, VINČA Institute of Nuclear Sciences, University of Belgrade, Belgrade, Serbia*

[2]*Faculty of Physics, University of Belgrade, PO Box 368, 110001 Belgrade, Serbia*

[3]*Synchrotron SOLEIL, F-91192 Gif sur Yvette, France*

danijelad@vin.bg.ac.rs

Azobenzenes (AB) are a class of molecules characterized by a core structure consisting of two phenyl rings connected by a double N=N bond, which enables isomerization upon UV or visible light. The *trans* conformation, which is more stable under ambient conditions, converts to the *cis* conformation upon illumination with 365 nm UV light. The photoisomerization is reversible to the original conformation either through illumination at 450 nm or via thermal treatment (Biwas *et al.* 2016). These properties make azobenzenes effective photoswitchers in a wide range of applications. Functionalization of noble metal nanoparticles with azobenzene molecules can affect both the photoisomerization of the molecule and the surface plasmon resonance of the nanoparticle, see Köhntopp *et al.* 2016, Titov *et al.* 2015, and Chu *et al.* 2019. The final properties of this hybrid nanosystem are governed by competing light-driven reactions within both components. Here we present the results of a study on the photoinduced properties of gold nanoparticles functionalized with azobenzene and two derivatives – hydroxy AB (AB-OH) and thiolated AB (AB-SH) upon UV, visible, and IR light illumination. Insight into the nature of processes occurring in this nanosystem was gained by investigating the valence band structure using synchrotron-radiation VUV aerosol photoemission spectroscopy. An overlap between the valence bands of the AB molecules and nanoparticles was observed, confirming that charge transfer can readily occur between the constituents.

References

Biswas T K, Sarkar S M, Yusoff M M, and Rahman M L (2016) *J. Mol. Liq.*, ***214***, 231.

Chu Z, Han Y, Bian T, De S, Král P, and Klajn R (2018) *J. Am. Chem. Soc*., **141**, 1949.

Köhntopp A, Dittner M, and Temps F (2016) *J. Phys. Chem. Lett.*, **7**, 1088.

Titov E, Lysyakova L, Lomadze N, Kabashin A.V, Saalfrank P, and Santer S (2015) *J. Phys. Chem.,* **119**, 17369.

MOMENTUM SPECTROSCOPY AS A TOOL TO UNRAVEL CHARGE DYNAMICS IN MOLECULAR CLUSTERS

Mathieu Gisselbrecht

Department of Physics, Lund University, Lund, Sweden.

mathieu.gisselbrecht@fysik.lu.se

Momentum spectrometers have revolutionized the study of small, isolated quantum systems in the gas phase by enabling coincidence measurements of the full 3D momentum of charged particles. Jahnke *et al.* (2015) demonstrated, in atomic and molecular dimers, that new electronic decay channels for energy transfer can be opened between the constituents of the cluster. Extending such studies to larger clusters is of fundamental importance for understanding for instances processes relevant to atmospheric chemistry. In a seminal work, Kulmala *et al.* (2007) showed that when molecules such as NH_3, H_2SO_4, or volatile organic compounds mix with water clusters, the nucleation mechanism is significantly modified, leading to clusters that can act as efficient condensation centers. However, investigations of the interaction of these clusters with VUV and X-ray radiation remain scarce.

Here, we extend coincidence momentum spectroscopy to larger clusters with sizes up to ~1 nm, comprising a few tens of atoms or molecules. In a series of studies, Oostenrijk *et al.* (2018, 2019) employed site-selective ionization to localize initial charges and probe charge and proton transfer mechanisms within hydrogen-bonded networks. Such processes are expected to play a key role in the reactivity of organic compounds. More recently, Ganguly *et al.* (2022) showed that structural changes in CO_2 clusters can enhance the production yield of O_2^+, a mechanism relevant for CO_2-rich planetary atmospheres such as Mars. Finally, we present our first results aimed at understanding charge solvation following ionization, using electron spectroscopy on mass-selected cluster.

References

Ganguly S *et al.* (2022) *Comm. Chem.,* **5**, 16.
Jahnke T *et al.* (2015) *J. Phys. B,* **48**, 082001.
Kulmala M *et al.* (2007) *Science,* **318**, 89.

Oostenrijk B *et al*. (2018) *Phys. Chem. Chem. Phys*., **20**, 2932.
Oostenrijk B *et al*. (2019) *Phys. Chem. Chem. Phys*., **21**, 25749.

FROM GAS-PHASE TO LIQUID PHASE: PROBING THE ELECTRONIC STRUCTURE OF AMINO ACIDS WITH X-RAY SPECTROSCOPY

Juliette Leroux[1], Nicolas Velasquez[2], Florian Trinter[2], Markus Ilchen[1], Laura Pille[3], Lucas Schwob[3], Aarathi Nair[1], Jean-Yves Chesnel[4] and Sadia Bari[3]

[1]*Department of Physics, Universität Hamburg, 22607, Hamburg, Germany*

[2]*Fritz-Haber-Institut der Max-Planck-Gesellschaft, Faradayweg 4-6 14195, Berlin, Germany*

[3]*Deutsches Elektronen-Synchrotron DESY, 22603 Hamburg, Germany*

[4]*CIMAP, CEA/CNRS/ENSICAEN/Université de Caen Normandie, 14050 Caen, France*

juliette.leroux@uni-hamburg.de

The isolation of biomolecules in the gas phase eliminates all interactions with the solvent, allowing for stepwise control of these interactions by progressively increasing the number of bound water molecules, thereby bridging the gap between isolated molecules and aqueous conditions. A single water molecule can already induce significant structural changes in the molecule, such as the location of the protonation site or geometry (see Voss *et al.* 2018; Leroux *et al.* 2025).

Over the past thirty years, efforts have been made to develop experimental techniques for studying hydrated species in the gas phase. Comparing the gas-phase structure with the singly hydrated gas-phase structure provides insight into the influence of molecular water on its properties. In contrast, performing a liquid-phase study allows us to gain insights into the influence of water as a solvent and approach the conditions relevant to biology. Moreover, the addition of a solvent allows charge redistribution between the molecule and the solvent, thereby altering the local charge distribution and 3D structure.

Soft X-ray radiation provides a local probe into the atomic environment based on the electronic excitations of core electrons to unoccupied molecular orbitals, thereby capturing both the electronic and geometric structures of the system under investigation. In this study, we first combined X-ray absorption spectroscopy with tandem mass spectrometry to obtain information about the electronic structure of singly hydrated, protonated phosphotyrosine. We further explore the influence of

the solvent on phosphotyrosine and address ultrafast charge-transfer dynamics using Auger–Meitner spectroscopy (AMS) in aqueous solution in the soft X-ray range and extend it to the tender X-ray domain.

References

Leroux J, Chesnel J-Y *et al*. (2025) *Chem. – Eur. J.*, **31**, 202403665.
Voss J M, Fischer K C, Garand E (2018) *J. Mol. Spectrosc*., **347**, 28.

INTRA/INTER MOLECULAR CHEMISTRY IN NANO- SOLVATED GLYCINE CLUSTERS

Ville Lindblom[1], Sumit Srivastav[2], Aditi Pradhan[3], Shilpa Sahu[1], Ivo Vinklarek[3], Jochen Kuepper[3], Patrik Rousseau[2], Noelle Walsh[4], Mathieu Gisselbrecht[1], Stacey L. Sorensen[1], Per Eng-Johnsson[1] and Sylvain Maclot[2]

[1]*Department of Physics, Lund University, Box 118, Lund, 221 00 Sweden*

[2]*Université Caen Normandie, ENSICAEN, CNRS, CEA, Normandie Univ, CIMAP UMR6252, F-14000 Cean, France*

[3]*Center for Free-electron Laser Science CFEL, Deutsches Elektronen-Synchrotron DESY, Notkestr. 85, 22607 Hamburg, Germany*

[4]*MAX IV Laboratory, Lund University, Box 118, Lund, 221 00 Sweden*

Ville.Lindblom@fysik.lu.se

Three-dimensional electron and ion imaging spectrometry in coincidence is used to study the chemistry of glycine clusters, after inner-shell electron ionisation. In this study, we investigate the intra-cluster reactivity mechanisms as well as the effect of solvation on these processes. Recently, it has been shown that radiation impact on amino acid clusters can lead to intra-cluster reactivity that include peptide bond formation (see Rousseau *et al.* 2020). By investigating the amino-acid cluster we can, therefore, develop a deeper understanding of the formation of larger biological molecules such as peptides, while also revealing the role hydration or solvation may play in intermolecular chemistry. This experiment was carried out at the MAX IV Laboratory in Lund, Sweden, at the FlexPES beamline. A reaction microscope was used to study the products after the clusters had interacted with radiation. Specifically, both pure and hydrated glycine clusters were studied after ionisation of a C1s, N1s and O1s electron. The mass spectra of the glycine clusters reveal that there are certain "magic" numbers, meaning that some cluster sizes are more stable than others. Specifically, glycine clusters containing three and six glycine molecules were much more prevalent than any other. Three bonded glycine molecules were also more stable at higher initial charge states, because they very often occur in coincidence with other ionised cluster sizes. In contrast, the glycine cluster of six glycine molecules was stable in events in which only one charged particle was detected. Figure 1 shows

how the cluster dynamics changes due to site-selectivity. The clusters are 79n+1 Da in size (n=2-5); the peaks between these values are due to fragmentations of one or more glycine molecules of the cluster. A significant observable difference is how the cluster loses a fragment of 36 Da at a much higher rate after ionisation at one of the oxygen sites. This was initially attributed to the loss of two water molecules from the pure glycine cluster.

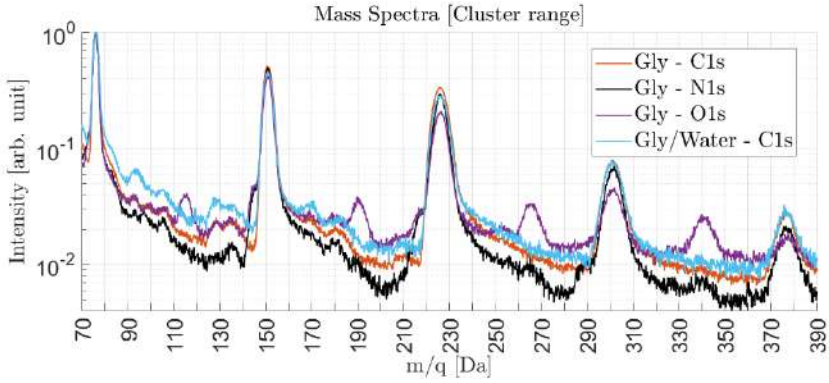

Figure 1: Mass spectra for glycine clusters at different ionisation edges. Orange (C1s), black (N1s) and purple (O1s) are pure glycine clusters, while blue (C1s) is glycine and water mixed clusters.

References

Rousseau P, Piekarski D G, Capron M *et al.* (2020) Polypeptide formation in clusters of β-alanine amino acids by single ion impact, *Nat Commun*, **11**, 3818.

THEORETICAL INSIGHTS INTO THE UV PHOTORESPONSE OF BIOMOLECULES

Ana Martin-Somer[1] and Lara Martinez-Fernandez[2]

[1]*Departamento de Química, Universidad Autónoma de Madrid, Módulo 13, 28049, Spain*

[2]*Departamento de Química Física de Materiales, Instituto de Química Física Blas Cabrera, CSIC, 28006, Madrid, Spain*

lmartinez@iqf.csic.es

The interaction of biomolecules with ultraviolet (UV) radiation populates electronically excited states whose evolution determines their photophysical and photochemical response. While efficient relaxation pathways often preserve molecular integrity, competing reactive channels can lead to chemical transformations that compromise biological function. These processes include photodimerization (Martinez-Fernandez and Improta 2021), ionization and the formation of reactive radical species (Banyasz *et al*. 2017). Selected examples of these processes will be discussed in DNA, where theoretical studies have provided detailed insight into the excited-state mechanisms governing both photostability and photodamage (Martínez Fernández *et al*. 2022). In contrast, the UV photoresponse of proteins and their constituent amino acids and peptides remains comparatively less explored from a theoretical perspective. Particular attention will be devoted to our investigation on the photodissociation in protonated peptides(Martínez-Fernández *et al*. 2024) and recent efforts aimed at elucidating charge-transfer processes in proteins, highlighting their potential role in shaping the photoresponse of larger biomolecular systems.

References

Banyasz A, Martínez-Fernández L, Balty C, Perron M, Douki T, Improta R and Markovitsi D (2017) *J. Am. Chem. Soc*., **139**, 10561.

Martínez Fernández L, Santoro F and Improta R (2022) *Acc. Chem. Res.*, **55**, 2077.

Martinez-Fernandez L and Improta R (2021) in *DNA Photodamage: From Light Absorption to Cellular Responses and Skin Cancer*, The Royal Society of Chemistry.

Martínez-Fernández L, Ranković M L, Canon F, Nahon L, Giuliani A, Milosavljević A R and Martin-Somer A (2024) *RSC Adv.*, **14**, 16809.

DEGRADATION OF POLYMER BUILDING BLOCKS DUE TO REACTIONS WITH IONOSPHERIC STATE SELECTED O^+ (4S, 2D) ION ANALOGS

Cíntia A. P. da Costa[1,2], Nandana Pattathadathil[1], Nicolas Solem[3,4], Roland Thissen[3,4], Christian Alcaraz[3,4], Matteo Michielan[1], and Daniela Ascenzi[1]

[1] *Dipartimento di Fisica, Università di Trento, Trento, 38123, Italy*

[2] *Aix Marseille Univ, CNRS, Institut Origines, PIIM, Marseille, France*

[3] *Université Paris-Saclay, CNRS, Institut de Chimie Physique, Orsay, 91405, France*

[4] *Synchrotron SOLEIL, L'Orme des Merisiers, 91192 Saint Aubin, Gif-sur-Yvette, France*

cintia.da-costa@univ-amu.fr

Polymeric materials are widely used in aerospace applications due to their resistance, flexibility and electrical and thermal insulation properties. Polymers used to coat space instruments in Low Earth Orbit region (up to 2000 km above Earth's surface) experience erosion caused by the primary atmospheric components at these altitudes, O and O^+. Ground-based atomic oxygen exposure experiments have been conducted (see, for instance, Shpilman *et al.* 2008), but the precise chemical erosion mechanisms are still not well described in the literature. The goal of this study is to investigate reactions of O^+ ions at selected ground and first excited states (^4S and ^2D, respectively) with representative molecules of polymers that could be taken to the gas phase. We aim to evaluate the extent of the reactivity (by measuring integral reactive cross sections, CSs) and their dissociation patterns (by determining the branching ratio, BR, for each product channel) and, if possible, extrapolating whether this behavior is consistent with that of the complete polymer in the solid phase. The degradation of N-methylmaleimide and diphenyl ether were taken as representatives of a Kapton macromolecule. Experiments were conducted at the French Synchrotron SOLEIL with the CERISES setup (Cunha de Miranda *et al.* 2015) a guided ion beam tandem mass spectrometer that couples ion generation via tunable VUV light with octupolar RF guiding and trapping of ions to measure absolute integral CSs and product BRs for ion-molecule reactions as a function of photon energy. O^+ was produced by dissociative photoionization of O_2 in the range 18.5 to 24 eV

and collision energy (ranging from 0.1 – 10 eV in the reference of the Center of Mass (CM)). Figure 1 shows results for the reaction of $O^+(^4S)$ with N-methylmaleimide ($C_5H_5NO_2$) as a function of the collision energy. The most abundant products are due to dissociative charge transfer and are observed at *m/z* 54 ($C_3H_2O^+/C_3H_4N^+$), 82 ($C_4H_2O_2^+/C_4H_4NO^+$) and 67 (C_3HNO^+), with little dependence on the collision energy (lower CSs values at $E_{CM} < 1$ eV are an artifact of the ion lens extraction system).

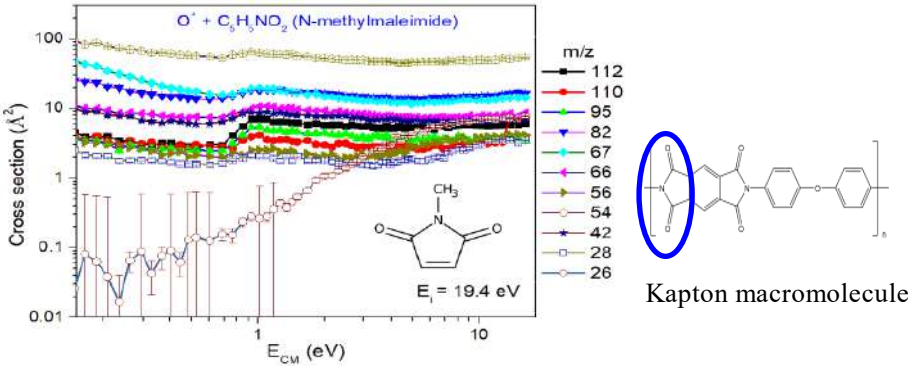

Figure 1: Cross sections for the ionic products of the reaction of O+(4S, hv= 19.4 eV) with N-methylmaleimide and their evolution with collision energy at the center of mass.

Acknowledgments: The research is carried out within the National Recovery and Resilience Plan (NRRP), Mission 4, Component 2, Investment 1.1, Call for tender No. 1409 (14.9.2022) by the Italian Ministry of University and Research (MUR), funded by the European Union – NextGenerationEU – Project Title P20223H8CK "Degradation of space-technology polymers by thermospheric oxygen atoms and ions: an exploration of the reaction mechanisms at an atomistic level" - CUP E53D23015560001. Thanks to Laurent Nahon & DESIRS team @SOLEIL SRF for assistance under Proposal No. 20240422. The results presented in this work are based upon work from COST Action COSY (CA21101), supported by COST (European Cooperation in Science and Technology).

References

Cunha de Miranda B *et al* (2015) *The Journal of Physical Chemistry* A, **19**, 6082.
Shpilman Z et al (2008) *Review of Scientific Instruments*, **79**, 2885044.

PHOTOELECTRON CIRCULAR DICHROISM AS A SENSITIVE PROBE OF ANOMERIC STRUCTURE IN GAS-PHASE SUGARS

Michele Pugini[1], Viktoria Brandt[1], Deb Pratim Mukhopadhyay[2], Nicolas Velasquez[1], Florian Trinter[1], Lukáš Tomaník[1], Gustavo Garcia[2], Laurent Nahon[2], and Bernd Winter[1]

[1]*Fritz-Haber-Institut der Max-Planck-Gesellschaft, Faradayweg 4-6, 14195 Berlin, Germany*

[2]*Synchrotron SOLEIL, L'orme des merisiers, Départementale 128, 91190 Saint Aubin, France*

mpugini@fhi-berlin.mpg.de

Chiral molecules are indispensable for life, and within living systems are found almost solely in one of two mirror-image enantiomeric forms. In the specific case of monosaccharides, for which the D-enantiomer dominates in biology, a particular stereocenter arises, namely the anomeric carbon (labeled as site 1 in Fig. 1), which corresponds to the locus of specific isomers called anomers in sugars. The hydroxyl group attached to this carbon atom can freely interconvert between axial (α) and equatorial (β) orientations via a ring-opening process known as mutarotation. The resulting α and β anomers are two different stereoisomers of the same monosaccharide with the same handedness, with the β anomer being the more stable form in aqueous solution as a consequence of the anomeric effect (Alagubin *et al.* 2021).

The mechanism underlying the interconversion between anomers is not yet fully understood. A first step toward elucidating the mechanism of mutarotation is the molecular-level characterization of individual anomers. To this end, we investigate substituted glucopyranosides, namely methyl-α-D-glucopyranoside (α-mGlu) and methyl-β-D-glucopyranoside (β-mGlu). In these molecules, methylation prevents anomeric interconversion, thereby rendering the individual anomers spectroscopically accessible; see Fig. 1.

While the stereoelectronic nature of the anomeric effect is expected to induce only subtle differences in the valence photoelectron spectra, photoelectron circular dichroism (PECD)—defined as the forward–backward asymmetry in the photoelectron flux along the photon propagation axis upon photoionization of

chiral molecules with circularly polarized light—has been shown to be exquisitely sensitive to minor changes in molecular structure and conformation (Dupont *et al.* 2022; Hadidi *et al.* 2021). PECD should therefore be well suited to distinguish between the α and β anomeric forms.

In addition, performing the experiments in a solvent-depleted environment allows the exclusion of solvent interactions, so that only intramolecular interactions need to be considered. We combined an aerosol thermodesorption source (Gaie-Levrel *et al.* 2011) with electron-ion coincidence measurements, detecting valence photoelectron images of nascent neutrals following ionization by VUV circularly polarized light. Our results show a pronounced anomer-specific PECD effect for the studied sugars.

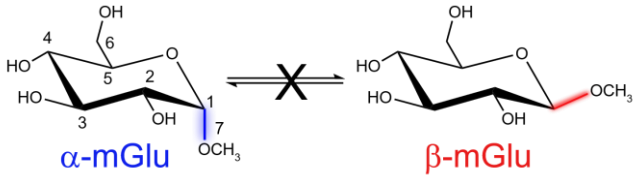

Figure 1: Schematics of methyl-α-D-glucopyranoside (α-mGlu) and methyl-β-D-glucopyranoside (β-mGlu). C1 is the anomeric carbon.

References

Alabugin, I V *et al.* (2021) *Chemical Society Reviews*, **50**, 10212.

Dupont J *et al.* (2022) *J. Phys. Chem. Lett.,* **13**, 2313.

Gaie-Levrel F *et al.* (2011) *Phys. Chem. Chem. Phys.*, **13**, 7024.

Hadidi R et al. (2021) *Commun. Chem.*, **4**, 72.

INDUCED PHOTOELECTRON CIRCULAR DICHROISM ONTO AN ACHIRAL CHROMOPHORE

Etienne Rouquet[1,2,3], Gustavo Garcia[2], Laurent Nahon[2], Valeria Lepere[1], Rodolphe Vuilleumier[4] and Anne Zehnacker[1]

[1] *Institut des Sciences Moléculaires d'Orsay (ISMO), CNRS, Université Paris-Saclay, Orsay, France*

[2] *Synchrotron SOLEIL, L'Orme des Merisiers,Départementale 128, Saint-Aubin, France*

[3] *Physikalisches Institut, Universität Münster, Münster, Germany*

[4] *Chimie Physique et Chimie du Vivant (CPCV), École Normale Supérieure, Sorbonne Université, Paris, France*

etienne.rouquet@uni-muenster.de

Photoelectron Circular Dichroism (PECD), the forward/backward asymmetry in the angular distribution of the electrons resulting from the ionization of a chiral molecule by a circularly polarized light, see Powis 2000 , is a very sensitive probe of molecular structure, see Dupont 2022, Hadidi 2021, and Turchini 2017.

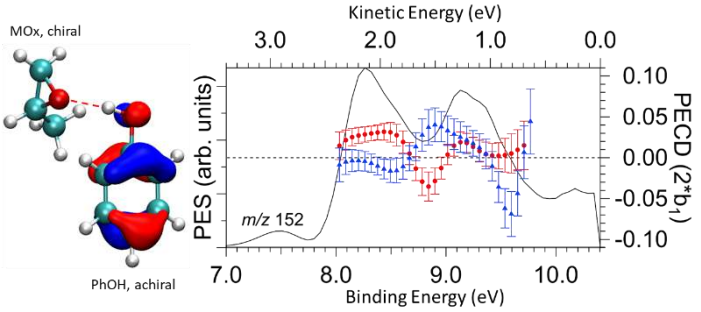

Figure 1: Left, structure of the most stable Phenol:Methyloxirane complex. Right, PES and PECD spectra for both enantiomers (blue and red) of the complex

While it was historically studied using synchrotron facilities, recent developments show PECD using laser setups, both in the femto- and nanosecond time scale, see Lee 2022. Using a ns-laser and a resonance-enhanced multiphoton ionization energy scheme, it is possible to selectively ionize different conformers of the

same molecule in the gas phase, which enhances the analytical potential of PECD. One major drawback of this phenomenon is the need of an accessible excited electronic state, i.e. the presence of a chromophore within the molecule. To tackle the issue, we thought of using a method already evidenced for circular dichroism in absorption, see Allenmark 2003 and Rizzo 2010. More specifically, it is the use of molecular complexes, separated in two moieties. One part is chiral, but does not have a chromophore, and the other is a non-chiral moiety with a chromophore. We recorded induced PECD of methyloxirane (MOx) via a molecular complex with phenol (PhOH) using VUV synchrotron radiation, see Rouquet 2023. In the gas phase, using helium as a carrier gas, we were able to form PhOH-MOx complexes whose structure and orbitals were previously calculated, showing a non-chiral HOMO located solely on the PhOH moiety. However, what we saw is a non-zero chiroptical response originating from the ionization of the complex, due to the electron scattering off the chiral molecular potential. Using this method, it is possible to enlarge the scope of PECD as an analytical tool, allowing to gain extensive molecular information of chiral molecule, as well as conformer-specific chiroptical response for virtually any system. We then successfully applied this technique using a ns-laser 2 photon energy scheme, providing conformer-selective PECD results. We first applied it to a single molecular system 1-indanol, see Rouquet 2024, before confirming our synchrotron-based results on conformer selected Phe:MOx molecular complexes, see Rouquet 2026. Two structures of the complex were observed in the gas phase, involving hydrogen bonds with both lone pairs of the MOx oxygen atom, revealing a mirrored deformation of the achiral phenol for each structure.

References

Allenmark S (2003) *Chirality,* **15**, 409.
Dupont J *et al.* (2022) *J. Phys. Chem. Lett.*, **13**, 2313-2320.
Hadidi R *et al.* (2021) *Commun. Chem.,* **4**, 72.
Lee H *et al.* (2022) *Phys. Chem. Chem. Phys.,* **24**, 27483.
Powis I (2000) *J. Chem. Phys.*, **112**, 1.
Rizzo P *et al.* (2010) *Chirality,* **22**, E67.
Rouquet E *et al.* (2023) *Nat. Commun.,* **14**, 6290.
Rouquet E *et al.* (2024) *Angew. Chem. Int. Ed.,* **63**, e202401423.
Rouquet E *et al.* (2026) *Angew. Chem. Int. Ed.,* **65**, e3631400.
Turchini S (2017) *J. Phys. Condens. Matter,* **29**, 503001.

PROBING AND TRANSFORMING HYDRATED BIOMOLECULES WITH X-RAYS: A THEORETICAL PERSPECTIVE

Petr Slavíček[1]

[1]*University of Chemistry and Technology, Prague, Technická 6, 16628, Prague*

petr.slavicek@vscht.cz

X-rays have long been used to disentangle the structure of biomolecules. With liquid-jet photoelectron spectroscopy, the same atom-specific sensitivity can now be extended to molecules in water, where C 1s and heteroatom core-level spectra become fingerprints of protonation, hydration, and local chemical environment. In the first part of the talk, I will discuss this idea for biomolecular solutes. Recent liquid-jet XPS of uracil, combined with maximum-overlap DFT, non-equilibrium continuum solvation, and QM/MM sampling, shows how long-range polarization and explicit dynamical hydration determine core-level binding energies; for deprotonated uracil, comparison with theory identifies N1 as the aqueous deprotonation site (Fournier *et al*. 2026). Related studies of amino acids demonstrate that aqueous photoelectron spectra directly report on the gas-to-solution change of molecular form, for example in proline (Credidio *et al*. 2024), while indole illustrates that individual hydrogen bonds can be separated from the nonspecific solvent background (He *et al*. 2023). The theoretical toolbox for such analyses is now mature enough for quantitative assignments, and internally consistent liquid-phase chemical-shift data may ultimately make XPS a more empirical structural probe of solutions (Tomaník *et al*. 2026).

The second part of the talk will move from structure to radiation-induced dynamics. I will focus on doubly ionized biomolecule-water complexes, where the initial state may be a localized biomolecular dication or a charge-delocalized pair, and where the subsequent dynamics depend strongly on how the state is prepared. State- and time-resolved measurements on hydrated pyrrole show that local double ionization can trigger proton transfer to water within about 50-60 fs (Zhou *et al*. 2025). In a complementary inner-valence ionization pathway, nuclear-motion-mediated intermolecular Coulombic decay (ICD) is observed: after ionization of pyrrole, the N-H...O hydrogen bond contracts, increasing the ICD efficiency and encoding femtosecond nuclear motion in the kinetic-energy-

release spectrum; by contrast, hydrated pyridine, where the biomolecule acts as a hydrogen-bond acceptor, remains close to a frozen-geometry limit (Zhou *et al*. unpublished results). I will discuss how localized and delocalized dicationic states, potential-energy surfaces, nonadiabatic and adiabatic molecular dynamics, and kinetic-energy-release/electron spectra can be combined into a theoretical description of these processes. Together, these examples show how X-ray and electron spectroscopies, supported by molecular simulations, can probe and rationalize both the static structure and the radiation-driven transformation of hydrated biomolecules.

References

Credidio B, Thürmer S, Stemer D, Pugini M, Trinter F, Vokrouhlický J, Slavíček P and Winter B (2024) From Gas to Solution: The Changing Neutral Structure of Proline upon Solvation. *J. Phys. Chem. A*, **128**, 10202-10212.

Fournier M, Procházka M, Dupuy R, Derbali E, Ajili Y, Hochlaf M, Palaudoux J, Slavíček P and Nicolas C (2026) Liquid-Jet XPS and Theoretical Computations Reveal Solvation-Driven Shifts and the Deprotonation Site in Uracil. Manuscript.

He L, Tomaník L, Malerz S, Trinter F, Trippel S, Belina M, Slavíček P, Winter B and Küpper J (2023) Specific versus Nonspecific Solvent Interactions of a Biomolecule in Water. *J. Phys. Chem. Lett.*, **14**, 10499-10508.

Tomaník L, Trinter F, Slavíček P and Winter B (2026) Electron spectroscopy for chemical analysis of liquids. *Chem. Sci.*, **17**, 6156-6164.

Zhou J, Wu L, Belina M et al. (2025) State- and time-resolved observation of ultrafast intermolecular proton transfer in hydrated biomolecules. *Nat. Commun.*, **16**, 5838.

ELECTRON INDUCED REACTIVITY IN AQUEOUS MEDIA USING A LIQUID MICROJET

Samrat Saha[1,2], Anirban Paul[1], Volodymyr Malynovskyy[1], Miloš Ranković[1], Juraj Fedor[1] and Pamir Nag[1]

[1]*Heyrovský Institute of the CAS, Dolejškova 3, 182 00 Prague 8, Czech Republic*

[2]*Department of Surface and Plasma Science, Faculty of Mathematics and Physics, Charles University, V Holešovičkách 2, Prague, Czech Republic*

samrat.saha@jh-inst.cas.cz

When high-energy radiation, including charged particles, passes through matter and living cells, it transfers energy to the medium, leading to the generation of secondary electrons. Since about 80% of living cells consist of water, the interaction of primary radiation with H_2O also plays an important role. Ionization of water molecules results in the formation of secondary electrons and water cations, which can further react or decompose to form hydroxyl radicals and prehydrated electrons, the latter acting as precursors to solvated electrons. Hydroxyl radicals and solvated electrons can also contribute to damage in living cells, including DNA single- and double-strand breaks (see Boudaïffa *et al.* 2000; Halliwell *et al.* 2021). Therefore, it is important to quantify their formation by primary radiation in aqueous media and to study their reactivity.

Our research group in Prague developed a unique recirculating liquid microjet setup (see Nag *et al.* 2023) to study electron-induced chemical reactivity in the solvated phase and to quantify the dose of solvated electrons. The experimental setup consists of a high-vacuum-compatible recirculating liquid microjet and an electron gun that delivers a tunable electron beam with energies ranging from 60 to 800 eV. Following irradiation, the liquid sample can be collected for ex-situ analysis or recirculated for subsequent irradiation experiments.

To understand the effect of hydroxyl radicals produced by the primary electron beam in aqueous TRIS (2-amino-2-(hydroxymethyl)propane-1,3-diol) solutions, we irradiated a 19.3 mM TRIS solution with a 300-eV electron beam. After the irradiation for different number of passes, the sample was collected and analyzed using a UV–Vis spectrometer. The measurements revealed clear evidence that TRIS reacts with hydroxyl (OH•) radicals generated through electron-induced dissociation of water molecules (see Nag *et al.* 2023). On the other hand, to

quantify solvated electrons, we implemented the two-electron reduction of nitrate ions (NO_3^-) to nitrite ions (NO_2^-), as shown in Equation 1.

$$NO_3^- + 2\ e_{hyd}^- + 2\ H^+ \rightarrow NO_2^- + H_2O. \quad (1)$$

We irradiated aqueous $NaNO_3$ solutions with an electron beam at different incident energies, ranging from 60 to 600 eV, for multiple passes. The irradiated samples were mixed with 2,3-diaminonaphthalene (2,3-DAN), which selectively reacts with NO_2^- to produce fluorescent 2,3-naphthotriazole (2,3-NAT). The fluorescence yield of the product provides a quantitative measure of the electron dose produced within the liquid microjet, as shown in Figure 1 (Saha *et al.,* unpublished).

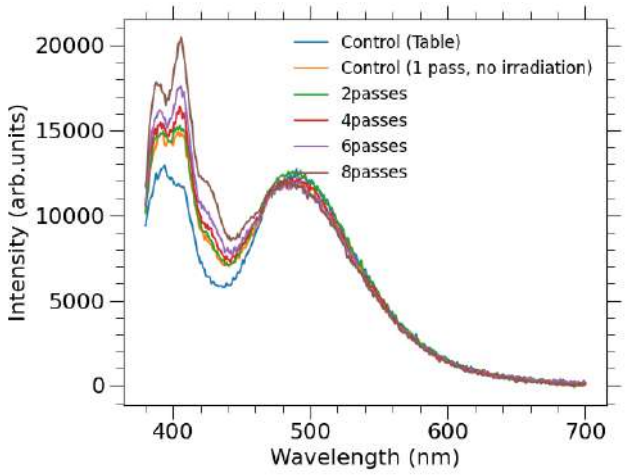

Figure 1: Fluorescence spectra from 380 to 700 nm of the reacted sample.

References

Boudaïffa B, Cloutier P, Hunting D, Huels MA and Sanche L (2000) *Science*, **287**, 1658.

Halliwell B, Adhikary A, Dingfelder M and Dizdaroglu M (2021) *Chem. Soc. Rev*., **50**, 8355.

Nag P, Ranković M, Schewe HC, Rakovský J, Sala L, Kočišek J and Fedor J (2023*) J. Phys. B: At. Mol. Opt. Phys.*, **56**, 215201.

Saha S, Polena J, Sicard-Roselli C, Malynovskyy V, Slavíček P, Ranković M, Fedor J and Nag P, *Chem. Sci.,* (about to submit).

BOND FORMATION FOLLOWING ACTIVATION OF GAS-PHASE AMINO ACID CLUSTERS

T.J. ten Napel[1], B.M. Szihalmi[1], J.K.D. Bergsma[1], A.H. Kramer[1], R.J. Mackey[1], O. Kavatsyuk[2], V. Zamudio-Bayer[4], J. T. Lau[4], J.C. Poully[3] and T. Schlathölter[1,2]

[1]*University of Groningen, Zernike Institute for Advanced Materials, 9747 AG Groningen, Netherlands*

[2]*University of Groningen, University College Groningen, 9718 BG Groningen, Netherlands*

[3]*CIMAP UMR 6252 (CEA/CNRS/ENSICAEN/Université de Caen Normandie), Boulevard Becquerel, 14070 Caen Cedex 5, France*

[4]*Helmholtz-Zentrum Berlin für Materialien und Energie, Abteilung Hochempfindliche Röntgenspektroskopie, 12489 Berlin,Germany;*

t.a.schlatholter@rug.nl

The possible extraterrestrial origin of life's building blocks has been debated for decades. Amino acids, the fundamental constituents of proteins, have been identified in primitive meteorites, and gas-phase glycine has been detected in the coma of comet 67P/Churyumov-Gerasimenko (see Altwegg *et al.* 2016). These molecules are thought to form on icy dust grains in the interstellar medium (ISM) or protosolar nebulae (PSN) (see Ciesla and Sandford 2012), although direct detection of an amino acid in either environment has yet to be achieved.

More complex biomolecules may form in the interstellar medium (ISM) and protosolar nebulae (PSN) through bottom-up synthesis from small precursors or top-down fragmentation of larger species. An intermediate pathway involves energetic processing of non-covalent molecular clusters, triggering intra-cluster bond formation (ICBF). Recent studies demonstrated ICBF and peptide bond formation in amino acid clusters induced by keV ion impact (see Altwegg *et al.* 2016) and vacuum ultraviolet (VUV) photon absorption (see Ciesla and Sandford 2012). However, the effects of more energetic photons (soft X-rays) on amino acid clusters remain unexplored. Such X-ray-driven chemistry may be relevant in X-ray-dominated regions (XDRs), including planetary nebulae, supernova remnants, and environments around young stellar objects. Similarly, the

interaction of atomic hydrogen (H) with amino acid clusters remains largely unexplored, despite the high abundance of atomic H in many astrophysical environments and its potential role in driving chemical transformations.

We have employed near-edge soft X-ray absorption mass spectrometry (NEXAMS, (see González-Magaña *et al.* 2012)) to investigate soft X-ray induced process in protonated clusters of the amino acid serine. The clusters were produced by means of electrospray ionization and the experiments were performed at the IonTrap end station of the BESSY II synchroton (Helmholtz Zentrum Berlin, Germany). We will present new data on the X-ray induced formation of covalent bonds between serine-cluster constituents. In addition, we will discuss the influence of the cluster environment on the molecular electronic structure and its manifestation in NEXAMS spectra.

For the H-induced processes, we employed an experimental setup in Groningen in which electrosprayed, protonated serine and glycine dimers were accumulated in a radiofrequency ion trap and exposed to gas-phase H atoms. Fragmentation pathways and intracluster reactions were subsequently characterized by mass spectrometry. Preliminary results indicate that H attachment is invariably dissociative and frequently triggers intracluster bond formation.

References

Altwegg K *et al.* (2016) *Science Advances*, **2**, e1600285.

Ciesla J and Sandford S A (2012) *Science*, **336**, 452–454.

González-Magaña O, Reitsma G, Tiemens M, Boschman L, Hoekstra R and Schlathölter T (2012) *Journal of Physical Chemistry A*, **116**, 10745.

Licht O *et al*. (2023) *Angewandte Chemie International Editions*, **62**, e202218770.

Rousseau P *et al*. (2020) *Nature Communications*, **11**, 3818.

VACUUM ULTRAVIOLET PHOTOABSORPTION SPECTROSCOPY OF BENCHMARK ORGANIC MOLECULES

F. Ferreira da Silva[1], F. Kossoski[2], A. Lozano[3] A. S. Barbosa[4], S. V. Hoffmann[5], N. C. Jones[4] and M. Mendes[1]

[1] *Department of Physics, Nova School of Sciences and Technology, 2829-516 Caparica, Portugal.*

[2] *Laboratoire de Chimie et Physique Quantiques (UMR 5626), Universite´ de Toulouse, CNRS, UPS, France.*

[3]*Institut de Recherche en Astrophysique et Planétologie (IRAP), Université de Toulouse, CNRS, CNES, 9 Avenue du Colonel Roche, Toulouse, France*

[4]*Departamento de Física, Universidade Federal do Paraná, Caixa Postal 19044, Curitiba 81531-980, PR, Brazil*

[5]*ISA, Department of Physics and Astronomy, Aarhus University, Ny Munkegade 120, 8000 Aarhus C, Denmark*

f.ferreiradasilva@fct.unl.pt

Vacuum ultraviolet (VUV) photoabsorption spectroscopy constitutes a powerful tool for probing the electronic structure of isolated molecules, providing access to valence, Rydberg and ionization continua states that govern their photophysical and photochemical behaviour. In this contribution, we present recent results on the absolute photoabsorption cross sections of a series of molecular systems of fundamental and applied interest, including halogen-substituted pyrimidines[1,2] and simple organic molecules such as propylene oxide[3], and trichloroanisole[4], over the 3.0–11.0 eV photon-energy range. Measurements were performed using high-resolution synchrotron radiation, enabling the characterization of the lowest-lying electronic excitations and the identification of extensive Rydberg manifolds converging to the first ionization energies. The experimental spectra are supported by state-of-the-art quantum chemical calculations, allowing detailed assignments of the observed spectral features and assessment of the influence of molecular structure, heteroatom substitution and halogenation on the excited-state landscape. Particular emphasis is placed on the evolution of valence-Rydberg interactions and on the spectroscopic signatures

associated with substitution effects in biologically relevant pyrimidine derivatives. For the simple organic molecules, the measurements provide benchmark data for understanding the electronic response of oxygenated, aromatic and halogenated systems to VUV radiation. The resulting absolute cross sections and electronic-state assignments contribute to a growing database required for modelling radiation-driven processes in planetary atmospheres, plasma environments and biologically relevant media, while providing new insights into the relationship between molecular structure and electronic excitation dynamics.

References

[1] – M. Mendes et al. (2021) *Int. J. Mol. Sci.* **22,** 6460.
[2] – F. Kossoski et al. (2025) *Phys. Chem. Chem. Phys.,* **27,** 9687.
[3] – M. Mendes et al. (2026) *Phys. Chem. Chem. Phys.,* **28,** 7645.
[4] – M. Mendes et al. (2023) *Phys. Chem. Chem. Phys.,* **25,** 25361.

AUTHORS' INDEX

E

F

G

H

I

J

K

L

M

S

T

U

CIP - Каталогизација у публикацији
Народна библиотека Србије, Београд

537.56(082)
539.186.2(082)
539.121.7(082)
533.9(082)

SUMMER School and International Symposium on the Physics of Ionized Gases (33 ; 2026 ; Beograd)
Book of Abstracts / 33rd Summer School and International Symposium on the Physics of Ionized Gases - SPIG 2026, f25-28 August 2026], Belgrade, Serbia ; [organized by] Institute of Physics Belgrade [and] Serbian Academy of Sciences and Arts. - Belgrade : SASA : Institute of Physics, 2026 (Beograd : Skripta Internacional). - 264 str. : ilustr. ; 24 cm

Tiraž 200. - Bibliografija uz svaki rad. - Registar.

a) Јонизовани гасови -- Зборници b) Атоми -- Интеракција -- Зборници v) Плазма -- Зборници

COBISS.SR-ID 198869001

SPECTROSCOPIC APPLICATIONS OF LASER-INDUCED PLASMA IN THE CONTEXT OF ARTIFICIAL INTELLIGENCE

Jin Yu

School of Physics and Astronomy, Shanghai Jiao Tong University, Shanghai 200240, China

jin.yu@sjtu.edu.cn

Laser-induced breakdown spectroscopy (LIBS) emerged as a scientific discipline in 1962, merely two years after the invention of the laser. Owing to its broad application prospects, the technique has attracted significant attention since its inception and has long been regarded as an ideal solution for analytical detection based on laser-induced emission spectroscopy. Between 1964 and 1965, the Jarrell Ash Company in the United States developed an instrument known as the *Laser Microprobe*, marking one of the earliest explorations into the commercial use of LIBS.

Today, after more than six decades of continuous advancement, LIBS research has matured into a vibrant and innovative academic ecosystem that attracts and inspires a growing number of research teams worldwide. With this strong scientific foundation in place, the field is now well-positioned for meaningful progress toward industrial application and commercialization. The early commercial developments envisioned 61 years ago are gradually coming into clearer view, supported by new technological capabilities and emerging industrial needs.

The pace of technological progress has not slowed; we have already entered the era of artificial intelligence. Alongside powerful new methods for information processing, unprecedented demands for digitalization and intelligent manufacturing—epitomized by Industry 4.0—have emerged. Against this backdrop, this report draws on the foundational research and applied practice of the LIBS team at the School of Physics and Astronomy, Shanghai Jiao Tong University, to explore new opportunities and new modalities for LIBS development, as well as new prospects for its commercialization in the context of artificial intelligence. The aim is to offer a modest contribution that may spark further discussions.